AN ELECTRON SPIN RESONANCE STUDY OF CONFORMATIONAL EFFECTS IN FREE RADICALS DERIVED FROM ALIPHATIC ALCOHOLS AND ETHERS

by

ALEXANDER GIBSON BRIGGS

B.Sc., Mount Allison University, 1975
M.Sc., University of St. Andrews, 1977

A DISSERTATION SUBMITTED IN PARTIAL FULFILMENT
OF THE REQUIREMENTS FOR THE DEGREE OF
DOCTOR OF PHILOSOPHY
in the Department
of
Chemistry

We accept this dissertation as conforming
to the required standard

_____
Dr. Paul R. West

_____
Dr. R.H. Mitchell

_____
Dr. F.P. Robinson

_____
Dr. D.E. Lobb

_____
Dr. R.W. Olafson

_____
Dr. Y.L. Chow

UNIVERSITY OF VICTORIA

November 1982

Supervisor: Dr. Paul R. West

ABSTRACT

Variable temperature ESR studies of radicals generated photolytically from simple aliphatic alcohols and ethers in cyclopropane solution reveal complex linewidth effects. Isotropic modulation of the proton hyperfine splittings (hfs) through restricted rotation about C-O and C-C single bonds is observable in the region 230>T>150K. Such effects can be distinguished from anisotropic viscosity-dependent line broadening.

In spectra from alcohol radicals resolved 2nd order structure causes no ambiguity in the interpretation. Restricted rotation about $\dot{C}_\alpha$-OH modulates $a_{\alpha H}$ and $a_{\beta H}$ *out-of-phase* with a_{OH} in the series $R\dot{C}HOH$ [R = CH_3, C_2H_5, $C_2H_5CH_2$, $(CH_3)_2CHCH_2$, $(CH_3)_3CCH_2$]. A general model for the process is discussed. In cases three and four restricted C_β-C_γ rotation allows the diastereotopic inequivalence of the β-protons to be manifested as a broadening of $\tilde{M}_\beta$ = 0 components. Preferred conformations consistent with all the foregoing modulation effects and with observed H_β and H_γ splittings are presented. The analysis is supported by results for radicals $R\dot{C}HOR'$ from related ethers and by spectral simulation.

The spectrum of the 1-hydroxycyclohexyl radical demonstrates previously unobserved fine structure and a low-temperature linewidth effect tentatively attributed to radical site inversion.

A second series of alcohol-derived radicals $R_1R_2R_3\dot{C}CHOH$ with an increasingly bulky C_α substituent has been studied. The H_α hfs provide evidence of a steric flattening not hitherto observed. This effect

correlates well with literature values of steric parameters for the $R_1R_2R_3C$ substituent. In the case $R_1,R_2 = CH_3$, $R_3 = C_2H_5$ an observed specific γ-H interaction is assigned to a locked conformation of the crowded system.

A series of highly alkylated cyclic ethers has been examined. The dramatic temperature-dependent changes in the spectrum of the 5,5-dimethyl-1,3-dioxan-2-yl radical are attributed to restricted ring flipping. A fast exchange limit spectrum has been obtained for the first time in such systems, allowing evaluation of thermodynamic parameters. The 2,4,8,10-tetraoxyspiro[5,5]undecan-3-yl radical exhibits similar behaviour. The 2,2,5,5-tetramethyl and 5,5-diethyl-2,2-dimethyl-1,3--dioxan-4-yl radicals have fixed conformations which give rise to enhanced values of $a_{\gamma H}$ in agreement with theoretical calculations. In the latter case a splitting of 4.27 G is assigned to a single γ-methylene proton in behaviour analogous to $R_1R_2R_3C\dot{C}HOH$.

EXAMINERS:

Dr. Paul R. West

Dr. R.H. Mitchell

Dr. F.P. Robinson

Dr. D.E. Lobb

Dr. R.W. Olafson

Dr. Y.L. Chow

TABLE OF CONTENTS

LIST OF TABLES

Table

LIST OF FIGURES

Figure

Figure

Figure

Figure

LIST OF ABBREVIATIONS

a_i	hyperfine splitting constant of a nucleus (or nuclei) i
$\|a_i\|$	the magnitude, or absolute value, of a_i
Bu	butyl
Bu^t	tertiary-butyl
D	deuterium
dtbp	di-*t*-butyl peroxide
E_a	activation energy
ESR	Electron Spin Resonance
G	gauss (see footnote page 8)
g-value	spectroscopic splitting constant of an electron
$\Delta G_c^{\ddagger}$	free energy of activation at the coalescence temperature
hfs	hyperfine splitting(s)
IR	infra-red
k	rate constant
m_i	nuclear spin quantum number for a single nucleus i
M_i	nuclear spin quantum number for a group of equivalent nuclei (equation 3, page 4)
$\tilde{m}_i$	spectral index number for a single nucleus i (see page 67)
$\tilde{M}_i$	spectral index number for a group of equivalent nuclei (cf. equation 3, page 4)
NMR	nuclear magnetic resonance
Ph	phenyl
T	temperature
T_c	coalescence temperature

UV	ultraviolet
VT	variable temperature

ACKNOWLEDGEMENTS

Special thanks are due to Dr. Paul R. West for his understanding support and guidance throughout the course of this work. I am also grateful to the University of Victoria for the award of a Postgraduate Research Fellowship and to the Chemistry Department for the use of its research facilities.

Implicit in the fact of the ensuing dissertation are the contributions of many without whom the project would have been impossible. These include, among others, special efforts in the design and construction of a variety of equipment by the electronic, mechanical and glass-blowing workshops, and it has been a pleasure to work with these people. I would like to thank Terry Wiley for his assistance, and especially for dealing with the inevitable problems associated with complex instrumentation. The contribution of Academic Systems personnel in adapting the simulation programs for use is also gratefully acknowledged.

The friendship of my fellow graduate students and other members of the department has played a major role in making my sojourn in Victoria an enjoyable one.

Finally, I would like to thank Mrs. Eleanor Lowther for her patience and skill in the typing of this dissertation.

DEDICATION

To my mother and father

and my brother

As a young lion torn from the forest
is tame and playful, allowing
caresses, and joining in every frolic
so we found chemistry;
but as it grew to its full size and
formidable strength, — it became a thing
no longer to be played with;
demanding all care, attention, and respect.

John Scoffern,
Chemistry No Mystery,
1839

PREFACE

This dissertation presents the results of research undertaken to examine the interplay of stereoelectronic, steric and conformationally dependent effects on ESR spectral parameters in a range of aliphatic alcohol and ether-derived free radicals.

Chapter I is a discussion of electron spin resonance spectroscopy as a technique for investigating the conformations and configurations of organic free radicals.

It was necessary to examine a variety of experimental techniques in order to establish, for the first time in the research group, a system appropriate to the study. The choice of substrates incurred particular problems which will be discussed. The development of the experimental system was an important component of the project and is treated in detail in Chapter II.

The third chapter presents the exchange effects observed in the spectra of a variety of α-hydroxyalkyl radicals and discusses the mechanisms from which they arise, these being primarily restricted rotation about single bonds. Conformational aspects are also treated.

Chapter IV deals with conformational effects in the spectra of radicals derived from 1,3-dioxanes and related spiro ethers. Some interesting specific γ-proton hyperfine interactions here are related to remote splittings in α-hydroxyalkyl radicals.

Chapter V examines the degree of bending in a series of β-alkyl substituted alcohol radicals with emphasis on the effect of steric

interactions when the substituents are large.

The syntheses of compounds used as substrates are presented in Chapter VI.

Some notes on the use of the computer programs in simulation of ESR spectra follow the dissertation as Appendix A.

CHAPTER I

ESR SPECTROSCOPY: A TECHNIQUE FOR STUDYING THE STRUCTURE OF ORGANIC FREE RADICALS

1. SPECTRAL PARAMETERS AND THEIR INTERPRETATION

The ESR technique has progressed a great deal since the time when it was possible to suggest that "chemists would...be interested in simply establishing the presence or absence of free radicals."[1] Remarkable advances in detection and resolution over the last two decades have seen ESR spectroscopy develop into a powerful battery of sophisticated techniques to extend our understanding of diverse physical and chemical properties of paramagnetic species. Detailed information has been obtained on radical structure and conformation,[2,3,4] kinetics and mechanisms of radical reactions,[5] electron spin relaxation and structural organization in various media,[6] electron distribution in molecules,[7] and processes and structures in biomolecules.[8,9,10] Many of these topics have been mentioned[11,12] or discussed[13,14] in recent reviews.

Early interest by physicists has resulted in an extensive understanding of the theory of electron spin resonance, the basic elements of which are now available in texts[9,10,15-19] and brief summaries.[20,21] Comprehensive treatments of the theory and practical aspects of design, construction and use of ESR spectrometers have been published.[22,23]

Since the present work is concerned with the structure of the organic radicals *per se*, it is not within the scope of this dissertation

to discuss the basic theory of magnetic resonance phenomena. Accordingly, this section emphasizes the measured spectral parameters and their relationship to particular properties of the observed radical species. Aspects of theory will be introduced as required.

The isotropic ESR spectrum of a free radical in fluid solution is characterized by a g-value, and spin-spin splitting giving rise to the multiplicity, separation and relative intensity of the lines. Further information may be obtained from lineshape and linewidth.

(a) g-Values

When microwave radiation is applied to an unpaired electron in a magnetic field (H), absorption of energy will occur if the resonance condition (Equation 1) is satisfied,

$$h\nu = g\beta H \qquad (1)$$

where h is Planck's constant, ν is the microwave frequency and β is the Bohr magneton for the electron. The dimensionless proportionality factor g is called the spectroscopic splitting constant of the electron. For an electron not associated with any nuclei the value of g is 2.00232. In an organic radical the unpaired electron has both spin angular momentum and a component of angular momentum resulting from its orbital motion. The orbital angular momentum depends on the geometry of the molecule, or more fundamentally on the electronic wave function. As a result, the interaction of the total angular momentum vector with a magnetic field differs depending on the orientation of the radical with respect to the field direction. The anisotropic properties of the g-value can be measured in single crystal experiments. For free

radicals in non-viscous solution the anisotropy in g is averaged to zero by Brownian tumbling. In viscous solution, however, g-factor anisotropy can manifest itself through line broadening. The low anisotropy of carbon-centered π radicals gives them observed g-values which differ little from the free spin value (2.00232), (e.g. for $C_2H_5\cdot$, g = 2.00260).[24] Small differences in the observed g-value are related, for example, to partial delocalization of the unpaired electron onto oxygen or halogen atoms bonded to the radical center (e.g. for $CH_3\dot{C}HOH$, g = 2.00334,[25] for $CH_3COCH_2\cdot$, g = 2.00441).[26] Where the range of basic functional groups is restricted to alcohols and ethers the very limited trends which have been observed[27] are of little diagnostic value.

(b) Hyperfine Splittings

(i) General Information

Spin-spin splitting in isotropic organic radical spectra reflects interactions of the electron with the local magnetic fields of active nuclei, e.g. ^1H, ^{13}C, ^{15}N, ^{19}F, ^{35}Cl, ^{37}Cl. As a result of their relatively low energy compared to electron-electron coupling these nuclear interactions are referred to as hyperfine splittings (hfs). The resulting multiplicity of the ESR signal then depends on the number and magnetic moments (nuclear spin, I) of the interacting nuclei. For n equivalent nuclei, in the ideal first order unbroadened spectrum, one observes 2nI + 1 lines appearing in a binomial intensity distribution. The separations of the lines correspond to the differences in local field experienced by the unpaired electron due to different nuclear spin states. When an absorption occurs the electron spin quantum number

($M_S = \pm \frac{1}{2}$) changes by unity ($\Delta M_S = \pm 1$) while the nuclear spin angular momentum vector does not change ($\Delta M_I = 0$). These are the selection rules.

The line positions are a function of the hyperfine splitting constants (a_i) as indicated in equation 2. If there are n groups of equivalent* nuclei and r_i nuclei in the i^{th} group then the k^{th} line in the spectrum will be found at the magnetic field H_k given by equation 2. In this equation H' is the magnetic field of resonance in the absence of

$$H_k = H' - \sum_{i=1}^{n} a_i M_i \qquad (2)$$

nuclear hyperfine interaction, and M_i is defined as;

$$M_i = \sum_{j=1}^{r_i} m_{Ij} \qquad (3)$$

where m_{Ij} is the nuclear spin quantum number of each nucleus j in the i^{th} group. The hyperfine splitting constant due to interaction with nuclei of the i^{th} group is a_i.** The fact that each spectral line is associated with a unique set of nuclear spin quantum numbers has important consequences in both motional processes and in second order effects (see Chapter III).

---

* The term *equivalent* will be more rigidly defined in the context of dynamic ESR (Chapter III). Equation 2 is consistent with the later definition.

** In order to have positive M_I values displaced to high field it is assumed that $a_i < 0$ in equation 2 (see Chapter III).

(ii) The Origin of Hyperfine Splitting

Three different magnetic interactions of nuclei and the electron can be identified.

One mechanism of interaction is the dipolar coupling of the nuclear and electron spins. Such coupling is anisotropic but averages to zero for freely tumbling radicals in solution.

When electron orbital angular momentum is significant its interaction with the nuclear spin represents a second mechanism. This situation tends to have little importance for the majority of alkyl radicals.[20]

Most important in isotropic spectra of organic radicals is the Fermi contact interaction resulting from spin density in a molecular orbital having atomic s orbital character associated with the nucleus in question. Most organic carbon-centered radicals have their unpaired electron density in π molecular orbitals derived from atomic 2p orbitals (node at the nucleus). Accordingly no *direct* contact interaction is expected. It is important to distinguish here between spin density and unpaired electron density. If the other electrons in a molecule were completely unaffected by the presence of a partially filled MO (i.e. unpaired electron) then the spin density would be exactly the unpaired electron density. However, *spin polarization* occurs so that spin density is induced in other orbitals including those with s atomic character associated with nuclei up to four bonds removed from a localized (unconjugated) organic π radical.

As mentioned, most aliphatic and aromatic radicals are of the π type, with either a localized 2p electron or one delocalized in an extended conjugated π system. In either case no *unpaired* electron density is associated with the hydrogen nuclei if a strictly planar system is maintained. *Spin polarization* of the hydrogen valence electron by the unpaired electron in the π system is then postulated (Figure 1).

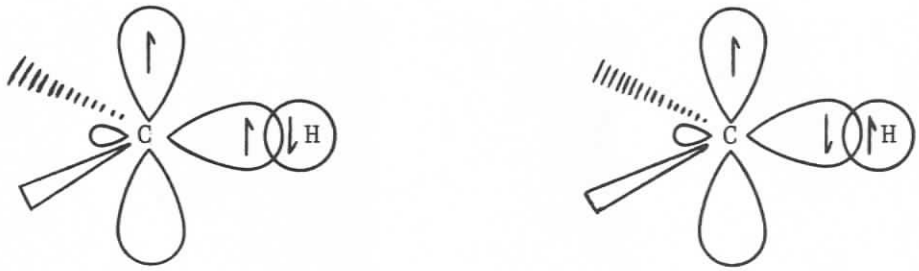

(a) (b)

FIGURE 1: Spin polarization. Configuration (a) is favoured.

This mechanism does not involve a transfer of unpaired electron density to hydrogen. The indicated association of "parallel" spins provides a finite component of *spin density* at both the carbon and hydrogen nuclei. Spin polarization implies that the configuration in Figure 1(a) is energetically more favourable than the one in 1(b). This can be understood by considering Hund's rule.* Clearly both carbon and hydrogen

* "...as far as possible electrons will go into orbitals so that they have parallel spins."[28]

now have net spin density in an "orbital" having "s" character. For hydrogen the spin is of opposite sign to that in the carbon p orbital and accordingly a negative sign is applied to the hyperfine splitting ($a_{\alpha H}$).* For α-carbon, spin density of the same sign is induced and so $a_{\alpha C}$ remains positive.

Given the importance of the isotropic Fermi contact interaction, proton hyperfine splittings can be a sensitive indicator of spin density distribution in organic free radicals.

For planar radicals having completely delocalized π electron systems the semi-empirical molecular orbital theory (HMO) provides a reasonable indication of unpaired electron distribution. Consider the molecular orbital ψ_i occupied by the unpaired electron in a molecular framework of n carbon atoms

$$\psi_i = C_{i1}\phi_1 + C_{i2}\phi_2 + \ldots + C_{in}\phi_n \qquad (4)$$

as a linear combination of atomic $2p_z$ orbitals (ϕ_j)(Equation 4). Then in the normalized expression (i.e. $C_{i1}^2 + C_{i2}^2 + \ldots + C_{in}^2 = 1$) the square of the coefficient C_{ij} of the atomic orbital ϕ_j is the probability that the unpaired electron is on atom j (Equation 5).

$$\rho_j = C_{ij}^2 \qquad (5)$$

In this expression ρ_j is the unpaired electron density on atom j. Experimental observations of proton hyperfine couplings revealed a

---

* The notation used is the usual one for designating nuclei in free radicals, *viz:*

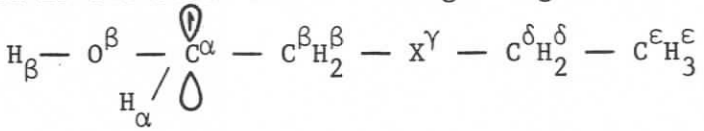

proportionality relationship between these aromatic hydrogen hfs and unpaired electron densities, (Equation 6), often referred to as the McConnell equation. Q typically falls in the range -20 to -30 gauss.*

$$a_H = Q\rho_C \tag{6}$$

For series of radicals not greatly different from each other good correlation for a given Q value is observed. In methyl radical, for example (a_H = -23.0 G)[3] the value of ρ_C is clearly unity and Q = -23 G. In the benzene radical anion the unpaired electron density at each carbon must be ρ_C = 1/6. Experimentally a_H = -3.75 as predicted. Simple HMO calculations, however, do not predict the negative sign of the coupling constant. As well, finite hyperfine splittings are often observed for protons attached to carbons predicted to have zero unpaired electron density by the simple Hückel approach. However, extended HMO theory introduces electron correlation and forecasts the spin polarization phenomena that are observed.[16,17,29,30]

The large hyperfine splittings observed for protons of methyl groups attached to π systems were not accommodated by the spin polarization hypothesis alone. Accordingly a second "hyperconjugative" mechanism was proposed that allowed the unpaired electron in the carbon $2p_z$ orbital to couple directly with one of the electrons in the β-C—H

---

* Hyperfine splittings in this dissertation are reported in Gauss (G), common practice in North America. More strictly, splittings are reported in millitesla (mT) derived from the SI unit of magnetic flux density, the Tesla (10G = 1 mT). Note that Gauss is the cgs unit of magnetic induction and the use of the cgs magnetic intensity unit, the Oersted (Oe), would be more correct and is occasionally used.[21] For the purposes of the ESR experiment 1 G = 1 Oe. In the Physics literature hyperfine interaction is usually reported in MHz ($a_{MHz} \simeq 2.80\ a_{gauss}$).

σ bond, leaving the other with a small component of positive spin density.[17] Note that a valid linear combination of the atomic orbitals of the three hydrogens and the carbon of the methyl group can be generated to provide a molecular orbital of appropriate π symmetry. Such hyperconjugation may be visualized as a partial contribution to the radical structure from a no-bond resonance representation such as that in Figure 2(b).

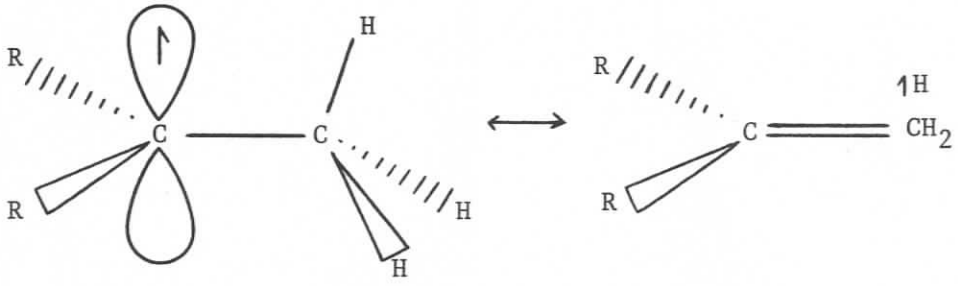

(a) (b)

FIGURE 2: Hyperconjugation.

Coplanarity of C_β, H_β and the axis of the $2p_z$ orbital at the radical site is implied. A positive coupling constant is predicted and observed. As well, an angular dependence of the β-proton splitting is anticipated and most often expressed by an equation of the form;[3,31]

$$a_{\beta H}(\theta) = Q_\beta(\theta)\rho_\alpha \qquad (7)$$

where θ is the dihedral angle between the axis of the half-occupied $2p_z$ orbital and the C_β-H bond (Figure 3). The spin density ρ_α is assumed to

be unity and the function $Q_\beta(\theta) = B_o + B \cos^2\theta$. Thus;

$$a_{\beta H} = B_o + B \cos^2\theta \qquad (8)$$

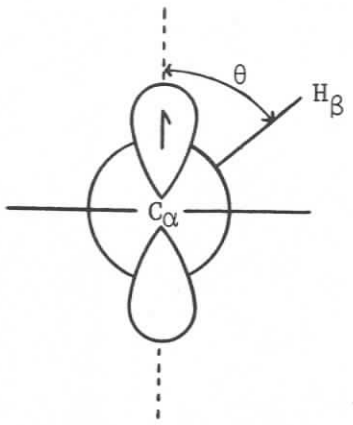

FIGURE 3: Newman projection along C_α-C_β defining the dihedral angle θ.

As a result, the constant B_o, which is independent of the torsional angle θ, can be interpreted as a spin polarization term.[15] Experimentally since $-2 < B_o < 2G$ it is often neglected (i.e. $B_o \longrightarrow 0$).

The validity of the hyperconjugation mechanism has been questioned. For example, the H_β hfs interaction can be interpreted in terms of a spin polarization mechanism provided the same angular dependence is adopted (see refs. 15, 32 and references therein). The relative contributions to a_β by the two mechanisms remains a matter of discussion. Indeed the distinction between them has not always been made clear. For this reason King[29] has argued, following Luz,[33] against the use of the term hyperconjugation, preferring instead to speak of *spin delocalization*. This controversy notwithstanding, Equation 8 appears to maintain[34] its empirical usefulness in discussions of the conformation about the

C_α-C_β bond in organic radicals, and will be adopted in later discussion in this dissertation. It also seems appropriate to use the terms *spin polarization* (which does not involve transfer of electron density) and *spin delocalization* (which does involve fractional migration of electron density) throughout the remainder of this work.

While rotation about C_α-C_β will clearly affect the (average) magnitude of $a_{\beta H}$, it is important to note that other specific electronic effects of β-heteroatoms (and β-substituents bearing heteroatoms) have been identified. In particular, the p_z orbital of an oxygen atom (N.B.: the oxygen lone pairs are not equivalent[35,36]) adjacent to the radical center is expected to have significant positive spin density when its axis is parallel to that of the p_z orbital at the radical center (Figure 4). This induces a negative spin density at the hydrogen nucleus in the

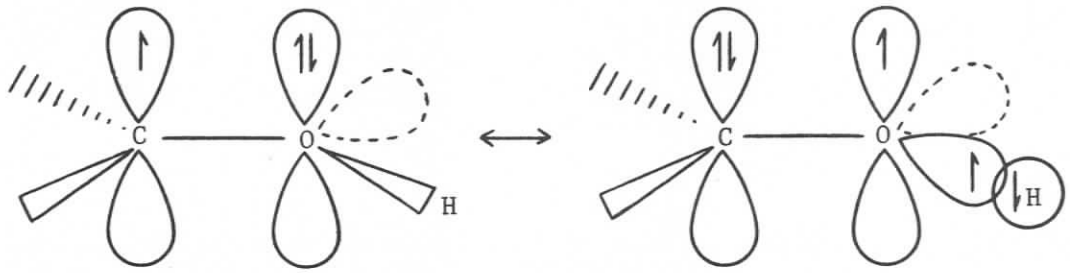

(a) (b)

FIGURE 4: Conjugative spin delocalization to oxygen.

case of a hydroxyl group, resulting in a negative hfs (a_{OH}) which is at a maximum (magnitude) when the proton is in the nodal plane of the π

system.[37] When the proton is in the plane of the axis of the carbon $2p_z$ orbital and the oxygen atom ($\theta = 0$) however, the spin delocalization mechanism is active (cf. Figure 2) and the hyperfine splitting (a_{OH}) is expected to be positive.

Hyperfine splitting arising from remote centers, specifically H_γ, H_δ, and H_ε can be extrapolated from the foregoing discussion. Long range proton hyperfine coupling has been reviewed by Gilbert[14] and in detail by King.[29] The same two mechanisms discussed above are still considered to be operative. In cases where more than one bond intervenes the spin polarization contribution may be assigned to any of three different processes. These have been defined as: (1) a direct (i.e. through space) polarization of the electrons of the C-H bond (Figure 5(a)), (2) a mixed direct-indirect polarization (Figure 5(b)), and (3) a purely indirect (through-bond) mechanism of successive polarizations analogous to Figure 1.

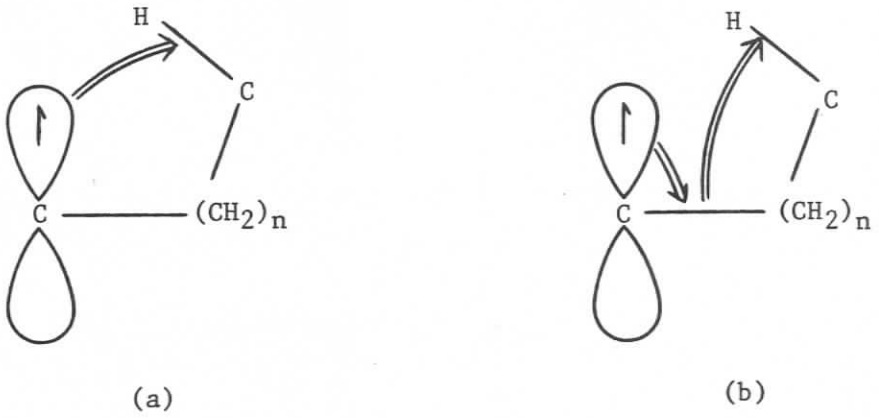

FIGURE 5: Long range spin polarization mechanisms (a) direct, (b) mixed direct-indirect.

Contributions of this last type are expected to be of little significance at nuclei more than one bond removed from the radical center. Direct contributions, on the other hand, do not depend on the size of n nor on dihedral angles in the intervening framework, but they do rely heavily on favourable stereochemistry. The direct polarization contribution to hyperfine splitting from the fragment in Figure 6(a), for example, would be negligible, while the conformation in Figure 6(b) would allow a more significant interaction. Mixed direct-indirect

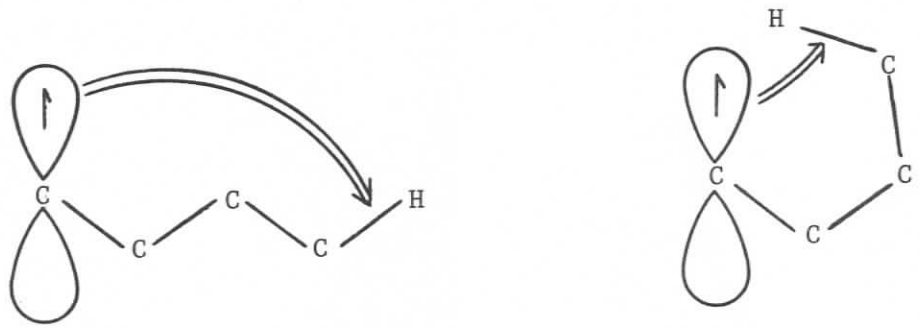

(a) (b)

FIGURE 6: Stereochemical dependence of direct spin polarization.

contributions, of which several may exist depending on n, are expected to have only a small overall contribution, even in geometrically favourable cases. Clearly, then, as a mechanism of transfer of spin density in long range hyperfine splitting, spin polarization will be a minor factor and significant only in cases of highly favourable stereochemistry.

Spin delocalization can contribute to long range interactions in two ways.[29] First, electron delocalization can occur within the bonding framework, an indirect process (cf. Figure 4, but repeated to more distant centers). The second involves delocalization directly between *non-bonded* atoms. This can be visualized as a partial contribution to the radical structure from a configuration such as that shown in Figure 7(b). (This has been called homohyperconjugation.) These *spin delocalization* processes also depend completely on favourable geometry.

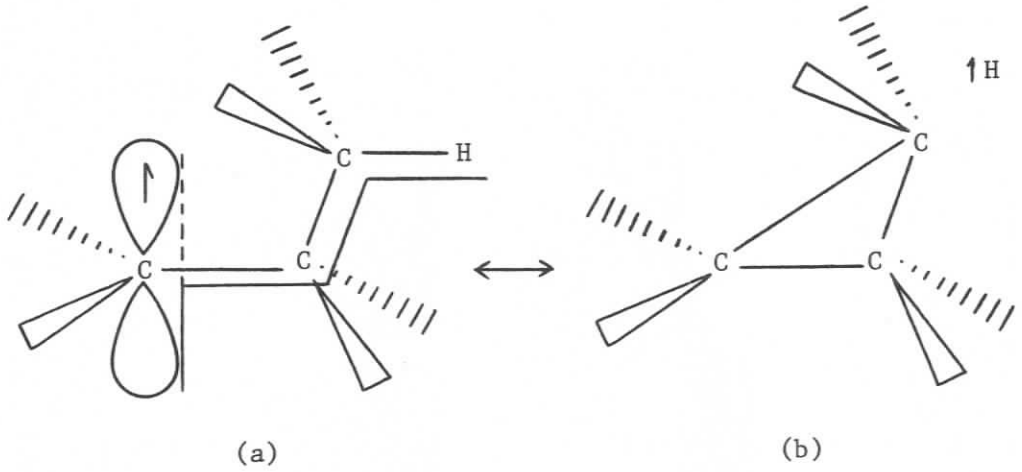

(a) (b)

FIGURE 7: Direct spin delocalization showing W-plan arrangement of bonds.

A variety of radicals exhibiting significant long range hyperfine splittings has been studied. Typically these have rigid or semi-rigid cyclic or polycyclic frameworks of known geometry that predispose the molecular orbitals to the operation of one or both of the above mentioned effects.[29] Indeed, amazingly large splittings have been reported, even for δ and ε protons. For example, Smith et al.[38] have assigned a

coupling of 1.04 G to the terminal methyl protons of the radical in Figure 8, which suggests to them conformation shown.

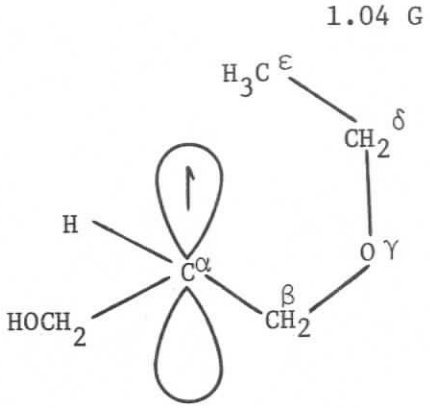

FIGURE 8: Long-range hfs in an open-chain structure.

It is recognized that the ether linkage provides an enhanced opportunity to observe long range coupling.[29] Both through-bond and through-space interactions have been invoked to explain the extremely large splitting (+22.49 G) assigned for the bridgehead C-4 proton (γ) in the bicyclo-[2,2,1]hexan-2-yl radical[39,14e] (Figure 9).

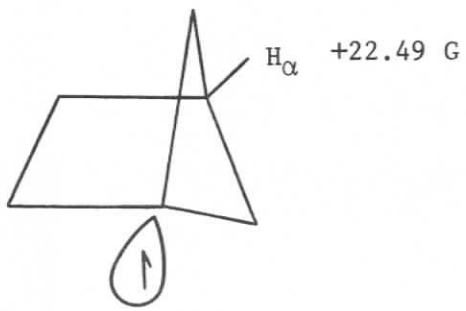

FIGURE 9: Exceptionally large $a_{\gamma H}$ in a rigid bicyclic system.

More data are required to establish a reliable theoretical and empirical basis for predicting long range splittings in most cases. Assignment of splittings in complex molecules can be difficult. Since the sign of the splittings is frequently not known it is difficult to assess the relative importance of spin polarization and spin delocalization contributions. Also it is not always clear what geometrical changes occur in going to the radical. Moreover, geminal H_γ splittings can be *opposite* in sign. These are observed in "frozen" conformations but then average to a low observed value at higher temperature[40] (see also Chapter IV). Such a phenomenon can clearly affect assignments when low temperature limit spectra are not available. Moreover, bulky or highly electronegative substituents can lead to electronic effects that distort predictions based on the behaviour of the parent radicals.

The most useful "rule of thumb" for prediction of large long range splittings is the W-plan concept (Russell et al.[41,29]). A periplanar zigzag arrangement of remote bonds with respect to the $2p_z$ orbital at the radical center (Figure 7) maximizes splitting by the terminal nucleus. It should be pointed out that the simple intuitive spin delocalization mechanism illustrated in Figure 7 does not explain why this arrangement should be more favourable for long range splitting than the anti-W arrangement (Figure 10). However, both calculations by Ellinger et al.[32,42] and experimental observations[29] are consistent with low anti-W-plan splittings. A clearer understanding of the relative contributions to hyperfine splitting of spin polarization and spin delocalization in simple alkyl radicals has been provided by the non-

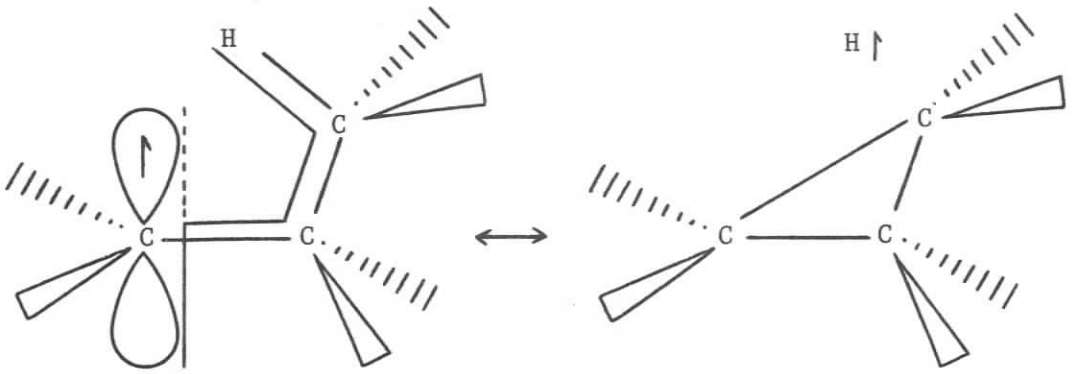

(a) (b)

FIGURE 10: Anti-W-plan arrangement of bonds—unfavourable for significant long-range hfs.

empirical calculations of Ellinger et al.[32,42] (see Chapters III and IV).

(c) Second Order Splittings

For free radicals in solution second order splittings arise from non-degeneracies in the hyperfine energy levels which result when the total spin angular momentum of a group of several equivalent nuclei is taken into account. Details of the theory have been presented by Fessenden[43] and by de Boer and Mackor,[44] and some aspects are discussed by Ayscough.[19] In most cases the second order splitting of lines that are degenerate in the first order treatment is smaller than the observed linewidth and remains unresolved. Three conditions contribute to observation of second order splittings: (1) narrow linewidths ($\leqslant$ 0.2 G); (2) relatively large groups of equivalent protons; and (3) large hyperfine splittings ($\geqslant$ 10 G).[19] In favourable instances some of the first order lines appear as resolved multiplets. These multiplets are not

centered on their first order positions but are "shaded" toward lower field. Also the second order pattern for each first order line (having a different $|M_I|$) is different.

It is important to recognize the presence of second order splittings for the interpretation of some spectra. Even more critical in the present work, incompletely resolved second order splittings cause an apparent increase in observed linewidth and an asymmetry in lineshape. Thus an apparent decrease in line intensity (based on "peak height") is encountered. While second order splittings provide no additional information the patterns can serve to confirm the assignment of a complex first order spectrum.

Some of the radicals reported in this dissertation show second order effects. In these cases confirmation of assignment has been undertaken by computer simulation (see Chapter II, 2) and by comparison with the predictions of theory.[43,44]

2. RADICAL CONFIGURATION

(a) Introduction

In the ensuing discussion a distinction is made[3] between configuration and conformation. Conformation refers to the geometry of a radical as defined by dihedral angles of rotation about single bonds (see earlier comments in section 1(b)). In this section configuration means the detailed arrangement of the atoms attached to the radical center, e.g. whether the radical is planar, tetrahedral, or intermediate between these extremes. Non-planar radical centers are referred to as being "bent."

Throughout the treatment of mechanisms of nuclear hyperfine coupling in section 1(b) it was assumed that the radical center was adequately described by sp^2 hybridized orbitals on the carbon atom. In many cases, though, deviations from planarity dramatically affect the hyperfine splittings of α and β nuclei. Kochi has presented a detailed review[3] (see also ref. 14).

(b) Radicals as Vibrating Species

Since radicals have out-of-plane vibrational modes[14e,45] the designation "bent" is simplistic (Figure 11). Accordingly, "planar" radicals have a vibrational potential function with a minimum at $\phi = 0$.

FIGURE 11: Radicals are vibrating species.

Here we define ϕ as the angle between the nodal plane of the semi-occupied p_z orbital and the bond joining the radical center to an α substituent. A non-planar radical has a vibrational potential function with a symmetric double minimum in a bent configuration with an energy barrier for inversion.[46] Given that α and β hyperfine splitting

constants are a function of the degree of bending (ϕ) their magnitude and temperature dependence for a particular species must rely on the amplitude of the vibration, the height of the inversion barrier, and the number of vibronic states below that barrier. Accurate analysis of the vibronic wave function of a free radical is difficult at best and impossible in complex cases. Thus most discussions of hyperfine splittings as a function of temperature neglect the effect of vibrational averaging.[3] In summary the terms planar and bent must necessarily remain an approximate description of radical configuration.

To supplement information on bending derived from $a_{\alpha H}$ other relevant data such as; (1) ^{13}C hfs at the radical center, (2) the effects of isotopic substitution, (3) molecular orbital calculations, and (4) comparison with other radicals may be used.

(c) Factors that Affect Configuration

(i) General Survey

The ϕ dependence of hyperfine splittings arises ultimately because bending translates as a change in orbital hybridization at the radical center. Such a change alters the relative importance of the spin polarization and spin delocalization mechanisms of hyperfine coupling.

What factors, then, cause these changes in hybridization? Two determinants are invoked by Norman et al.[27] and supported in part by others (cf. Ingold[34]). They are; (1) geometrical constraints within the radical, and (2) conjugatively electron releasing substituents. A proposal[47,48] that α configuration for acyclic species is determined by substituent electronegativity alone seems inadequate (*vide infra*)(but

see ref. 49). An alternative molecular orbital explanation by Bingham and Dewar[50] involves the destabilization of the planar geometry due to antibonding interactions with the substituents. However, this approach has been criticized by Bernardi et al.,[49] whose calculations indicate that electronegativity and π conjugation are the active factors, with electronegativity being dominant. Gregory et al.[51] have pointed out that in some cases the electronegativity and π conjugation effects oppose each other.

Consideration of actual physical data in the context of the two factors suggested by Norman et al.[27] allows an empirically useful picture of bending to emerge.

In the most elementary example of the methyl radical the vibrational potential minimum occurs at the planar configuration (a_H = 23.04 G). Calculated values of a_H and $a_{^{13}C}$ for methyl radical as a function of ϕ are shown in Table 1.[3]

TABLE 1: INDO calculations of the angular dependence of H_α and ^{13}C coupling constants for methyl radical[3]

	ϕ	$a_{\alpha H}$ (G)	$a_{^{13}C}$ (G)
	0°	-22.96	46.0
	5°	-21.18	54.7
	10°	-16.85	77.46
	15°	-12.26	108.03
(tetrahedral)	19.5°	- 8.99	138.57
Experimental		22.83 (-20°C) 23.04 (-177°C)	38.34 (-177°C)

As bending increases, the s-character of the semi-occupied orbital increases causing increasing positive spin density at the carbon nucleus and a concomitant increase in through-bond induction of positive spin density to the hydrogen nucleus. Thus a_H decreases in magnitude while becoming more positive. Replacement of one or two hydrogens by methyl groups causes little deviation from planarity as evidenced by $a_{\alpha H}$ for ethyl radical (-22.38 G) and isopropyl radical (-22.11 G). There has been some controversy about the configuration of the *t*-butyl radical (ref. 14, 52 and references therein) centering on evident lack of agreement on the shape of its vibrational potential function. More recent results firmly conclude that the radical is undergoing rapid inversion with a small energy barrier[53,14f] (see also ref. 54).

(ii) Structure

Structural constraints within a species can force non-planarity at the radical center. Thus while most large alicyclic radicals, cycloheptyl ($a_{\alpha H}$ = 21.78 G), cyclohexyl (21.3 G), cyclopentyl (21.48 G), and cyclobutyl (21.2 G), may be judged essentially planar, cyclopropyl radical provides an example in which the significant bending created by ring strain leads to $a_{\alpha H}$ = -6.66 G. An intermediate degree of bending is observed for the 2-bicyclobutyl radical (1). In this case the very

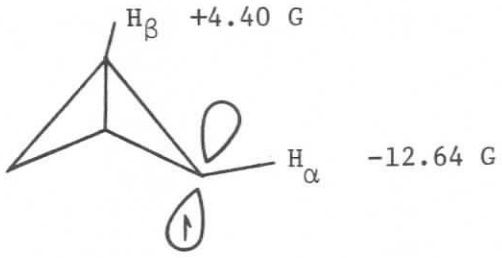

1

low value of $a_{\beta H}$ would indicate that these protons lie close to the nodal plane of the half-occupied p_z orbital if a conventional $\cos^2\theta$ relationship is operative.

Non-planarity is also observed in the 7-norbornenyl radical (2) where the original authors[55] suggested that $a_{\alpha H}$ was positive in sign. This assignment has been questioned by Kawamura[56] and by Ingold et al.[46]

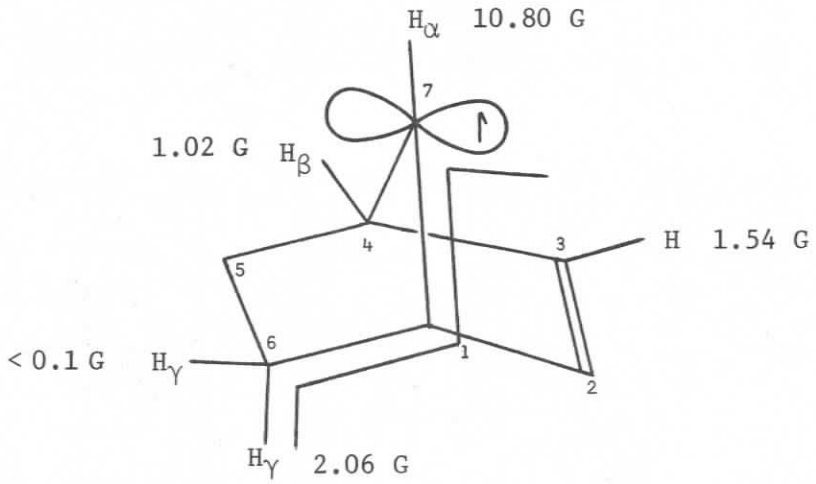

2

Nonetheless it is clear that there is significant bending. Again a low value of $a_{\beta H}$ (1.02 G) is observed. Note as well the relatively large value of $a_{\gamma H}$ (2.06 G) for the 5 and 6 *endo* protons which conform to the favourable W plan for long range splittings.

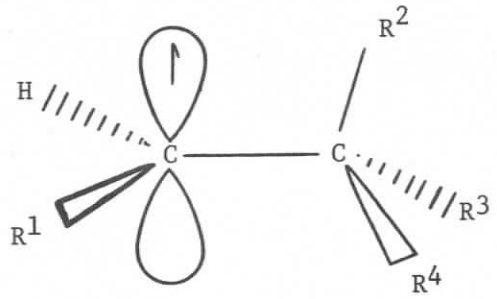

3

In some acyclic radicals (3) steric factors may also influence configuration if substituents R^1-R^4 are sufficiently bulky. Such deformations will be distinct phenomena but closely related to conformational preferences (rotation about C_α-C_β) which also attempt to minimize steric interactions.[3,57] Few studies appear to have focused directly on this aspect and some relevant examples in the present work will be discussed further in Chapter V.

(iii) Conjugatively Electron Releasing Substituents and Electronegativity

The effects of conjugatively electron releasing substituents on radical configuration are no less significant than those of geometrical constraint. Successive replacement of hydrogen by fluorine in methyl radical causes a large change in the hyperfine splittings[3,58] (Table 2).

TABLE 2: Hyperfine splittings for fluoromethyl and fluoroethyl radicals (G)

Radical	$a_{\alpha H}$	$a_{\alpha F}$	$a_{\alpha}{}^{13}C$	$a_{\beta H}$	$\phi°$
$\cdot CH_3$	-23.0	-	38.5	-	0
$\cdot CH_2F$	-21.1	+64.3	54.8	-	5
$\cdot CHF_2$	+22.2	+84.2	148.8	-	12.7
$\cdot CF_3$	-	+142.4	271.6	-	17.8
free electron in pure 2s orbital			1190.		
$\cdot CH_2CH_3$	-22.38	-	-	+26.87	-
$\cdot CHFCH_3$	-17.31	+59.21	-	+24.48	-
$\cdot CF_2CH_3$	-	+94.01	-	+13.99	-

The configuration of trifluoromethyl radical is nearly tetrahedral (for sp^3 hybridization $\phi = 19.5°$) and has a corresponding large barrier to inversion (calculated 27 Kcal/mol). Such changes in $a_{\alpha H}$ are expected for a highly electronegative substituent in $\cdot CH_2X$. The p-character of the C-X bond in a X-$\dot{C}$-H fragment should be increased,[27,47] creating an increase in the s-character of the unfilled orbital. This effect in molecules has been discussed by Bent.[59,60] The large negative value of $a_{\alpha H}$ would be thereby diminished in magnitude. However, the further large change in $a_{\alpha H}$ upon introduction of a second electronegative substituent ($\cdot CF_2H$, Table 2) would not be predicted from electronegativity considerations alone. Finally, the highly electronegative ammonia substituent does not induce bending in $\cdot CH_2\text{-}\overset{\oplus}{N}H_3$ for which $a_{\alpha H} = -25$ G (see ref. 27).

In summary, conjugative electron delocalization must also be postulated as a significant source of bending. A contribution to the overall structure of the type shown (4b) would tend to increase electron density at C_α and initiate bending toward a tetrahedral geometry to relieve electron-electron repulsion.[27,61] One might expect this dona-

$$\dot{C}H_2 - \ddot{X} \longleftrightarrow \ddot{C}H_2 - \dot{X}^{\oplus}$$

4a 4b

tion to be enhanced for oxygen, which is less electronegative than fluorine. However, reduction in bending from the electronegativity factor (inductive effect) for oxygen may work in the opposite direction and lead to a similar net degree of bending for the two heteroatoms.

TABLE 3: hfs for some oxygen substituted acyclic alkyl radicals

Radical	$a_{\alpha H}$ G	$a_{\beta H}$ G	$\lvert a_{\beta Me}/a_{\alpha H}\rvert$	Temp. °C	Ref.
$\cdot CH_2OH$	-17.38	-	-	26	25
$\cdot CH_2OCH_3$	-17.24	-	-		62
$\cdot CH_2OCH_2CH_3$	-16.8	-	-	RT	61
$\cdot CH_2OC(CH_3)_3$	-17.3	-	-	-107	63,64
$CH_3\dot{C}HOH$	-15.37	+22.19	1.44	26	25
	-15.0	+22.4	1.49		61
$CH_3CH_2\dot{C}HOH$	-15.06	+21.40	-	26	25
$CH_3(CH_2)_2\dot{C}HOH$	-15.3	+20.0	-	29	25
$CH_3\dot{C}HOCH_3$	-13.7	+22.0	1.60		61
$CH_3\dot{C}HOCH_2CH_3$	-14.1	+21.8	1.55	-40	62
	-13.96	+22.28	1.60		61
$CH_3CH_2\dot{C}HO(CH_2)_2CH_3$	-13.91	+20.83	-	-40	62
$CH_3(CH_2)_2\dot{C}HO(CH_2)_3CH_3$	-14.21	+18.85	-	-40	62
$CH_3O\dot{C}HOCH_3$	+12.12	-	-		65,61,27
$(CH_3)_3CO\dot{C}HOC(CH_3)_3$	11.1	sign assigned -ve in ref. 66			66
$HO\dot{C}HOH$	+12.3	a_{OH}=3.5			67
	+12.75	a_{OH}=3.10		15	68

(d) Configuration in Oxygen Substituted Radicals

Table 3 shows some hyperfine splittings for oxygen substituted acyclic alkyl radicals. All the information for the hydroxymethyl radical suggests a nearly planar species[3] ($a_{\alpha H}$ = -17.38) and $a_{\alpha H}$ gives no indication that this situation differs for $\cdot CH_2OCH_3$. Higher homologues in both the alcohol and ether-derived series do have H_α hfs that indicate

more pronounced bending. However, the decrease in $|a_{\alpha H}|$ on going from $\cdot CH_2OH$ to $CH_3\dot{C}HOH$ is also consistent with some delocalization of spin to the methyl group (*vide infra*). Therefore Norman et al.[61] have argued that, for alkyl radicals having a methyl and an electronegative substituent, the ratio $|a_{\beta Me}/a_{\alpha H}|$ is a better indicator of bending than just $a_{\alpha H}$ alone. The ratio increases with bending. ($a_{\beta H}$ is decreased by bending, *vide infra*.) While such a correlation was apt for the range of radicals reported,[61] it is of limited applicability in the present work since α-Me is present in only a few cases (Table 3). It is interesting that while $\cdot CH_2OC(CH_3)_3$ appears planar (considering $a_{\alpha H}$ only, cf. $\cdot CH_2OH$), the radical $\cdot CH_2OCH_2CH_3$ would appear to be slightly bent. It is tempting to infer a slight steric flattening at the radical center in the former case. However, rotational disruption of the conjugation interaction with oxygen might well have the same effect and such a conclusion must be drawn with caution.

Note the effect of introducing a second oxygen substituent. The radical $CH_3O\dot{C}HOCH_3$ has an H_α hfs indicative of severe bending. The alicyclic ether radicals (Figure 12) confirm the increase in bending with increasing substitution of oxygen for carbon and illustrate additional increases caused by geometrical constraint. The large value of $|a_{\alpha H}|$ for radical (6) relative to that for (5) cannot be attributed to ring strain. It has been proposed that conjugative electron delocalization is enhanced in (6) by the much smaller dihedral angles between the oxygen p-type lone pair and the semi-occupied $2p_z$ orbital on carbon[27,46] giving $a_{\alpha H}$ in species (6) a higher positive value due to "back hyper-

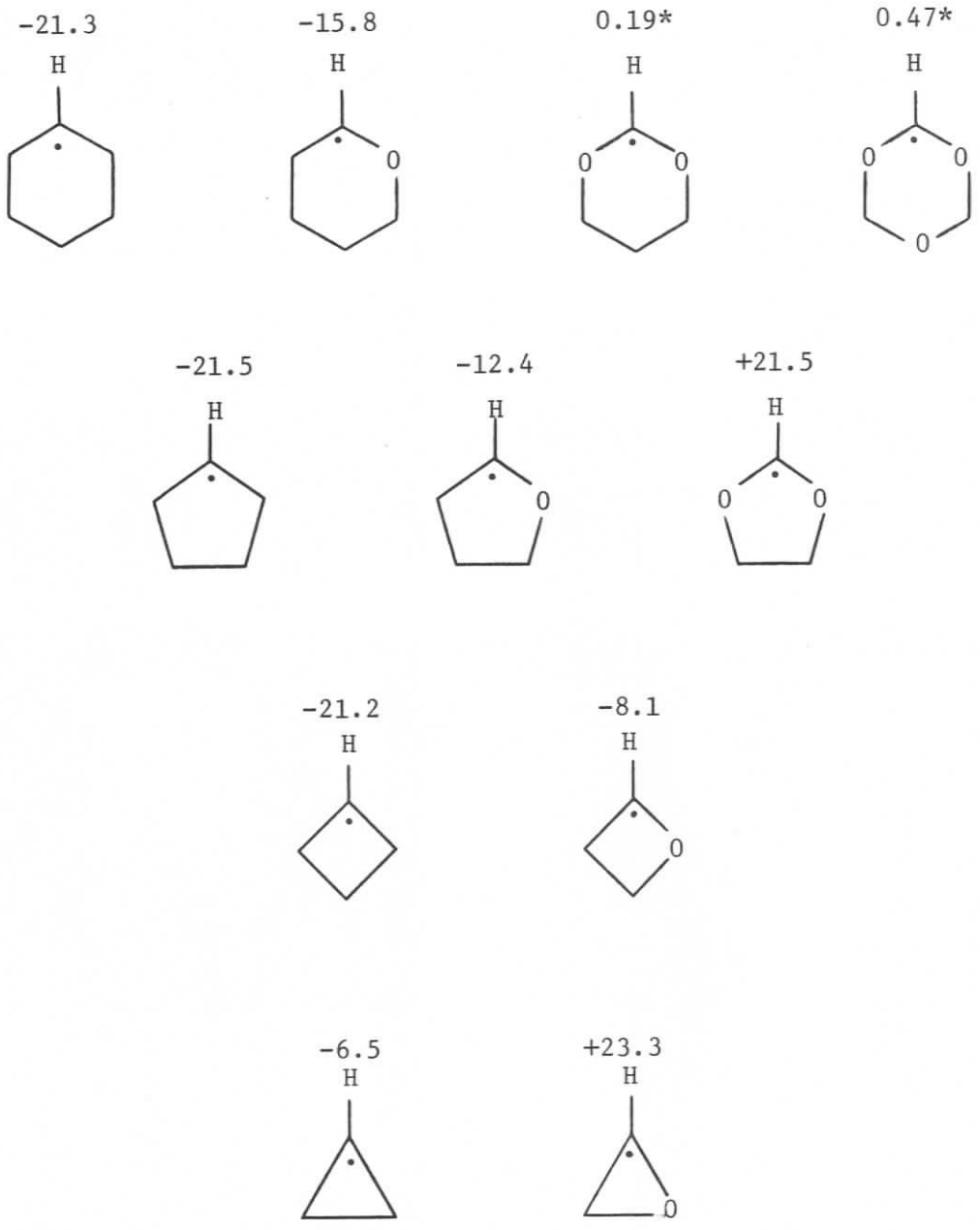

FIGURE 12: $a_{\alpha H}$ for some alicyclic radicals[27] (see also ref. 69).

*sign undetermined

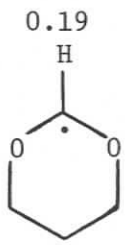

5

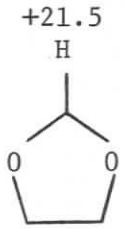

6

conjugation."[46] Ingold et al.[70] have reported that the 2-methoxy-1,3-dioxolan-2-yl radical (7) is pyramidal with a high inversion barrier ($\geqslant$10 Kcal/mol).

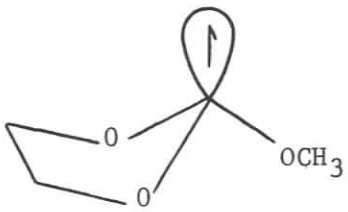

7

Radical species bearing several α-oxygen substituents reveal the effects of bending at C_α on β-proton splittings, though clearly the changes observed are much less pronounced than for $a_{\alpha H}$.[27] Precise correlations are largely restricted to the simplest cases of an α-methyl group in free rotation. The spin delocalization mechanism (conjugatively electron releasing substituent) which gives rise to the major component of H_β hfs (see Section 1, Figure 2) is disfavoured by non-planarity (Figure 13).[3] In part hindered rotation[65,71] of the methyl group may result in an average dihedral angle less favourable for interaction.

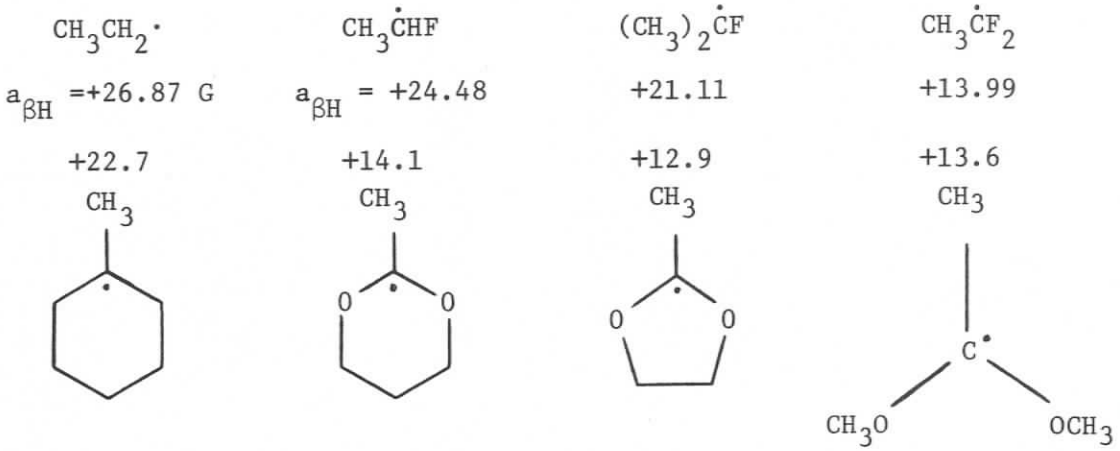

FIGURE 13: β-methyl hfs dependence on bending.

In the less extreme cases a methyl substituent may be thought of as contributing weakly to bending.

Conversely a conjugatively electron withdrawing α substituent (e.g. ——CF_3) should decrease bending in favourable cases. Compare $a_{\alpha H}$ in the series $\cdot CH_2OH$ (-17.4), $CH_3\dot{C}HOH$ (-15.4), and $CF_3\dot{C}HOH$ (-18.16).[3] The flattening effect in the last species is consistent with an overall structure represented by the contributors (8a,b,c).[27]

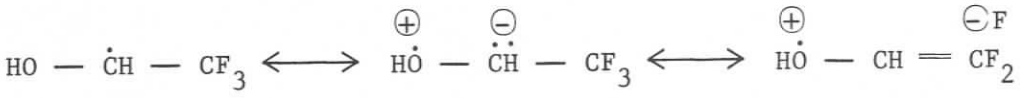

8a 8b 8c

One further consideration should be noted. An increase in the (reduced) mass of the substituents at a radical center will in general

diminish the average amplitude of vibration and hence increase the observed value of $|a_{\alpha H}|$. The effect of altering the mass of a substituent can be considered in detail only in the simplest of cases (e.g. $\cdot C^2H_3$).[3]

In summary it is clearly evident that the factors determining α-bending (conjugatively electron releasing substituents, structural constraints, and electronegativity) provide only a qualitative (semi-quantitative) understanding of the recorded parameters. Since these diverse effects can operate in a cooperative and occasionally opposing fashion it is not surprising that considerable controversy exists in the literature. Accordingly the above presentation has been restricted to a description of the often opposing hypotheses. The present work was not designed to reconcile the conflicting views of various authors (e.g. Krusic and Kingham[72] and Chen and Koch[73]; Griese and Beckhaus[74]; also Bingham and Dewar[50] and Bernardi et al.[49]). It will be appropriate to comment later on the applicability of the several mechanisms of bending in the present work. Obviously it is important to exercise caution when using $a_{\alpha H}$ as a monitor of bending.

(e) Solvent Effects

As pointed out by Ayscough[15] the solvent may have significant effects on the ESR spectra of radicals in solution. The possible broadening of lines due to anisotropy in the g-factor or hfs when Brownian tumbling is slowed in solvents of high viscosity (i.e. usually at low temperatures) has been mentioned (see Section 1). Consideration of relaxation broadening is deferred to the next section.

Solvent molecules may have a discrete organization in the first and subsequent solvation spheres of the solute radical which can lead to special effects in the observed spectrum. Solvation effects are most pronounced for radical ions. Redistribution of spin to the counter-ion is one potentially important interaction for such species. Uncharged organic radicals in organic solvents are typically much less perturbed by their environment. However, in the present context it is important to recognize both hydrogen bonding and the potential for proton exchange between alcohol-derived radicals and solvent in protic (usually aqueous) solutions. Hyperfine splitting due to hydroxyl protons can nevertheless be observed for alcohol radicals in the neutral conditions of the neat alcohol[25] or non-polar solvent (e.g. cyclopropane; this dissertation). In aqueous solution proton exchange is pH dependent. Using an aqueous flow system Fischer[75] showed that a_{OH} for $\cdot CH_2OH$ is observed at pH = 1.40 but not at pH = 1.03 due to rapid exchange. (*Intramolecular* exchange phenomena are discussed in Chapter III.) In Shiga's early work[76] ESR spectra of α-hydroxyalkyl radicals in aqueous acid medium showed no a_{OH}. Stone and Maki[77] have commented on the differences in ESR parameters for a series of semiquinones in protic and aprotic solvents. Loth and Graf[78] have recently reported intra and intermolecular hydrogen bonding and proton exchange studies for hydroxylic radicals in various solvents.

In the case of radicals in the ether series, hydrogen bonding effects seem minimal. Lucken and Poncioni[79] have reported ESR parameters for α-alkoxy radicals previously studied by Norman et al.[27] Although

their substrates were dissolved in di-*t*-butyl peroxide (1:1, no other solvent) the hfs did not differ significantly (± 0.2 G) from those recorded in flow experiments (Norman et al.[27]) employing aqueous solutions containing Ti^{+3} and H_2O_2. The precision of the measurement (± 0.1 G[27]) suggests that the two sets of results are virtually identical. Moreover, later results[40,71] for the same ether substrate dissolved in di-*t*-butyl peroxide and cyclopropane are closely similar. (See also Chapter IV.)

Griller[80] has pointed out that the tacit assumption that ESR experiments are carried out at constant volume is incorrect. Solvents, in general, contract on cooling. In a series of constant temperature experiments at varying high pressures he demonstrated that, in three different solvents (cyclopentane, acetone, ethanol) the change in nitrogen hfs for di-*t*-butyl nitroxide radical was almost completely due to the change in volume of the solvent. He did not speculate as to the mechanism causing the change in a_N.

In this dissertation, and in many other published works, significant changes in hyperfine splitting as a function of temperature are attributed to intramolecular processes (e.g. rotation about a single bond). If the free radicals could be observed in the absence of a solvent they would have barriers to rotation or inversion that were somewhat lower than those measured in solution. The anticipated changes in hfs (linewidth effects) might not then occur within a readily accessible temperature range. Clearly then the ESR parameters related to intramolecular dynamic processes which are measured as a function of

temperature for radicals in solution retain their validity in the context of most solution chemistry, which is also carried out at constant pressure, though often at low temperatures.

The assumption is made in this work that the solvent (usually cyclopropane) is not involved other than through Van Der Waals' contact with the radicals, and that the observed radicals have no interactions with the remaining substrate or initiator.

3. ESR LINEWIDTHS

This section briefly outlines the most important mechanisms which can contribute to line broadening in ESR spectra.[17,15,10] In each case the likelihood of importance in the present research is indicated. Where appropriate, references to other sections of this dissertation are provided.

It is useful initially to list for reference the mechanisms to be considered, which can be divided into two broad categories, *viz.*

(a) Inhomogeneous broadening

  (i) Inhomogeneous applied magnetic field

  (ii) Anisotropic interactions in the g-factor and in hfs, slow molecular tumbling

  (iii) Unresolved hfs

(b) Homogeneous broadening

  (i) Spin-lattice relaxation including power saturation

  (ii) Electron spin-electron spin dipolar interaction

  (iii) Electron spin-nuclear spin dipolar interaction

(iv) Chemical processes

1. Electron spin exchange
2. Electron transfer
3. Proton exchange

(v) Spin rotation interaction

(vi) Time-dependent hfs.

Inhomogeneous broadening refers to situations in which the unpaired electron in each of several free radicals is subjected to a slightly different magnetic field on a static or time-averaged basis.

It is assumed that, using a modern spectrometer and accessories, the applied field throughout its sweep is sufficiently homogeneous not to be a significant cause of line broadening.

In Section 1 of this chapter it was pointed out that in sufficiently non-viscous solutions the anisotropies in the g-factor and hfs are averaged to zero by rapid Brownian tumbling of the radicals. This condition does not hold when solutions become more viscous, usually because of decreasing temperature. The result, in general, is an asymmetric broadening of lines which will be different for each line of the spectrum. This "viscosity broadening" will be mentioned in later chapters.

Large linewidths are in some cases attributed to unresolved hyperfine splittings. These may be long range hfs (e.g. H_γ, H_δ) or second-order splittings (*vide supra* Section 1(c)).

Homogeneous line broadening refers to cases in which the static plus time averaged magnetic fields are the same at each unpaired electron

but the instantaneous magnetic field is not. It is usually characterized by the relaxation time T_2 which is inversely proportional to the observed spectral linewidth.

Spin lattice relaxation refers to an unpaired electron in the higher energy state (in a magnetic field) giving up energy to its surrounding environment, e.g. solvent. The spin lattice relaxation time (T_1) is characteristic of the mean lifetime of a given spin state in the absence of other relaxation mechanisms. If spin lattice relaxation is inefficient (i.e. T_1 is large) then the energy levels rapidly become equally populated and no spectrum is observed. If, on the other hand, spin lattice relaxation is very fast (i.e. T_1 too short) then the uncertainty in its energy (Heisenberg uncertainty principle) can cause extreme line broadening. In non-viscous liquid solutions spin-lattice relaxation usually is not the limiting factor for observing narrow lines. If the applied microwave power is too great the spin-lattice relaxation may fail to be effective. The difference in spin state populations is reduced and transitions occur so quickly that any observed absorption is broadened by the uncertainty in the energy of the spins. Thus for optimal conditions of signal intensity (sensitivity) and resolution it is important that the applied microwave power not be too high. There is, in fact, a relatively narrow range of optimality (see Chapter II, 2).

The field effect of electron spins in mutual proximity while very significant in solids is usually insignificant for radicals in non-viscous solutions. The dipolar interaction of an unpaired electron with a neighbouring nuclear spin (whether in the radical or the solvent) is

averaged to zero in solutions of low viscosity.

For radicals in solution the linewidth limit is most often imposed by electron spin exchange. This refers to a mutual exchange of spin states on collision of two radicals having unpaired electrons of opposite spin and is thus concentration dependent. This relaxation mechanism limits the lifetimes of the spin states without changing the relative populations. It is often the greatest contributor to T_2', the spin-spin relaxation time. The measured relaxation time T_2 (from observed linewidth) is related to spin-lattice and spin-spin relaxation times by Equation 9.

$$\frac{1}{T_2} = \frac{1}{T_2'} + \frac{1}{2T_1} \tag{9}$$

Usually $T_1 \gg T_2'$ so that $T_2 \simeq T_2'$. Since most solutions are magnetically dilute this condition allows one to obtain quite narrow linewidths ($\leqslant 0.1$ G) in the absence of other effects. The Lorentzian character of the line shape is attributed to spin-spin relaxation.

If some chemical process occurring in the sample causes a change in the magnetic environment of the unpaired electron, line broadening can result. If during a bimolecular collision the unpaired electron is transferred to a previously diamagnetic molecule the field position of resonance will generally change. This mechanism is not considered to contribute significantly to observed linewidths in the present research.

Proton exchange was discussed at the end of the previous section in this chapter.

Radicals in the gas phase are free to rotate and this rotation sets up a magnetic moment which, in the presence of an external magnetic

field, is oriented in space. The resultant dipole-dipole interaction is thus not averaged to zero and results in very complicated spectra. In liquids at ambient or lower temperatures oriented molecular rotation is usually quenched (disrupted). Thus this mechanism does not contribute to the observed linewidth.

Time-dependent hfs are often caused by a specific complexing equilibrium or an intramolecular rotation changing the local magnetic environment of the unpaired spin. This phenomenon is, in large measure, the subject of Chapter III and will be dealt with there.

In the absence of significant line broadening mechanisms the amplitude of an absorption peak is directly proportional to the number of radicals giving rise to that absorption (i.e. concentration).

The amplitude of the usual first derivative absorption curve is inversely proportional to the square of the linewidth. Thus peak intensity rather than actual linewidth is more commonly used as an indicator of line broadening.

CHAPTER II

GENERATION OF TRANSIENT ORGANIC FREE RADICALS AND THEIR DETECTION BY ESR SPECTROSCOPY

1. BACKGROUND: CHEMICAL

Perhaps the central problem in studying aliphatic free radicals is their fleeting existence in solution, where decay in their concentration occurs rapidly via dimerization with a bimolecular rate constant of *ca.* 10^9 $\ell mol^{-1}s^{-1}$, the diffusion controlled limit at room temperature.[2,5,81] Consequently, continuous generation of the desired radical is undertaken in order to maintain an acceptable stead-state concentration for study. The electron spin resonance technique has a practical detection limit of *ca.* 10^{-7} M for high resolution work. At required scan times for fully resolved spectra the concentration must be sustained for at least several minutes. If analysis of motional effects, at the standard established for stable aromatic ion radicals, is to be applied to transient radicals such high resolution spectra must be obtained. Recently spectrometers designed to study very fast radical processes have been developed (see, for example, refs. 6 and 13 and references therein), but such experiments do not have the same high resolution requirement.

(a) Radiolytic Radical Generation

The first method used to produce a steady-state concentration of radicals sufficiently high to be studied by ESR was irradiation of liquid hydrocarbons in the spectrometer cavity by an electron beam from

a 2.8 MeV van de Graaff generator. This important work by Fessenden and Schuler[24] virtually laid the foundation for the entire field of ESR studies of transient free radicals in solution. It was particularly significant that high resolution was obtained by working at low temperatures in solvents of low viscosity. Later radiolysis of aqueous solutions was developed by Fessenden and Eiben.[82] While once again high resolution was obtained experiments were naturally restricted to relatively high temperatures. However, the primary products of aqueous radiolysis, e^- and $\cdot OH$, presented a highly successful indirect radical initiation procedure.

The somewhat complex experimental considerations of the electron bombardment technique have been presented by Fessenden and Schuler.[83] This and other radical generation techniques have been reviewed by Fischer[2] and more recently by Norman.[5]

(b) Photolytic Radical Generation

(i) Flowing Solution Methods

A more accessible technique in terms of cost and experimental complexity was pioneered by Livingstone and Zeldes.[25] This involved UV irradiation of dilute alcohol solutions of H_2O_2 as they flowed through the cavity of an ESR spectrometer. Radical generation involved photolytic production of hydroxyl radical (Reaction 1).

$$H_2O_2 \xrightarrow{h\nu} 2HO\cdot \qquad (1)$$

$$RCH_2OH + \cdot OH \longrightarrow R\dot{C}HOH + H_2O \qquad (2)$$

This species subsequently abstracted a hydrogen atom from the alcohol

(Reaction 2) to give the free radical of interest. By flowing the solutions reaction products that would give rise to interfering radicals were removed. At a given flow rate the observed spectrum remained relatively constant and reproducible. In experiments of this type the hydroxyl radical is not observed due to g-factor anisotropy.[84] Later more generally applicable initiators were developed (*vide infra*) and it is now feasible to irradiate flowing solutions of organic molecules in a variety of solvents. For example acetone can be use, and the radical formed on irradiation, acetone triplet, is a suitable species for H-atom abstraction in many cases, obviating the use of dissolved peroxides. Unfortunately abstraction from acetone also occurs, giving a strong spectrum from $\cdot CH_2COCH_3$ which may interfere.

(ii) Static Solution Methods

Ultraviolet irradiation of static solutions offers significant advantages over the flow method. Experiments can be conducted over a wider range of temperatures and only very small quantities of substrate are required. The technique was introduced by Vanderkooi and Fox,[85] Krusic and Kochi,[86,87] and Hudson and Hussain.[88] Krusic and Kochi [86,87] obtained isotropic spectra as low as -140°C, illustrating the suitability of cyclopropane as solvent for a variety of substrates. Spectra of simple saturated alkyl radicals showing alternating linewidth effects (see Chapter III), previously inaccessible, were obtained using this technique.

(iii) Reactions in Photolytic Radical Generation

Griller[81] has classified photolytic reactions used in ESR studies according to whether the radical of interest is formed directly by irradiation of an appropriate molecule (Reaction 3, R' may or may not be a radical)

$$R—R' \xrightarrow{h\nu} R\cdot + R' \qquad (3)$$

$$\text{photolabile molecule} \xrightarrow{h\nu} R\cdot \qquad (4a)$$

$$R\cdot + R' \longrightarrow R'\cdot + R \qquad (4b)$$

or rather in a subsequent radical-molecule reaction (Reaction 4).

In the former category a number of different precursors specific to individual radicals of interest have been used. They share the criterion of homolysis employing accessible ultraviolet photon energies. Such species include diacyl peroxides, peresters, azoalkanes and ketones, among others.[2,5,81] For example, Norrish Type I cleavage of the photo-excited triplet of a ketone (Reaction 5) often occurs, and with a good quantum yield.[2] Photodecarboxylation of diacyl peroxides (Reaction 6) has provided a very efficient and versatile procedure.[2,81]

$$R—\overset{\overset{O}{\|}}{C}—R' \xrightarrow{h\nu} R—\overset{\overset{O}{\|}}{C}\cdot + \cdot R' \qquad (5)$$

$$R—\overset{\overset{O}{\|}}{C}—O—O—\overset{\overset{O}{\|}}{C}—R \xrightarrow{h\nu} 2\ CO_2 + 2R\cdot \qquad (6)$$

In free radical terms the second method actually involves an initiation sequence. Irradiation of a suitable peroxide forms alkoxy or hydroxy radicals which then react with the chosen substrate. In this

respect di-*t*-butyl peroxide has found wide application. It is relatively inert and does not deteriorate on long storage. It has a favourable solubility in a variety of organic solvents, including undiluted substrates, and it has a low freezing point (*ca.* -40°C). Di-*t*-butyl peroxide is cleaved with a quantum efficiency near unity at 253.7 nm (Reaction 7) to give two reactive *t*-butoxy radicals[89] which, conveniently, are not observed by ESR spectroscopy in solution[84] (see Chapter I).

$$(CH_3)_3COOC(CH_3)_3 \xrightarrow{h\nu} 2(CH_3)_3CO\cdot \qquad (7)$$

The reactivity of *t*-butoxy in H-atom abstractions from a wide range of substrates has been reviewed.[2,81]

It the present study H-atom abstraction from a range of alcohols and ethers is involved. Abstraction occurs preferentially from a carbon atom bonded to oxygen although abstraction from the hydroxyl group of alcohols has been observed.[90,91] This preference over abstraction from other carbon centers is due to the stereoelectronic effect of the oxygen atom which lowers the energy of the transition state (9) for the reaction.

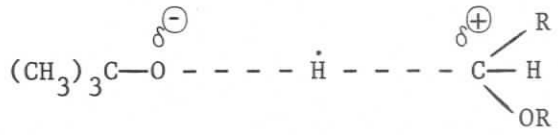

9

The low steady-state concentration of other species is then readily understood. For example, the relative reactivities to $(CH_3)_3CO\cdot$ at -60°C of cyclopentane and tetrahydrofuran are 1.0 and 2.8×10^3 respectively.[34]

Thus photolysis of a solution of di-*t*-butyl peroxide and 1-propanol gives 1-hydroxylprop-1-yl radical (Reaction 8).

$$(CH_3)_3CO\cdot + CH_3CH_2CH_2OH \longrightarrow CH_3CH_2\dot{C}HOH + (CH_3)_3COH \qquad (8)$$

When the substrate is 2-methyl-1,3-dioxane (10) abstraction is preferentially from the carbon bonded to two oxygen atoms resulting in the 2-yl radical (11), but the 4-yl radical (12) is also observed in significant concentration.[92] However, it should be noted that the relative

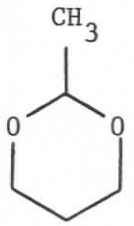

10

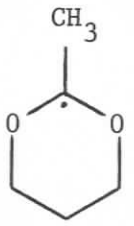

11

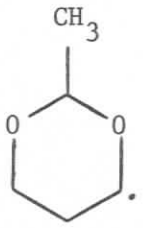

12

rates of abstraction can vary widely with structure, particularly for cyclic ethers where oxygen lone pairs have a discrete conformational relationship to the incipient radical.[34,70,93] For example, hydrogen abstraction from the 2-position of tetrahydrofuran by $(CH_3)_3CO\cdot$ is facile. In this case the p-type lone pair on oxygen makes an angle of 30° with the abstracted hydrogen.[34] In contrast, hydrogen abstraction from the bridgehead is not observed in the case of the bicyclic ether (13) for which the angle in question is 90°.[34]

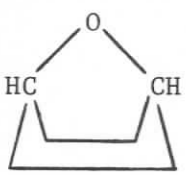

13

(c) Chemical Radical Generation

Another method of free radical production involves an aqueous flow system in which a steady-state concentration is generated by a chemical reaction. The technique was introduced by Piette et al.,[94] Saito and Bielski,[95] and Dixon and Norman.[96,97] The reactions employed have been reviewed by Norman[5] and Fischer.[2]

Such systems usually utilize a redox process involving metal ions. Many are based on the Fenton reaction (Reaction 9). Other examples are shown in Reactions 10 and 11. In the case of Reactions 9 and 11 the

$$Fe^{+2} + H_2O_2 \longrightarrow Fe^{+3} + {}^{\cdot}OH + OH^- \quad (9)$$

$$Ce^{+4} + RCHO \longrightarrow R\dot{C}O + Ce^{+3} + H^+ \quad (10)$$

$$Ti^{+3} + H_2O_2 \longrightarrow Ti^{+4} + {}^{\cdot}OH + OH^- \quad (11)$$

initially formed radical rapidly reacts with organic molecules present to form the species of interest, most often by simple H-atom abstraction (e.g. Reaction 12).

$$\cdot OH + RH \longrightarrow H_2O + R\cdot \quad (12)$$

The Ti^{+3}/H_2O_2 system, first introduced by Dixon and Norman,[96,97] has been widely used in both acidic and basic aqueous solution. Above pH = 3 complexation of Ti^{+3} with $EDTA^{-1}$ prevents its hydrolysis. The reactions of this Fenton-like system have been reviewed by Norman.[98,99]

The procedure involves a continuous rapid-flow apparatus which contains the Ti^{+3} solution (as $TiCl_3$) and the H_2O_2 solution in separate reservoirs and mixes them immediately (*ca.* 50 ms) before the combined

solution enters the flat cell in the ESR cavity. The substrate molecule can be included in solution with either the Ti^{+3} or the H_2O_2, or in a reservoir feeding a third stream if necessary. Spectra are then obtained during continuous flow. Rates of about 100 to 150 mℓ/min for each stream are required. In many instances this method provides intense signals and it has the advantage of simple experimental apparatus (cf. radiolysis[83]). The chosen substrate must be both soluble and stable in aqueous solution since other redox solvents are expensive or cause precipitation problems. In practice steady-state concentrations of isomeric radicals not readily observed by continuous photolysis may be present, complicating the spectra (•OH is apparently somewhat less selective than $(CH_3)_3CO•$). The greatest disadvantage of the method, though, is that a large amount of substrate is required.

2. BACKGROUND: TECHNICAL

(a) Photolysis Systems

The source of UV irradiation is invariably a high pressure mercury capillary lamp, or a mercury-xenon or xenon short-arc lamp of 0.5, 1, or 2 kW rated power. Lamps which have a higher overall power rating may not be expected to be dramatically more effective in general since the radical production rate depends on the luminous flux at the sample (*inter alia*). Thus it is better to have a relatively small arc length given the small volume of solution actually under detection by the spectrometer. Arc lamps are in most common use, but for pulse studies highly collimated laser flash photolysis has been used.[6]

A good quality quartz lens (usually Suprasil) of high transparency to UV light and of high power (f-number = 1) is needed near the lamp to collect the light as efficiently as possible. The resulting parallel beam is then focussed on the sample through slits in the front of the ESR cavity by a second lens which of necessity, given the focal length, must be placed between the poles of the magnet.

Infra-red radiation leads to heating of the sample and cavity affecting the tune and, incidentally, the actual temperature of the experiment. If the beam is passed through an infra-red filter cell this heating effect can be avoided (see Section 3).

Intensity losses in such a system are such that a typical 1 kW lamp may ultimately provide only about 1 W of radiation incident on the sample.[2]

Wong[100] has reported a significant increase in rate of radical production (and signal intensity) by focussing UV light on the end of a light pipe (Suprasil quartz rod) fitted into a modified cavity front-plate. The enhancement occurred in spite of a loss of Q, the filling factor, in the cavity modification.

(b) Temperature Considerations

Current variable temperature accessories (e.g. Brüker ER-4111) provide integral temperature setting and reproducibility for static samples from -150° to +25°C (and higher with slight modification). In contrast sample temperatures in flow systems are difficult to adjust and maintain over a wide range due to thermal gradients. Thus flow experiments are restricted to the range *ca.* -70° to +20°C

ESR signal intensities are improved at low temperatures because of the Curie Law and because radical recombination is slowed.

If solvents become too viscous on cooling, though, linewidths will increase as anisotropy increases at slow rates of Brownian tumbling. The early success of Krusic and Kochi[86,87] using static samples at low temperatures depended on the low viscosity of both the solvents cyclopropane and ethane in the cold and on the relatively low MW, low polarity substrates that were used.

Also the photolysis technique avoids the reduction in initiation rates that lower temperatures introduce in chemical reactions, though abstraction (e.g. Reaction 8) may be slowed.

(c) Solvent Considerations

(i) Static Solutions

The choice of a suitable solvent for samples in standard (*ca.* 3 mm i.d.) ESR tubes is very important. Given the sample volume of such a standard tube the solvent must have a low dielectric constant for tuning. Inertness in both initiation (photolysis) and subsequent reactions is required. For the physical reasons cited above it must be liquid over a wide range of temperatures and have a low viscosity. High solubility of the substrate over this temperature range is desirable.

Only a few solvents meet these criteria. Cyclopropane (b.p. -33°C) is widely employed, although cyclopentane, ethane and propane have been used. More polar solutes may require certain of the freons or even methanol, with corresponding trade-offs in viscosity and dielectric loss. For biological modelling when H_2O_2 is used, aqueous solutions are

commonly adopted media. In this case a flat cell (thickness typically 0.010-0.025 inch) is used to avoid overloading the cavity Q. A simple and inexpensive method of obtaining variable temperature ESR spectra of lossy solutions has been reported recently.[101] However, the capillary tubes used would not be suitable for photolysis.

All solutions to be studied must be free of dissolved oxygen to avoid undesirable peroxy radical formation. Solvents of relatively high boiling point are conveniently deoxygenated by purging with nitrogen or argon. A dry ice condenser is necessary to successfully retain volatile solvents in the purging operation. In practice for static samples several freeze-pump-thaw cycles (using liquid nitrogen) on a vacuum line are undertaken.

Low boiling solvents (e.g. cyclopropane, trichlorofluoromethane) and indeed liquids of higher boiling point (e.g. cyclopentane, acetone, 1,1,2-trichloro-1,2,2-trifluoroethane) are sealed in the sample tubes under vacuum at liquid nitrogen temperatures. After sealing even tubes containing propane or cyclopropane can be handled safely at room temperature.

The distinct advantage of the sealed tube method of sample preparation is the small amount of substrate that is required, typically 200-500 mg (*ca.* 1-3 mmol). Both highly purified and relatively expensive (e.g. labelled) substrates are then accessible. However, depletion of substrate on prolonged irradiation (changing signal intensity) and interference from accumulated products are the trade-offs.

(ii) Flowing Solutions

The photolysis flow technique involves a solution of substrate (*ca.* 0.05 to 0.2 M) and an initiator (e.g. peroxide, ketone) being drawn, by gravity or aspirator suction, through a cylindrical tube or flat cell in the spectrometer cavity. The solution is passed through a heat exchanger arrangement[2,25] for cooling before entering the cavity. Useful flow rates in the range 0.2 to 4 mℓ/min are typical, although the difficulty of insulation between the heat exchanger and the cavity necessitates much higher flow rates (*ca.* 25 mℓ/min) to maintain low temperatures (e.g. -70°C).[2] Thus for high resolution (long scan times) relatively large quantities of substrate are necessary.

The use of a flat flow-cell minimizes dielectric loss when polar solvents are required. Formation of either highly labile initial products or light-absorbing species would also dictate a flow technique approach.

3. APPARATUS AND TECHNIQUES FOR THE PRESENT RESEARCH

(a) Instrumentation

(i) Spectrometers

Two ESR spectrometers were available in the present work, a Brüker ER-200 tt (photolysis—static samples) and a Varian E-6S (photolysis—aqueous flow). Both X-band spectrometers were operated at 100 kHz modulation frequency employing conventional TE-102 cavities. For high resolution work the Brüker instrument offered the following additional capabilities:

(1) A Brüker ER-4111 variable temperature unit providing digital selection of integral temperatures from -150° to +30°C (higher with modification).

(2) A B-NM 12 NMR oscillator (gaussmeter) providing accurate field calibration and 7-digit display of field position. A frequency counter was not available.

(3) A dedicated B-NC 12 data system offering computerized data accumulation and on-line simulation capabilities.

(ii) Data Accumulation and Simulation

Spectral accumulation employed the newest version of the Brüker accumulation program available at any time, i.e. EPRMEAS-FT (1973), EPR-79, EPR-79C, and EPR-80 respectively. The simulation program supplied by Brüker was EPRCAL (1973) which calculates isotropic spectra to first order by initially constructing the appropriate line diagram.

Off-line simulation was carried out by the University's IBM 4341 central computer. Spectra demonstrating second order effects were simulated using the program (QCPE-210) by P.J. Krusic. Spectra involving intramolecular exchange effects were simulated using the program ESREXN (QCPE-209) by J. Heinzer,[102] which is based on the density matrix formalism.[102] Both programs were obtained from the Quantum Chemistry Program Exchange. For further discussion of these two programs see Appendix A.

(iii) Comments on Instrumentation and Measurement

1. Temperature Control. A non-commercial VT system adapted for use with the Brüker instrument was employed for a few early experiments but did not have the valuable temperature selection capabilities of the

4111-VT unit. With samples that deteriorated rapidly on irradiation the ability to select and achieve new temperatures rapidly was essential.

2. Field Calibration. Unfortunately the B-NM 12 gaussmeter was not functioning during most of the experiments.

3. Data Accumulation. Several attempts to enhance the signal-to-noise ratio of spectra from samples of well-behaved substrates by computer accumulation of repeated scans, either slow (>5 s/sweep) or fast ($\leqslant 5$ s/sweep), proved futile with the hardware/software system described. In our judgement the main reason for this was that the number of data points sampled (1024) was inadequate to achieve the resolution required for spectra having many lines and small hyperfine splittings. Furthermore the positional integrity of repeated scans appeared insufficient to avoid real absorption lines actually cancelling themselves in the memory. These types of problem have been discussed by Swartz, Bolton and Borg,[8] and applications of computers to ESR spectroscopy have recently been reviewed by Vancamp and Heiss.[103]

4. Precision. All of the hyperfine splittings reported were measured directly by inspection. The estimated precision of each result is indicated in the table where it appears. Clearly, expanded scale scans improve the precision. In some spectra the broad nature of the signals and/or the relatively poorer signal-to-noise ratio result(s) in considerably reduced precision, particularly in reference to spectra involving dynamic processes. In such situations appropriate limits are given.

5. g-Values. Representative g-values were obtained using the absorption due to hydroxymethyl radical as an accurately known internal standard.[25] In view of the inherent linewidths of the alcohol-derived radicals and probable narrow range of g-value variation under the influence of the alkyl substitution parameter being studied no attempt was made to measure the g-value for all the radicals reported.

The g-values for acyclic α-hydroxy and α-alkoxy substituted alkyl radicals lie in the range 2.0030-2.0033, which is greater than that for the α-unsubstituted radicals (2.0024-2.0027).[27] A second α-oxygen substituent causes a small decrease in g. These variations have been discussed by Norman et al.[27] in terms of spin delocalization and bending.

6. Linewidths. Assessment of relative linewidths was based on peak amplitudes and confirmed by appropriate simulation employing both dynamic and static programs.

7. Power Saturation. For linewidth purposes the optimum power setting was required. Examination of the saturation behaviour of the 2-hydroxyprop-2-yl radical using the Brüker ER-200 tt gave the curve shown in Figure 14. All the ESR spectra were obtained at 25 db power attenuation, the maximum in the plot shown.

(b) The Photolysis System

An essential element of the present work has been the establishment of a functioning lamp system, the first experimental requirement of the study. Several local constraints were present including: (1) the need for portability due to lack of services and for use with both spectrometers; (2) the configuration of the Brüker magnet.

FIGURE 14: Peak height (intensity) vs. $(\text{power})^{\frac{1}{2}}$ for isopropanol radical line at -30°C using Brüker spectrometer.*

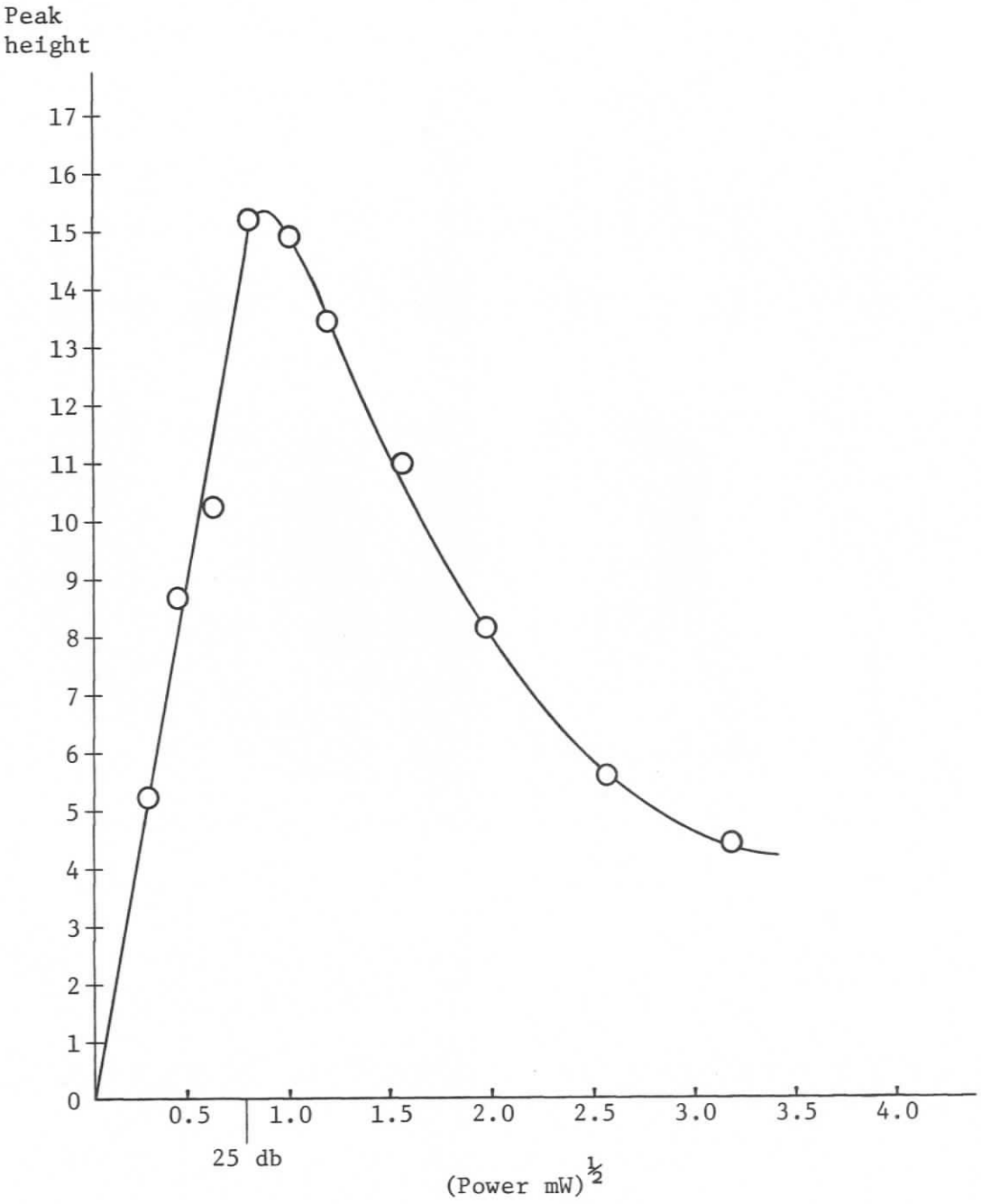

*Data is avg. of two determinations. No account was taken of slight sample deterioration during measurement.

(i) The Lamp Unit

The lamp unit consisted of an Illumination Industries model SEB base fitted with a PEK AH6-2-B high pressure mercury capillary arc rated 2 kW and having an arc length of two inches. (At the time of writing these lamps are no longer commercially available.) Having made this choice it was then necessary to have constructed a cooling system which would circulate distilled water from a cooled reservoir through the lamp water jacket at $\geqslant 1.2$ gal/min and a high voltage power supply designed specifically for the unit. For portability the lamp was supported by a wheeled trolley upon which rested a large (*ca.* 20 gal) plastic barrel, the cooling reservoir. Within this container was a similar smaller vessel of *ca.* 5 gal capacity which contained the distilled water to be circulated through copper coils in the outer cooling reservoir and subsequently through the lamp water jacket. This arrangement is pictured schematically in Figure 15. The water circulating system was fitted with a pressure switch which would cut power to the lamp in the event of a significant drop in the water pressure. The ice-filled outer reservoir allowed operation of the lamp for *ca.* 2 hours before draining and refilling with ice was necessary.

The lamp system described was adaptable to the use of an AH6-1-B 1 kW lamp having an arc length of 1 inch. Another special power supply had to be constructed for this adaptation which, though used only on a trial basis, may become the configuration of necessity if the AH6-2-B lamps remain unavailable.

FIGURE 15: Self-contained 2 kW lamp system (viewed from top).

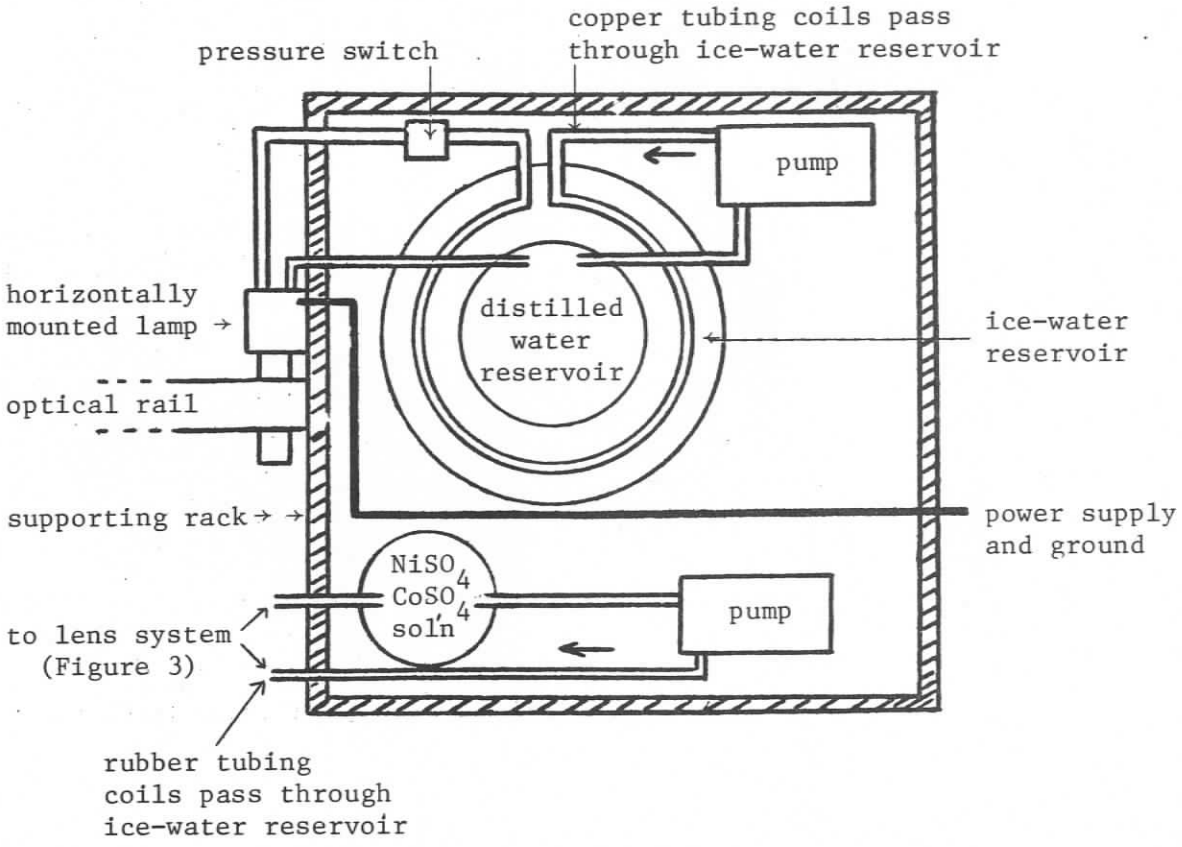

The apparatus is mounted on a 4' x 4' trolly with screw stabilizers. The power supply is a separate wheeled unit.

(ii) The Lens System

The lenses were suspended in machined fittings from a short length of optical rail which projected from a rack on the side of the trolley (Figures 15 and 16). This arrangement permitted adjustment of the lamp-to-collecting lens distance and the focussing lens-to-sample distance.

In order to collect light efficiently from the 2-inch source relatively large lenses were initially selected. It was possible to use a pair of 3 inch diameter lenses (focal length = 3 inches, f-number = 1) in conjunction with the Varian instrument. Photolysis experiments with this arrangement caused undesirable heating in the spectrometer cavity. This heating was eliminated by placing between the lenses a cylindrical cell (dia. 9 cm, length 3 cm) having flat quartz end faces and through which was circulated an aqueous solution of $NiSO_4$ (1.14 M) and $CoSO_4$ (0.2 M). This solution absorbed the undesirable infrared component of the irradiation.[2] Ultraviolet transmitting solution filters have been discussed in the literature.[104,105]

The Brüker configuration is more constraining. With rapid-scan coils in place the pole separation is only 5.5 cm and this dimension extends 13 cm from the sample. Thus it was necessary to obtain Suprasil lenses of a diamter (2 inches) that would fit between the pole faces when mounted, and still be of sufficient power (f-number = 1) to be efficient in the collection and delivery of UV intensity. Finally, thin lens mounts of non-ferrous metal had to be constructed.

The use of the smaller lenses in conjunction with the Brüker instrument caused no apparent cavity heating and the IR filter cell was

FIGURE 16: ESR flow-photolysis system.

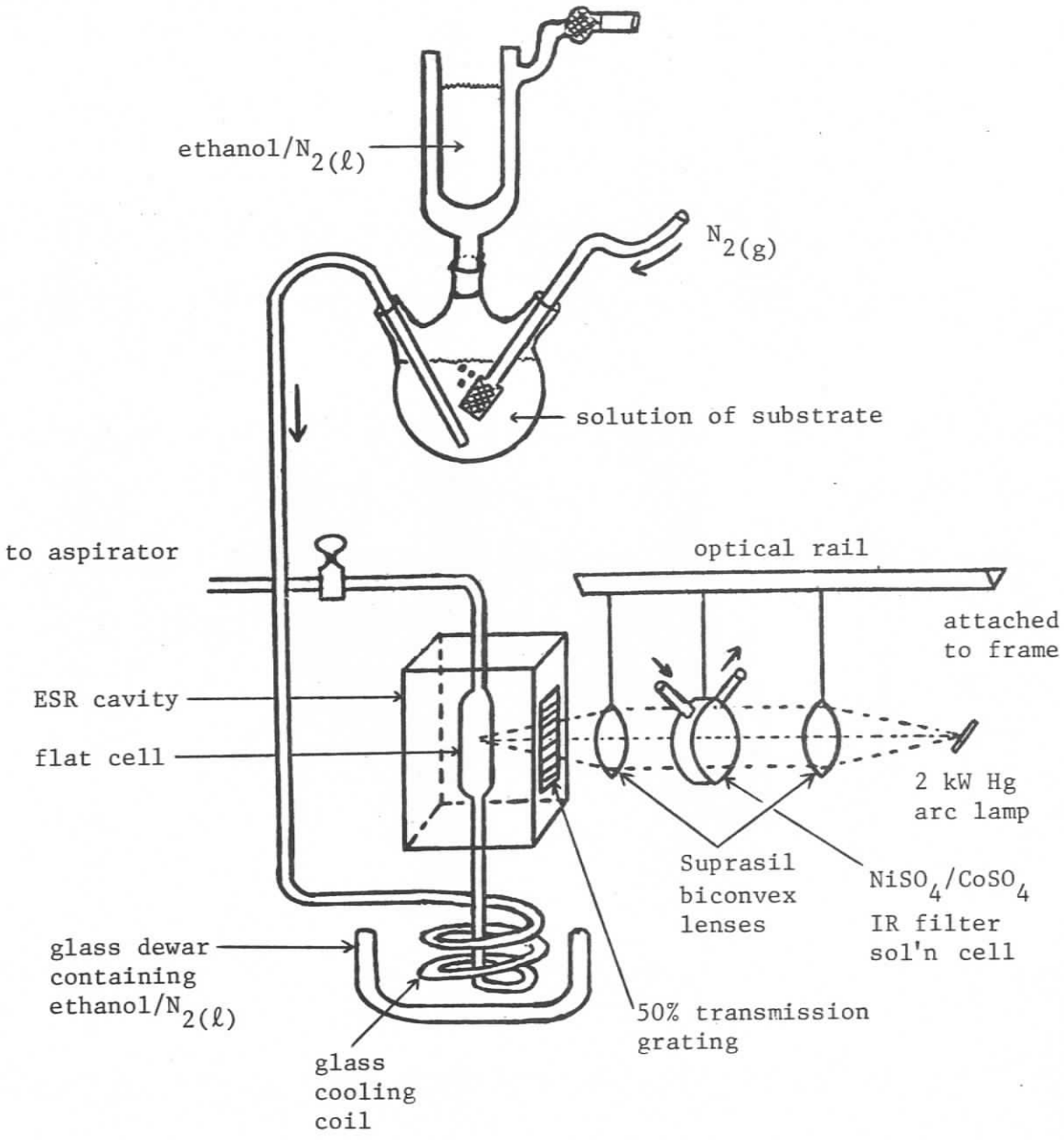

therefore removed from the system.

A pair of Herasil lenses of similar diameter were tried earlier and found less satisfactory, a function both of their lower power (f-number = 1.5) and of the different quality of the quartz. Therefore, in spite of cost, Suprasil lenses of f-number = 1 must be selected.

The final arrangement allowed installation of a spherical mirror (dia. 3 inches, focal length 2 inches) behind the lamp with the intention of increasing UV intensity at the sample. Whether or not a significant gain was made is difficult to assess since after only a few hours irradiation the silvering material had begun to vapourize, leaving the mirror partially transparent. The mirror used is the Oriel 6149 rear reflector and should be judged in terms of its resistance to this light.

(iii) Safety

An important concern in the operation of a high intensity lamp is safety. Direct personal exposure, especially visual, to such a lighted source must be avoided. With this in mind a finned cylindrical aluminum housing with a rectangular port in the side was constructed and placed around the lamp, clamped to the lamp base. In spite of the desirability of such a simple arrangement the housing proved unusable due to the very considerable heat which built up in it and which was not dissipated by the air-cooled fins. This heat contributed to leakage of water from the lamp base as well as other problems and its use had to be abandoned. The lamp was subsequently shielded in a less confining shroud of metal foil and black cloth.

A pair of no. 10 welder's goggles was used to look at the focussed spot when adjusting the final position of the trolley/lamp system in front of the cavity grid.

It was also necessary to cover the plastic coated pole faces of the Brüker magnet with aluminum foil to avoid damage from stray yet intense light.

(iv) Use of the Photolysis System

In the initial 18 months of operation lamp lifetime was a delaying and expensive problem. The AH6-2-B lamps occasionally gave only a few hours service and it was not unusual for a lamp, either new or previously used, to explode on ignition. Other lamps gave 10 to 20 hours service and exceptionally 26 hours was achieved (manufacturer advertised life 80 hours). Shortening of lamp life is expected on repeated start-up but additional factors were clearly involved:

(1) Lamp orientation—difficulties were partially reduced by horizontal rather than vertical mounting of the lamp.

(2) Opaque deposits—the black deposits which usually build up on the outside of lamps that have been used for some hours can be easily cleaned off by dismantling the water jacket, but in cases where this was done the lamp frequently failed to re-light and had to be discarded. More frequent changing of the distilled water in the circulating reservoir might help alleviate this problem.

In summary, the establishment and maintenance of a functioning photolysis system has been one of the most difficult experimental problems associated with this research.

(c) Sample Presentation

In this work the utility of UV photolysis of samples in sealed tubes, of photolysing flowing solutions, and of the multi-stream redox aqueous flow technique were initially assessed for the substrates of interest. The disadvantages of the aqueous redox method (*vide supra*) worked to dictate photolysis as the method of choice.

(i) The Photolysis Flow Technique

The early emphasis of the research was on the use of a single stream slow-flow system (Figure 16). In this case the abstracting radical (hydroxyl, *t*-butoxyl or acetone triplet) was generated photolytically. An acetone (or methanol) solution (500 mℓ) of the chosen substrate (0.05 M) was passed through a cooling coil in a dewar of ethanol/liquid nitrogen placed immediately beneath the cavity. The solution was then drawn upward by aspirator suction through the flat cell in the cavity. Typically, the flow rate was 2-4 mℓ/min, though flow rates of $\geqslant$20 mℓ/min were necessary for temperatures $\leqslant$-40°C. Unfortunately it proved very difficult to control or even to know accurately the temperature of the solution as it entered the flat cell. Moreover the solvents amenable to this flow system give radicals whose ESR signals overlap, in many cases, those of the radical being studied. This latter restriction is especially apparent in the present project where steric constraints are present in the substrates.

In an attempt to deal with the former problem a small steel heat exchanger was built. This device was small enough to fit inside the standard VT insert dewar supplied by Varian for use with static samples.

We thought this might make temperature control easier since it did not rely on a cold solvent bath and since the small heat exchanger could be placed closer to the cavity. The device was partially successful but difficulties continued to plague the system. In particular very low temperatures could not be achieved and many unwanted signals from solvent-derived radicals interfered.

Initial attempts to use a flow/photolysis system with the Brüker instrument indicated that the Brüker sample cavity is very temperature sensitive and it was not expedient at that time to devise a thermally insulated construct in which the flat cell could be contained.

(ii) The Sealed Tube Sample Technique

In the present work the use of relatively polar alcohols and high molecular weight ethers presented sharply enhanced problems in solubility and solvent selection relative to less polar small molecules. With this in mind, and in consideration of the problems discussed above, the preparation of samples in sealed tubes proved the only technique[87] suitable to this work.

The substrate (*ca.* 1-3 mmol), di-*t*-butyl peroxide (0.2 mℓ) and a solvent (*ca.* 1-2 mℓ) were added to a quartz ESR tube in reverse order of freezing point. The tube, previously attached by a graded seal to a short pyrex tube and ground glass joint, was then connected to a vacuum line. Next it was alternately cooled in liquid nitrogen, evacuated and, after isolation from the vacuum manifold by a stopcock, thawed. This process was repeated twice to ensure complete removal of dissolved oxygen, and the tube was re-frozen and closed with a flame above the graded seal.

It was best to thaw the tubes quickly by immersion in a graduated cylinder full of water at *ca.* 35°C.

Due to a delay in obtaining cyclopropane we initially tried as solvents Freon-11 (trichlorofluoromethane), Freon-113 (1,1,2-trichloro-1,2,2-trifluoroethane), acetone, di-*t*-butyl peroxide and cyclopentane. None of these was well suited to the desired application. Substrates were not adequately soluble in the freons. Di-*t*-butyl peroxide precluded experiments below *ca.* -40°C, its freezing point. Cyclopentane results in an easily detected steady-state concentration of cyclopentyl radical. Acetone also gives rise to an ESR spectrum (from $\cdot CH_2COCH_3$) and has a relatively high dielectric constant. Regular sample tubes (o.d. *ca.* 4 mm, i.d. *ca.* 3 mm) containing acetone were impossible to tune. Acetone solutions could, however, be used when placed in specially made ESR tubes which had several cm of narrower quartz tubing (o.d. 3 mm) joined on their ends. At this stage a reported[106] method of improving signal intensity by adding *p*-methoxyacetophenone to samples provided no significant enhancement for our substrates.

When cyclopropane became available the sample preparation procedure was modified to accommodate the fact that its boiling point is -33°C. The cyclopropane cylinder was attached to the vacuum line. After the substrate/peroxide mixture had been degassed in the usual way the evacuated manifold, now closed to the frozen samples, was closed to the pump and opened briefly to the cylinder. The maniford was then opened to the pump and evacuated. After repeating this flushing procedure the manifold, closed to the pump, was filled with a low pressure of cyclopropane which

was then condensed into each of the sample tubes (up to 4) one at a time. The cyclopropane was carefully replenished in the manifold as required. After re-evacuation of the manifold and the cold sample tubes, now filled with solid cyclopropane, the tubes were sealed individually while still open to the pump. They were then placed in a cold ethanol bath (*ca.* -90°C) and shielded from direct light for storage until use. It was found that even if the bath warmed slowly to $\geqslant 0°C$ (e.g. over several days) the tubes did not ever break. The standard technique just described was used throughout the remainder of the research.

CHAPTER III

CONFORMATIONAL STUDIES OF α-HYDROXY AND α-ALKOXY ALKYL RADICALS: TIME-DEPENDENT HYPERFINE SPLITTINGS

1. LINE BROADENING DUE TO CONFORMATIONAL INTERCHANGE—BASIC THEORY

This section illustrates by the use of relevant examples the theoretical background necessary for interpretation of linewidth effects which arise from intramolecular dynamic processes, specifically rotation about single bonds. The topic has been covered in detail in several reviews.[1,3,107-110]

If the magnetic environment of a nucleus is changed as a result of a transition between conformational potential minima then the hyperfine splitting due to that nucleus will also change. Consider a radical which can exist in two such conformations A and B, and which has a proton ($m_I = \pm\frac{1}{2}$) whose hyperfine splitting is a_1 and a_2 in the two forms respectively.[17] At slow interconversion rates the ESR spectrum will consist of two doublets (Figure 17 case c) with line separations given by a_1 and a_2. At fast interconversion rates a single doublet is observed (Figure 17 case a) having an averaged hfs $\bar{a}$ given by Equation 10,

$$\bar{a} = p_A a_1 + p_B a_2 \qquad (10)$$

where p_A amd p_B are the relative populations of the forms A and B respectively. At intermediate interconversion rates (i.e. exchange

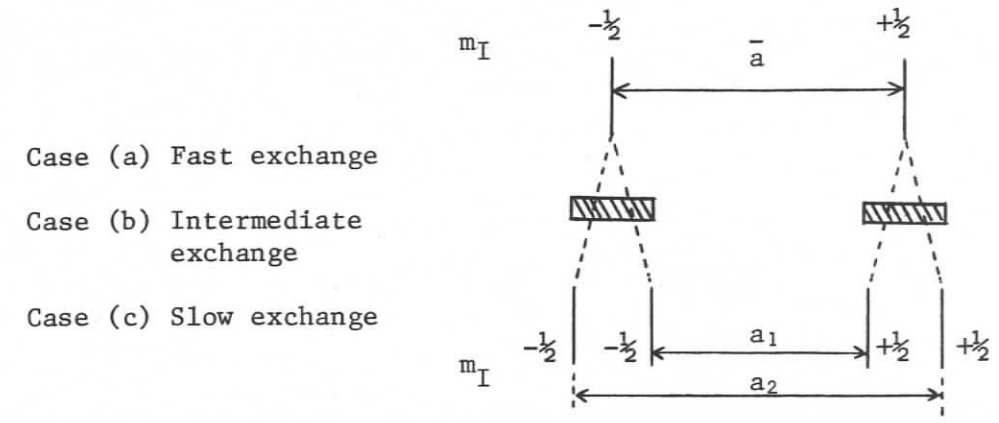

FIGURE 17: Line diagram for the ESR spectrum of a radical in which one proton can exist in either of two environments.

rates approximately equal to the difference in hfs expressed in frequency units) the spectrum will consist of broadened lines (Figure 17 case b). It can be shown that in this case the contribution to the linewidth, $T_2^{-1}(m)$, from modulation of the isotropic hfs is proportional to the mean square fluctuation in splitting, $p_A p_B (a_1 - a_2)^2$, and m^2 as given in Equation 11.[110] In this expression γe is the electron magnetogyric ratio,

$$T_2^{-1}(m) = \gamma_e{}^2 \tau\, p_A p_B\, (a_1 - a_2)^2\, m^2 + T_{2,0}^{-1} \qquad (11)$$

τ is the mean lifetime of the species A and B $\left[\tau = \tau_A \tau_B / (\tau_A + \tau_B)\right]$, and $T_{2,0}^{-1}$ is the linewidth in the absence of exchange. The change from form A to form B does not involve any change in nuclear spin quantum number (m_I). Thus there is a direct correspondence between ESR lines of species undergoing slow exchange and ESR lines observed at fast interconversion rates.

The average hfs $\bar{a}_i$ of the i^{th} nucleus can be either positive or negative but it is not possible to determine which from a simple ESR

spectrum. If $\bar{a}_i$ is positive the high field lines correspond to negative values of the associated quantum numbers m_i and *vice versa*. It is useful for the interpretation of experimental spectra to introduce spectral index numbers $\tilde{m}_i$ which are always positive on the high field side of the spectrum. They are defined by Equation 12.[110]

$$\tilde{m}_i = -\frac{\bar{a}_i}{|\bar{a}_i|} m_i \qquad (12)$$

Before dealing with systems containing several nuclei it is necessary to introduce two further definitions.[110] If two nuclei have the same instantaneous hyperfine splitting they are said to be *completely equivalent*. If their hfs are not instantaneously equivalent but are equivalent when averaged over time they are said to be simply *equivalent*.

Consider the two equally populated low energy conformers of n-propyl radical (14).[3,87] The two β protons are magnetically equivalent in both conformers and thus form a completely equivalent group. The α protons are instantaneously inequivalent and have different hfs (which are exchanged in the process 14a $\rightleftharpoons$ 14b) whose sum is constant (Equation 13).

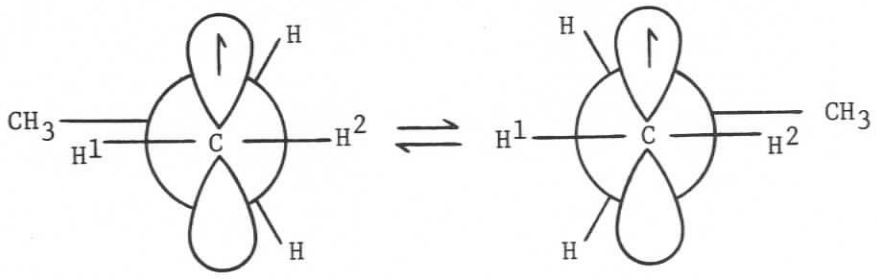

14a 14b

$$a_{H^1a} = a_{H^2b}$$

$$a_{H^2a} = a_{H^1b}$$

$$a_{H^1a} + a_{H^2a} = a_{H^1b} + a_{H^2b} \qquad (13)$$

In this type of process in which the hfs of one nucleus of an equivalent group increases while that of another nucleus decreases, the hfs of the two nuclei are said to be modulated *out of phase*.

The spectrum of n-propyl radical (14) (omitting a_β and a_γ, which do not change) will appear in the limit of slow exchange as a doublet of doublets due to the non-equivalent α-proton hfs (Figure 18 case a).

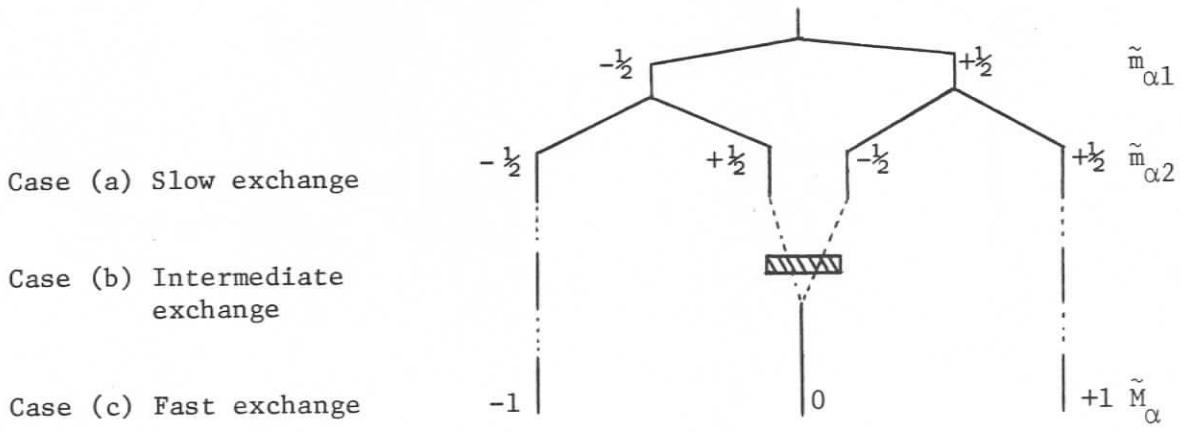

FIGURE 18: Effect of conformational interconversion on the α-proton multiplets in the ESR spectrum of n-propyl radical (14).[3,87]

As the exchange rate increases the two peaks near the center of the spectrum broaden as they begin to coalesce. When interconversion is rapid the splittings are averaged to $(a_{H^1a} + a_{H^2a})/2$, (Equation 10) and

the spectrum has the appearance of a 1:2:1 triplet. Thus Krusic and Kochi[87] observed that when conformational interconversions were slowed by cooling a sample of the n-propyl radical to -140°C the $\tilde{M}_{\alpha} = 0$ lines were broadened. However, in this as in most other cases the resolved low temperature (slow exchange) limit spectrum could not be obtained.

The broadening observed is manifest mainly as a decrease in amplitude of the first derivative peak since this is inversely proportional to the square of the linewidth.[17]

It is important to note that the peaks which broaden with decreasing exchange rates for this out-of-phase modulation mechanism are exactly the ones for which the two $\tilde{m}_i$ values are opposite in sign.

This out-of-phase modulation of the hyperfine splittings gives rise to linewidths which alternate across the spectrum and therefore came to be referred to as the Alternating Linewidth Effect. Relevant reviews have been referenced at the beginning of this section.

Two other types of line broadening effect which can arise from restricted rotation about single bonds have been identified.

The first of these is exemplified in the ESR spectrum of γ-chloropropyl radical (15),[3,111] a stick diagram of which is shown in Figure 19 (γ_H hfs not shown). In this case the outside lines ($\tilde{M}_{\beta} = \pm 1$) of the β-H triplet are broadened on cooling the sample to -132°C. This can be explained if the two β-proton hfs are instantaneously equivalent (i.e. the β protons are completely equivalent) but are modulated between two or more limiting values. A process which could cause the observed broadening pattern is 15a $\rightleftharpoons$ 15b.

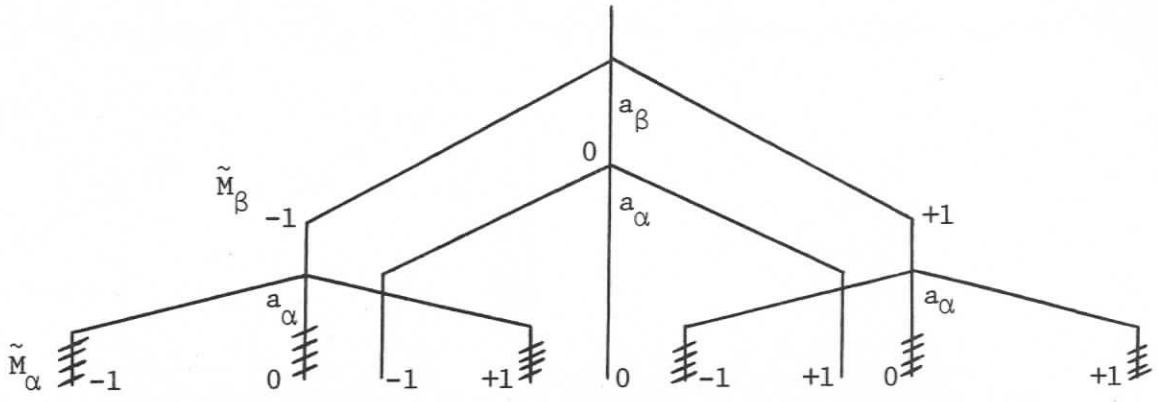

FIGURE 19: Line broadening due to in-phase modulation of β-H hfs in γ-chloropropyl radical (15). Cross-hatched lines are broadened on lowering sample temperature.

The β proton hfs are said to be modulated *in-phase* and the broadening is proportional to $\tilde{M}_\beta^2$ (see Equation 11). The lines in Figure 19 define the averaged spectrum in the limit of fast exchange.

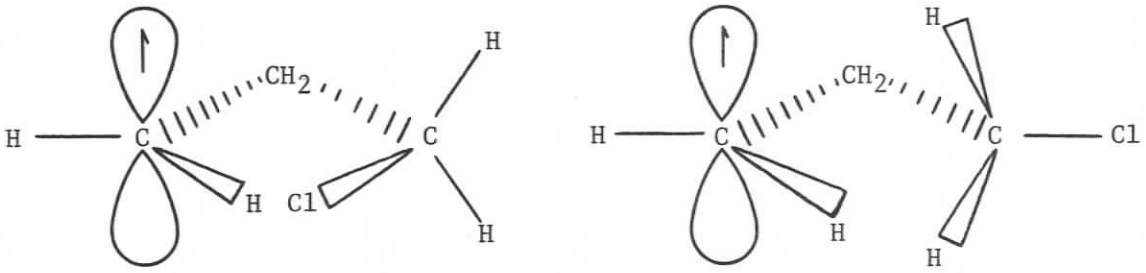

15a 15b

In both cases described above, i.e. in-phase and out-of-phase modulation of hfs, the observed broadening is always symmetrical with respect to the center of each hyperfine multiplet.

The third type of conformationally induced linewidth effect described by Kochi[3] is really a special case of modulation broadening involving *two* non-equivalent groups of nuclei and a conformational

change which gives rise to a large hfs difference for each group. His example, β-fluoroethyl radical, is somewhat complicated and it is therefore useful to consider a hypothetical case (16a ⇌ 16b). Suppose the conformations (16a) and (16b) are equally populated and that a_α decreases

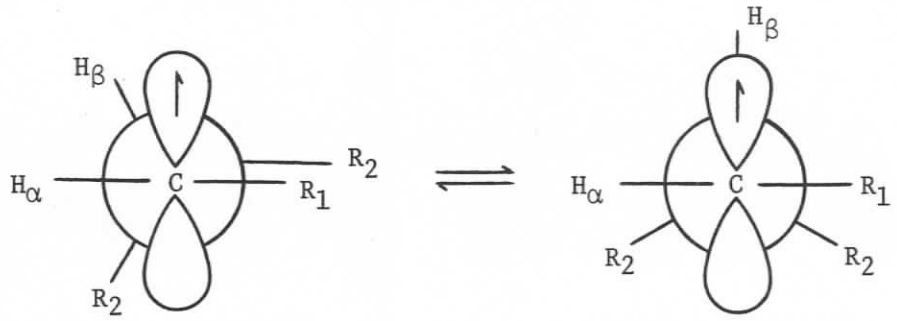

16a 16b

on going from (16a) to (16b), while a_β increases. A possible correlation diagram is shown in Figure 20.

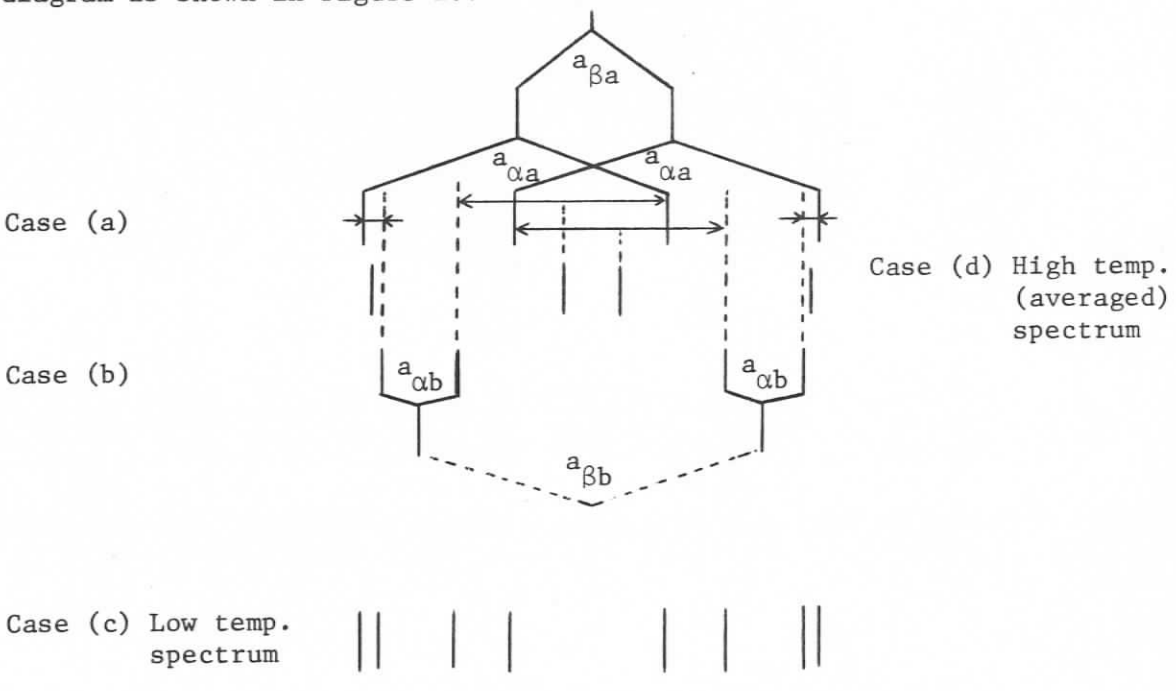

FIGURE 20: A correlation diagram for the hfs of the hypothetical interconversion 16a ⇌ 16b; case (a) spectrum of form (16a), case (b) spectrum of form (16b), case (c) superposition of spectra (a) and (b) (i.e. the slow interconversion limit spectrum), case (d) the spectrum at fast interconversion rates.

At slow interconversion rates the observed spectrum will be the superposition of (16a) and (16b) (Figure 20c). At fast interconversion rates the lines appear at the "center of gravity" of the correlated pair of lines (Figure 20d). At intermediate rates the lines which move over wide intervals of field are broadened more than those moving over a narrower interval. Thus the lines near the center of the spectrum in this example are broadened more than the outside lines and the broadening pattern is therefore not symmetric about the center of the hyperfine multiplets.

2. RELATED STUDIES—ACYCLIC SYSTEMS

(a) Rotation About Carbon-Carbon Bonds

The examples used in the preceding section to introduce linewidth effects involved only restricted rotation about carbon-carbon bonds. Both α-β and β-γ bond rotations have been invoked to explain experimentally observed temperature dependent linewidths.

A C_β-C_γ rotation of the type 17a $\rightleftharpoons$ 17b was suggested by Krusic et al.[87] to explain the out-of-phase modulation of the β-H hfs in n-butyl radical (17, X = H). Lloyd[112] has recently proposed the same rotation

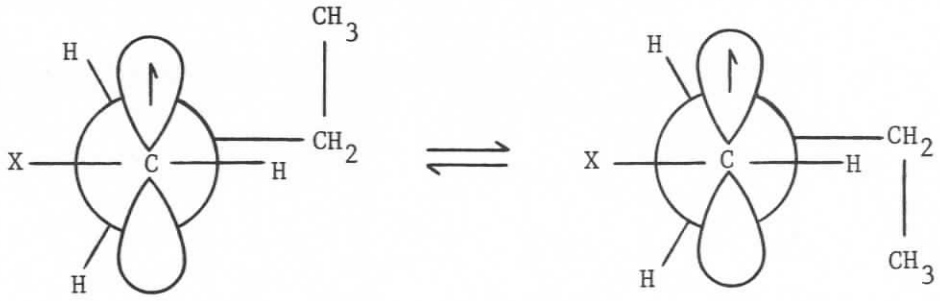

17a 17b

to account for the observed broadening (of $\tilde{M}_\beta = 0$ components) in the ESR spectrum of the radical from n-butanol (17, X = OH) and from n-butyl-isocyanate (17, X = NCO). He calculated the barrier for this rotation to be *ca.* 2 Kcal/mol. This is significantly higher than the barrier for C_α-C_β rotation in alkyl radicals, which is usually less than 1 Kcal/mol[3].

Related work has been presented by Scheffler et al.[183] which illustrates linewidth effects due to restricted C_β-P_γ rotation in the ESR spectra of 4-oxyl-3,5-di-*t*-butyl benzyltrialkylphosphonium radicals. Note from the structure given below that the restricted rotation affects substituents on the center β to the unpaired spin. (See also refs. 184 and 185.)

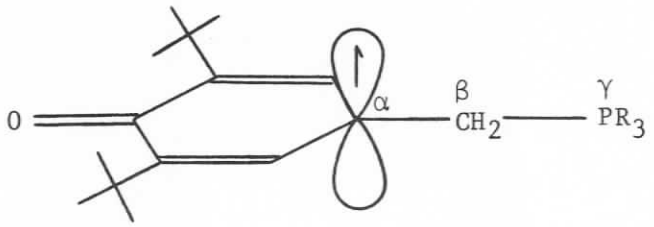

(b) Rotation About Carbon-Oxygen Bonds in Ether-Derived Radicals

Several interesting systems have been reported. Hudson et al.[62] and Krusic and coworkers[57] demonstrated the broadening of the $\tilde{M}_\alpha = 0$ lines in the spectrum of methoxymethyl radical as the sample temperature was lowered (Figure 21).[57] At -117°C these lines sharpened to a doublet of quartets, revealing the existence of a locked conformation in which the two α-protons are non-equivalent.

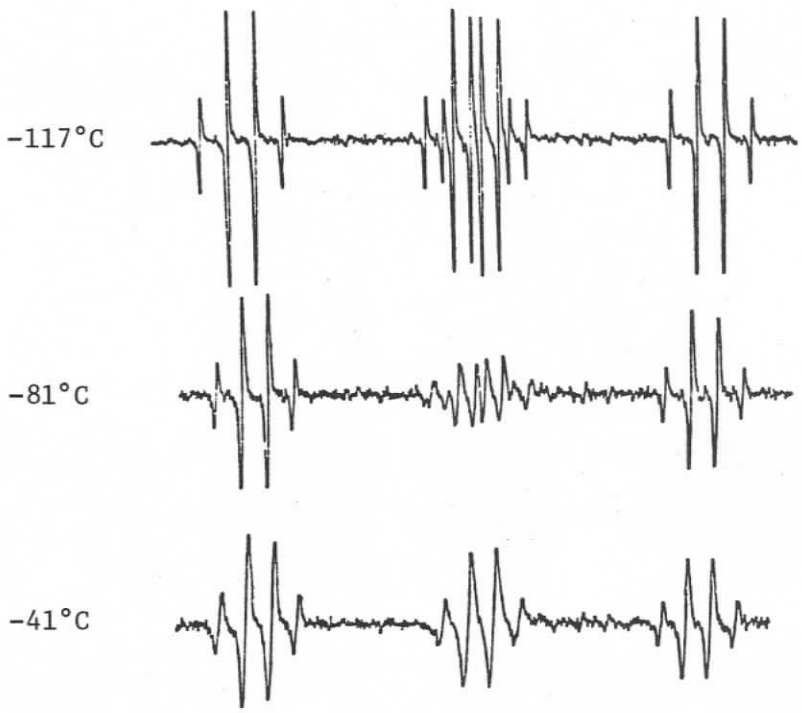

FIGURE 21: Experimental spectra for the methoxymethyl radical.

Splittings were assigned as in structure (18).[57] Krusic et al.[57] calculated the barrier for rotation to be about 5 Kcal/mol.

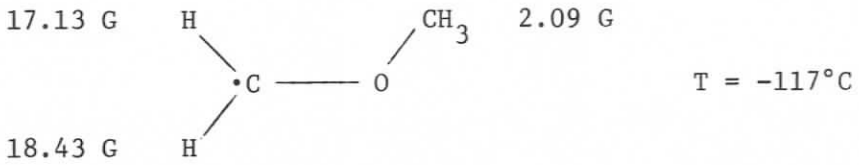

18

Similarly the radical (19) from *t*-butyl methyl ether shows broadening of the $\tilde{M}_\alpha = 0$ lines on decreasing the temperature as evidence of an out-of-phase modulation of the α-proton hfs.[3,64] At -151°C the ESR spectrum, a doublet of doublets of decets, indicates locked conformers

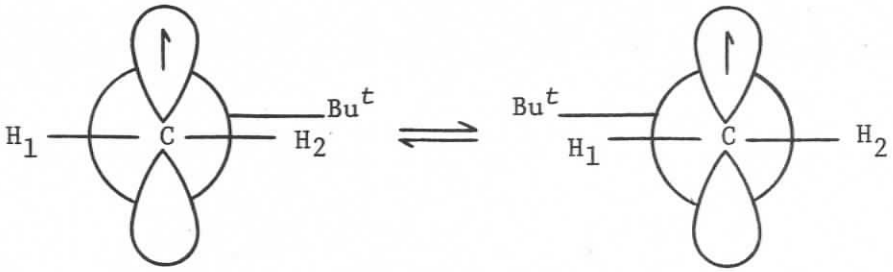

19a 19b

(19) in which the α-protons are not equivalent.[3]

Barriers to rotation of a methoxyl group in a series of cation radicals derived from aromatic precursors have been discussed by Sullivan.[113]

The ESR spectrum of the radical $\cdot CH_2OCH_2OCH_3$ from dimethoxymethane shows the expected triplet of triplets but at -49°C the center group is reduced in amplitude from that expected on the basis of a binomial 1:2:1 intensity ratio[114] (Figure 22). This $\tilde{M}_\alpha = 0$ broadening is explained in terms of the conversion 20a $\rightleftharpoons$ 20b analogous to the cases of methoxymethyl radical (18) and *t*-butoxymethyl radical (19). As the temperature is

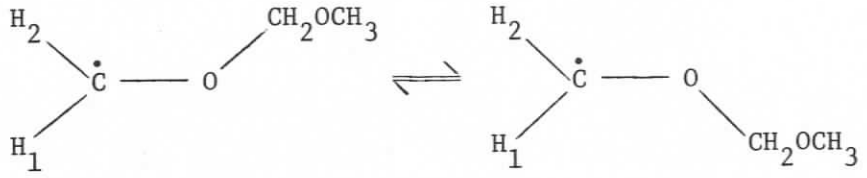

20a 20b

lowered this broadening continues until at -130°C the multiplet is resolved into the pattern expected for two non-equivalent α-proton hfs. However, on lowering the temperature from -70°C the $\tilde{M}_\gamma = 0$ components

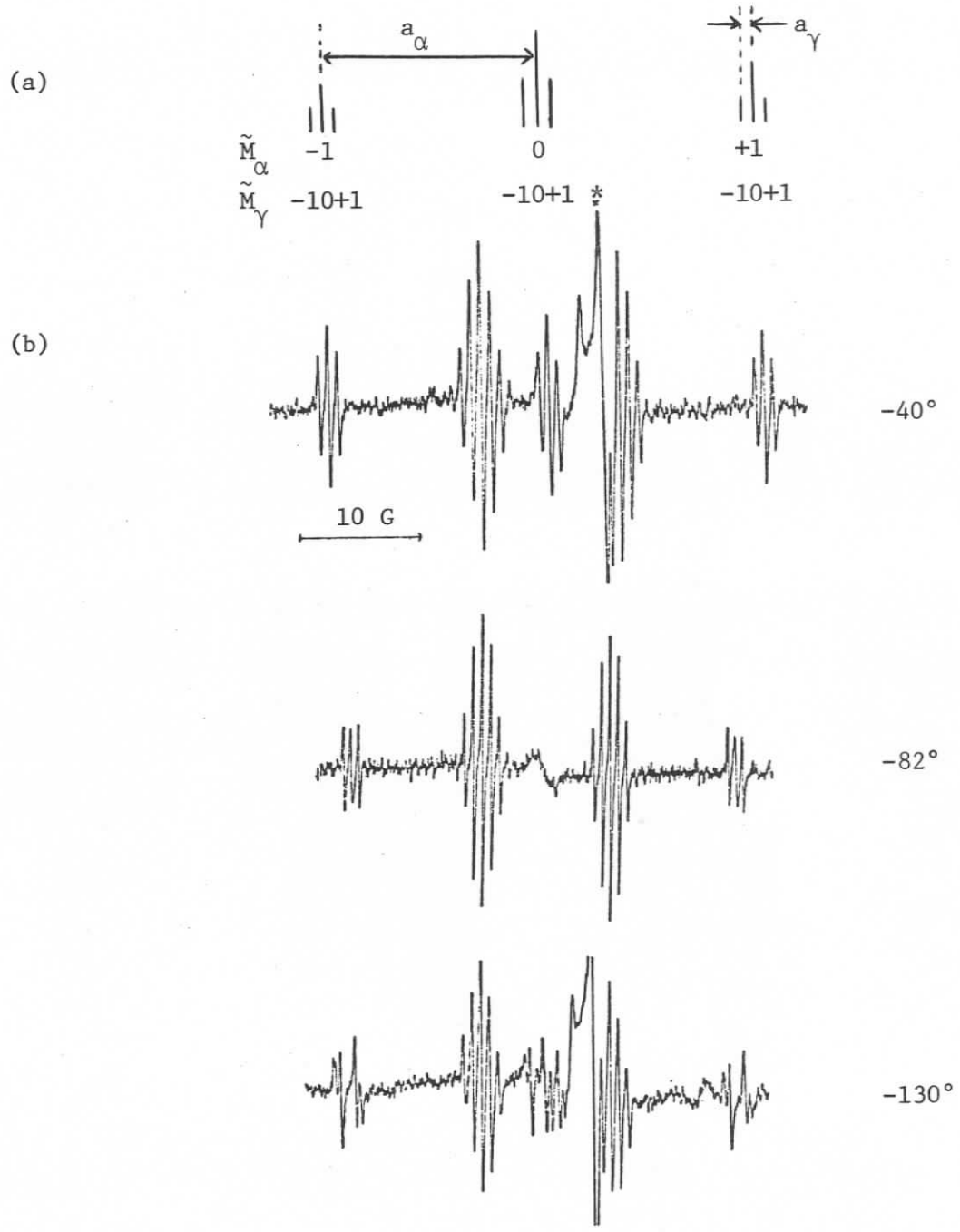

FIGURE 22: (a) line diagram, and (b) spectra for the radical $\cdot CH_2OCH_2OCH_3$ at various temperatures as observed by Gaze and Gilbert.[114] The additional doublet of septets is due to $\cdot CH(OCH_3)_2$, and the signal * arises from the cell.

begin to broaden and subsequently disappear. At -130°C these H_γ multiplets are each a doublet of doublets indicating non-equivalent H_γ hfs. As Gaze and Gilbert[114] point out, the interesting feature is that the broad central line $\tilde{M}_\gamma = 0$ which disappears on cooling reappears on the *outside* of the two H_γ lines which remain sharp, rather than on the inside as is usually the case (cf. Figure 18). This expansion of the H_γ hyperfine multiplet in the slow exchange limit can be explained only if the individual γ-proton hfs are of *opposite sign*. Thus at fast exchange rates when only the average $a_{\gamma H}$ is observed the width of the multiplet is decreased. The barrier for rotation about C_α-O_β was calculated to be *ca*. 4.1 Kcal/mol and for rotation about O_β-C_γ to be *ca*. 4.5 Kcal/mol.[114] The authors suggest[114] that conformation (21) could account for the observed splittings. The proton H_1 would be expected to have a

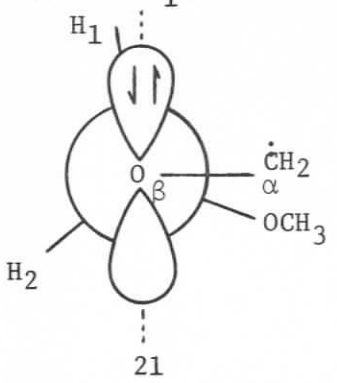

21

positive hfs due to its low dihedral angle with respect to the oxygen $2p_z$ orbital. The proton H_2 might well have a negative hfs arising from spin polarization, the long-range effect of which is enhanced by the intervening β-oxygen atom. Mutual exchange involving hyperfine splittings of opposite sign will be discussed further in Chapter IV.

(c) Hydroxyl Group Rotation

In the absence of steric constraints the rotation of a hydroxyl group attached to a radical center is described by a potential function having two minima in the nodal plane of the semi-occupied orbital on C_α. The magnitude of the hydroxyl proton hfs is determined by the relative contributions of the spin polarization and spin delocalization mechanisms described in Chapter I as the relative contributions are influenced by torsional oscillations. The temperature dependence of hydroxyl proton hfs has been treated theoretically by Sullivan.[115] Barriers to C_α-OH rotation for a series of cation radicals were found[115] to be in the range 3.2 to 10 Kcal/mol. A discussion of the temperature dependent splitting of hydroxyl protons is included in a more recent review by Sullivan and Menger.[37] Earlier treatments are also available.[116,117,118]

Linewidth effects due to modulation of hyperfine splittings by restricted rotation of hydroxyl groups have been observed, but usually for protonated quinones.[119-122] For example, Gough et al.[121,122] found that at low temperatures the hfs of the *meta* protons in mono-protonated benzosemiquinone radical (22) differed by 0.35 G, although the *ortho* proton hfs appeared unaffected.

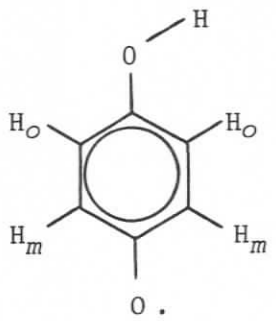

In recent studies designed to provide information about intramolecular hydrogen bonds, Loth, Graf and co-workers[78,123] demonstrate hydrogen hyperfine splittings due mainly to restricted C_α-OH rotation in a series of aromatic and aliphatic species. For the radical (23)

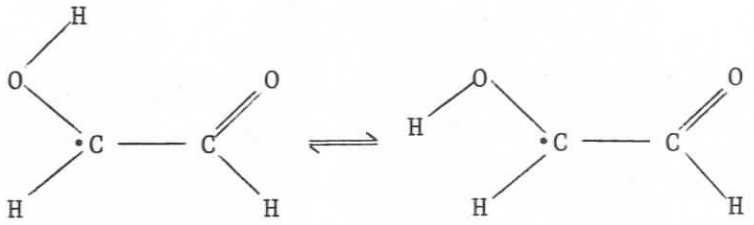

23a ⇌ 23b

formed by irradiating glyoxal (HCOCHO) in toluene these authors found[123b] that satisfactory spectral simulation was achieved when the change in hfs for each proton induced by C_α-OH rotation (23a ⇌ 23b) was less than *ca.* 0.4 G. The C-C rotational barrier is relatively high in (23) due to partial double bond character.

Krusic et al.[124] reported an alternating linewidth effect in the spectrum of $(CF_3)_2\dot{C}OH$ (24) due to restricted rotation of the OH group.

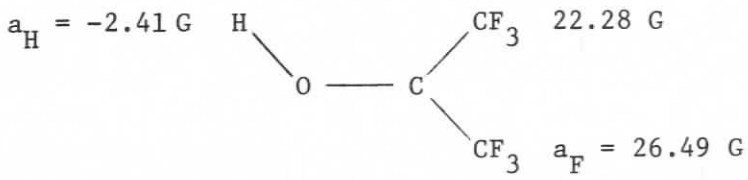

24

They suggested a planar conformation to account for the non-equivalent F_β hfs shown (24) at -140°C.

A much studied system is the hydroxymethyl radical (25). The alternating linewidth effect (Figure 23) for this radical was first

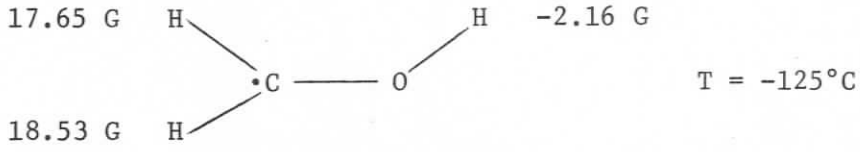

25

reported by Hudson[125] and independently by Krusic et al.[57] (see ref. 3).

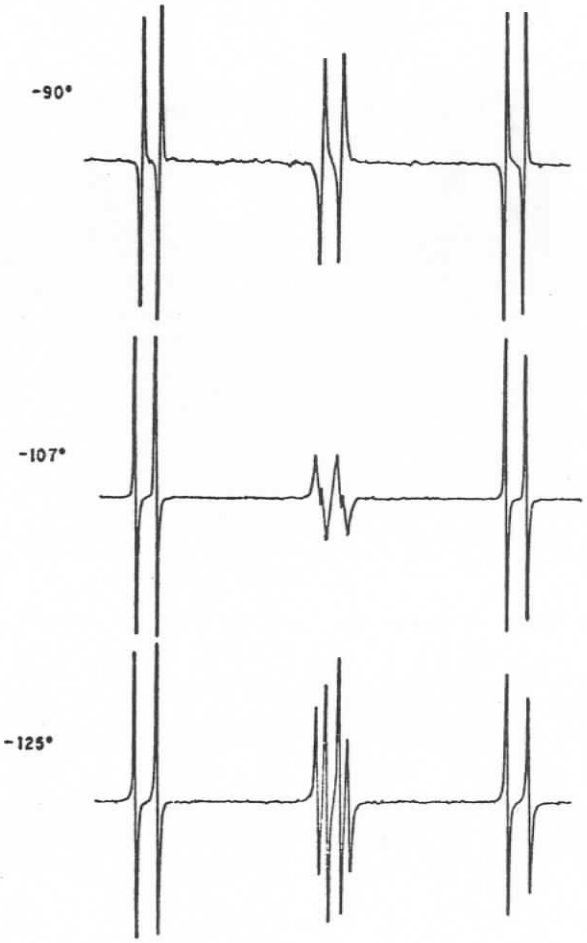

FIGURE 23: ESR spectrum of hydroxymethyl radical at various temperatures.[57]

At -125°C the two α protons are magnetically non-equivalent (25). Treatment of the linewidth effects by density matrix theory provided[57] an activation energy for rotation of 4.6 Kcal/mol, which compares favourably with the value obtained for $\cdot CH_2OCH_3$ (*vide supra*). Hudson[125] and Krusic et al.[57] suggest that the radical (25) is at most slightly non-planar. In contrast, *ab initio* SCF calculations by Ha[126] indicate an out-of-plane angle of 25° for the CH_2 group which results in an asymmetric rotational function with two different barriers (Figure 24). (See also ref. 127.)

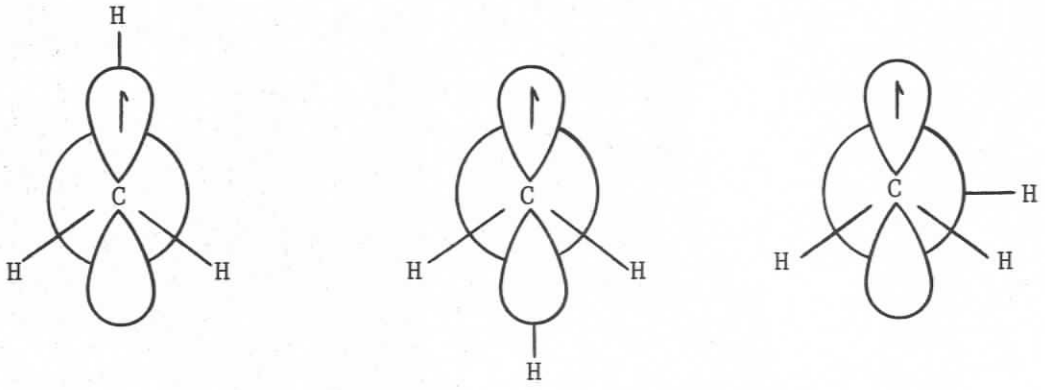

trans barrier
3.5 Kcal/mol

cis barrier
1.8 Kcal/mol

equilibrium

FIGURE 24: Asymmetric rotational barriers in $H_2\dot{C}OH$.[126]

Sargent and Grady[128] reported an additional linewidth effect for this radical in neat methanol. They observed that the two outermost lines ($\tilde{M} = \pm 3/2$)(Figure 25) are broadened and suggested a low amplitude torsional vibration process controlled by hydrogen bonding interactions as the cause of this in-phase modulation of a_α and a_{OH}.

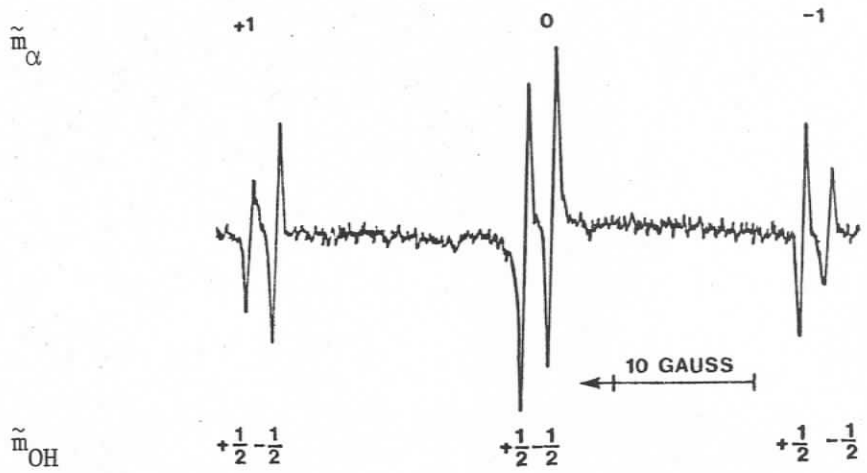

FIGURE 25: ESR spectrum of $\cdot CH_2OH$ in neat methanol[128] showing broadening of $\tilde{M} = \pm 3/2$ lines.

3. RESULTS OF THE PRESENT STUDY

The ESR spectra of many α-hydroxyalkyl radicals are well known[25,37,76,96,129-131] and some have been studied over a range of temperatures. Decreasing the sample temperature can cause linewidth effects in the spectra of such radicals which can be attributed to restricted rotation. Specifically, previous examples in section 2c, above, have shown that restricted rotation of a hydroxyl group can modulate the hfs of H_α ($\cdot CH_2\dot{O}H$[125,57], $HO\dot{C}HCHO$[123b]) and H_β ($HO\dot{C}HCHO$[123b], *cf.* $(CF_3)_2\dot{C}OH$[124]) and H_{OH} itself.[123b] Also, restricted rotation about C_β-C_γ can modulate $a_{\beta H}$ ($CH_3CH_2CH_2\dot{C}HOH$[112]). The results of the present research demonstrate both the generality of these effects and the necessity of considering more than one mechanism in arriving at an adequate interpretation of the low-temperature spectra of alcohol and ether-derived free radicals. Concomitantly α and β alkyl substitution effects on the important $R\dot{C}HOH$ class are revealed through the interesting

conformational information that arises from the analysis.

(a) C_α-OH Rotational Modulation of a_{OH} and $a_{\alpha H}$

Based on previous examples (section 2c) a modulation of a_α and a_{OH} can arise from restricted C_α-OH rotation in the radical (26) from 2,2-dimethylpropanol (neopentanol) which, in contrast to $\cdot CH_2OH$, has only one α-proton.

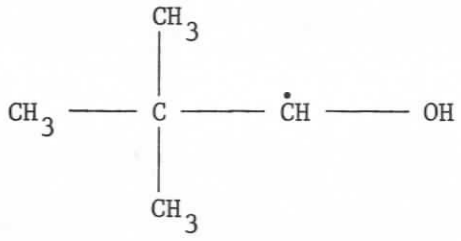

26

The hyperfine splittings for this radical are given in Table 4. The spectrum (Figure 26) consists of a doublet (a_α) of doublets (a_{OH}) of decets (a_γ) as illustrated in the accompanying stick spectrum. The two remote multiplets of low intensity (a = 22.5 G) are attributed to the *t*-butyl radical. The latter spectrum exhibits well-resolved second order structure.

As the temperature was lowered $|a_{OH}|$ increased (Table 4, Figure 43b) and the appearance of the multiplets changed (Figure 27) depending on the extent to which the individual lines of the H_γ decets overlapped. The γ proton hfs was virtually temperature invariant.

Upon cooling from -55°C the multiplets took on a highly asymmetrical appearance indicative of broadening of the inside lines (Figure 26a). Figure 28 illustrates this broadening in experimental and

TABLE 4: Hyperfine splittings for $(CH_3)_3\dot{C}CHOH$ (26) at various temperatures*

Temperature C°	$-a_\alpha$ ±0.05	$\lvert a_\gamma \rvert$† ±0.01	$-a_{OH}$ ±0.01
+20	13.48	0.312	0.175
+10	13.52		
0	13.54	0.320	0.325
-10	13.55		
-12		0.313	0.485
-14		0.313	0.525
-20	13.58		
-30	13.62	0.312	0.625
-40	13.63		
-43		0.290	0.775
-45	13.70		
-50	13.69	0.290	0.875
-55	13.70		
-60	13.73		
-60	13.73		
-70		0.30	
-80		0.30	

* All hfs are reported in gauss.

† Estimated error limits are given in this and subsequent tables, either at the head of the appropriate column or at a particular temperature. Error limits represent the extremes of the measurement and depend in this work (transient radical spectra) on linewidth, the relatively low S/N ratio and the inherent resolution of such studies.

(a)

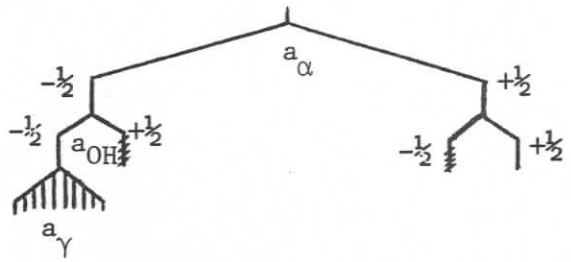

(b)

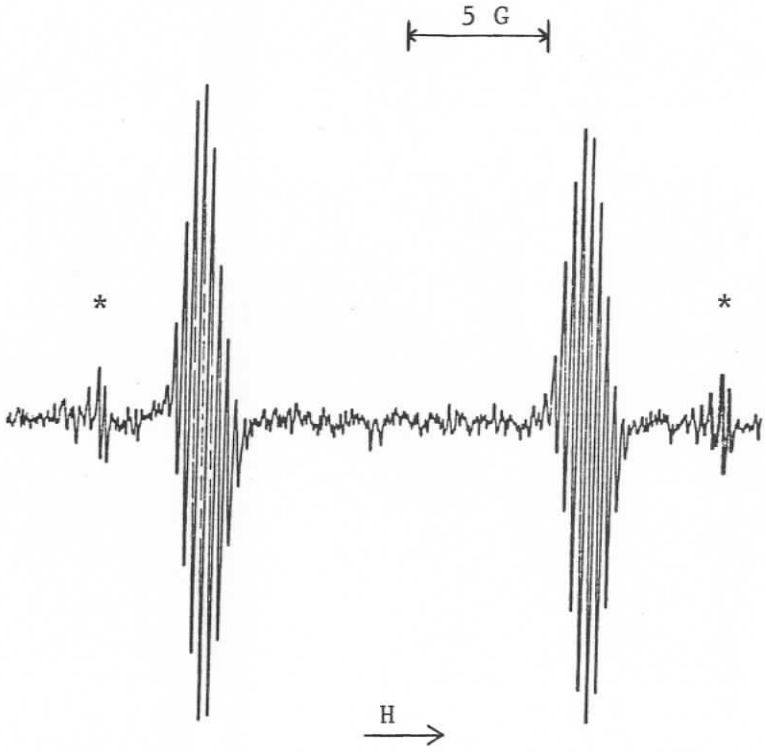

FIGURE 26: ESR spectrum of $(CH_3)_3\dot{C}CHOH$ (26) at -20°C. Line diagram is not to scale. Cross-hatched lines broaden at low temperature. Multiplets marked * are attributed to *t*-butyl radical.

Note: In all the spectra high field is to the right.

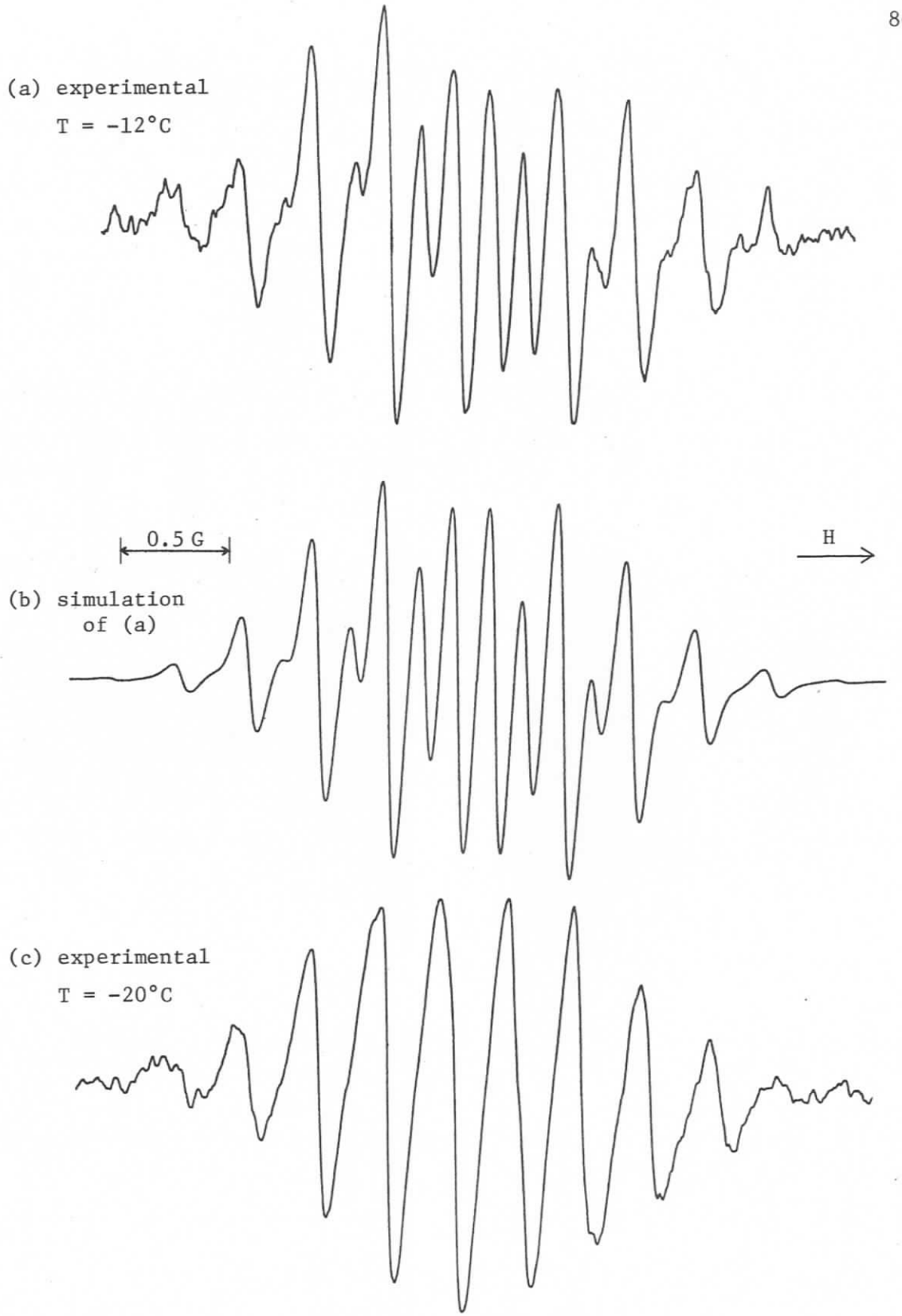

FIGURE 27: Low field multiplet in ESR spectrum of (26)
(a) -12°C, (b) simulation of (a), (c) -20°C.
(Figure continues)

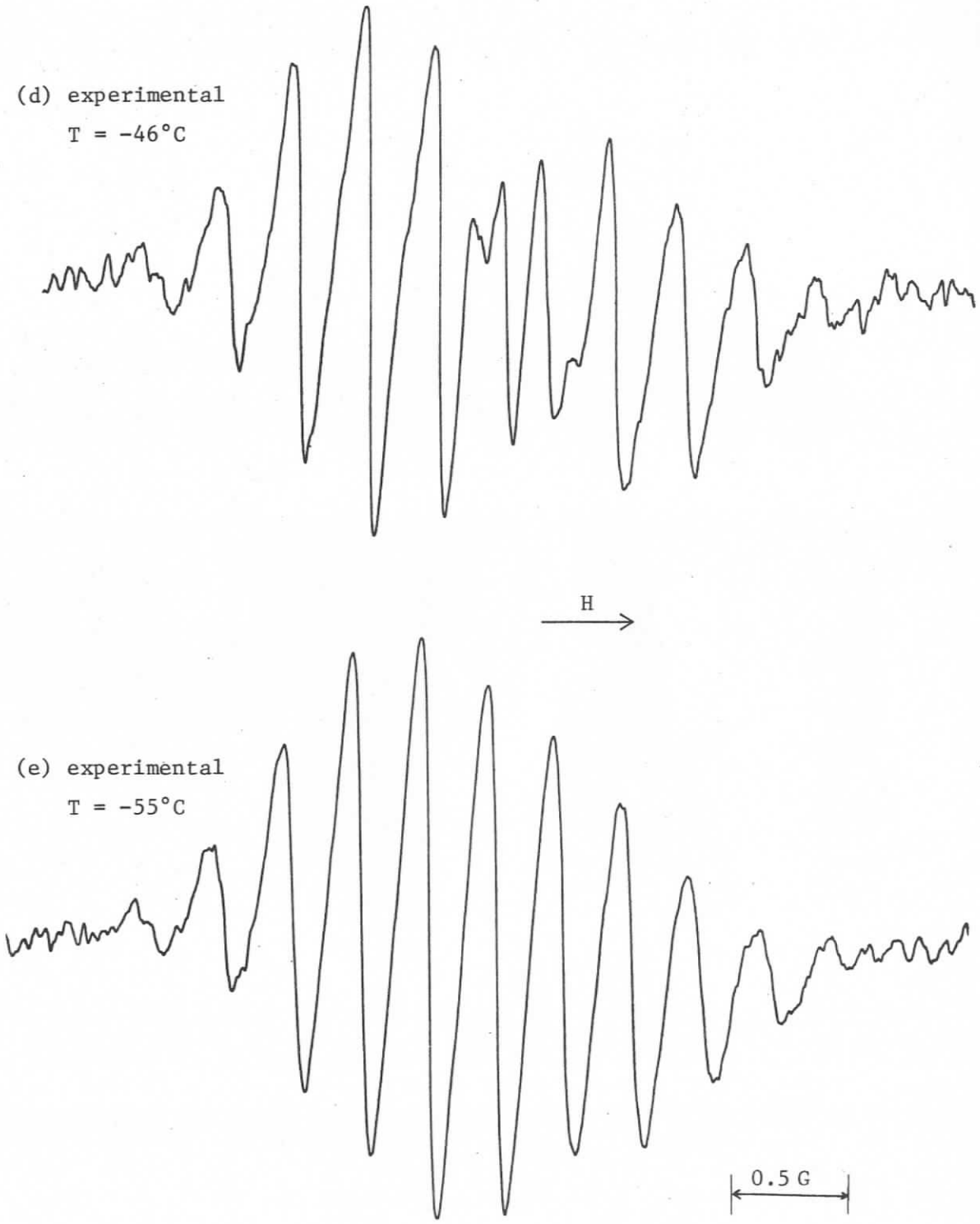

FIGURE 27 (continued): Low field multiplet in ESR spectrum of 1-hydroxyneopentyl radical (26), (d) at -46°C, (e) at -55°C.

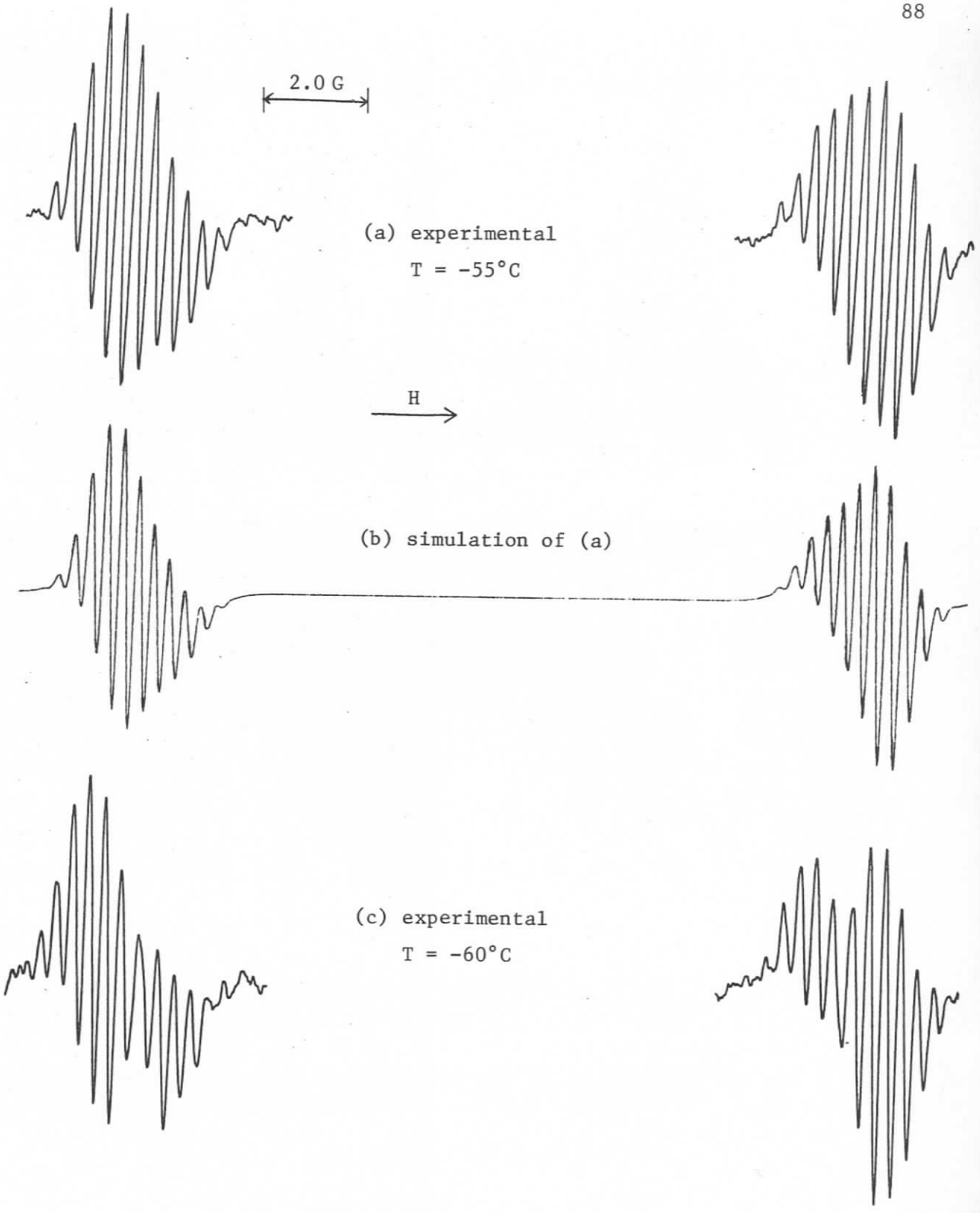

FIGURE 28: ESR spectrum of 1-hydroxyneopentyl radical (26), (a) at -55°C, (b) simulation of (a), (c) at -60°C. See page following.

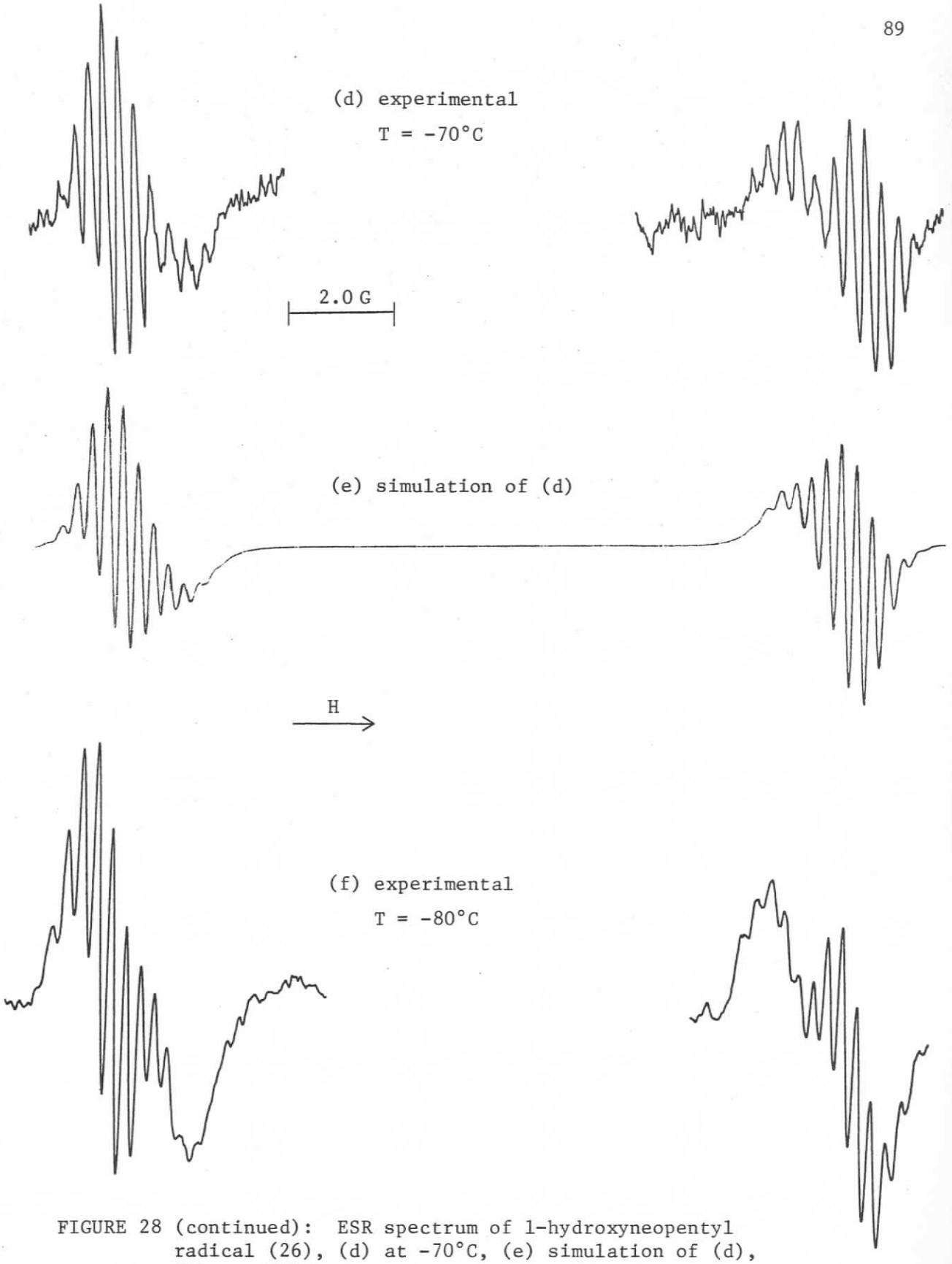

FIGURE 28 (continued): ESR spectrum of 1-hydroxyneopentyl radical (26), (d) at -70°C, (e) simulation of (d), (f) at -80°C.

simulated spectra. By -80°C these inside lines were broadened almost beyond resolution. Further cooling caused a decrease in the signal-to-noise ratio of the remaining lines and at -110°C no interpretable spectrum was observed.

The broadening of the inside lines is indicative of a process in which a_α and a_{OH} are modulated out-of-phase.* That is to say, a process is occurring in which $|a_\alpha|$ increases as $|a_{OH}|$ decreases and *vice versa*. The fact that the outside lines remain sharp is evidence that the sum $|a_\alpha| + |a_{OH}|$ is constant. This is reasonable since in the planar configuration (maximum -ve a_{OH}) delocalization to oxygen is maximized. The reduced spin density at C_α results in a minimum -ve a_α (i.e. lowest $|a_\alpha|$) and is illustrated by the following valence-bond representation (27).

$$R - \dot{C}H - OH \longleftrightarrow R - \ddot{C}H^{\ominus} - \dot{O}H^{\oplus}$$

27a 27b

On the basis of established work (*vide supra*) the modulating mechanism must be restricted rotation of the hydroxyl group. The process 28a $\rightleftharpoons$ 28b could account for the observed broadening but is not specifically required. Other species, namely $(CH_3)_2\dot{C}OH$, provide evidence (next subsection) that out-of-plane potential minima must be considered (e.g. 28c $\rightleftharpoons$ 28d).

---

*The term "out-of-phase modulation" refers here to the hfs of protons not in the same equivalent group. This usage has not been common, but see Sargent.[128]

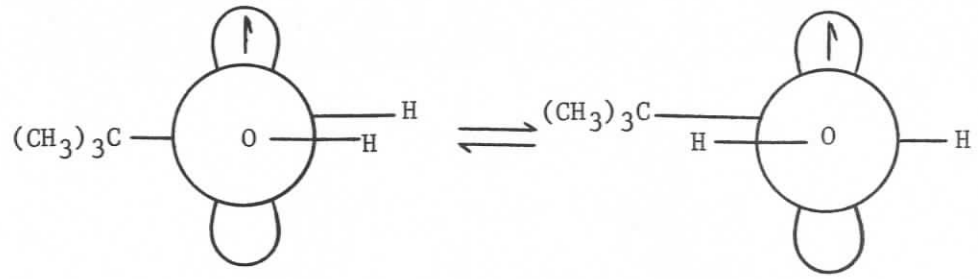

28a 28b

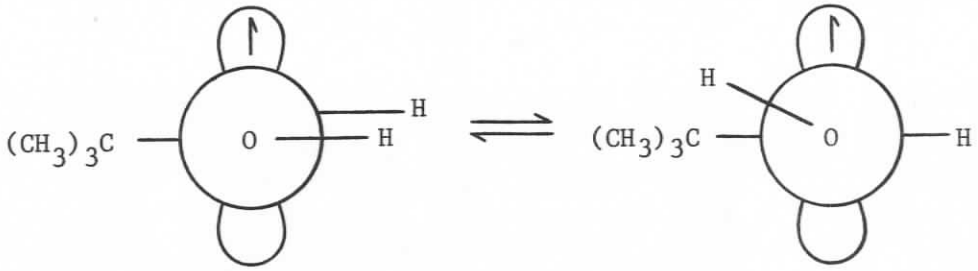

28c 28d

Note that the peaks which broaden when a_{α} and a_{OH} are modulated out-of-phase, are those for which the respective values of $\tilde{M}$ are opposite in sign (Figure 26).

Spectral simulation parameters are tabulated in Appendix A.

(i) Conformation and Long-Range Splittings

The γ-proton hyperfine plitting observed for the 1-hydroxyneopentyl radical (26)(Table 4) is significantly lower than that in neopentyl radical (29a,b). Ingold and Walton[132] have reported that $a_{\gamma H}$ = 0.96 G for the latter species at -48°C. At this temperature there is rapid rotation about the C_{α}-C_{β} bond due to the low sixfold rotation barrier.[132] Therefore θ_{Me} (29a) has an average value of 45°. [The rotational

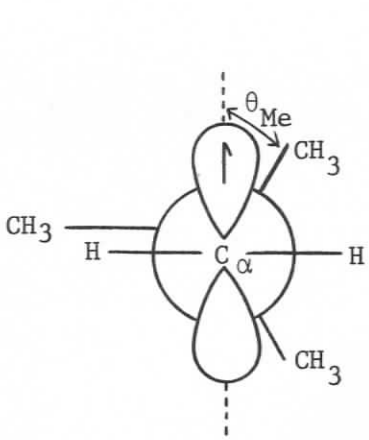

29a

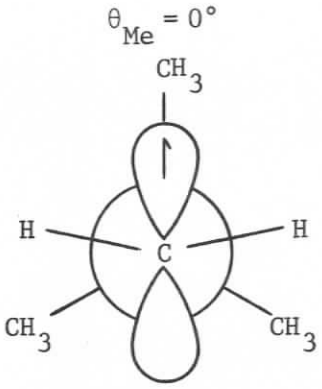

29b

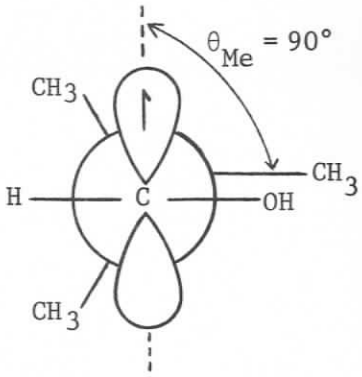

29c

potential minima for neopentyl radical (29a,b) have been calculated[133] to correspond to $\theta_{Me} = 0°$ with the radical center non-planar (29b).] A lower H_γ hfs for 1-hydroxyneopentyl (26) might be anticipated on the basis of spin delocalization to oxygen and increased bending at C_α (see Chapter V) for this species. However, conformational factors are probably also involved.

Karabatsos et al.[134,135] have reported a comprehensive NMR study of conformations of aliphatic aldehydes, some results of which are summarized in Table 5. If these aldehydes can be considered[112] reasonable conformational models for the α-hydroxyalkyl radicals then the preferred conformations of methyl-substituted acetaldehydes (methyl eclipsing carbonyl) suggest preferred conformations at $\theta_{Me} = 90°$ for 1-hydroxyneopentyl (29c).

The non-empirical calculations of Ellinger at al.[32,42] indicate that $a_{\gamma H}$ in n-propyl radical depends not only on θ_{Me} but also on θ_γ (30). The minimum steric interaction occurs for the conformation shown (30), where one hydrogen has $\theta\gamma = 180°$ and two hydrogens have $\theta\gamma = 60°$. Since the barrier to CH_3 rotation in 1-hydroxyneopentyl radical (29c) is

TABLE 5: Preferred conformations of aliphatic aldehydes (T = -30°C)

MONO SUBSTITUTED:

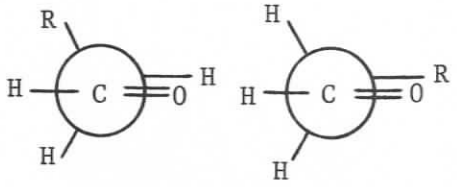

Aldehyde	R	%	%	R-$\dot{C}$H-OH
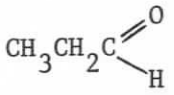	CH_3-	23	77	$CH_3CH_2\dot{C}HOH$
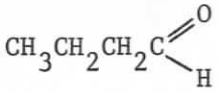	CH_3CH_2-	37	63	$CH_3CH_2CH_2\dot{C}HOH$
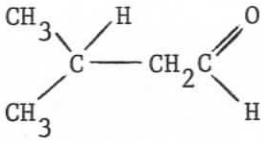	$(CH_3)_2CH$-	48	52	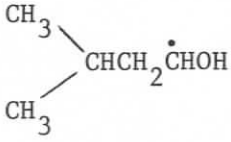
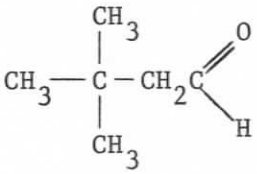	$(CH_3)_3C$-	80	20	$(CH_3)_3CCH_2\dot{C}HOH$

DISUBSTITUTED:

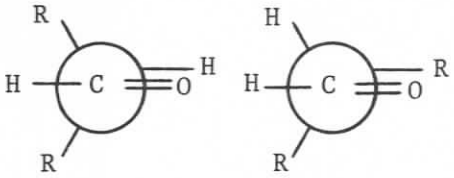

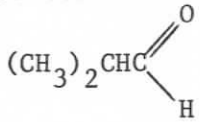	CH_3, CH_3	19	81	$(CH_3)_2CH-\dot{C}HOH$
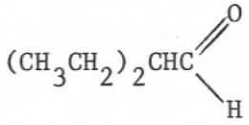	CH_3CH_2 CH_3CH_2	40	60	$(CH_3CH_2)_2CH-\dot{C}HOH$

expected to be larger than that for CH_3 rotation in n-propyl (cf. neopentyl, ref. 132) the CH_3 groups in this species (29c) may be frozen (on the ESR time scale) at temperatures above that at which the methyl of n-propyl freezes out, i.e. at *ca.* -163°C.[132,24] (Therefore it would be interesting to examine the temperature dependence of the splittings of the radical $(CH_3)_3\dot{C}CHOCH_3$. In general the onset of viscosity effects on ether-derived radicals occurs at much lower temperatures making such a study feasible.) Accepting the neopentyl analogy the overall equilibrium conformation of 1-hydroxyneopentyl radical is represented by structure (31)(neglecting, for the moment, C_α bending; see Chapter V). Using

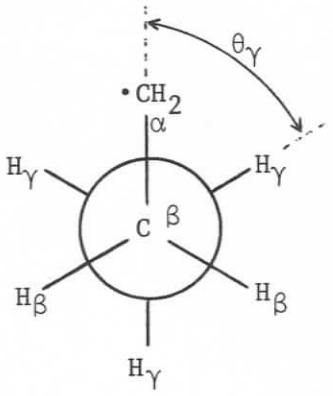

30

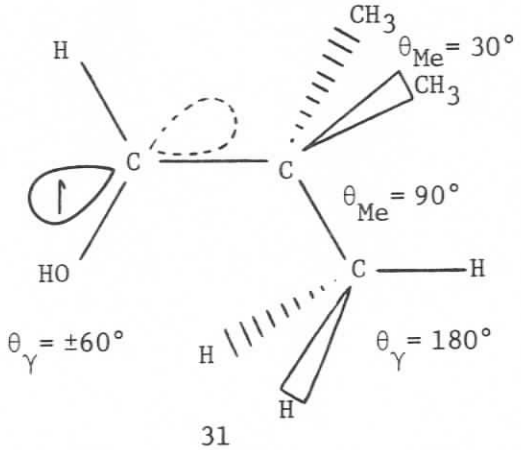

31

this conformation the average a_γ hfs can be calculated. Results based on quasilocalized MO's (see Ellinger et al.,[32] Table XIV) give a_γ(avg) = +0.37 G. This is in good agreement with the experimental value of 0.30 G (Table 4). While these two results are mutually consistent, this degree of agreement is not unique to the conformation $\theta_{Me} = 90°$, as $\theta_{Me} = 0$ gives the same result[32] (+0.37 G). Thus for 1-hydroxyneopentyl radical

(29c) we have only the aldehyde models[134,135] on which to base the notion of a $\theta_{Me} = 90°$ equilibrium geometry.

(b) C_α-OH Rotational Modulation of a_{OH} and $a_{\beta H}$

The results of Krusic et al.[124] for $(CF_3)_2\dot{C}OH$ suggest that restricted C_α-OH rotation should modulate the β-proton hfs in the radical $(CH_3)_2\dot{C}OH$ (32) from 2-propanol. We have indeed observed a selective line broadening pattern.

The spectrum is nominally a septet of doublets (Figure 29). Its expanded scale appearance is complicated by the presence of resolved second order components. This was noted by Livingstone and Zeldes[25] who also pointed out that a_{OH} becomes zero (unresolved) at -22.5°C. They suggested that resolved a_{OH} should reappear at lower temperatures but were unable to observe same at -42°C, the lowest temperature they could achieve with 2-propanol as substrate. Later Giacometti et al.[130] were able to show that a_{OH} for this species does pass through zero on cooling and become resolvable at temperatures below *ca.* -60°C, where it is presumed negative.

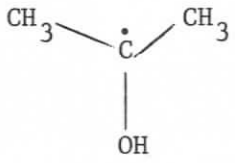

32

While the present results are in agreement with the above (Table 6) the hydroxyl proton splittings appear consistently more negative than those of Giacometti et al.[130] Figure 30 compares the computed and experimental spectra for -23°C (a_{OH} = 0 G). Peaks 1, 2 and 3 (not shown)

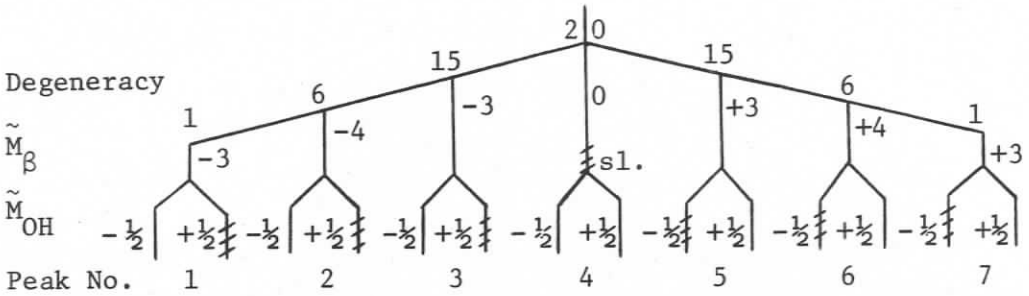

FIGURE 29: Line diagram for ESR spectrum of $(CH_3)_2\dot{C}OH$ (32). Cross-hatched lines are broadened at -90°C.

TABLE 6: Hyperfine splittings of 2-hydroxyprop-2-yl radical (32)

Temp. °C	a_β ±0.4 G	a_{OH} ±0.02 G
-18		+0.14
-23		0.0 |
-26		0.0 | unresolved
-33		0.0 |
-45		-0.18
-70	19.4	-0.37
-90		-0.55
-100		-0.69
-110		-0.80 ± 0.05

have the *same* appearance as peaks 7, 6 and 5 respectively and are not mirror images. Figure 31a shows that the hydroxyl proton hfs is again well resolved at -45°C and becomes more negative as the temperature is decreased. Note that such low temperature second order resolution

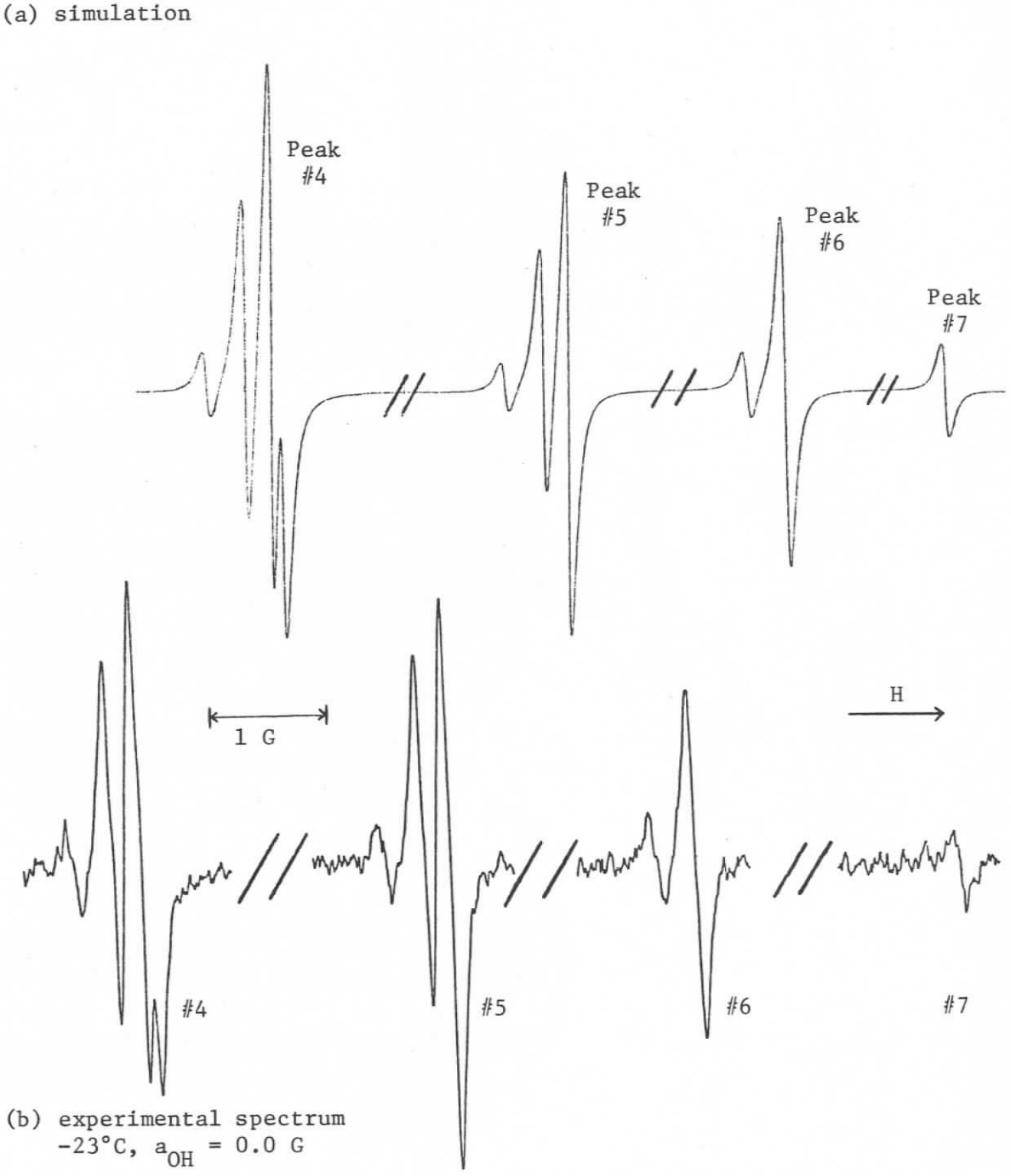

FIGURE 30: (a) Simulation of ESR spectrum of $(CH_3)_2\dot{C}OH$ (32), (b) experimental spectrum at -23°C, a_{OH} = 0.0 G.

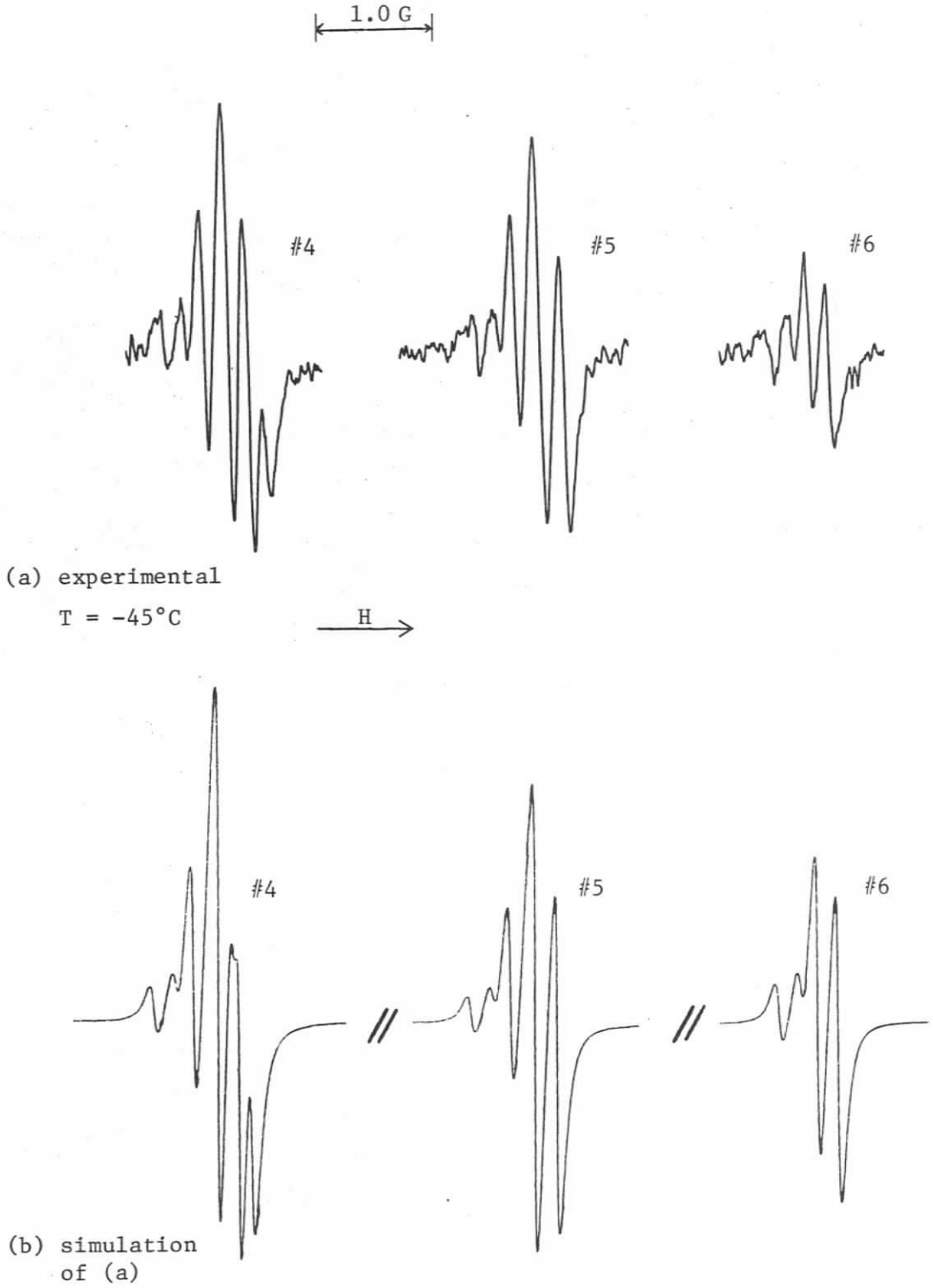

FIGURE 31: (a) Experimental spectrum of $(CH_3)_2\dot{C}OH$ (32) at -45°C (a_{OH} = -0.18 G), (b) simulation of (a). (Figure continues)

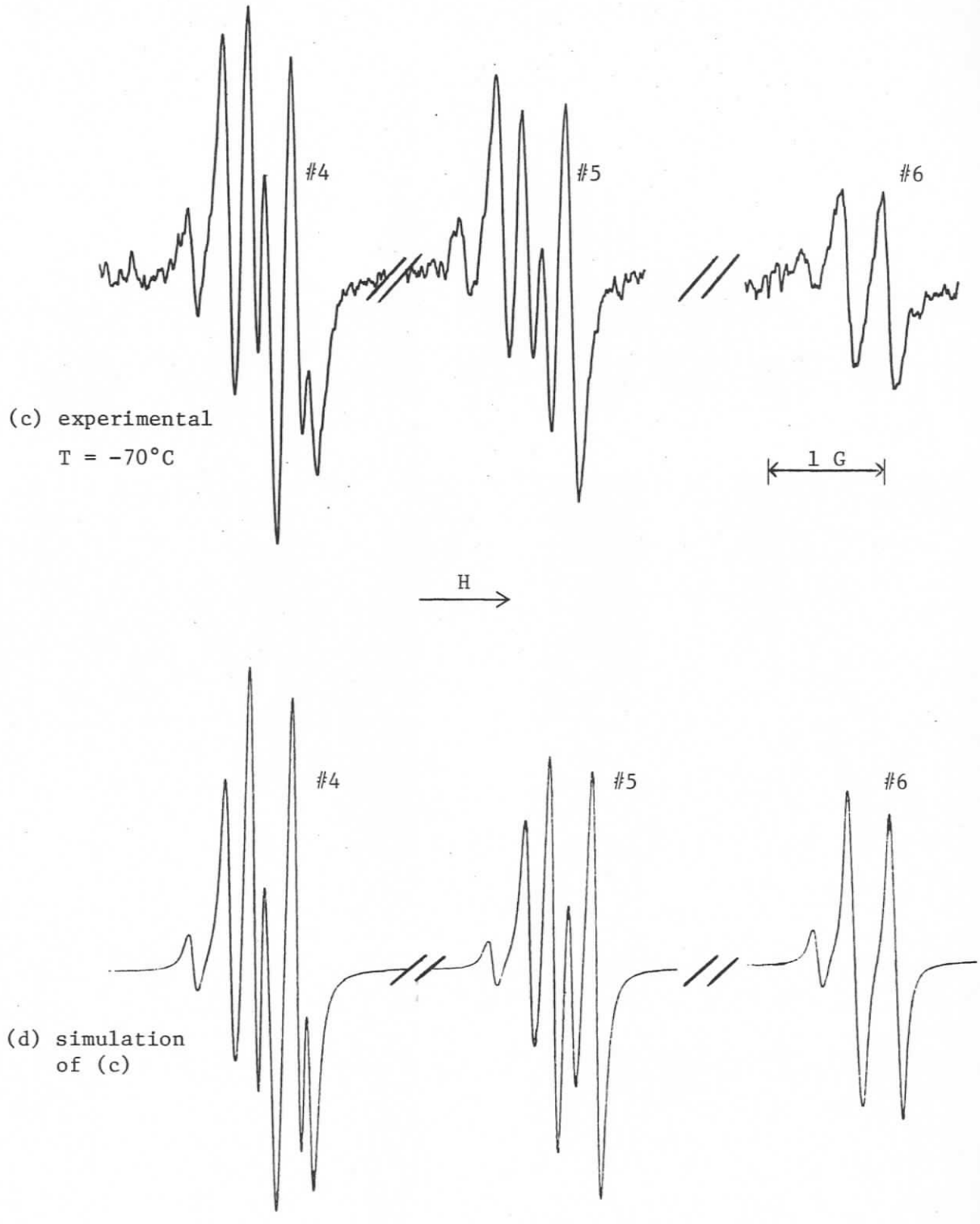

FIGURE 31 (continued): (c) at -70°C (a_{OH} = -0.37 G), (d) simulation of (c).

appears to have been achieved for the first time in the present study for this species. Detection of previously unreported line broadening effects is attributed to the enhanced resolution. At -90°C the inside lines are distinctly broadened (Figure 32), while both components of group no. 4 remain relatively sharp, though reduced in amplitude. Note again that the peaks which broaden initially are those for which $\tilde{M}_{\beta}$ and $\tilde{M}_{OH}$ are opposite in sign. Below -100°C all lines are broadened, undoubtedly due to viscosity effects.

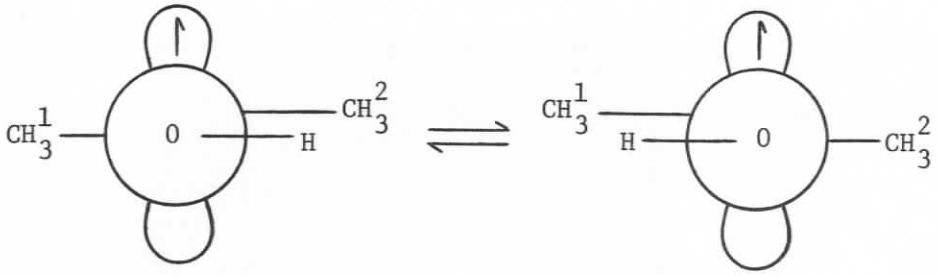

33a 33b

Interestingly, a symmetrical exchange model (33a $\rightleftharpoons$ 33b) in which a_{OH} is the same in the two coplanar potential minima does not allow simulation of the observed broadening pattern, and in fact very different results are obtained (components 2, 4 and 6 are all broadened completely). A model which does give the observed broadening is 34a $\rightleftharpoons$ 34b, which involves low-energy conformers in which the hydroxyl proton is twisted slightly out of the C_{β}-C_{α}-O plane. This is reasonable since the average splitting is positive above -23°C and increases with temperature. Figure 33 shows simulations of the observed broadening pattern based on the two-site exchange 34a $\rightleftharpoons$ 34b with

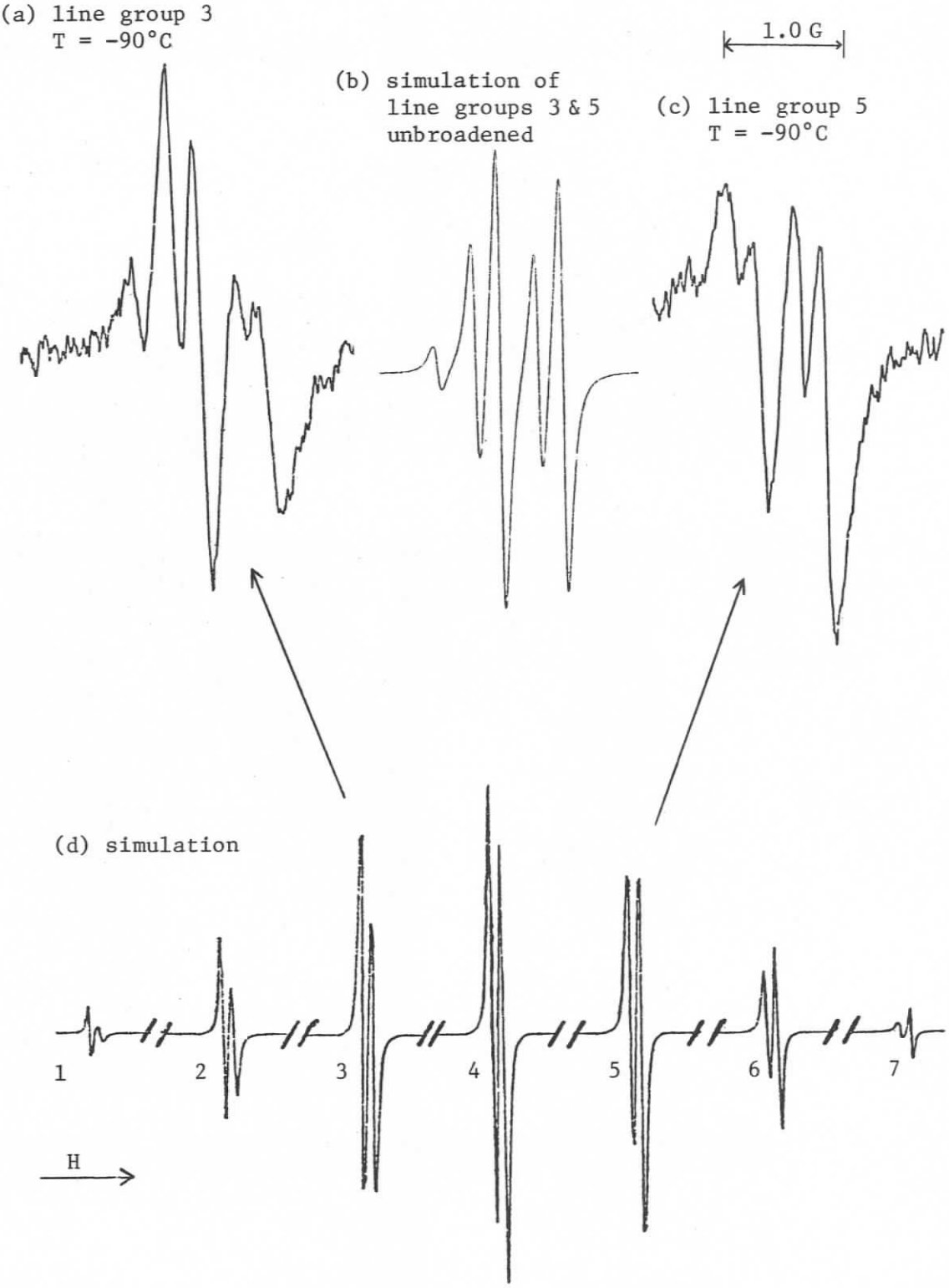

FIGURE 32: Line broadening in the ESR spectrum of $(CH_3)_2\dot{C}OH$ (32). Figure (d) is a simulation of the entire spectrum showing the onset of line broadening in the absence of second order hfs. (continued on following page)

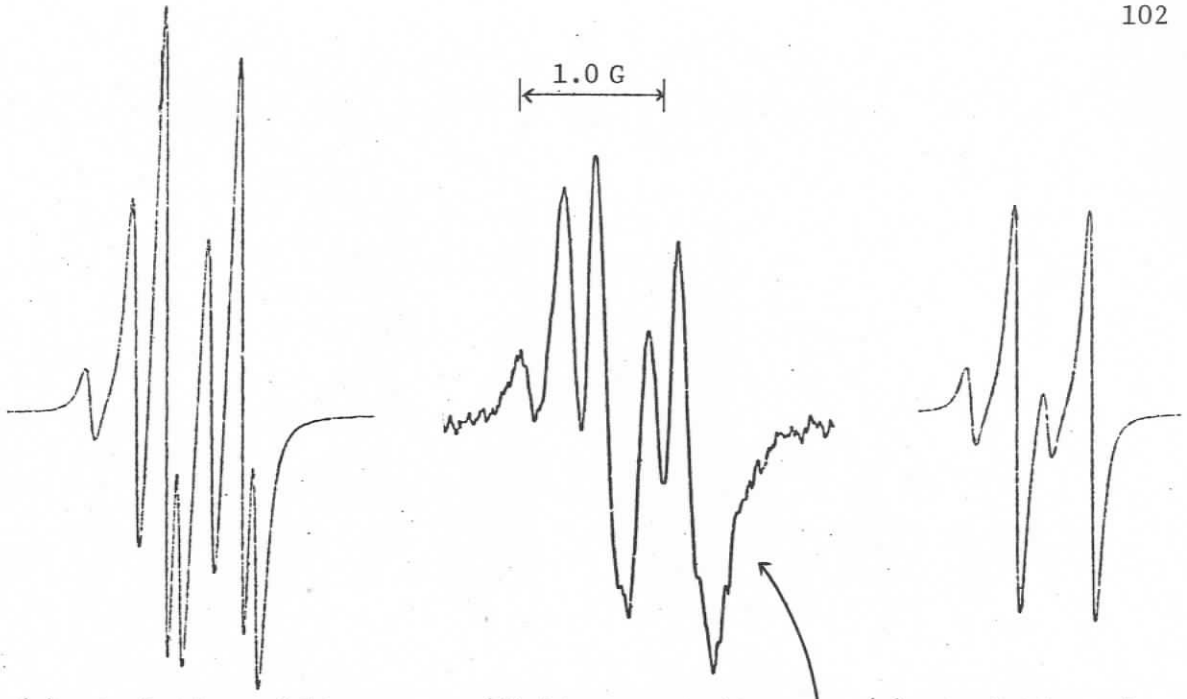

(e) simulation of line group 4 at -90°C

(f) line group 4 T = -90°C

(g) simulation of line group 6 at -90°C

FIGURE 32 (continued): N.B. Line group 4 was scanned at next lower gain and next higher modulation amplitude compared to lines 3 and 5.

(h) line group 6 T = -90°C

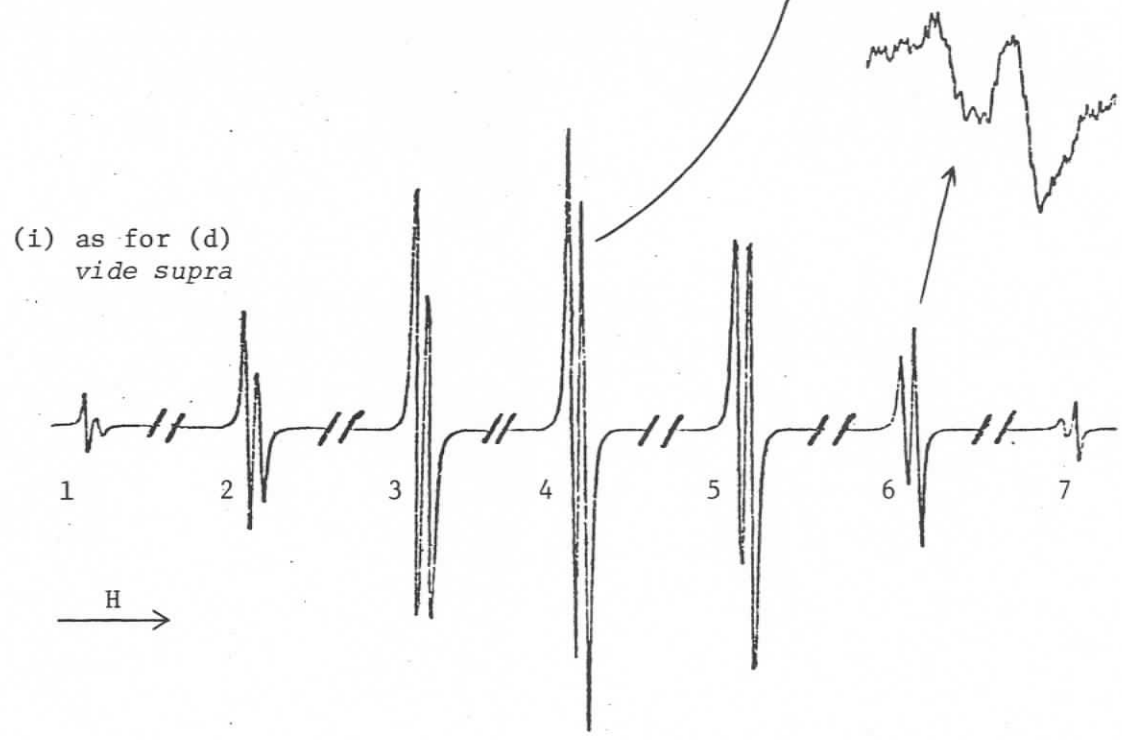

(i) as for (d) *vide supra*

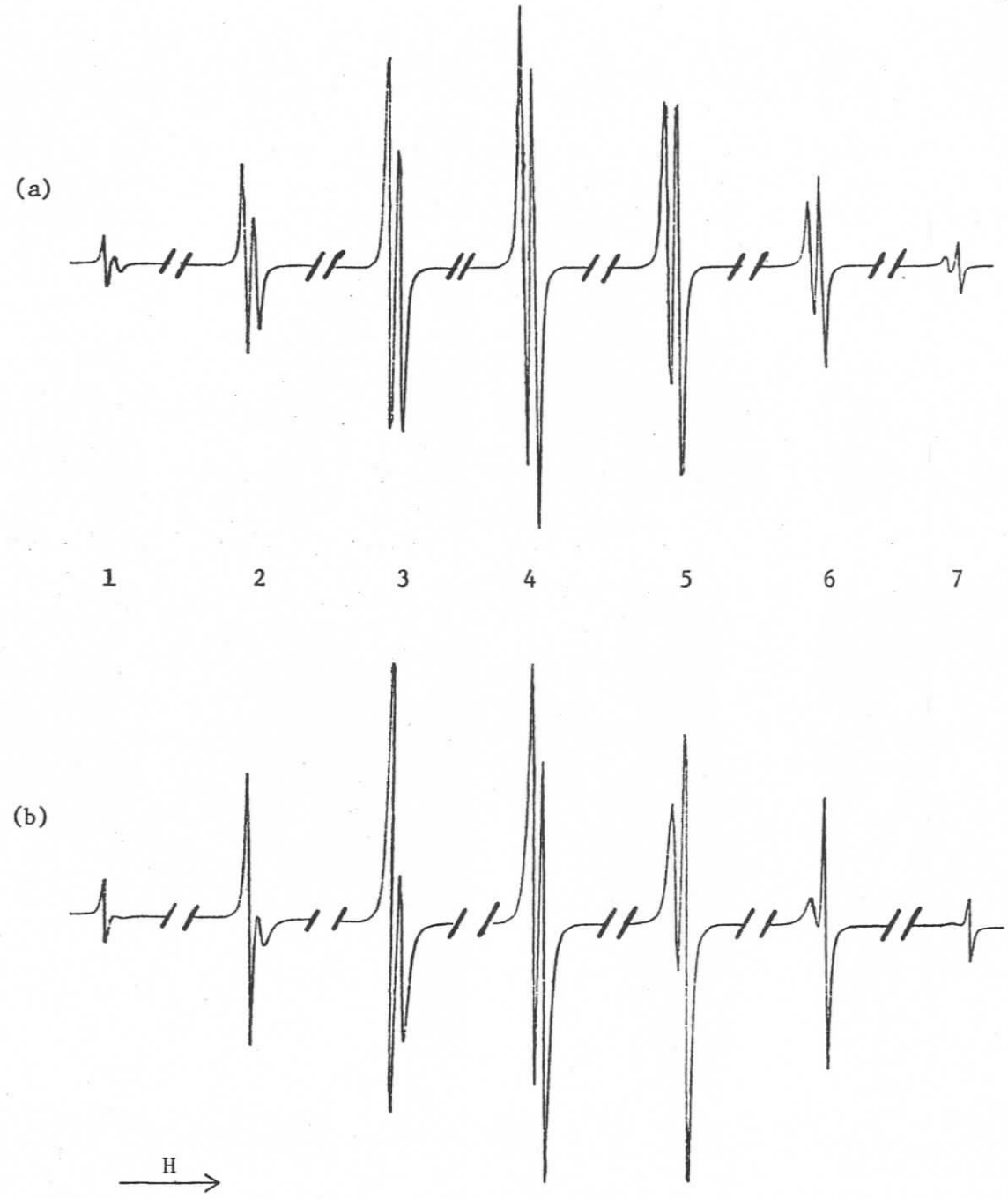

FIGURE 33: (a) Simulated spectra for two-site out-of-plane exchange for 2-hydroxyprop-2-yl radical (34). (b) Same simulation at a slower exchange rate (see Appendix A).

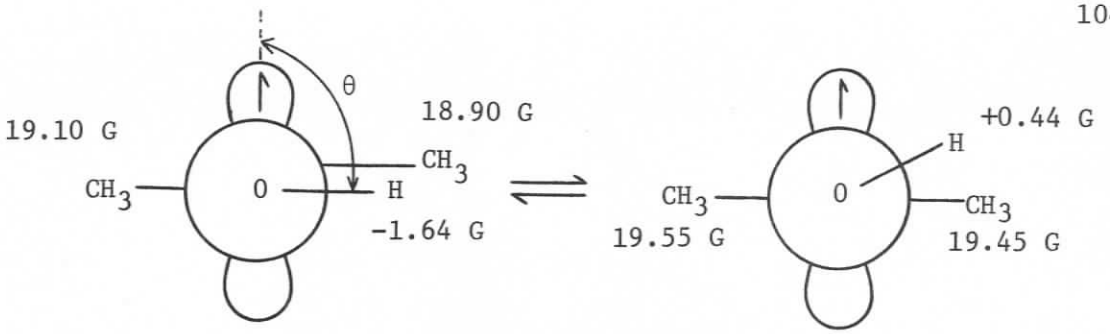

34a 34b

splittings as shown (see also Appendix A). The lowest value of a_{OH} (-1.64 G) is that used in the calculations of Krusic et al.[57] for θ = 90° in the planar hydroxymethyl radical. The other a_{OH} value (0.44 G) was chosen so that the average hydroxyl proton hfs, assuming equally populated conformers, was equal to the experimentally observed value. In the model illustrated the β protons have non-equivalent hfs when θ = 90° (34a)(*cf.* Krusic[57,124]). When $\theta \neq 90°$ (34b) the H_β splittings are increased, and the methyl protons *transoid* to the hydroxyl proton are assigned a slightly higher splitting than the protons of the *cisoid* methyl group. This is reasonable in terms of the expected spin density distribution. Note that in the simulation the "inside" lines broaden and the amplitude of the center multiplet (line group 4) is diminished relative to that of its neighbours (line groups 3 and 5). The extent of agreement with experimental observations is not affected by small changes in any of the splittings. Changes in spin density due to C_α bending are ignored in this simple model.

The logical extension of this is the six-site model (structures 35a-f, page 105). Simulation on this basis produce the same broadening pattern (Appendix A).

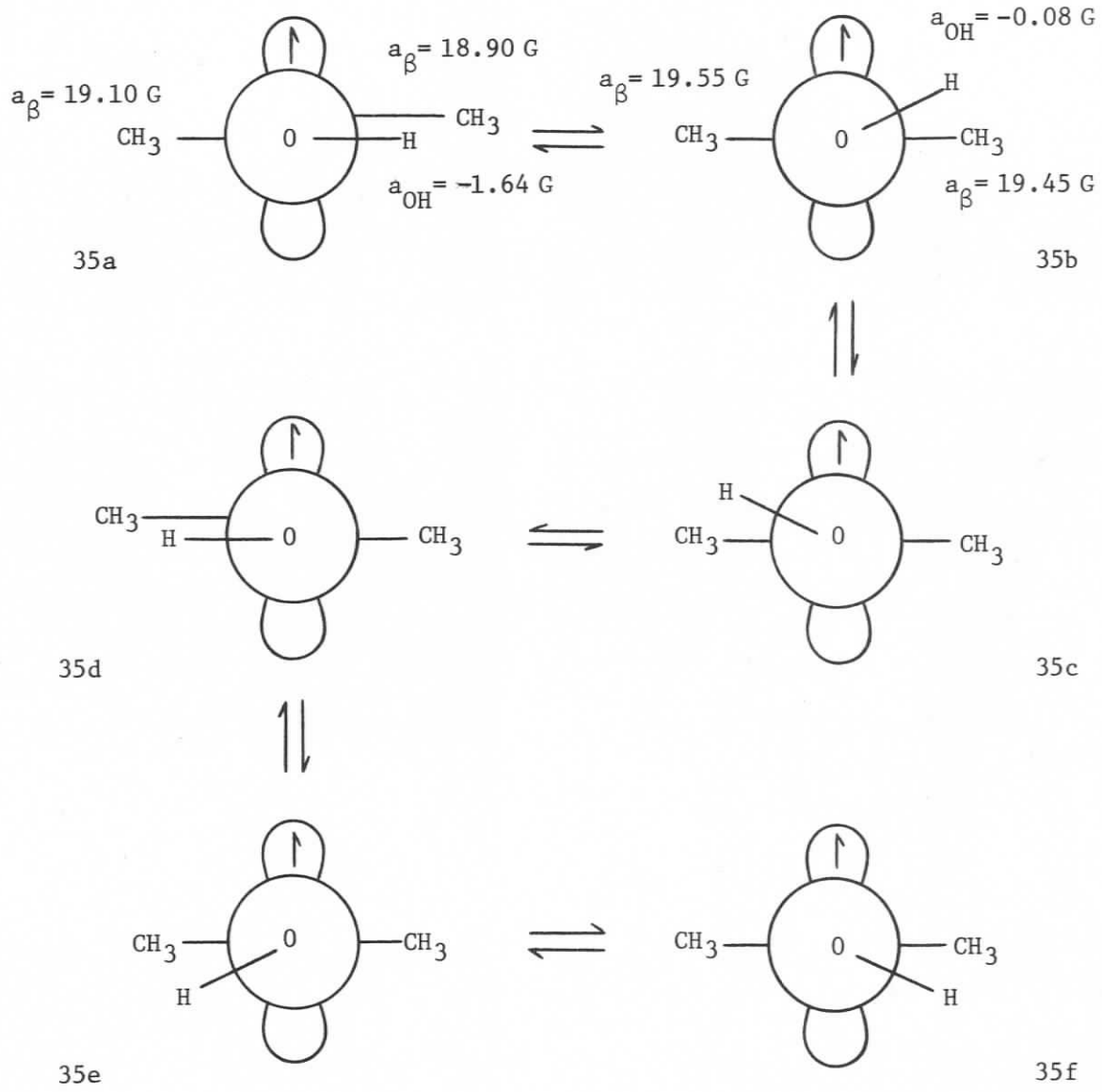
a_β= 19.10 G
a_β= 18.90 G
a_{OH}= -1.64 G
a_β= 19.55 G
a_{OH}= -0.08 G
a_β= 19.45 G
35a
35b
35c
35d
35e
35f

Thus not only do we observe modulation of a_β and a_{OH} by restricted hydroxyl group rotation but also the data support the notion of important rotational potential minima at angles θ other than 90°.

(c) C_α-OH Rotational Modulation of a_α, a_β and a_{OH}

(i) 1-Hydroxyethyl Radical

While Livingstone et al.[25] did not report linewidth effects in the ESR spectrum of 1-hydroxyethyl radical (36) down to -70°C they were able to resolve the second order splittings. The hydroxyl proton splitting was observed to pass through zero at *ca.* 30°C.[25] It becomes positive at higher temperatures.[130]

$$CH_3 - \dot{C}H - OH$$

36

In this work, low temperature ESR spectra of 1-hydroxyethyl radical (36) exhibit comparable splittings (Table 7), but at temperatures below *ca.* -80°C specific linewidth effects attributable to restricted C_α-OH rotation were observed. Figure 34 is the spectrum of $CH_3\dot{C}HOH$ (36) at -60°C along with a line diagram showing the observed low temperature line broadening pattern. Experimental and simulated spectra are shown in Figure 35 and Figure 36 respectively. The simulation, based on a model (e.g. 37a $\rightleftharpoons$ 37b) in which a_{OH} and a_α are modulated out-of-phase

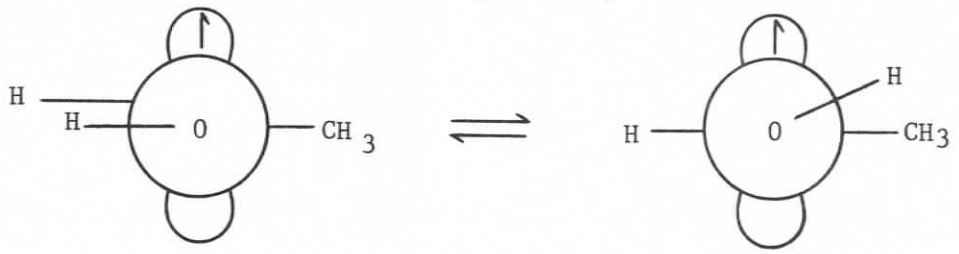

37a 37b

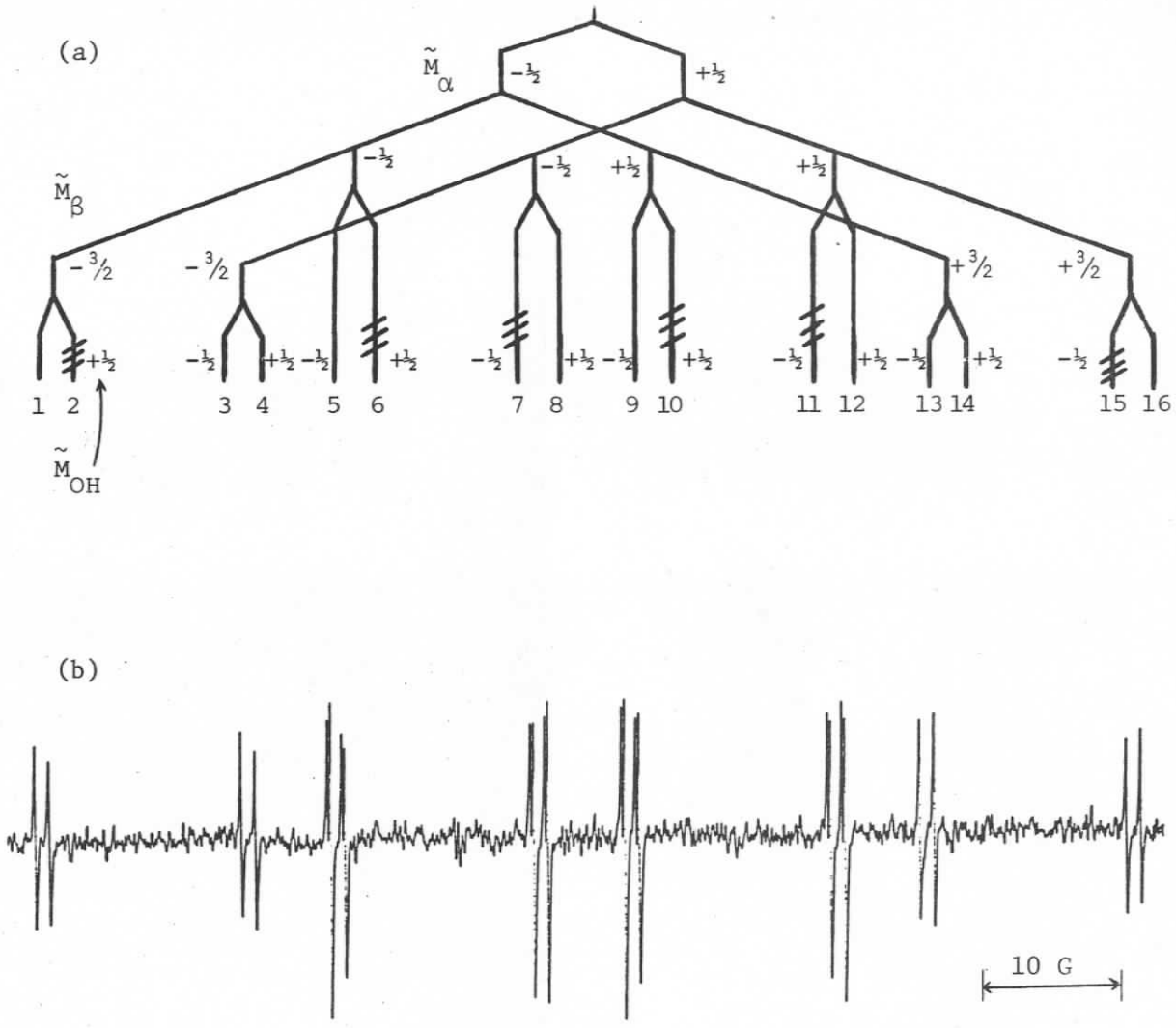

FIGURE 34: (a) Line diagram of ESR spectrum of $CH_3\dot{C}HOH$, not to scale. Broadened peaks are cross-hatched. (b) ESR spectrum of $CH_3\dot{C}HOH$ at -60°C.

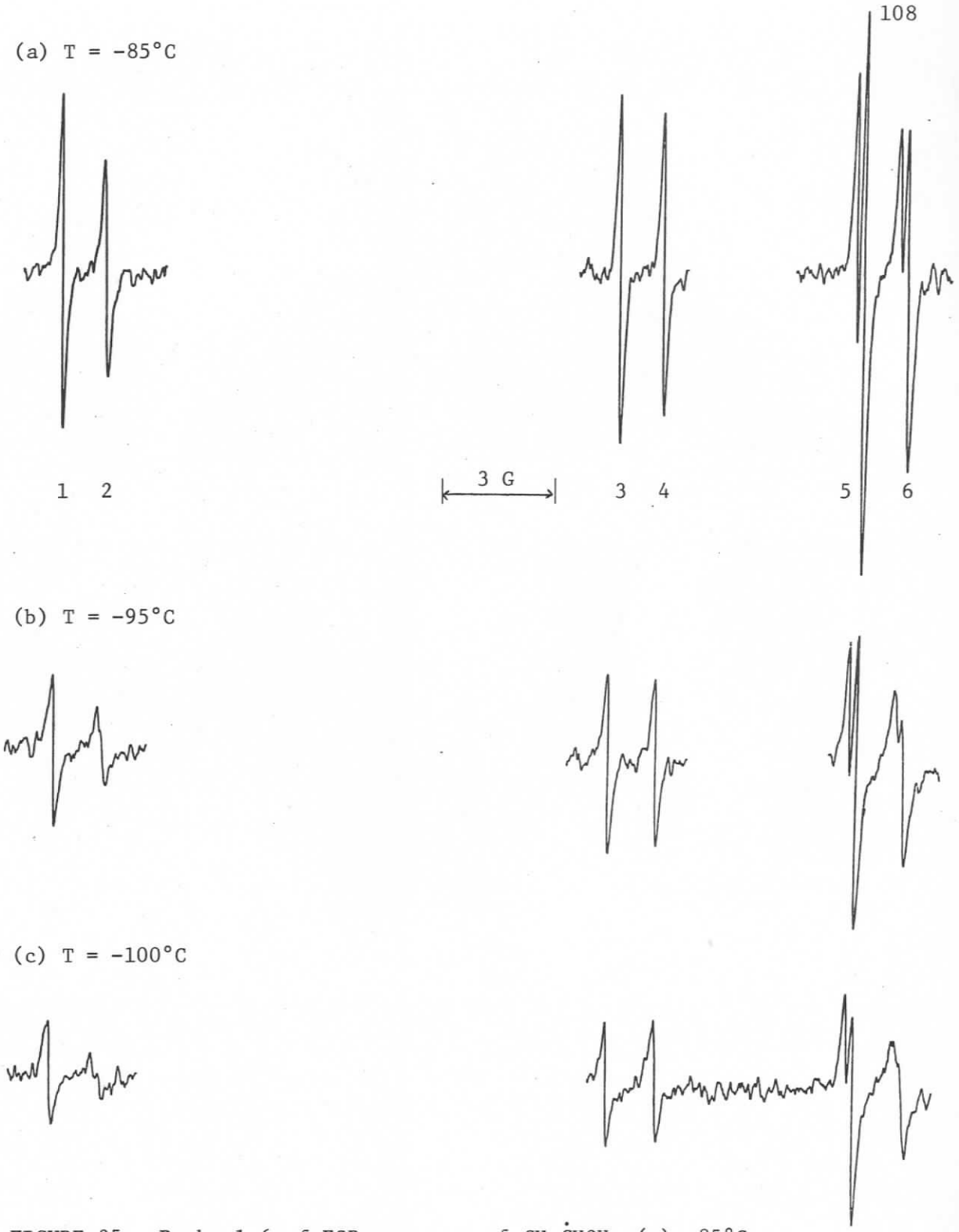

FIGURE 35: Peaks 1-6 of ESR spectrum of $CH_3\dot{C}HOH$, (a) -85°C, (b) -95°C, (c) -100°C. (Figure continues)

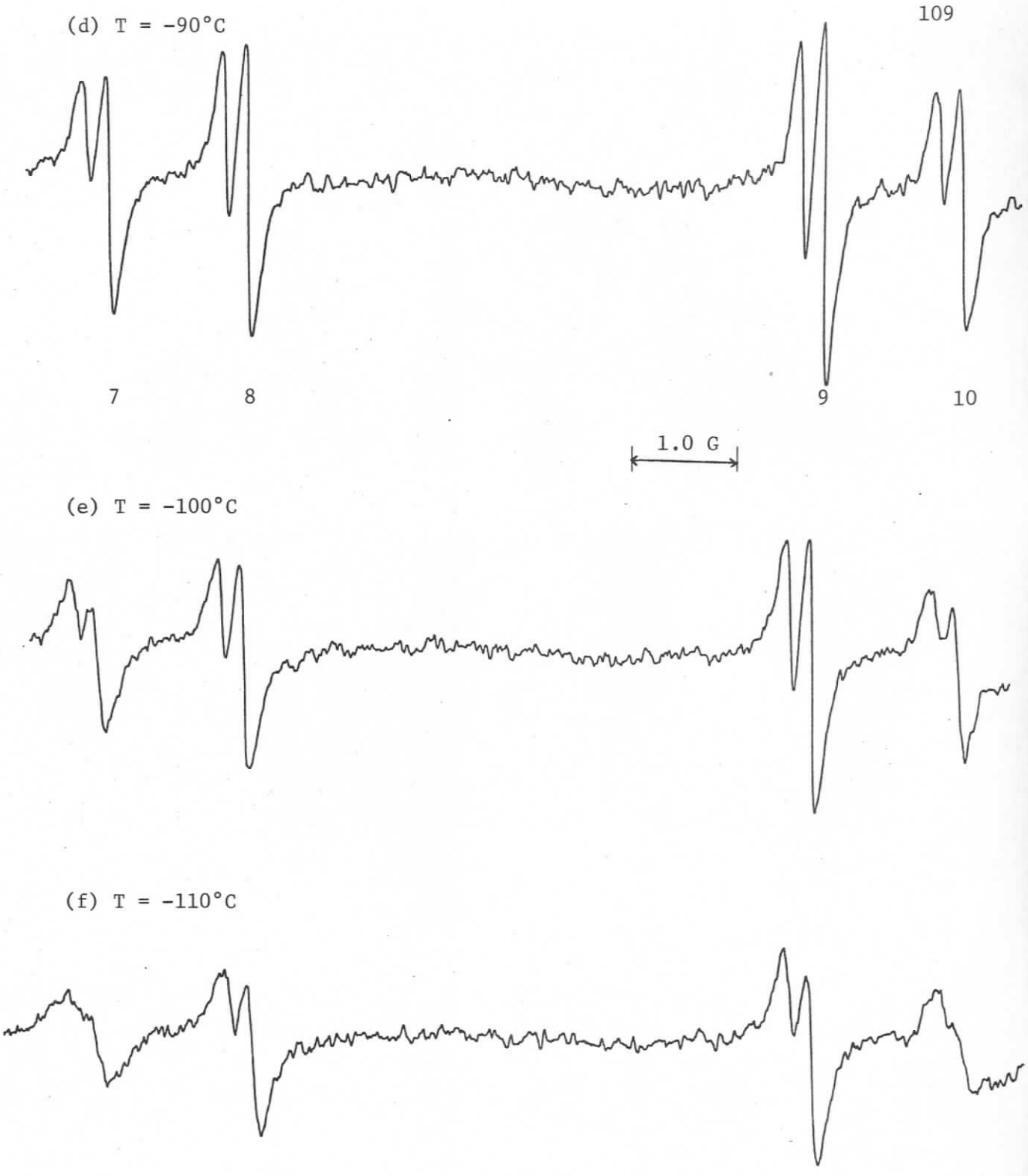

FIGURE 35 (continued): Peaks 7-10 of ESR spectrum of $CH_3\dot{C}HOH$, (d) at -90°C, (e) at -100°C, (f) at -110°C. Second order structure is clearly resolved.

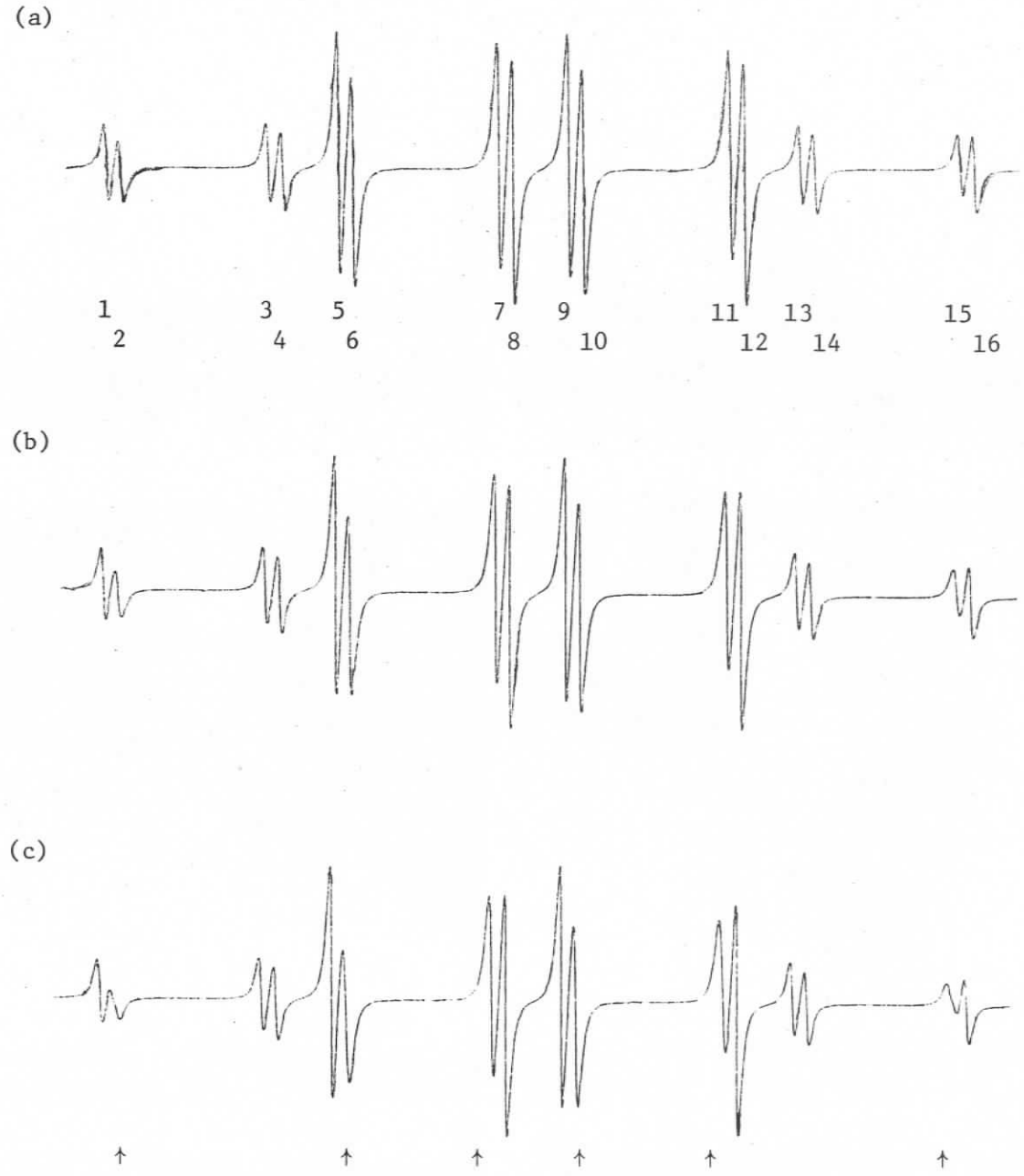

FIGURE 36: Simulation of ESR spectrum of $CH_3\dot{C}HOH$ based on modulation of a_α, a_β and a_{OH} by restricted C_α-OH rotation. Spectra a, b and c are at successively decreasing exchange rates (see Appendix A).

TABLE 7: Hyperfine splittings of 1-hydroxyethyl radical (36)

Temp. °C	$-a_{\alpha}$	$a_{\beta H}$	$-a_{OH}$
+20	15.1 ±0.2	21.9 ±0.2	not resolved ±0.02
+10			0.40
0.0			0.49
-10			0.60
-20			0.70
-30			0.82
-40	15.2 ±0.2	22.0 ±0.2	0.89
-60	15.30±0.2	22.1 ±0.2	1.04
-70	15.30±0.05	22.07±0.05	1.11
-80	15.33±0.05	22.11±0.05	1.25±0.05
-90	15.33±0.05	22.17±0.05	1.31±0.05
-100	15.33±0.10	22.11±0.05	1.35±0.05
-110	15.4 ±0.20	22.2 ±0.2	1.48±0.05

and a_{OH} and a_{β} are modulated out-of-phase reproduces the observed broadening pattern and the fact that the peaks in question are affected to different extents. (For simulation parameters see Appendix A.)

Anisotropic broadening which depends, *inter alia*, on $\tilde{M}^2$, sets in below *ca.* -120°C, although at this temperature second order splitting is still resolved (linewidth = 0.18 G).

Adams[129] concluded that for some simple 1-hydroxyalkyl radicals, including radical (36), there is no restriction to C_{α}-C_{β} rotation at room temperature. Our data show that a_{α} and a_{β} for $CH_3\dot{C}HOH$ (36) are virtually invariant over the whole temperature range (Table 7).

The thesis that the linewidth effects are specifically due to restricted C_α-OH rotation, and that restricted C_α-C_β rotation is not involved, is supported by the ESR spectrum (Figure 37) of $CH_3CH_2\dot{O}CHCH_3$ (from diethyl ether) which shows no linewidth effects even at -140°C. (For splittings, see Table 8.) This is because the rotation of an alkoxy group is not effectively restricted due to the larger angular momentum compared to a proton.

TABLE 8: Hyperfine splittings of $CH_3CH_2\dot{O}CHCH_3$

Temp. °C	$-a_\alpha$	a_β	$\lvert a_\gamma, \rvert$
	±0.1	±0.1	±0.1
-30	13.65	21.35	1.6
-40	13.85	21.35	1.65
-50	13.80	21.35	1.65
-80	13.85	21.55	1.7
-100	13.95	21.50	1.85
-130	14.1	21.6	1.85
-145	14.1	21.55	1.9

(ii) 1-Hydroxyprop-1-yl Radical

The ESR spectrum (Figure 38) of 1-hydroxyprop-1-yl radical (38) at -40°C (for example) shows well resolved hyperfine splitting (Table 9) from all protons. The additional hyperfine structure in the $\tilde{M}_\beta = 0$ multiplets is due to resolution of second order splittings (Figure 38a).

$CH_3CH_2\dot{C}HOH$

38

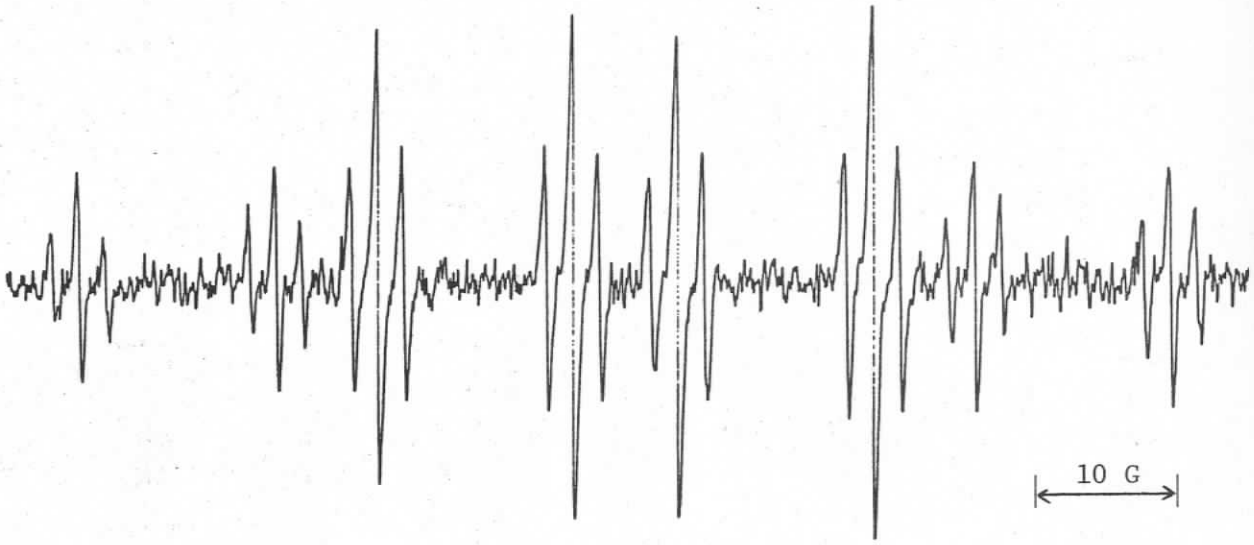

FIGURE 37: ESR spectrum of $CH_3CH_2O\dot{C}HCH_3$ at -140°C.

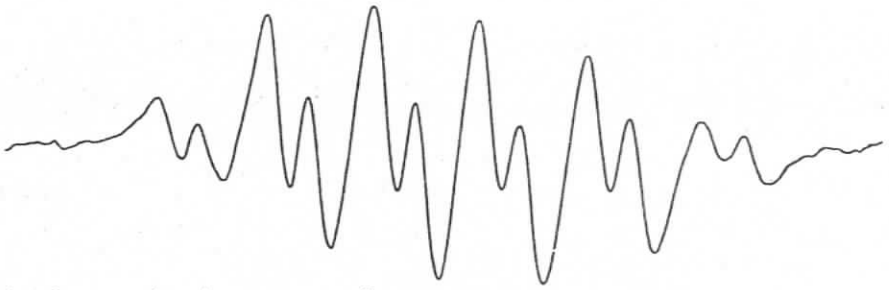

(a) high resolution scan of line group 3. The 1st order lines are twinned by 2nd order components. T = -40°C

0.5 G

(b) experimental, T = -40°C

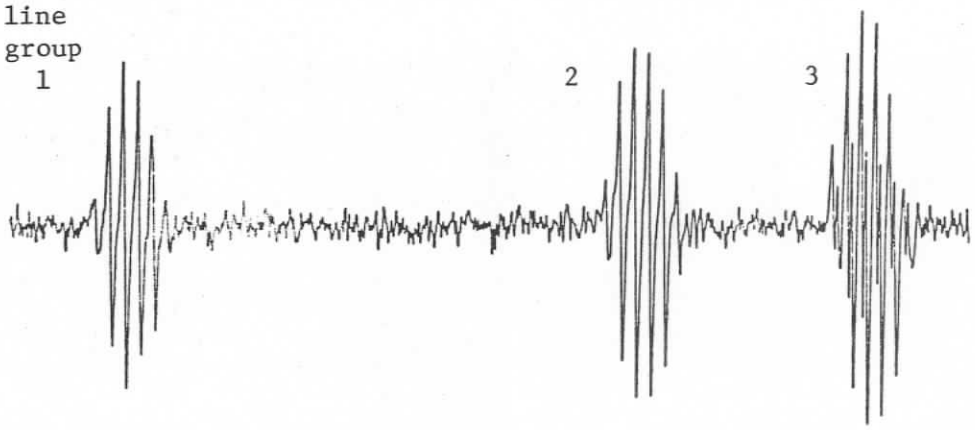

(c) simulation of (b)

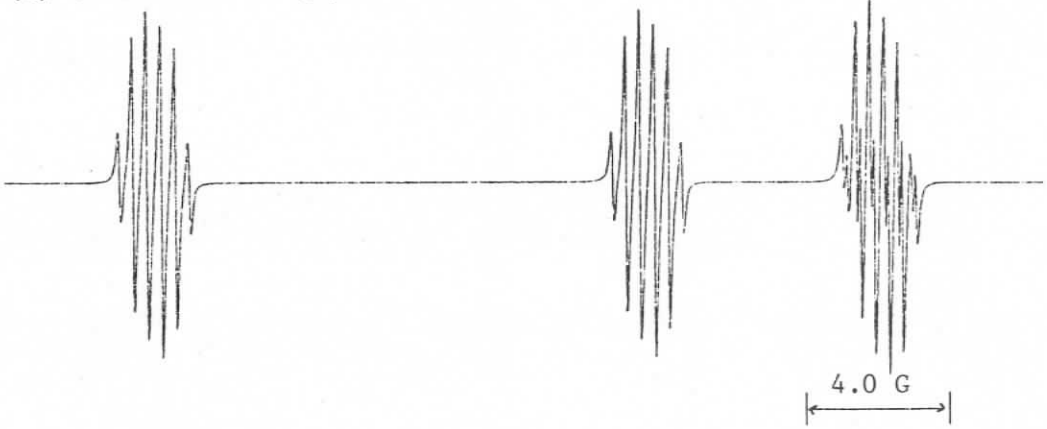

FIGURE 38: Low-field half of ESR spectrum of $CH_3\dot{C}H_2CHOH$ (38) at -40°C showing a high resolution scan of the line group having second order structure. The spectrum, with 2nd order splittings, is simulated in (c).

TABLE 9: Hyperfine splittings for 1-hydroxyprop-1-yl radical

Temp. °C	$-a_\alpha$	a_β	$\lvert a_\gamma \rvert$	$-a_{OH}$	$a_{2nd\ order}$
	±0.05	±0.05	±0.05	±0.05	±0.05
+20	14.68	20.9	0.37	0.40	
+10	14.74	21.12	0.42	0.38	
0	14.82	21.20	0.40	0.45	
-10	14.84	21.30	0.36	0.65	
-20	14.85	21.47	0.39	0.70	
-30	14.88	21.52	0.43	0.78	
-40	14.90	21.69	0.41	0.87	0.13
-50	14.97	21.88	0.45	0.97	
-60	14.94	21.89	0.44	1.08	
-70	14.94	22.07	0.42	1.12	
-80	14.94	22.22	0.44	1.20	
-90			0.50	1.30	

It is not necessary to invoke magnetic inequivalence to the β-protons as suggested by Livingstone et al.[25]

As the temperature was decreased some lines of the spectrum were broadened (Figure 39), and at different rates. Again restricted rotation of the hydroxyl group with a twofold potential minimum (e.g. 39a $\rightleftharpoons$ 39b) is a sufficient model for simulation of the observed effects.

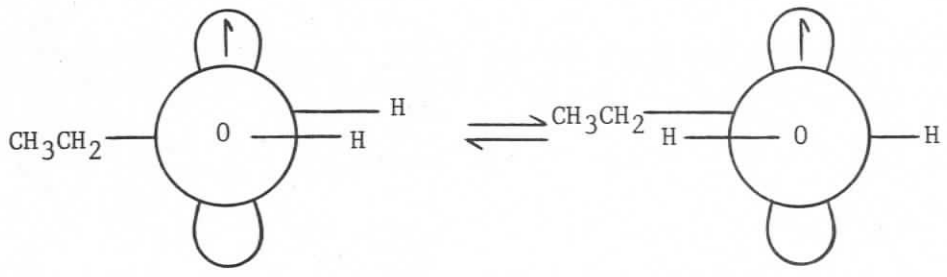

39a 39b

Experimental and calculated spectra are shown in Figures 40 and 41 respectively. Recall that the ESREXN program does not calculate second order splittings. (Simulation parameters in Appendix A.)

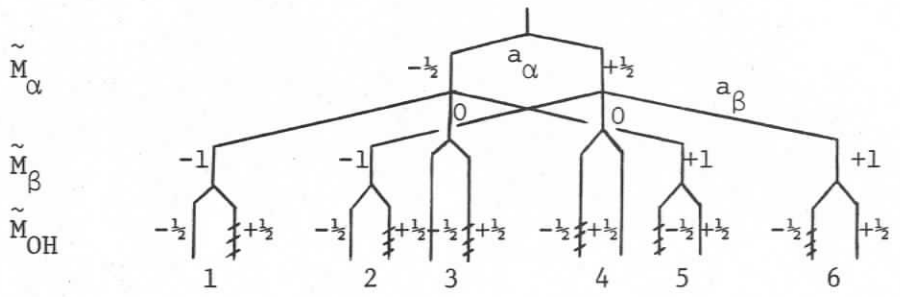

FIGURE 39: Line diagram for ESR spectrum of $CH_3\dot{C}HCH_2OH$. Gamma hfs omitted. Cross-hatched lines are broadened at low temperatures.

The line broadening pattern observed for this radical (38) is repeated in later examples which also have two β protons (i.e. contrast 2-hydroxyprop-2-yl, 1-hydroxyethyl).

In order to determine that anisotropic effects were not a major contributor to the broadening, a more dilute ($\leqslant ca.$ 0.4 M) sample of n-propanol in cyclopropane was prepared. The same effects were observed in its spectrum and sample life was significantly reduced.

At -90°C, however, anisotropic effects are manifest by the lack of second order resolution and by the complete disappearance of line group 1 (and 6, not shown)(Figure 40c).

We do not consider that any modulation effects arise from restricted C_α-C_β rotation (i.e. α-β rotation is unrestricted on the ESR time scale).

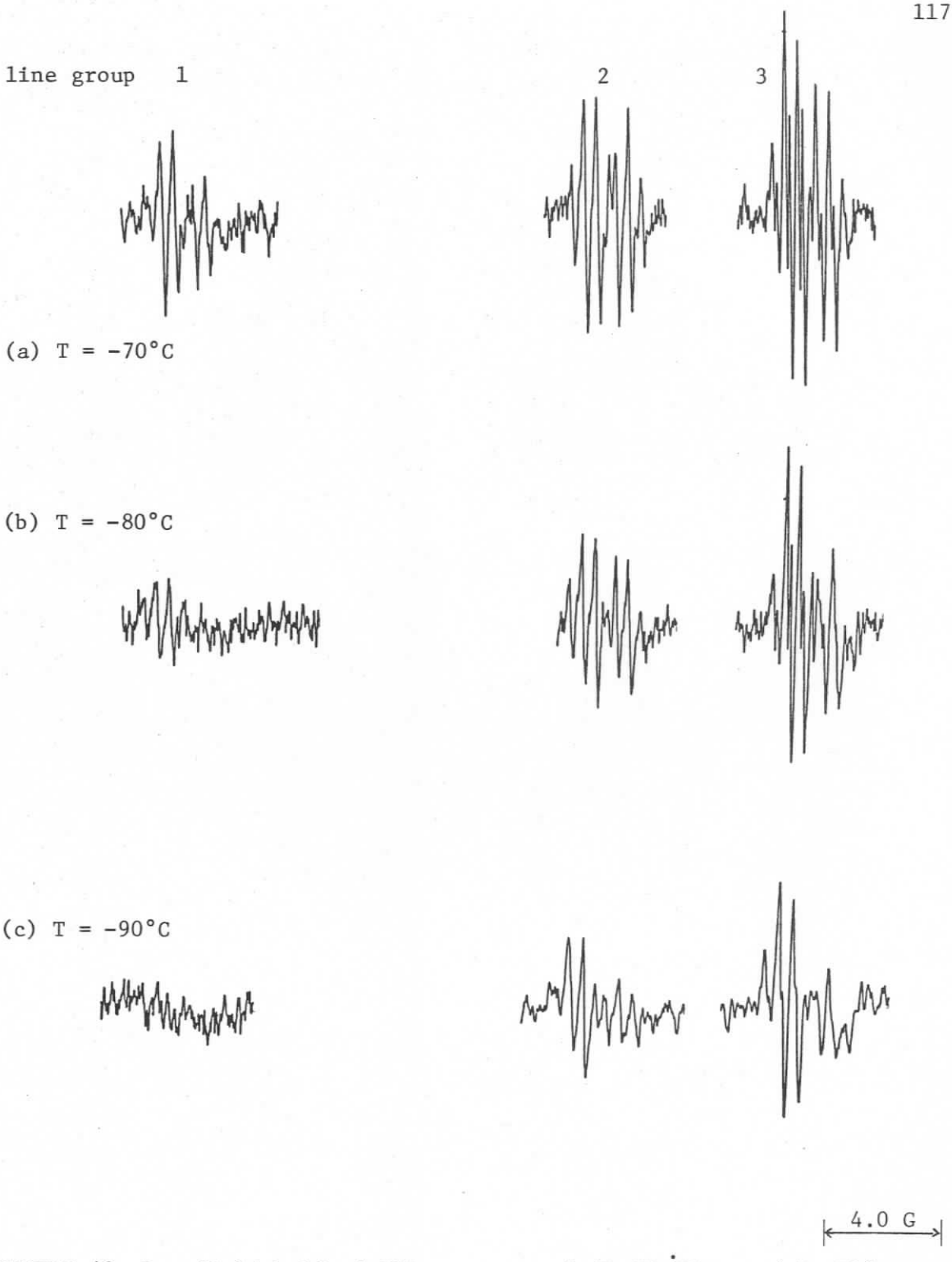

FIGURE 40: Downfield half of ESR spectrum of $CH_3CH_2\dot{C}HOH$ at (a) -70°C, (b) -80°C, (c) -90°C. Note that at -90° line groups 1 (and 6, not shown) are completely broadened by viscosity effects.

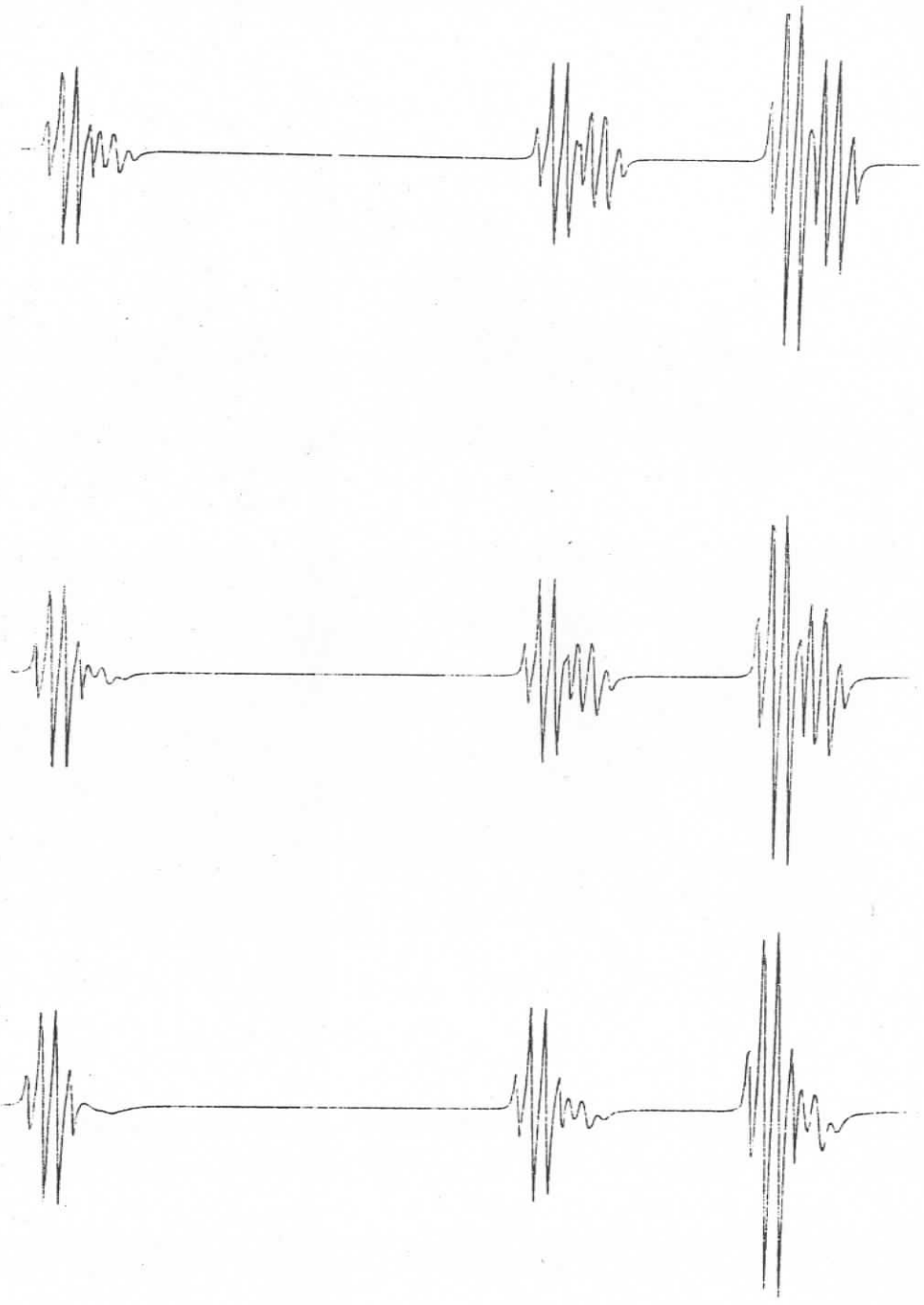

FIGURE 41: Simulation of low temperature ESR spectrum (low field half) of $CH_3CH_2\dot{C}HOH$. Rate constant for exchange decreases from top to bottom. Compare Figure 40.

The ESR spectrum (Figure 42) of the radical (40) from di-n-propyl ether shows no similar linewidth effects even at -120°C. The slight broadening of the $\tilde{M}_\beta = 0$ components at this temperature is probably due to

$$CH_3CH_2CH_2O\dot{C}HCH_2CH_3$$

40

incompletely resolved second order structure, as a_β increases with decreasing temperature (Table 10).

TABLE 10: Hyperfine splittings of $CH_3CH_2\overset{\gamma'}{C}H_2O\dot{C}H\overset{\beta}{C}H_2\overset{\gamma}{C}H_3$ (40) (g = 2.00331)(a_δ unresolved)

Temp. °C	a_α	a_β	$\lvert a_\gamma \rvert$	$\lvert a_{\gamma'} \rvert$
	±0.08	±0.08	±0.08	±0.08
-40	-13.60	20.36	0.44	1.68
-60	-13.56	20.50	0.40	1.72
-80	-13.60	20.84	0.44	1.76
-100	-13.64	21.30	0.52	1.80
-120	-13.84	21.84 *	0.56	1.88

* Calculated 2nd order splitting = 0.142 G @ -120°

Finally, in support of the proposal that the linewidth effects in the alcohol-derived radicals discussed to this point are not due to restricted C_α-C_β rotation, we note that Kochi et al.[3] observed no selective line broadening in the spectrum of $CH_3\dot{C}HF$ between -20°C and -140°C.

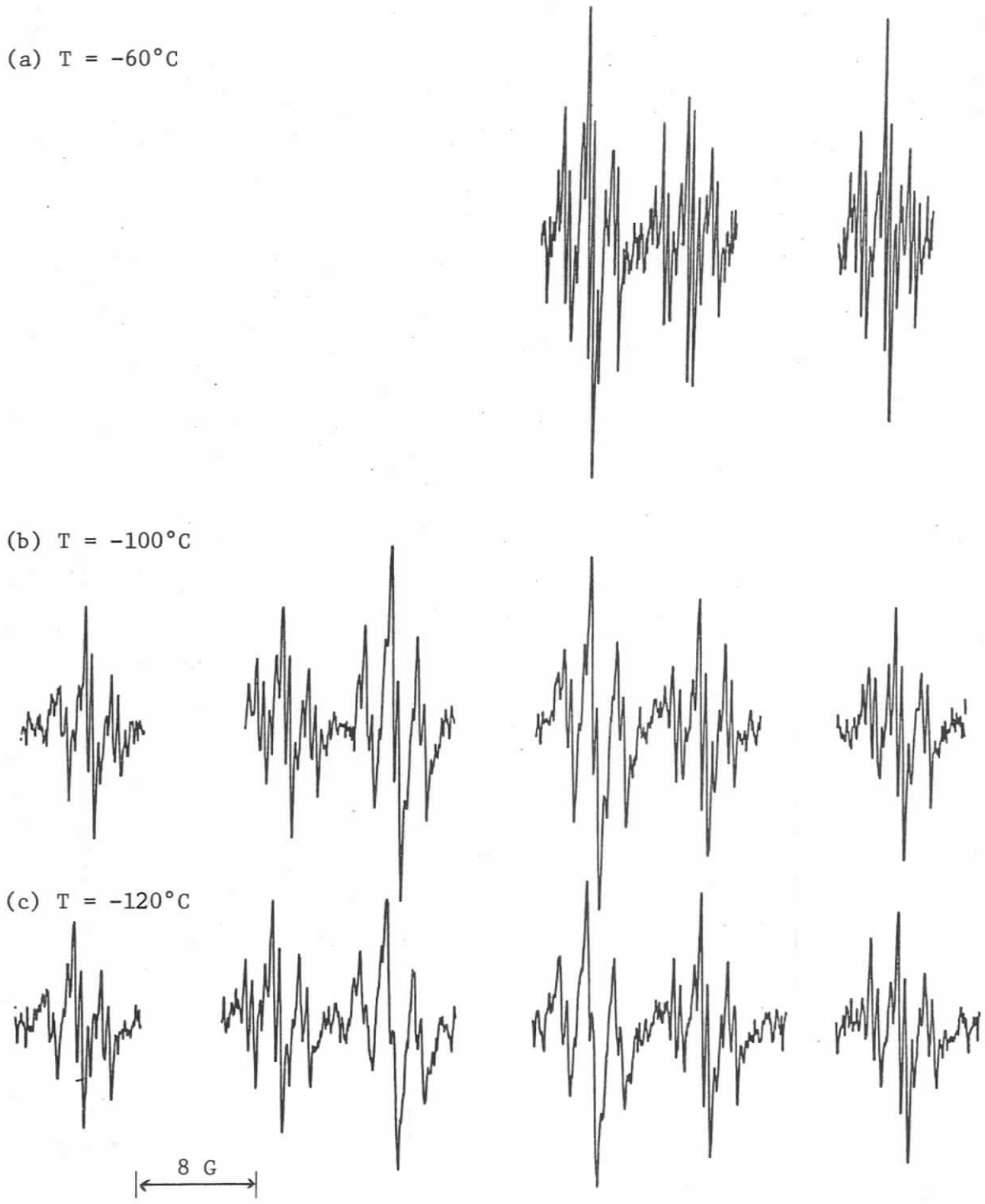

FIGURE 42: ESR spectrum of $CH_3CH_2CH_2O\dot{C}HCH_2CH_3$ (a) high field half of spectrum at -60°C, (b) whole spectrum at -100°C, (c) -120°C.

Conformation and Long-Range Splittings. In Chapter I the angular dependence of β-proton hyperfine splittings was described in terms of the commonly accepted equation 14, where B_o is usually assigned a low

$$a_\beta = B_o + B\cos^2\theta \qquad (14)$$

value and neglected. For discussions of alcohol radical conformations which utilize this relationship the constant B is calculated from the high temperature value of a_β for 1-hydroxyethyl radical (Table 7) as the splitting in the limit of free rotation about C_α-C_β (i.e. θavg = 45°). The values which result are given in Table 11.

TABLE 11: Calculated β-proton splittings in hydroxyalkyl radicals for various angles θ (B = 43.8 G)

for θ = 0°	a_β =	43.8	G
for θ = 30°	a_β =	32.85	G
for θ = 60°	a_β =	10.95	G
for θ = 90°	a_β =	0.0	G

Based on the aldehyde studies of Karabatsos et al.[134,135] (Table 5), the conformation (41) is expected to be preferred for 1-hydroxyprop-1-yl radical. Support for this suggestion comes from

θ = 30°

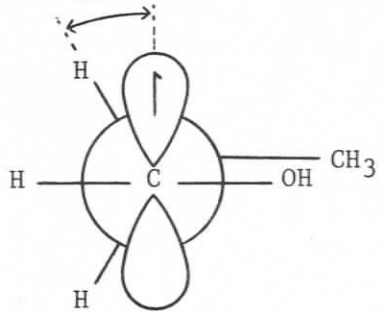

the large value of a_β and the fact that it increases sharply $\left(\frac{da_\beta}{dT} = -13 \text{ mG/C°}\right)$ with decreasing temperature (Figure 43a). The β-proton hfs of n-propyl radical, whose equilibrium conformation is (42), behaves similarly[3] $\left(\frac{da_\beta}{dT} = -29 \text{ mG/C°}\right)$.[24]

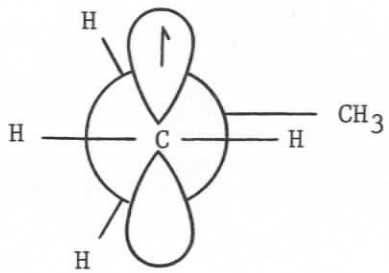

42

For both 1-hydroxyprop-1-yl radical (38) and the ether radical (40) the γ-proton hfs are near the low range (*ca.* $0.12 \leqslant |a_\gamma| \leqslant$ *ca.* 0.27)[32] predicted by the calculations of Ellinger et al.[32] for this $\theta_{Me} = 90°$ conformation for n-propyl radical (42).

Note that uncertainty in the measurement of changes in the small OH splitting is clearly revealed in Figures 43b and 43c, and trends are difficult to identify.

(d) Restricted Rotation About C_β–C_γ

(i) 1-Hydroxybut-1-yl Radical

The ESR spectra of 1-hydroxybut-1-yl radical (43) at +20°C and -20°C appear in Figure 44 accompanied by an appropriate line diagram. Hyperfine splittings are listed in Table 12. The quality of the spectrum

$$CH_3—CH_2CH_2\dot{C}H—OH$$

43

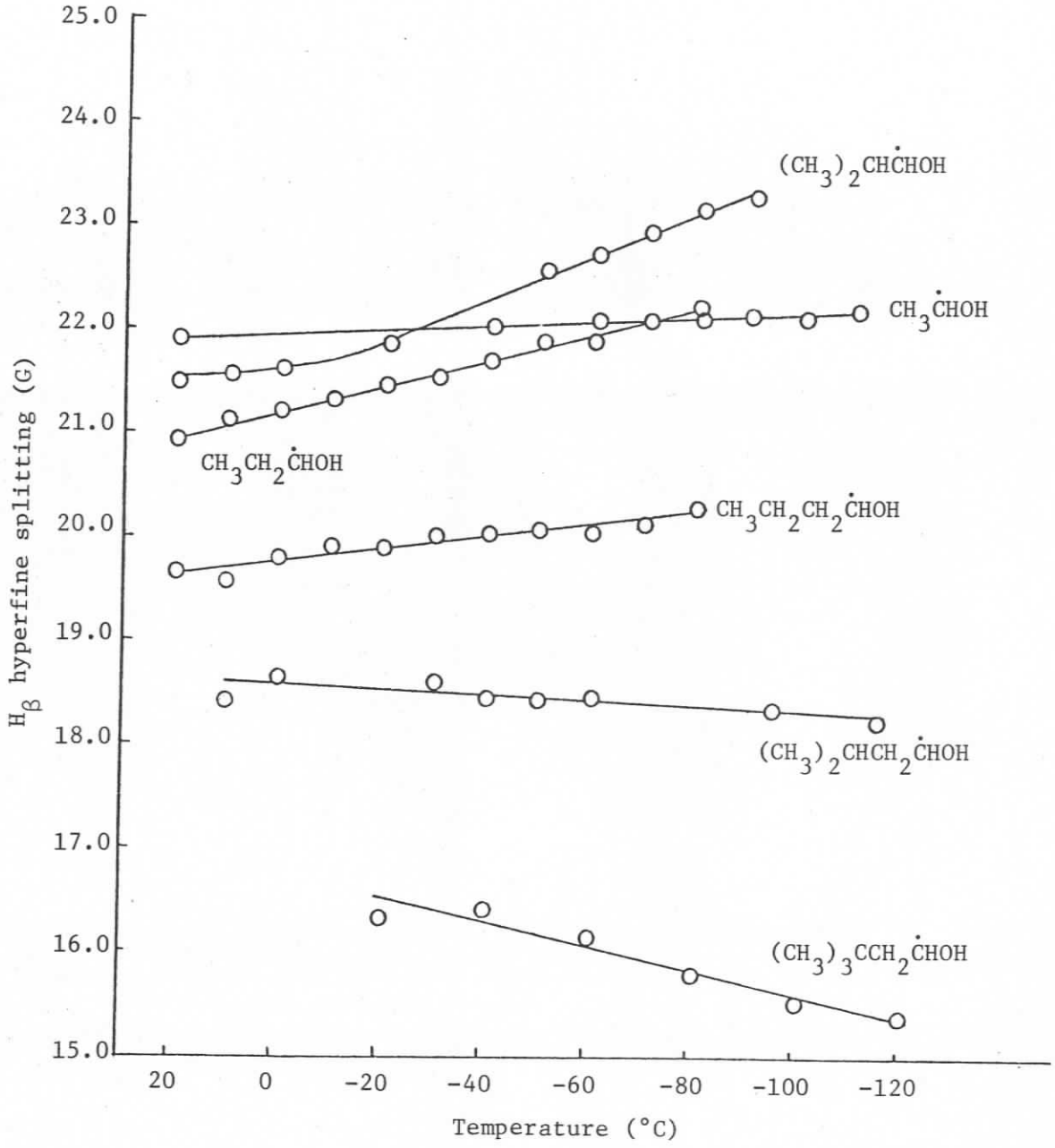

FIGURE 43a: Plot of $a_{\beta H}$ (G) vs. temperature (°C) for selected 1-hydroxyalkyl radicals.

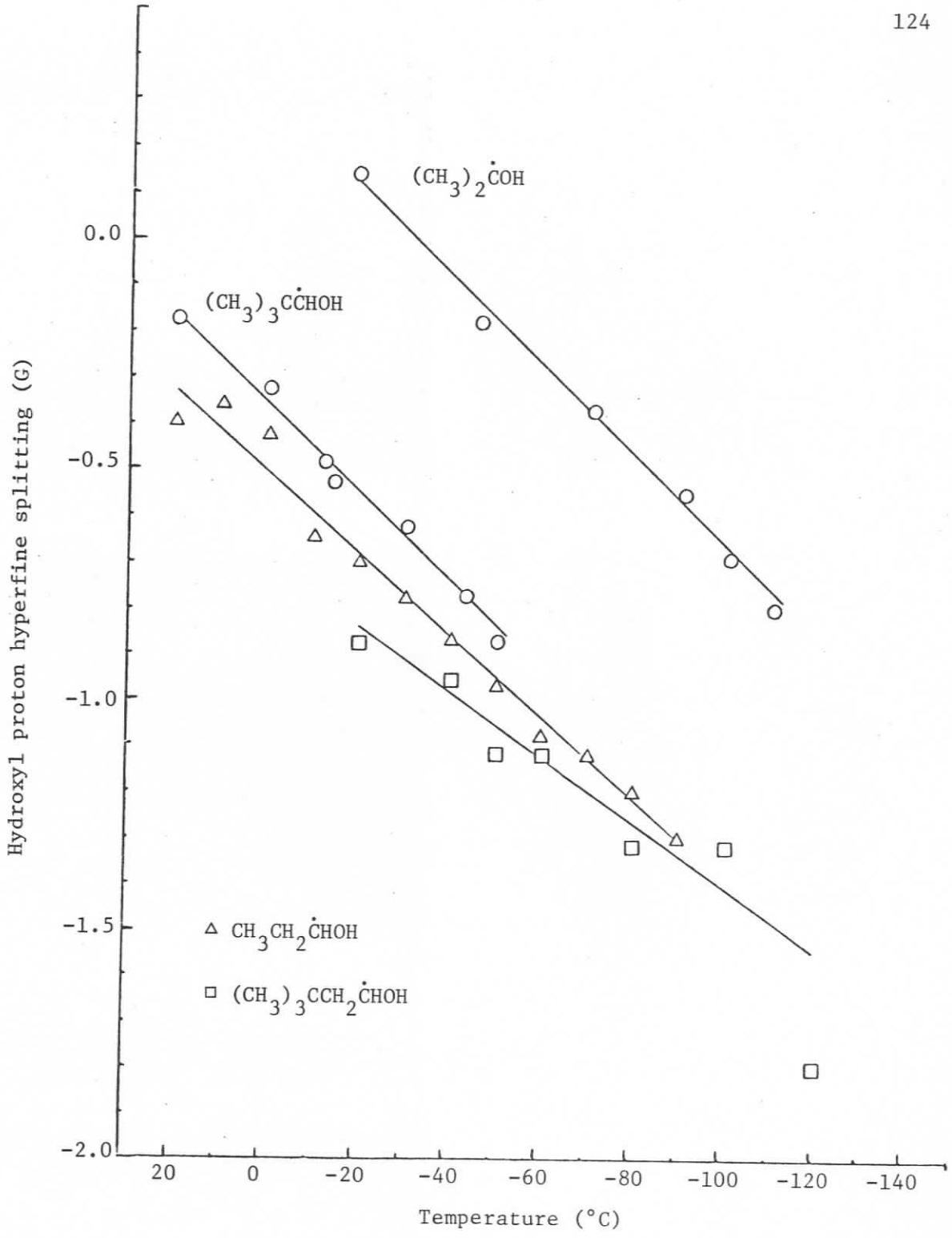

FIGURE 43b: Plot of a_{OH} (G) vs. temperature (°C) for selected 1-hydroxyalkyl radicals.

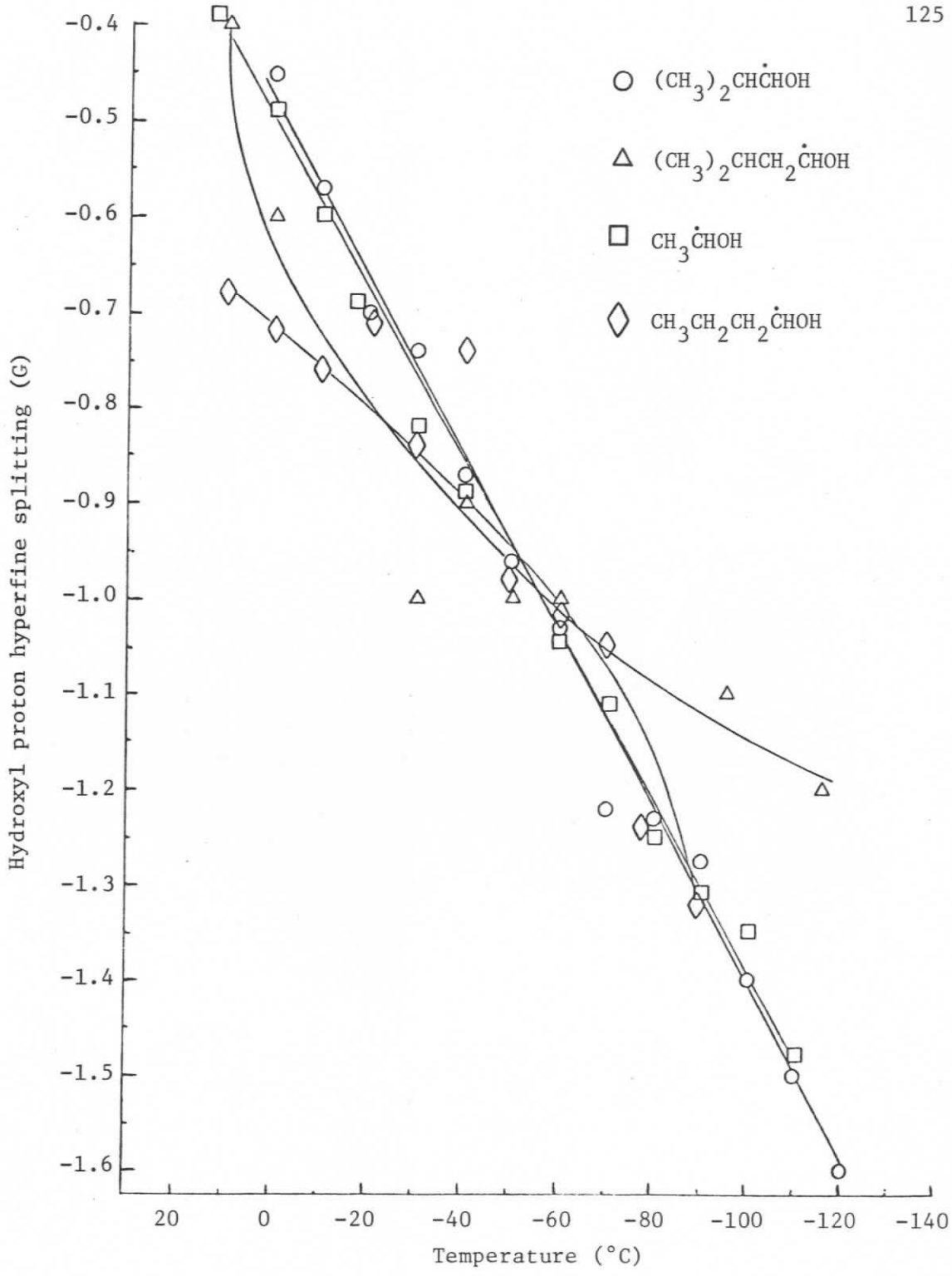

FIGURE 43c: Plot of a_{OH} (G) vs. temperature (°C) for selected 1-hydroxyalkyl radicals.

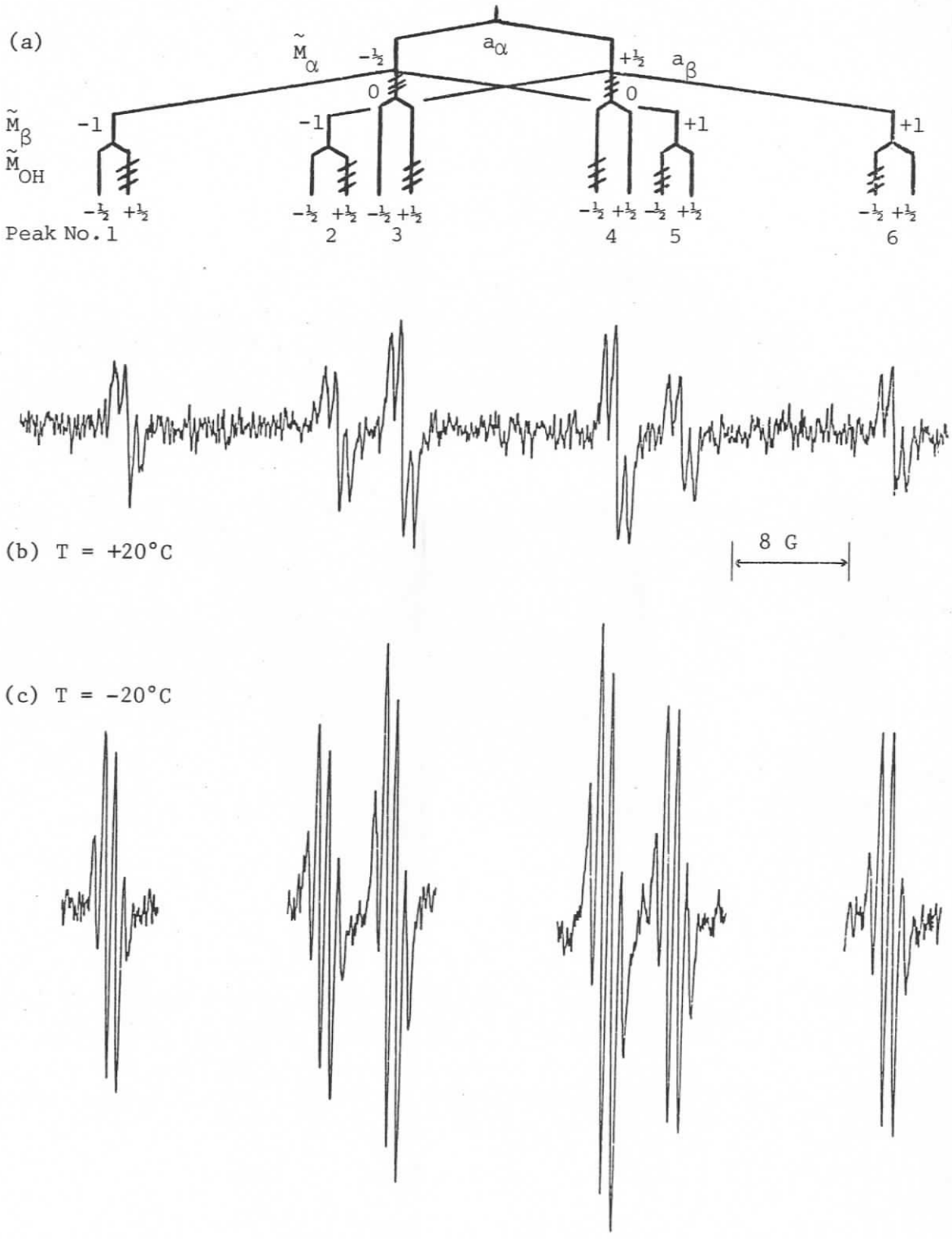

FIGURE 44: (a) Line diagram for ESR spectrum of $CH_3CH_2CH_2\dot{C}HOH$, not to scale, a_γ, a_δ omitted, (b) experimental spectrum at +20°C, (c) at -20°C.

TABLE 12: Hyperfine splittings in 1-hydroxybut-1-yl radical

Temp. °C	$-a_\alpha$	a_β	$\lvert a_\gamma \rvert$	$\lvert a_\delta \rvert$	$-a_{OH}$	$a_{2nd\ order}$
	±0.05	±0.05	±0.2	±0.02	±0.2	
+20	14.96	19.64	0.85		unresolved	
+10	15.04	19.56	0.70		0.68	
0	15.18	19.78	0.78		0.72	
-10	15.20	19.89	0.78		0.76	
-20	15.26	19.88	0.72		0.70	
-30	15.36	20.00	0.76		0.84	
-40	15.23	20.01	0.79	0.14	0.74	0.12
-50	15.31	20.05	0.73±0.02	0.14	0.98±0.02	0.12
-60	15.29	20.04	0.77±0.02	0.14	1.02±0.02	0.12
-70	15.38	20.12	0.88	0.14	1.05	
-80	15.54	20.29	0.86		1.24	
-90	15.48	-	0.92		1.32	

improved at moderately low temperatures (*ca.* -50°C) allowing clear resolution of a_δ and second order components (Figure 45), apparently for the first time.

As the temperature was decreased further the $\tilde{M}_\beta = 0$ components became less intense (Figure 46). Previously Lloyd[112] had suggested that this broadening was due to restricted rotation about C_β-C_γ modulating the two β-proton hyperfine splittings in an out-of-phase manner.

Our spectra (Figure 46) indicate not only the $\tilde{M}_\beta = 0$ broadening discussed by Lloyd but also the broadening pattern expected from restricted C_α-OH rotation (Figure 44a)(cf. 1-hydroxyprop-1-yl radical).

On the basis of β-proton hfs for the radical $CH_3CH_2CH_2\dot{C}HNCO$ in an adamantane matrix Lloyd[112] assigns the limiting H_β splittings of species

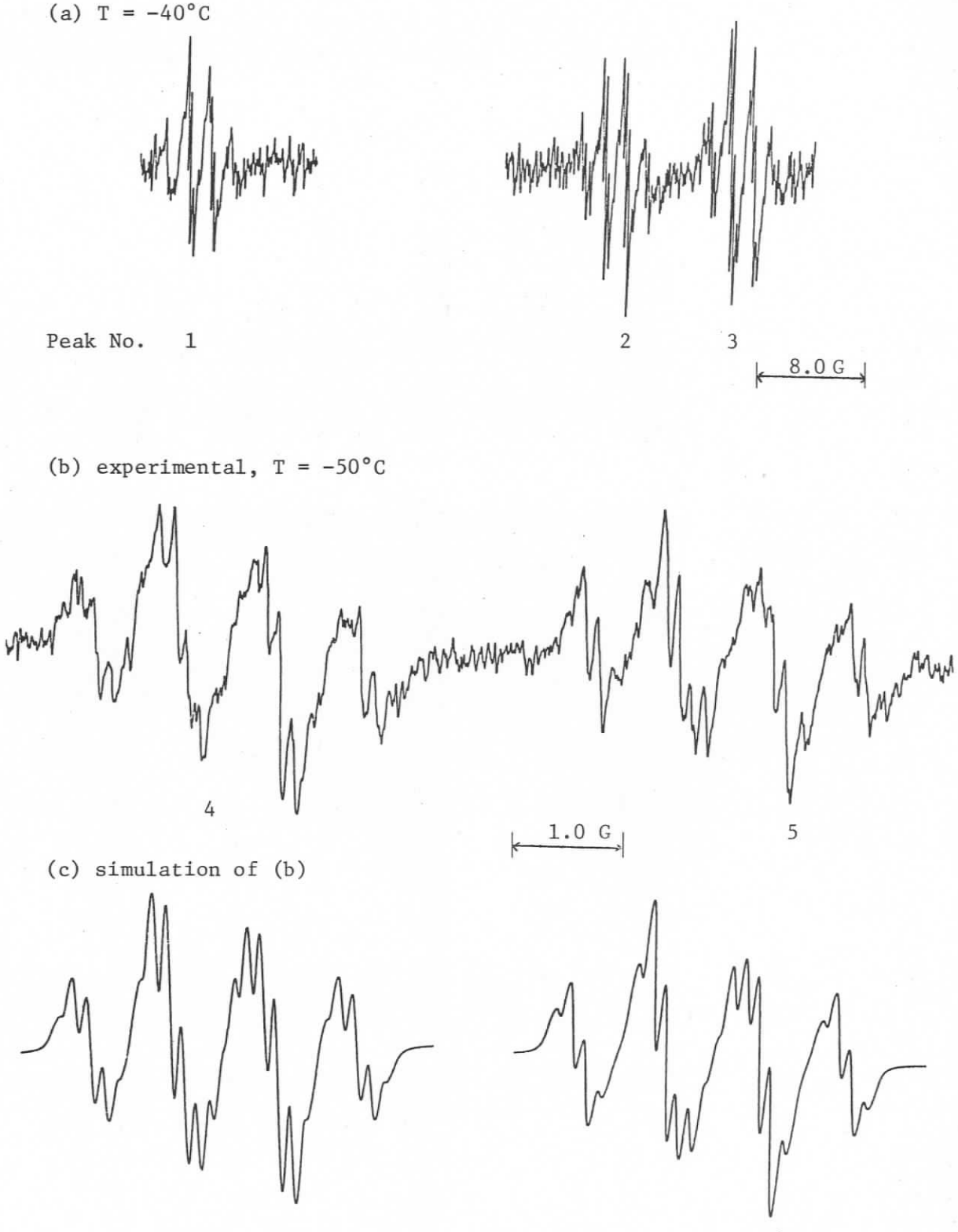

FIGURE 45: (a) Downfield half of ESR spectrum of $CH_3CH_2CH_2\dot{C}HOH$ at -40°C, (b) peaks 4 and 5 of spectrum at -50°C. Peak group 4 has second order structure. (c) Simulations of (b).

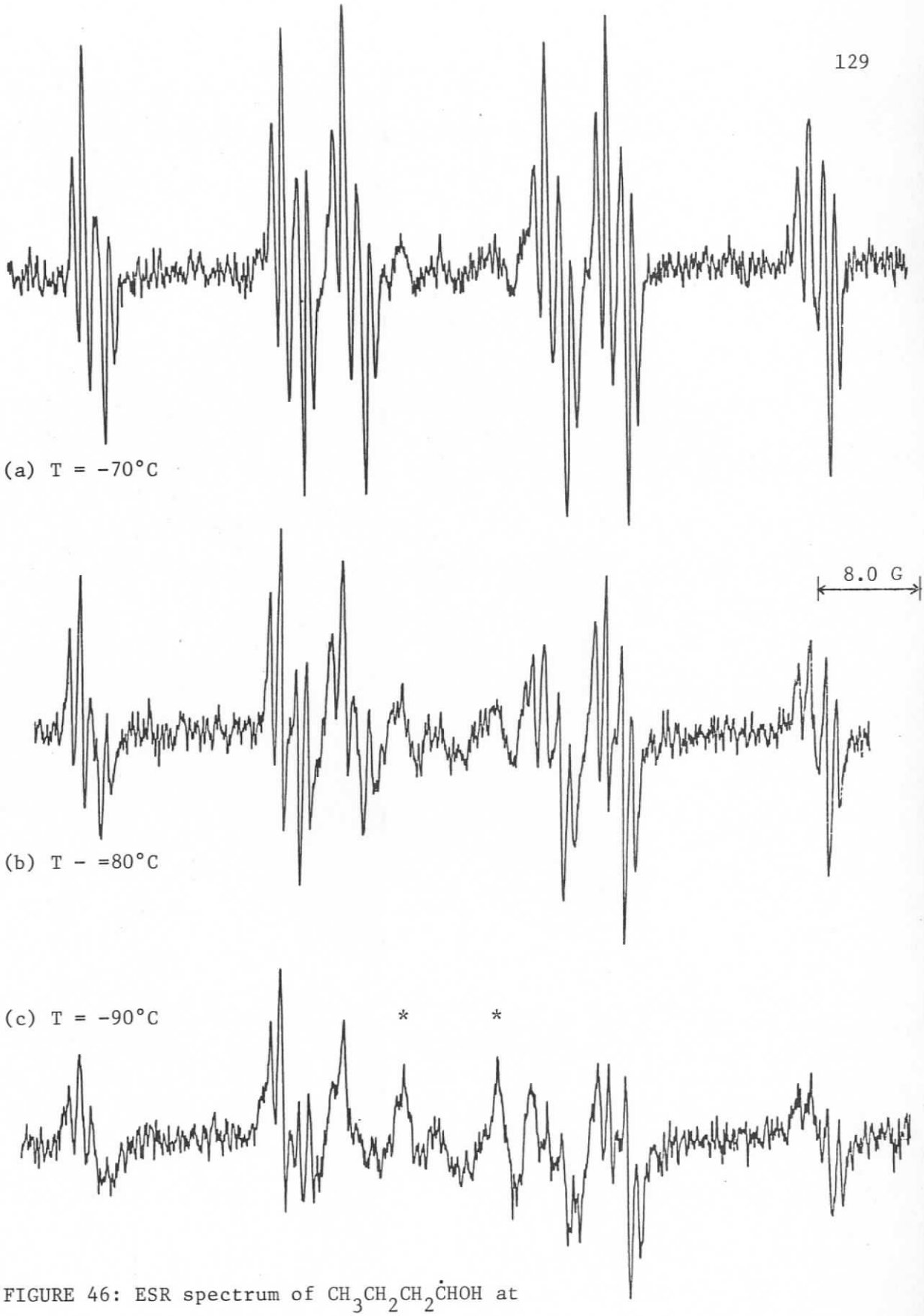

FIGURE 46: ESR spectrum of $CH_3CH_2CH_2\dot{C}HOH$ at (a) -70°C, (b) -80°C, (c) -90°C.
* see text

(43) the values 13.6 G and 25.2 G (Δa_β = 11.6 G). Detailed examination of the conformations that are involved in 1-substituted-1-butyl radicals indicates that Δa_β depends critically on the size of the 1-substituent and on the size of any substituent on the 3-carbon as these factors determine the relative populations of C_α-C_β rotamers. A further severe limitation on this model is that restricted rotation in the cavities of the adamantane matrix may determine the preferred C_α-C_β rotamers. Notwithstanding these criticisms of the value of Δa_β used by Lloyd,[112] values in the region 10-15 G are undoubtedly of the correct magnitude based on the observed lack of temperature-dependent behaviour of the γ-H multiplets. (For a detailed analysis see page 139.)

In the simulations it was also necessary to estimate the effects on hyperfine splittings arising from restricted rotation of the hydroxyl group. For this mechanism Δa values of *ca.* 2 G were found to be adequate by Graf et al.[123b] and such low values have been employed in this study (Figure 47).

To include a_{OH} derived broadening a (minimum) four site exchange model (e.g. 44) became necessary for the simulation. These structures (44) are used to illustrate the conformational exchange model involving rotation about the two bonds in question. They do not necessarily represent actual equilibrium conformations (*vide infra*).

As the sample temperature was decreased two peaks (marked * in Figure 46c) arose, apparently centered on the same g-value as the signals under study. Such lines do not accord with reapparance of sharp slow limit lines (see Figure 46b) and hence are likely due to accumulated

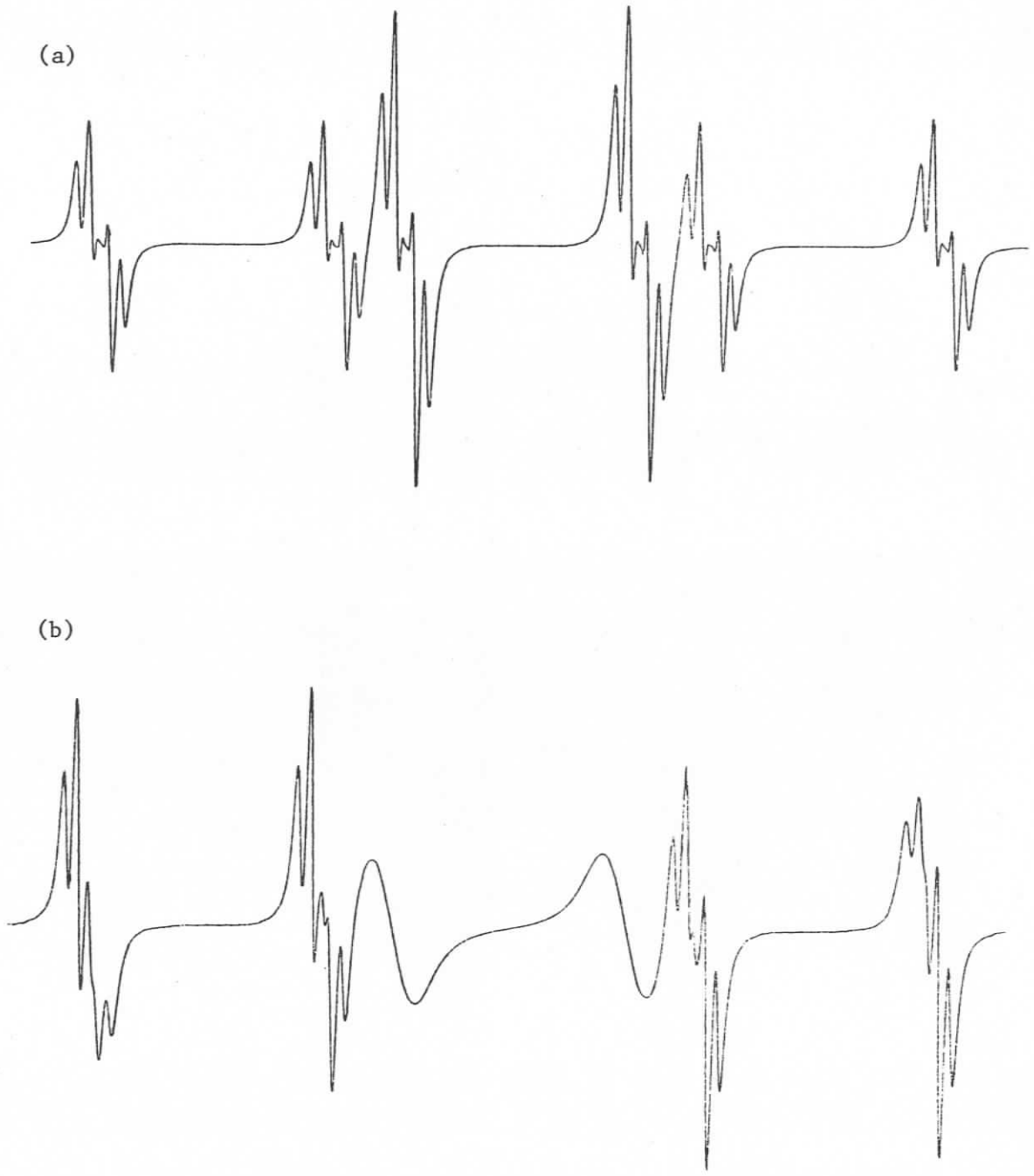

FIGURE 47: Simulation of the ESR spectrum of $CH_3CH_2CH_2\dot{C}HOH$ based on a four-site exchange model with $\Delta a_\beta \simeq 10$ G (see text and Appendix A). (a) Spectrum near high temperature limit, (b) spectrum at an intermediate exchange rate.

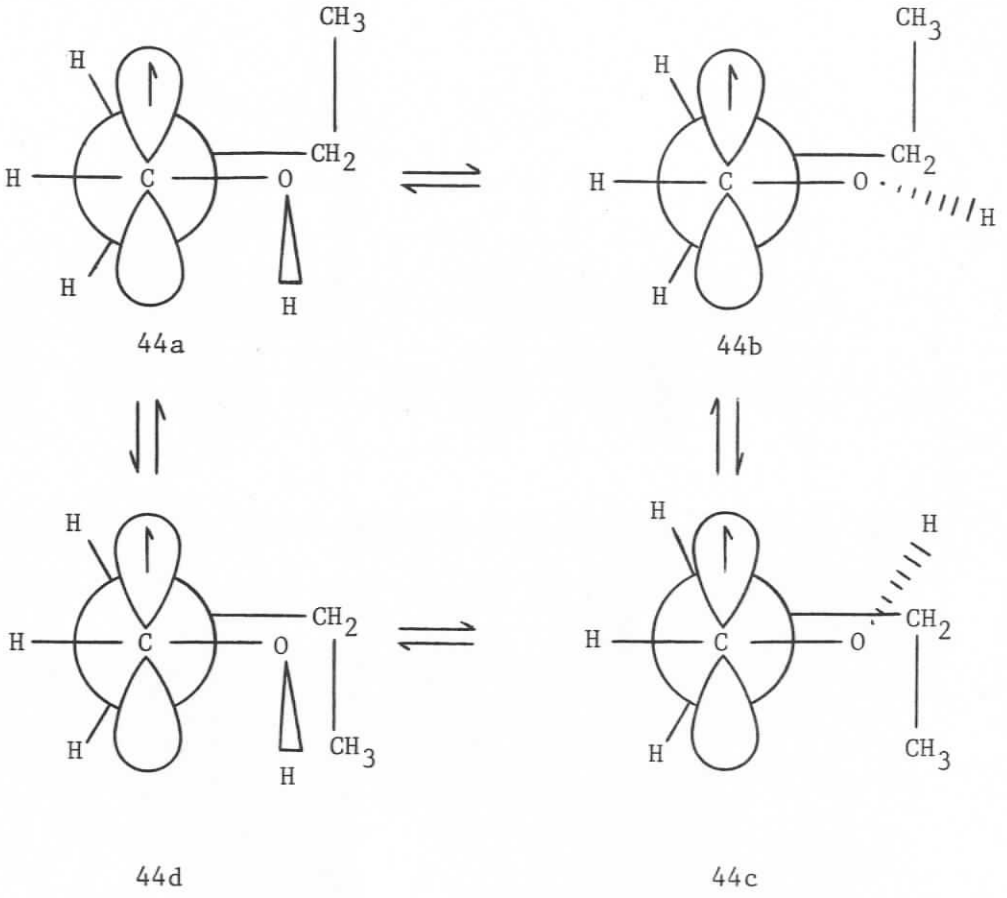

44a 44b

44d 44c

photoproducts. Similar lines occur in the case of 1-hydroxy-3-methylbut--1-yl radical (53)(*vide infra*).

Conformation and Long-Range Splittings. Two features stand out in a comparison of the hyperfine splittings of the 1-hydroxyprop-1-yl radical (Table 9) and the 1-hydroxybut-1-yl radical (Table 12). These are, first, the decrease in a_{β} by 1-2 G and, second, the increase in a_{γ} by a factor of two on going to the hydroxybutyl species. These changes may reflect a decreasing population of the conformation (45) and an increasing preference for the conformation (46). The conformational studies of

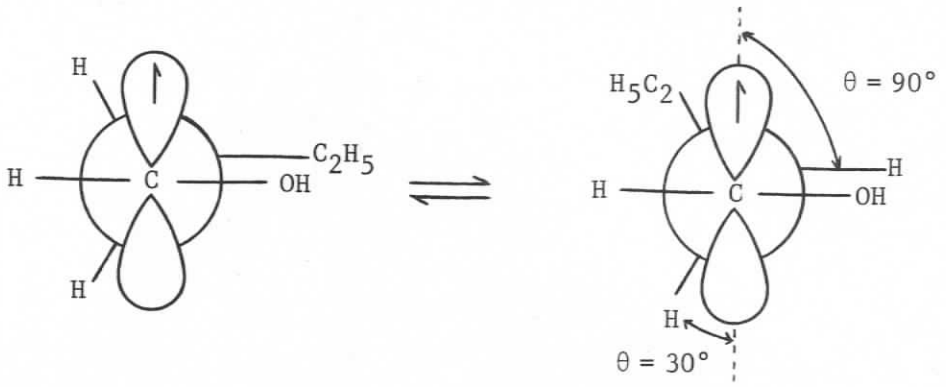

45 46

aldehydes by Karabatsos et al.[134,135] indicate that the population of the conformer having the 2-alkyl substituent as shown in structure (46) increases from 23% to 37% on going from propanal to butanal (Table 5). The conformers having a 2-hydrogen atom eclipsing oxygen are then the increasingly preferred rotamers for this molecule.[134,135] If the same is true for the 1-hydroxybut-1-yl radical then Equation 14 (Table 11) predicts a decrease in the average (observed) value of a_β on going to conformation (46)(i.e. experimentally $a_{\beta\ avg}$ = 22.07 G for the radical from n-propanol, and 20.12 @ -70°C for the radical from n-butanol).

The three probable low energy (staggered) C_β-C_γ conformations of the radical (46) are shown as structures (47a,b,c), in which the angle θ_γ (for the γ-protons) is either 60° or 180° (48). These values of θ_γ for the rotamer θ_R = 30° (47) are predicted by the calculations of Ellinger et al.[32] to lead to enhanced values of a_γ in n-propyl radical (relative to θ_R = 90°). By analogy in the present example such enhanced values could average to give a splitting in the observed range. Thus, if substantiated by further examples, it appears that γ-proton hyperfine

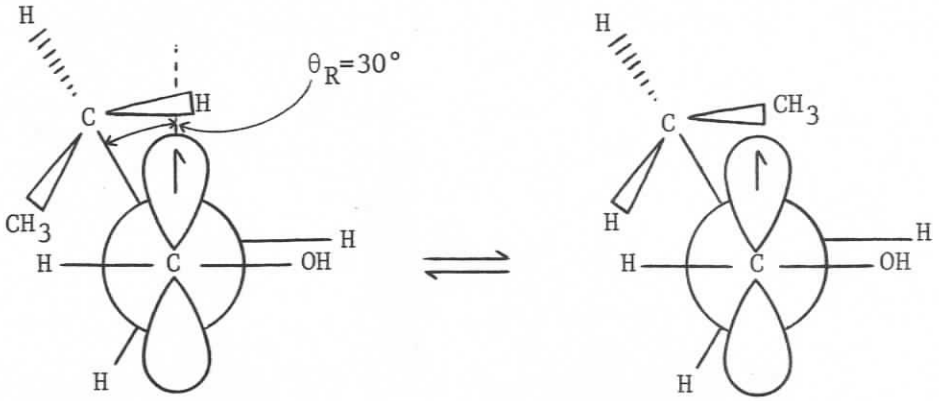

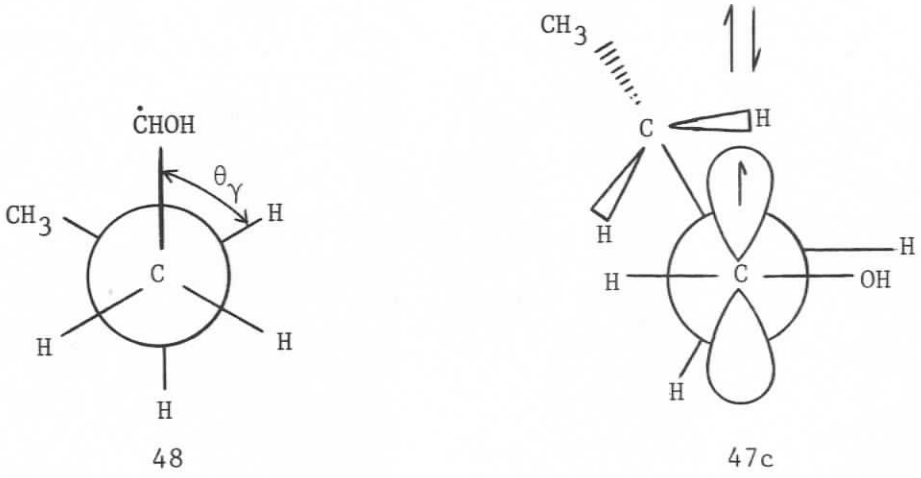

splittings can provide additional information about preferred C_α-C_β conformations.

Our results for the radical (49, R = CH_3) from 2-methyl-1-butanol are consistent with the preceding discussion. If conformation (50a, R = CH_3) is a preferred one we expect a low $a_{\beta\ avg}$. Experimentally, a_β = 19.75 G ±0.25 G at -50°C. The similar radical (49, R = C_2H_5) from

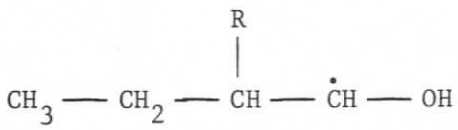

49

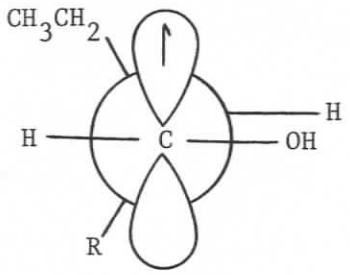

50a

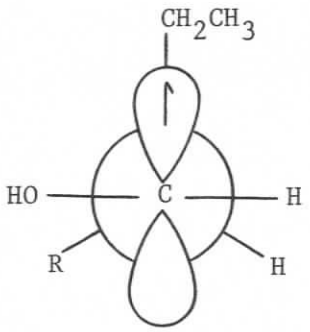

50b

2-ethyl-1-butanol gave an even lower value of $a_{\beta\ avg}$ (*ca.* 16 G) in aqueous solution at room temperature,[136] consistent with a significant population of conformer (50a, R = C_2H_5). (We found a_β 15.5 G ±0.25 G in a poorly resolved spectrum @ +15°C in cyclopropane.) However, an intermediate stable conformation (50b) cannot be ruled out for these species.

(ii) <u>1-(n-Butoxy)but-1-yl Radical</u>

The 1-(n-butoxy)but-1-yl radical (51) offers a test of the C_β-C_γ rotation modulation mechanism in the absence of a hydroxyl group.

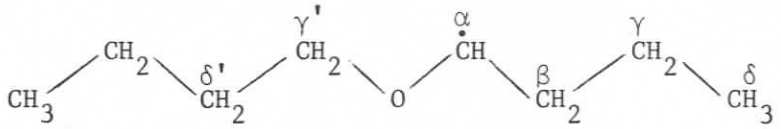

51

The spectrum (Figure 48) of this species contrasts with the spectra of similar radicals derived from diethyl ether and di-n-propyl ether in which no line broadening is observed (splittings in Table 13). In the present case the $\tilde{M}_\beta = 0$ components broaden beyond detection on cooling the sample to -110°C. The remainder of the spectrum remains isotropic

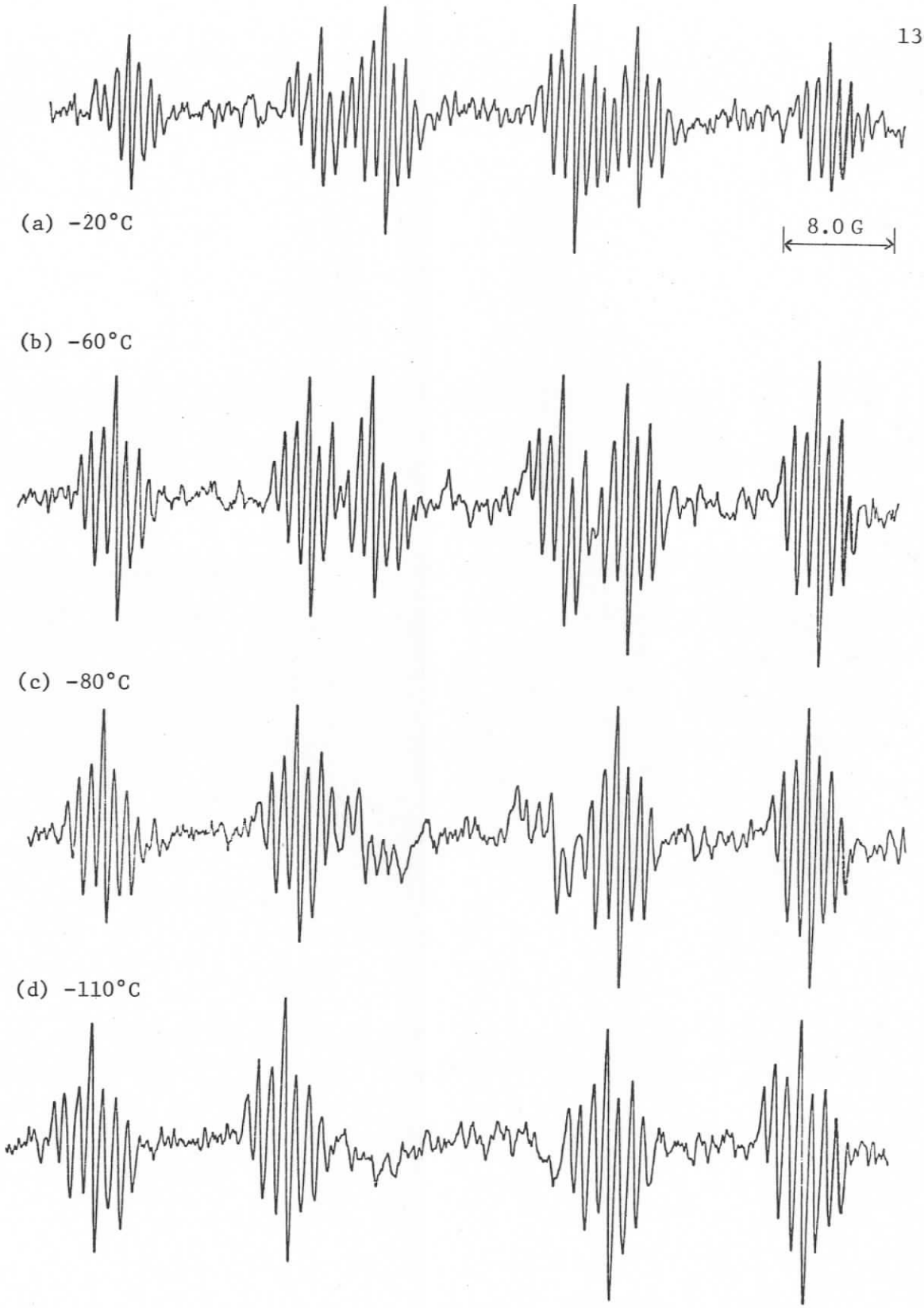

FIGURE 48: ESR spectrum of $BuO\dot{C}HCH_2CH_2CH_3$. (Figure continues)

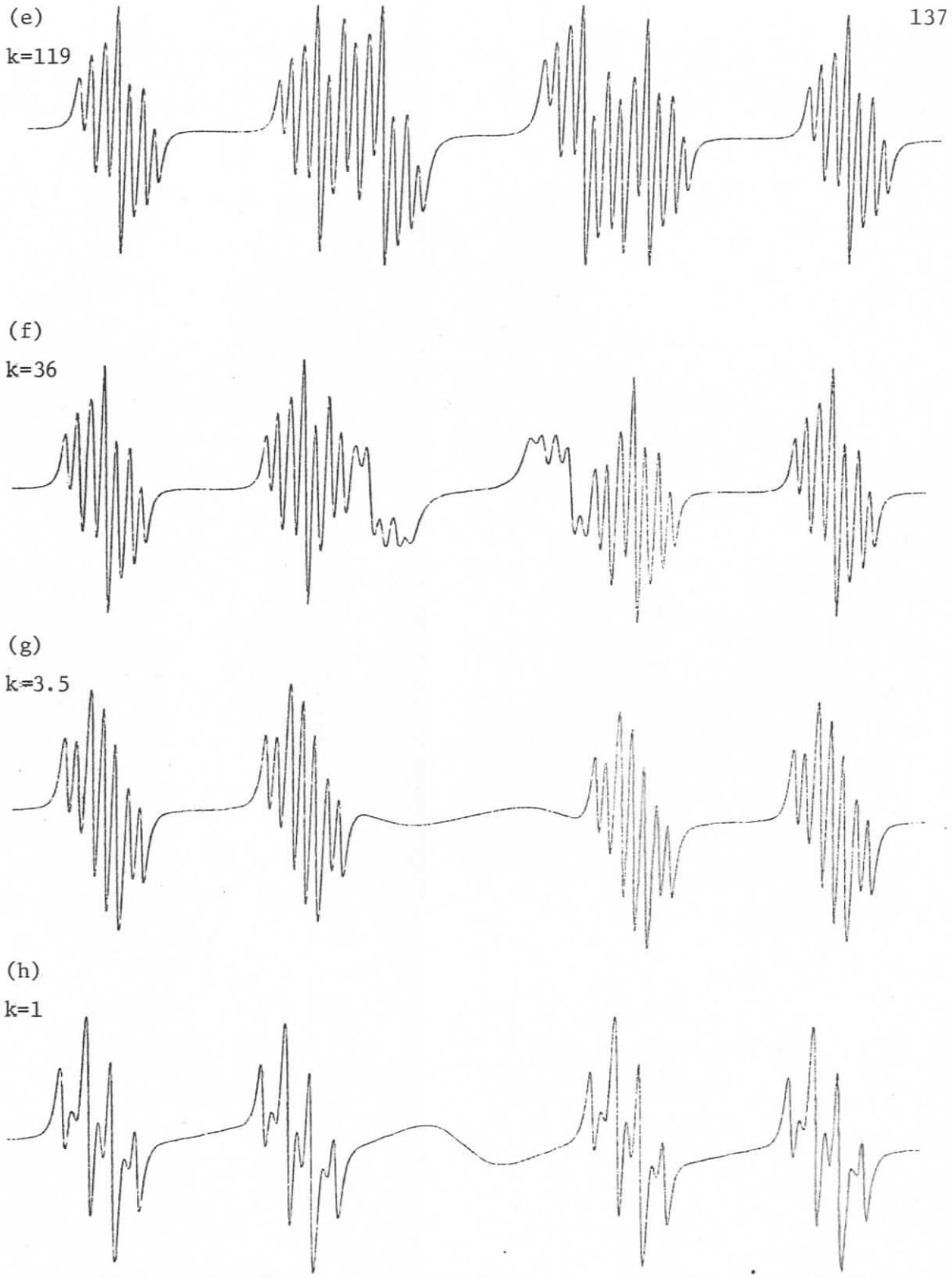

FIGURE 48 (continued): Simulations of ESR spectrum of $BuOCHCH_2CH_2CH_3$.
Compare (e) with (b), (f) with (c), (g) with (d). The relative rate constants are given. $\Delta a_{\beta H} = 15$ G $\Delta a_{\gamma H} = 2.2$ G. The last simulation shows that modulation of the γ-H splittings is not observed until below the rate constant (i.e. temperature) of coalescence for modulation of the β-H splittings.

TABLE 13: Hyperfine splittings for $BuO\dot{C}HCH_2CH_2CH_3$

Temp. °C	$-a_\alpha$	a_β	$\lvert a_\gamma \rvert$	$\lvert a_{\gamma'} \rvert$
	±0.1	±0.1	±0.1	±0.1
+10	13.80	18.66	0.80	1.60
0	13.88	18.56	0.88	1.60
-20	13.92	18.52	0.75	1.55
-40	13.88	18.64	0.76	1.70
-60	14.00	18.60	0.72	1.70
-80	14.04	18.70	0.80	1.76
-90	14.08	18.74	0.80	1.84
-100	14.12	18.80	0.80	1.88
-110	14.20	18.82	0.80	1.84
-130	14.36	18.94	0.96	2.00

and unbroadened to -130°C. There is no reappearance of the $a_{\beta H}$ components indicating that the low temperature limit is being approached. Thus we have further evidence that restricted rotation about C_β-C_γ is is the cause of the broadening of the $\tilde{M}_\beta = 0$ components in the spectra of these butyl radicals. This is the first demonstration of this effect in the spectrum of this ether-derived radical (51). Note that broad central lines due to accumulation of photoproducts do not arise for the ether radical (51) as they did in the spectrum of the radical from n-butanol (Figure 46). Since the spectrum retains high resolution to low temperatures and shows no additional line broadening due to restricted rotation about C_α-O it is a better example than 1-hydroxybut--1-yl radical for this $\tilde{M}_\beta = 0$ broadening effect.

An important point that has not been specifically addressed by Krusic et al.[87] or Lloyd[112] is the mechanism of modulation of the two β-proton splittings and the anticipated magnitude of the difference between them. Such differences are related to the magnetic inequivalence of the β-protons created by the asymmetry of the appropriate γ-group in a fixed conformation (about C_β-C_γ). This magnetic inequivalence is subsequently monitored as a result of the differential interaction of the two β-protons with the (rapidly rotating) radical center at C_α.

Such inequivalence in fact arises from all the populated conformations (about C_α-C_β), which may individually have drastically different values of $a_{\beta 1}$ and $a_{\beta 2}$. Accordingly several reservations must be expressed concerning the "fixed limits observed for the radical $CH_3CH_2CH_2\dot{C}HN{=}CO$ in the adamantane matrix:[112]

1. If the limit corresponds to frozen C_β-C_γ rotation, three conformers will be populated (52a-52c). In fact (52c) should be the dominant (anti) conformer in solution so that at a slow C_β-C_γ limit *no* resultant inequivalence in the β-H hyperfine splitting is observed. Therefore a fixed limit spectrum showing only differing β-H splittings may well be an adamantane artifact resulting from frozen C_α-C_β rotation. (Note the energy barrier 3.6 Kcal/mol in the solid is very different from the barrier calculated by Lloyd in solution, ~2.0 Kcal/mol, for the same radical.[112])

2. Secondly, at a slow C_β-C_γ limit we are always faced with estimating the population of the C_α-C_β conformers, i.e. (52d-52f), even if the C_β-C_γ conformation is correctly predicted. Once again $a_{\beta\ avg}$ for

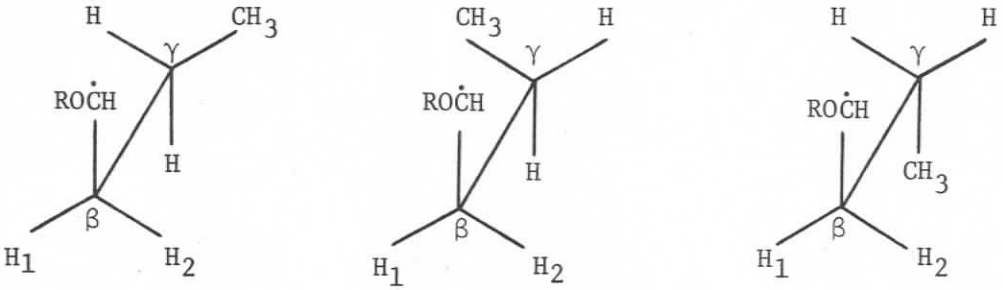

52a 52b 52c

Potential Energy Minima for C_β-C_γ Rotation

R = H, $CH_2CH_2CH_2CH_3$

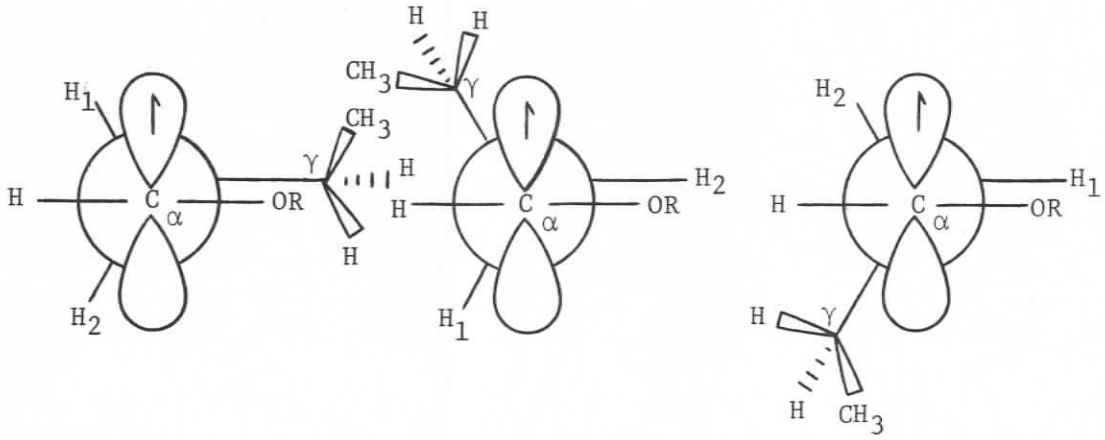

52d 52e 52f

Potential Energy Minima for C_α-C_β Rotation

for Case 52b

$CH_3CH_2CH_2CHN{=}C{=}O$ is 19.4 G in adamantane and 20.2 G in solution, so that the population of C_α-C_β conformers clearly changes.

3. Finally, the $a_{\beta\ avg}$ value will depend on the bulk of the α-substituent and the constant B (Equation 14) generated for β-H splitting. Clearly transfer of any fixed limits to a second species even in the same medium is suspect. Note $a_{\beta H\ avg}$ for the 1-hydroxybut-1-yl radical (43) is 20.29 G (@ -80°C) and for the ether radical (51) is 18.70 G (@ -80°C).

Clearly the slow limit values of $a_{\beta 1}$ and $a_{\beta 2}$ are difficult to obtain in the face of viscosity problems in suitably complex systems. However, they should be similar to values arising from the inequivalence in corresponding γ-chiral radicals where no time averaging is created by C_β-C_γ rotation. Such a system is the substituted phenoxyl series (e.g. 52g,h) reported by Fischer[185] in work from the Scheffler group.

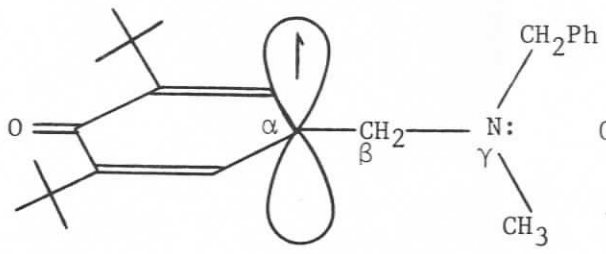

52g

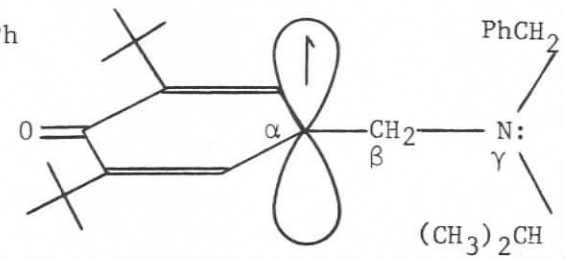

52h

These studies[185] have demonstrated the use of chiral β substituents (i.e. NR_1R_2) to provide an estimation of the magnetic inequivalence of the β-hydrogens. (Note that the two gauche conformers (52a) and (52b)

are *enantiomers*.) Accordingly, changes in the nitrogen substituents as in structures (52g) and (52h) create spectacular changes in the free rotation diastereotopic inequivalence of the β-protons. For radical (52g), $a_{\beta 1} - a_{\beta 2} = \Delta a_{\beta} = 1.74$ G (T = -40°C) while for radical (52h), $\Delta a_{\beta} = 11.00$ G (T = -45°C) (see also ref. 186).

Few diastereomeric shifts are reported for aliphatic transients though clearly they are anticipated. The phenomenon is well known for hindered nitroxides such as those reported by Gilbert et al.[187] for the species (52i). It should be recalled that changing R from CH_3CH_2 to

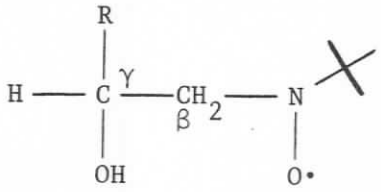

52i

$(CH_3)_2CH$ results in $\Delta a_{\beta H}$ (diastereotopic) going from 4.81 G to 7.74 G (for $a_{\beta\ avg}$ values of only 11.16G and 11.39 G respectively.)[187]

Clearly $\Delta a_{\beta H}$ values for simple transient π radicals can easily be of the order suggested by Lloyd[112] (i.e. *ca*. 12 G). Some indirect evidence for this magnitude is available. The fact that the γ-H splittings are also modulated by C_{β}-C_{γ} rotation has been overlooked. Note that the $\theta_{\gamma} = 60°$ and $\theta_{\gamma} = 180°$ (cf. structure 48) splittings for the conformations (52d-f) will also differ; based on both recent hydrocarbon work[132] and extensive work on cyclic ethers (see Gilbert et al.[40] and this dissertation, Chapter IV, section 2ai). Figure 48e-h shows simulations of the ESR spectrum of 1-(n-butoxy)but-1-yl radical based on a

two-site model in which $\Delta a_{\beta H} = 15$ G and $\Delta a_{\gamma H} = 2.2$ G (the limiting values are $a_{\beta H_1} = 26.32$ G, $a_{\beta H_2} = 11.32$ G, $a_{\gamma H_1} = +1.90$ G, $a_{\gamma H_2} = -0.30$ G, see also Appendix A). Given that interconversion between conformations (52a, R = Bu) and (52b) modulates both the β-H splittings and the γ-H splittings at the same *rate* it is clear that values of Δa_{β} in the range 8-15 G are necessary to accommodate the experimental lack of modulation of the γ-proton splittings.

(iii) The 1-Hydroxy-3-methylbut-1-yl Radical

The ESR spectrum of the 1-hydroxy-3-methylbut-1-yl radical (53) does not appear to have been observed previously, though an early attempt was made.[76] The hyperfine splittings are shown in Table 14.

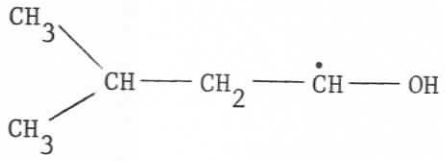

53

At +10°C the lines have their expected relative intensities. As the temperature is lowered the $\tilde{M}_{\beta} = 0$ components become less intense until at -95°C they are not detected (Figure 49), while the other lines remain sharp. The alternating linewidth effect can again be attributed to restricted rotation about C_{β}-C_{γ}, which modulates the two β-proton hfs mutually out-of-phase (*vide supra*). The simulations (Figure 50) are based on a two-site model for this restricted rotation only ($\Delta a_{\beta H} =$ 11.6 G, see Appendix A). The linewidth effects caused by restricted C_{α}-OH rotation appear only at very low temperatures for this species

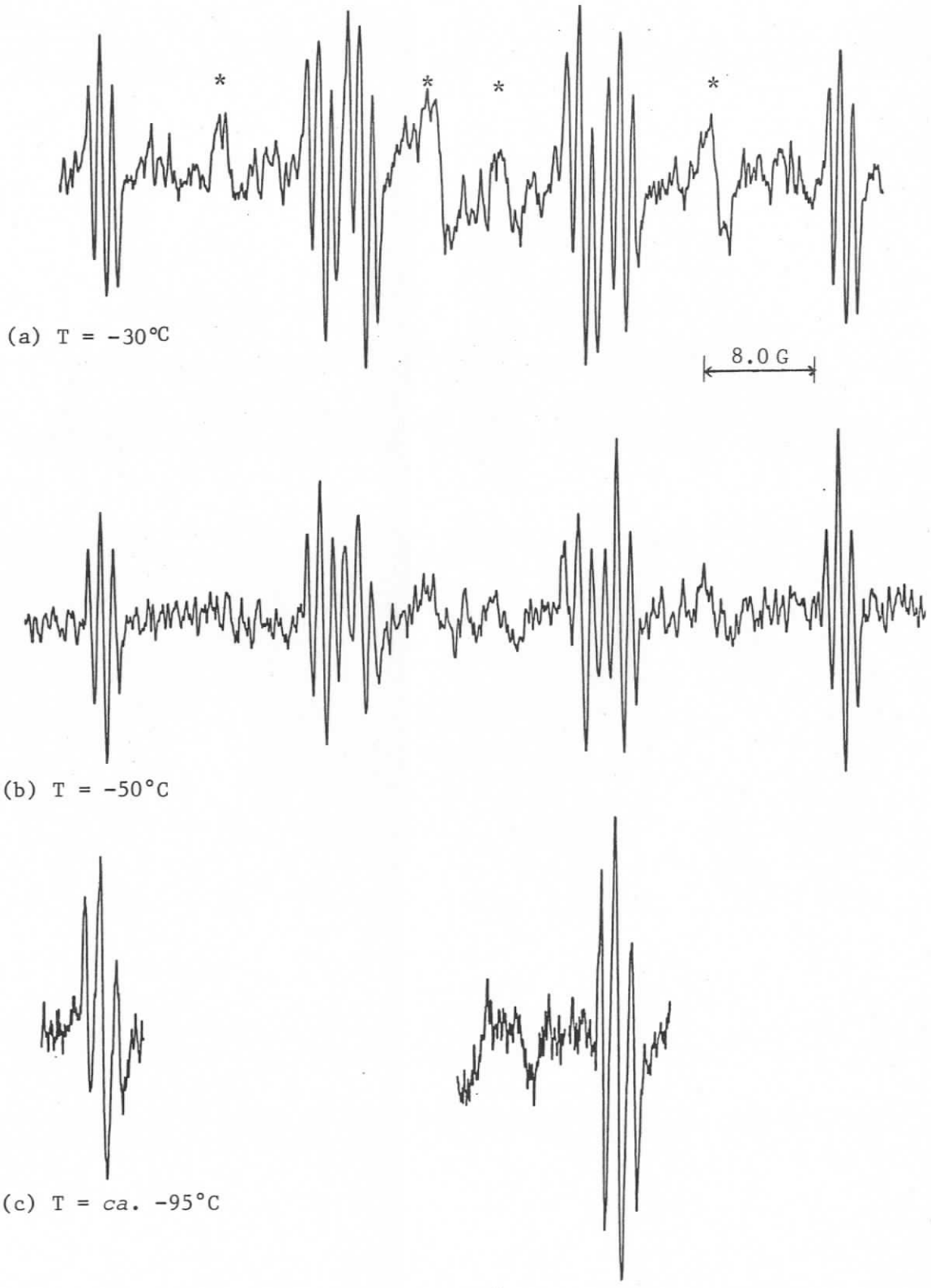

FIGURE 49: ESR spectrum of $(CH_3)_2CHCH_2\dot{C}HOH$ (53), showing broadening of $\tilde{M}_\beta = 0$ components at low temperature. *Additional signals were not identified.

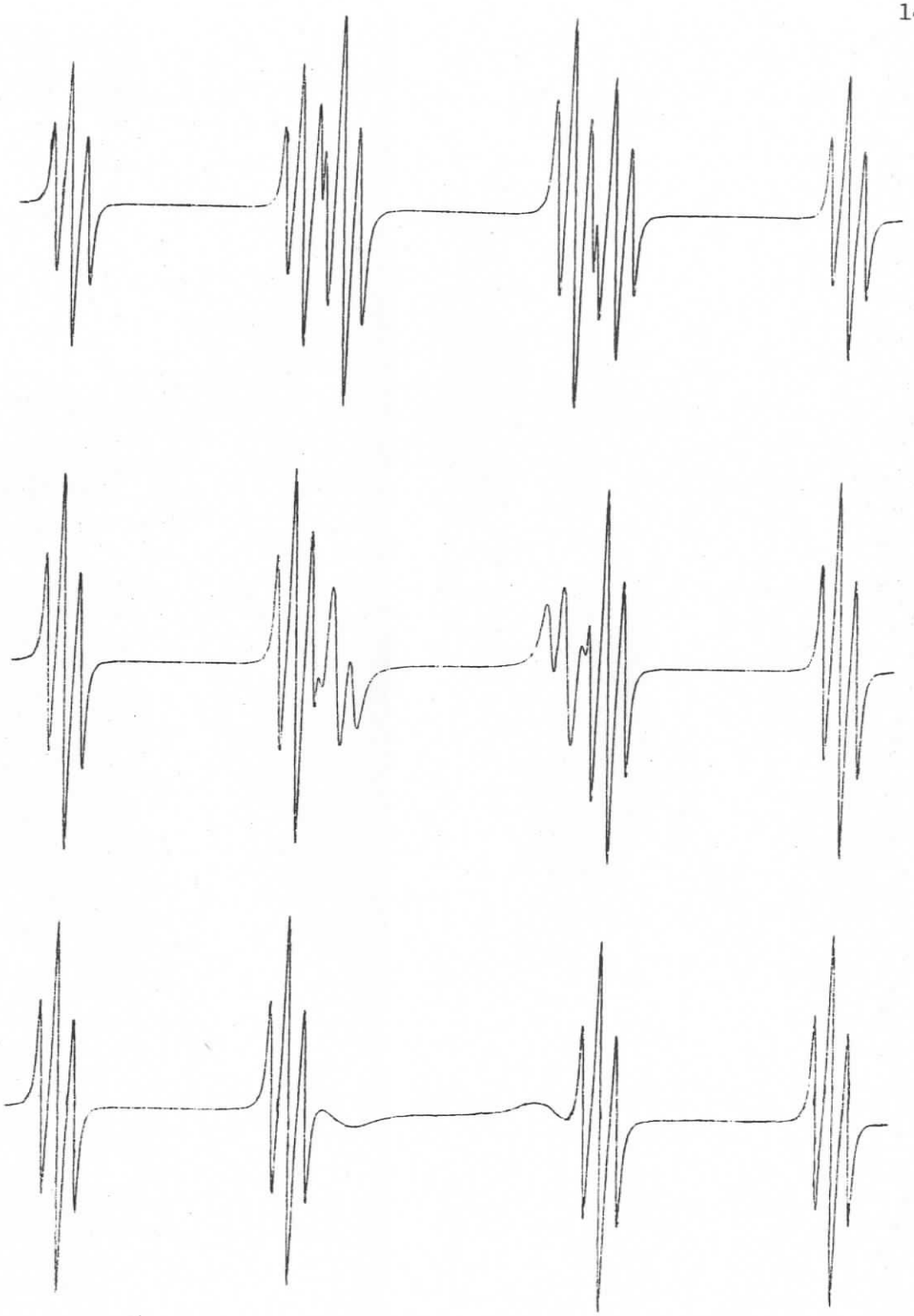

FIGURE 50: Simulation of alternating linewidth effect due to restricted rotation about C_β-C_γ in $(CH_3)_2CHCH_2\dot{C}HOH$ (53).

TABLE 14: Hyperfine splittings for 1-hydroxy-3-methylbut-1-yl radical (53)

Temp. °C	$-a_\alpha$	a_β	$\lvert a_\gamma \rvert$	$-a_{OH}$
	±0.01	±0.1	±0.4	±0.4
+10	15.40	18.40	1.0 ±0.05	0.40±0.05
0	15.56	18.60	0.95±0.1	0.60±0.1
-30	15.64	18.58	1.0	1.0
-40	15.68	18.42	0.9	0.9
-50	15.70	18.42	1.0	1.0
-60	15.72	18.44	1.0	1.0
ca. -95	-	18.34	1.1	1.1
-115	16.20	18.22	1.2	1.2

Note: A weak hfs of *ca.* 0.1 G was observed at high resolution and attributed to H_δ coupling poorly resolved.

(see inside lines of outer multiplets in Figure 51) indicating a faster rate in this case. No modulation of the γ-H hfs is expected here since the two preferred conformers, $\theta_{\gamma H} = \pm 60°$ (structure 55), should have nearly identical $a_{\gamma H}$.

The broadening of the $\tilde{M}_\beta = 0$ components for the radical (53) sets in at a higher temperature than in the case of the radical from n-butanol, indicating the expected higher energy barrier for rotation of the isopropyl group. Note that the inherent viscosity of the medium is also changing (Table 15).

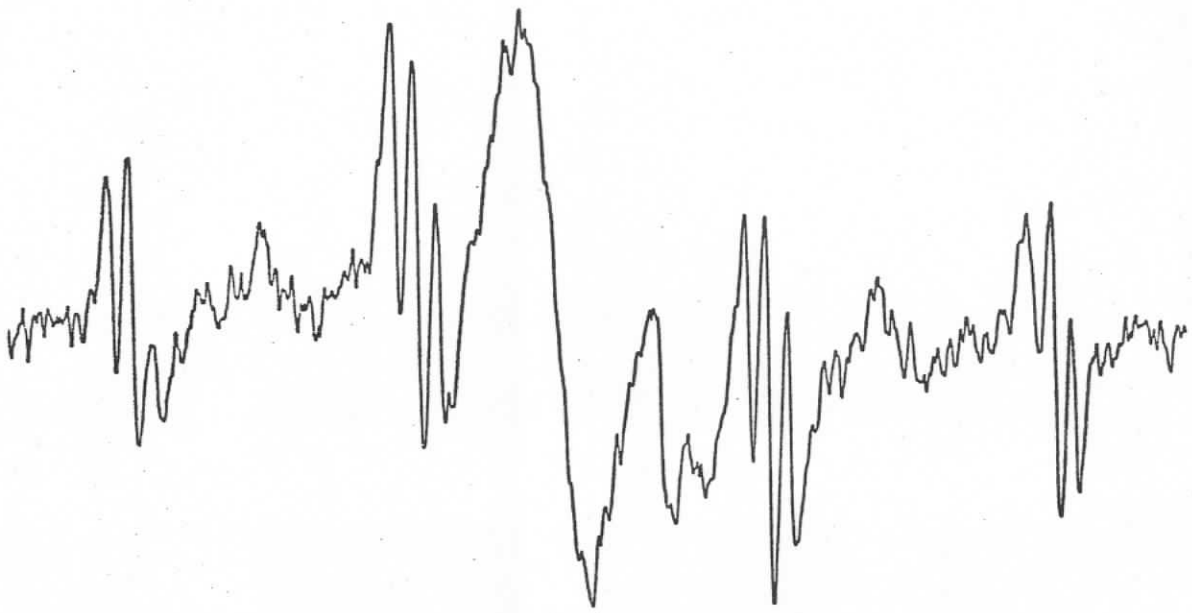

FIGURE 51: ESR spectrum of $(CH_3)_2CHCH_2\dot{C}HOH$ (53) at -115°C. The large peak near the center of the spectrum is unassigned.

TABLE 15: Viscosity of alcohols and ethers[137]

Compound	Viscosity (centipoise x 10^3)	Temp. °C
dimethyl ether	0.06584	-56.9
diethyl ether	2.79	0
	2.47	15
di-n-propyl ether	5.36	0.59
	4.48	15
di-n-butyl ether	7.41	15
methanol	6.23	15
ethanol	13.2	15
n-propanol	25.22	15
isopropanol	28.59	15
n-butanol	33.79	15
isobutanol	47.03	15
n-pentanol	46.50	15
3-methyl-1-butanol(isopentanol)	48.11	15
2-ethyl-1-butanol[138]	80.21	15
cyclohexanol[138]	41.07	30

Conformation and Long-Range Splittings. Karabatsos et al.[134] noted that as the 2-substituent in aliphatic aldehydes was made more bulky the conformational preference shifted in favour of a 2-hydrogen eclipsing the oxygen atom (Table 5). In the case of isopentanal this rotamer was found to be populated to the extent of 52%. The same conformation (54) is probably favoured for the radical (53). This is consistent with the relatively low value of a_β and its slight decreasing trend $\left(\frac{da_\beta}{dT} = +2.7 \text{ mG/C°}\right)$ on cooling (Figure 43a, Table 14). In a consistent pattern, a preference for this conformation (55c, 55d) would

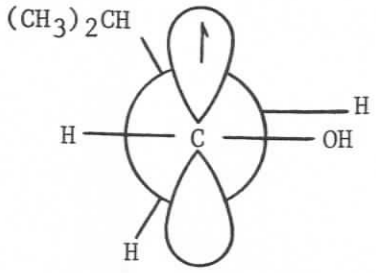

54

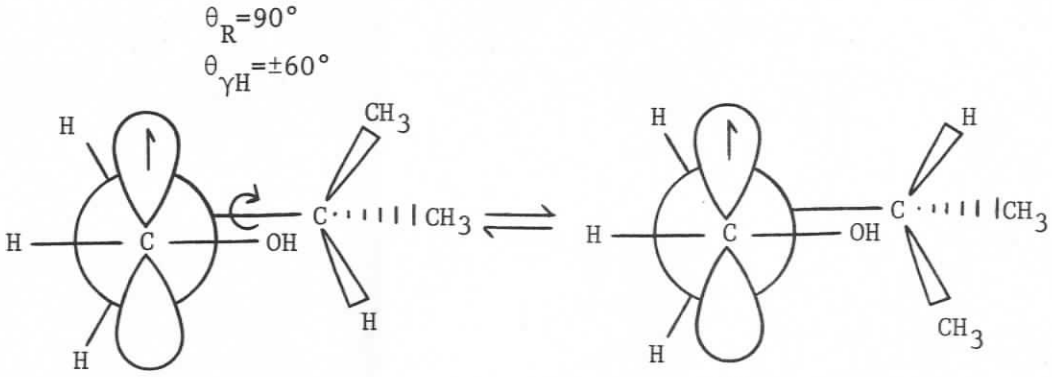

55a 55b

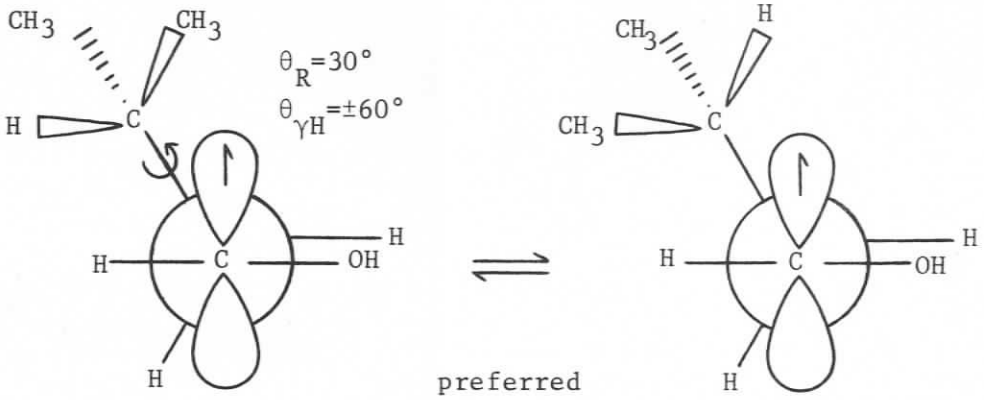

55c 55d

also enhance the single γ-proton hfs[32] and explain the large observed value (*ca.* 1.0 G, Table 14).

(iv) 1-Hydroxy-3, 3 -dimethylbut-1-yl Radical

The ESR spectrum of 1-hydroxy-3,3-dimethylbut-1-yl radical (56) is previously unreported. The hyperfine splittings are collected in Table 16. The unfortunate coincidence of some lines results in an

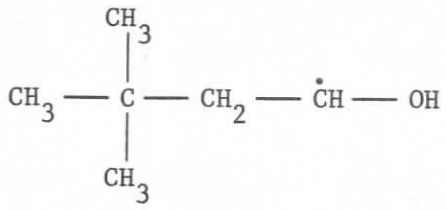

56

TABLE 16: Hyperfine splittings of 1-hydroxy-3,3-dimethylbut-1-yl radical (56)

Temp. °C	$-a_\alpha$	a_β	$-a_{OH}$	$\lvert a_\delta \rvert$
	±0.05	±0.05	±0.05	
-20	16.34	16.34	0.88	0.1
-40	16.36	16.40	0.96	
-50	16.26	16.20	1.12	
-60	16.28	16.16	1.12	
-80	16.60	15.80	1.32	
-100	16.72	15.52	1.32	
-120	16.90±0.2	15.40±0.2	1.80±0.2	

apparently anomalous intensity ratio (Figure 52a). However, the overlap is less severe at lower temperatures and broadening of the type expected from restricted C_α-OH rotation is clearly observed (Figure 52c,

(a) T = -40°C

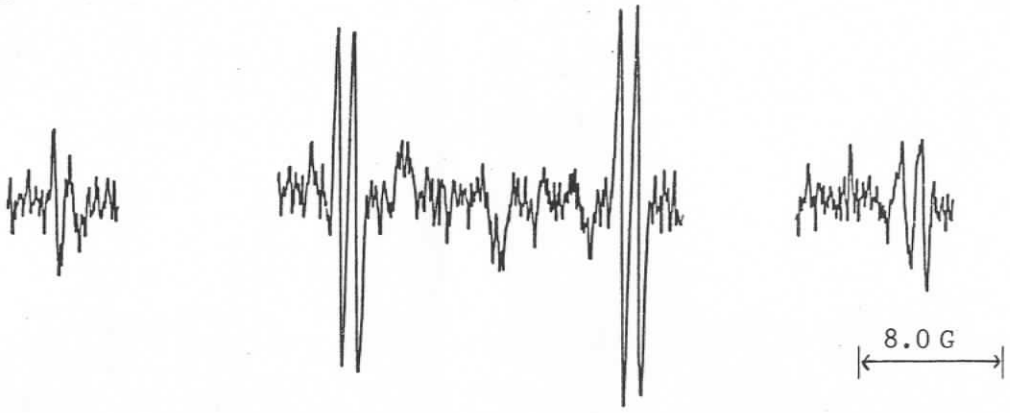

(b) T = -60°C

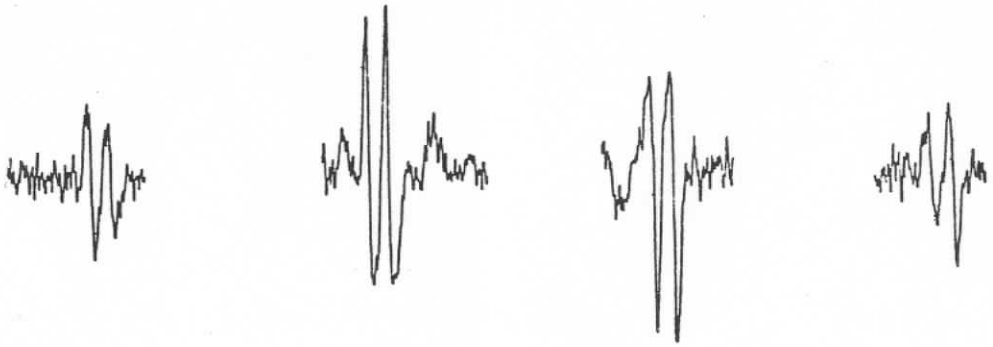

FIGURE 52: ESR spectrum of $(CH_3)_3CCH_2\dot{C}HOH$ (56) showing broadening due to restricted C_α-OH rotation. (continued)

(c) T = -80°C

(d)

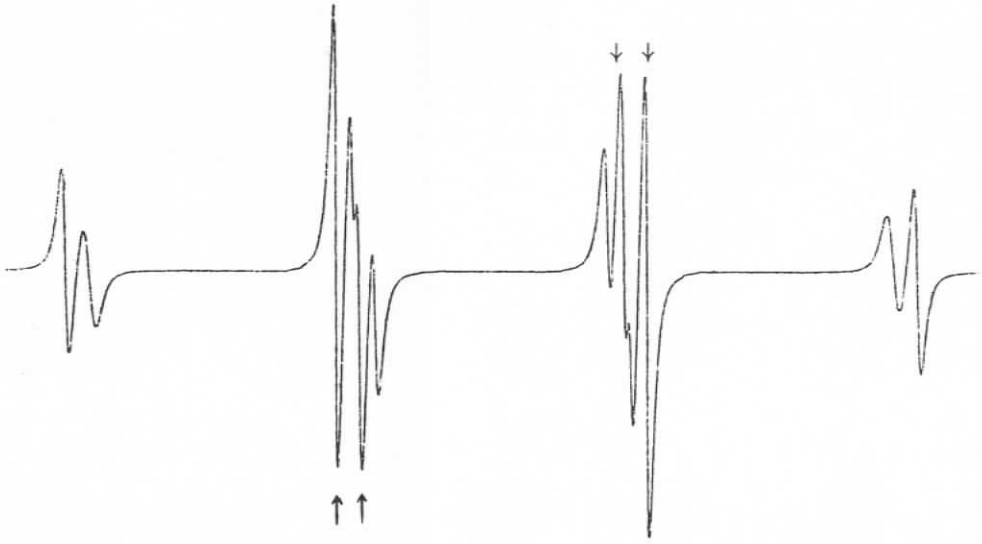

FIGURE 52 (continued): (c) Experimental spectrum at -80°C, (d) simulation of (c) showing linewidth effect due to restricted rotation about C_α-OH. Arrows indicate $\tilde{M}_\beta = 0$ lines.

cf. Figure 44a. Simulation in Figure 52d). Notably the $\tilde{M}_\beta = 0$ components in the spectrum of this species (56) are unbroadened. The symmetrical β *t*-butyl group has deactivated the C_β-C_γ rotational modulation mechanism. The low energy C_β-C_γ conformers are equivalent here.

Conformation and Long-Range Splittings. NMR studies on aldehydes indicate[134,135] that conformation (57) is populated to the extent of 80% for 3,3-dimethylbutanal. The low observed value of a_β (Table 16) is

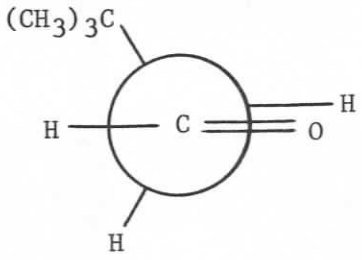

57

consistent with a preference for this conformation (58) in the case of the 1-hydroxy-3,3-dimethylbut-1-yl radical (56). Table 11 gives the expected values of β-proton hfs for angles θ of 90° and 30° in these species, which average to the observed value. The steady decrease in

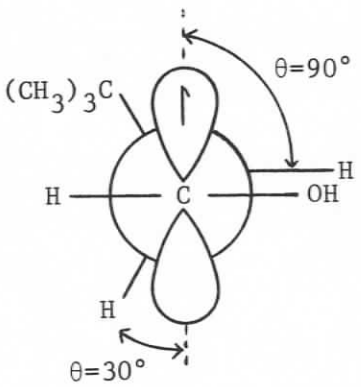

58

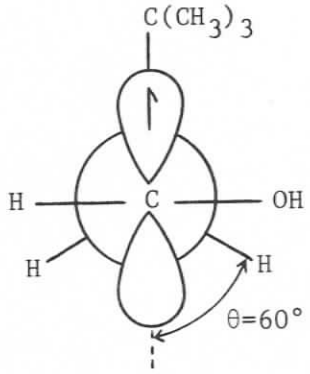

59

a_β with decreasing temperature $\left(\frac{da_\beta}{dT} \simeq +12 \text{ mG/C°}\right)$ (Table 16, Figure 43a) could, however, argue in favour of a preferred conformation (59) in which a_β is expected to be somewhat lower (Table 11, $\theta = 60°$). On the basis of considerations outlined in Chapter I, this latter conformation (59) would be the most favourable one for observing enhanced δ-proton hyperfine splittings. Indeed well resolved δ-splittings (a_δ = 0.1 G) are observed under high resolution conditions (Figure 53a). Thus this conformation (59) may be preferred for the radical (56).

It is important to note that Kochi[3] has suggested that the related radicals (60) and (61) may prefer the same symmetrical rotamer (62). Neither of these species exhibits significant selective line broadening and a for each is only minimally temperature dependent.[3] [The ether radical (63) does, however, exhibit an alternating linewidth effect as discussed early in this chapter. $T_c \simeq -107°C$][3,64]

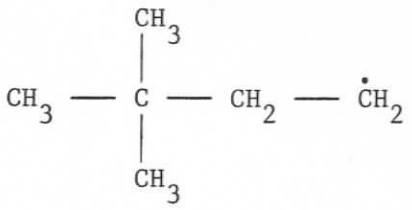

60

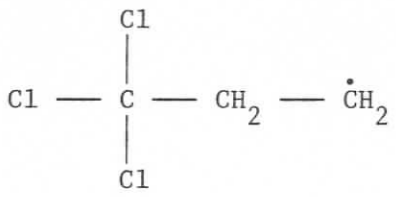

61

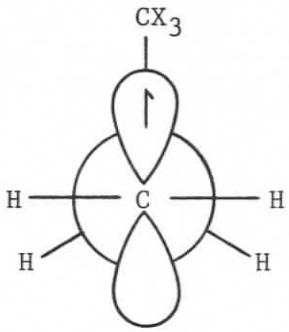

62

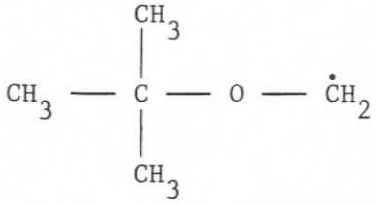

63

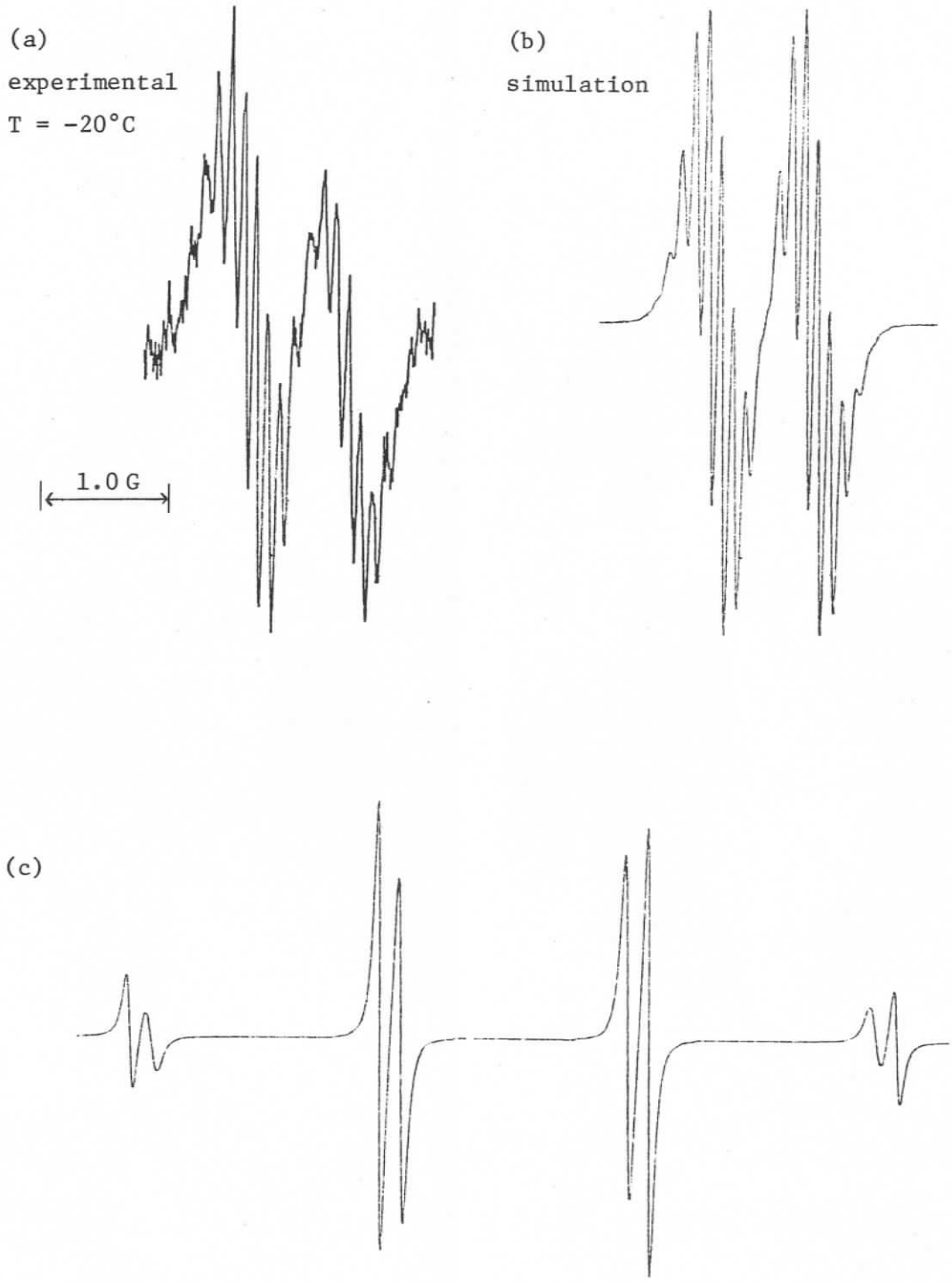

FIGURE 53: (a) Line group to left of center of spectrum at -20°C under high resolution conditions. (b) Simulation of (a) as a simple doublet of decets. (c) Note that when $a_\alpha \simeq a_\beta$ (e.g. @ -20°C) the broadening evident in this simulation is observed experimentally (Figure 53a) under high resolution conditions. [radical $(CH_3)_3CCH_2\dot{C}HOH$ (56)]

(e) Further Substitution—Two β Substituents

(i) 1-Hydroxy-2-methylprop-1-yl Radical

The hyperfine splittings of the 1-hydroxy-2-methylprop-1-yl radical (64) are given in Table 17. The relatively large value of a_β and its significant increase $\left(\frac{da_\beta}{dT} = -20 \text{ mG/C°}\right)$ with decreasing temperature (Figure 43a) are consistent with a preference for the conformation (65) (*cf.* the analogous aldehyde, Table 5). Also the γ-proton hfs is about half that observed for the β-branched radical (26) from neopentanol (Table 4).

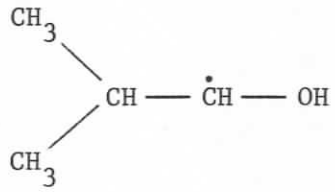

64

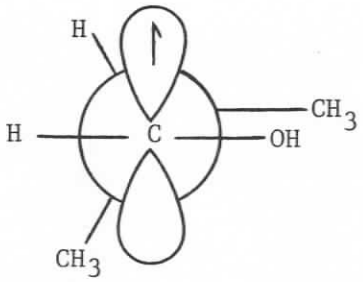

65

The line broadening pattern observed on cooling the sample (Figure 54) differs from all the 1-hydroxyalkyl radicals discussed previously. In this case the linewidth effect could not be simulated using a model in which both a_α and a_β were modulated out-of-phase with a_{OH} (i.e. by restricted rotation about C_α-OH) as before (Figure 55, also Appendix A). Instead a model in which a_β is modulated out-of-phase with a_α and in-phase with a_{OH} reproduces the experimental results best (compare Figures 54 and 55).

Such a result emphasizes the complex nature of the processes determining the sign and magnitude of changes in the *three* hyperfine

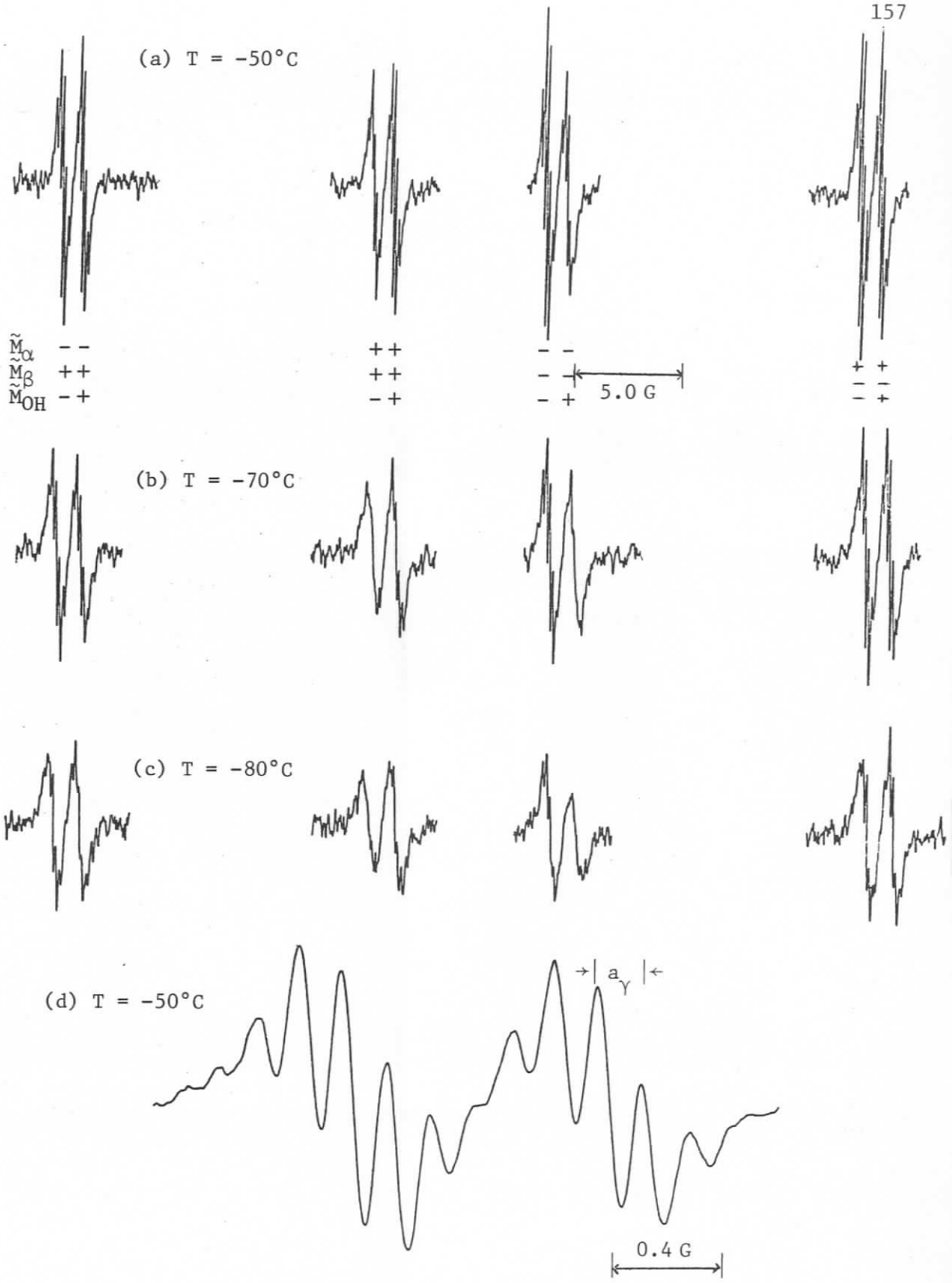

FIGURE 54: ESR spectrum of 1-hydroxy-2-methylprop-1-yl radical (64) (a) at -50°C, (b) at -70°C, (c) at -80°C, (d) high resolution on far left doublet, at -50°C.

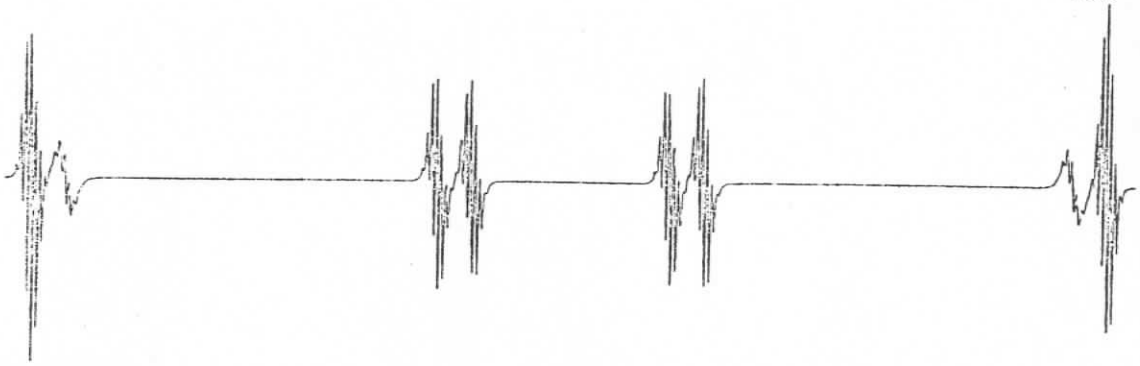

(a) a_{β} and a_{OH} modulated out-of-phase as in previous cases to show that the same model does not now apply (cf. Figure 54).

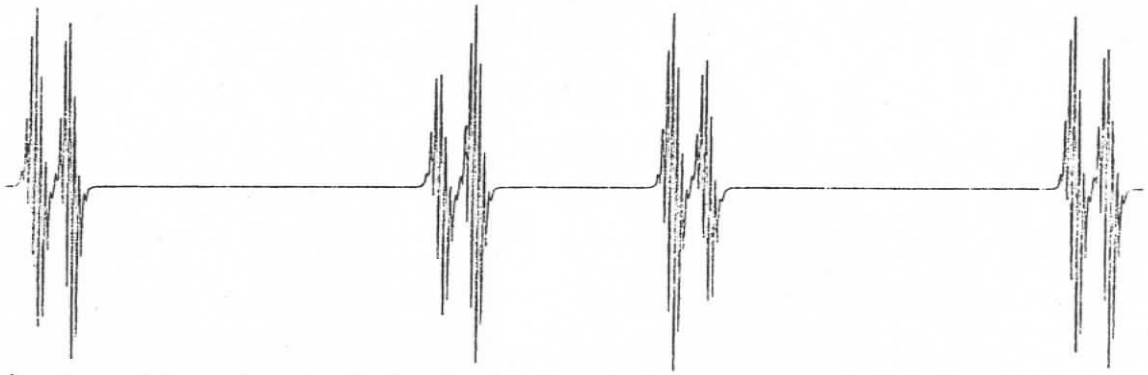

(b) a_{β} modulated out-of-phase with a_{α}, in phase with a_{OH}.

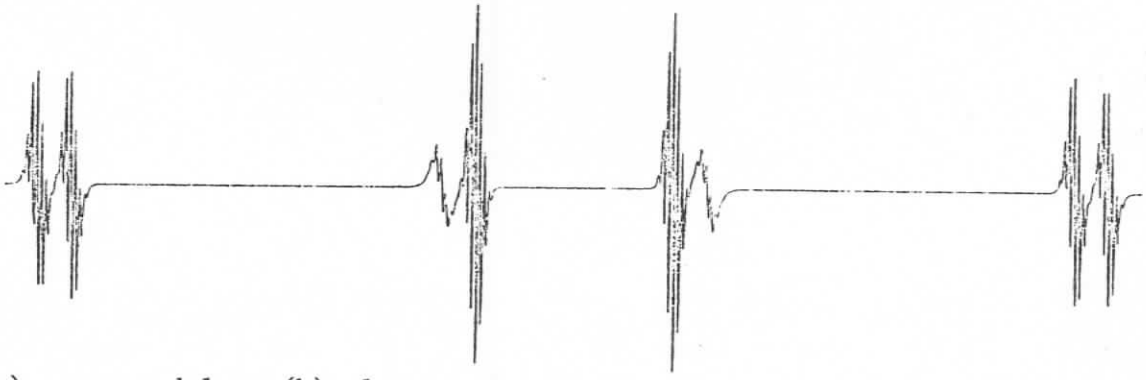

(c) same model as (b), lower rate constant.

FIGURE 55: Simulations of line broadening in the ESR spectrum of 1-hydroxy-2-methylprop-1-yl radical (64). (See Appendix A)

TABLE 17: Hyperfine splittings for 1-hydroxy-2-methylprop-1-yl radical (64)

Temp. °C	$-a_{\alpha}$	a_{β}	$\lvert a_{\gamma} \rvert$	$-a_{OH}$
	±0.05	±0.05		±0.05
+20	14.3 ±0.1	21.5 ±0.1		-*
+10	14.37	21.57		-*
0	14.50±0.1	21.6 ±0.1		0.45±0.1
-10	14.45	21.95	0.12±0.02	0.57±0.02
-20	14.54±0.1	21.85±0.1		0.70±0.1
-30	14.57	-		0.74
-40	14.60	-		0.87
-50	14.60	22.58	0.16±0.005	0.96±0.005
-60	14.63	22.73		1.03
-70	14.68	22.95		1.22
-80	14.70	23.17		1.23
-90	14.78±0.1	23.28±0.1		1.3 ±0.1
-100	-	-		*ca.* 1.4†
-110				*ca.* 1.5†
-120				*ca.* 1.6†

* incomplete resolution.

† higher linewidth, $\Delta H_{pp} \simeq 0.75$ G.

splittings ($a_{\alpha H}$, $a_{\beta H}$, and a_{OH}) created by coupled rotations about C_{α}-C_{β} and C_{α}-OH. Once again it is important to note that rotation about C_{α}-C_{β} is *not* restricted in the temperature range under consideration. Accordingly $a_{\beta H}$ is determined by (and modulated by changes in) two principal factors: recapping;

(1) Spin delocalization from C_{α} to oxygen increases for a planar C_{α}-OH conformation. The expected result is higher $\lvert a_{OH} \rvert$ and reduced

$|a_\alpha|$ and $|a_\beta|$.

(2) Rotation about C_α-OH effects changes in the C_α-C_β dihedral angles of stable conformations and hence in the spin delocalization (hyperconjugative) interaction with the β-hydrogens.

If we consider our two basic cases, i.e. (a) one β alkyl substituent with hence two β hydrogens, and (b) two alkyl substituents, the possible effects on a_β can be summarized in Scheme 1. Note for the radical from n-propanol (Scheme 1,i, $R = CH_3$) the displacement of the β hydrogens (with equivalent θ) causes a negligible change in a_β. Thus the modulation is C_α spin-density controlled (out-of-phase).

In the second case (Scheme 1,ii) displacement of β hydrogens creates a greater $|a_{\beta\ avg}|$ for decreasing $|a_{OH}|$, a conformationally induced hfs change in the same direction as the effect of C_α spin density change (i.e. again out-of-phase).

Finally, in the last case (Scheme 1,iii), since the θ angles for both β hydrogens are again similar, $a_{\beta\ avg}$ tends to be constant and the change in C_α spin density predictably will be the overriding factor (out-of-phase).

Note in all these cases small displacement of β hydrogens modulated by the restricted C_α-OH rotation is the phenomenon causing broadening and *not* restricted C_α-C_β rotation.

Now turning to the disubstituted case (from isobutanol, Scheme 1, iv), where the single β-H makes a critical low θ angle, we can easily envisage a case as shown where the net effect on $|a_{\beta H}|$ is to decrease in a synchronous fashion with $|a_{OH}|$ (i.e. in-phase) while the C_α spin density

SCHEME 1

(i)

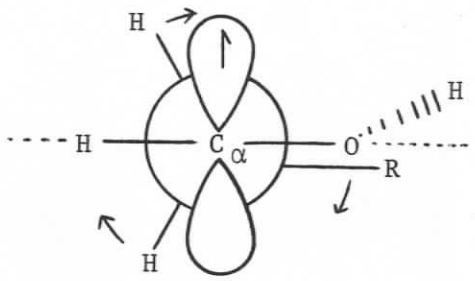

C_α-OH non-planar
lower $|a_{OH}|$

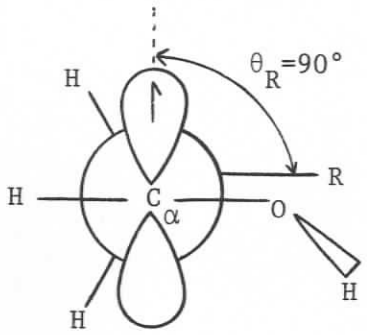

C_α-OH planar
higher $|a_{OH}|$

(ii)

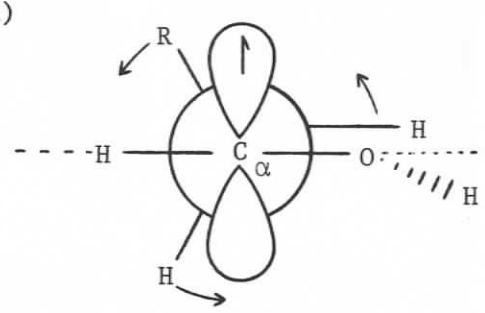

C_α-OH non-planar
lower $|a_{OH}|$
increased $|a_\beta|$

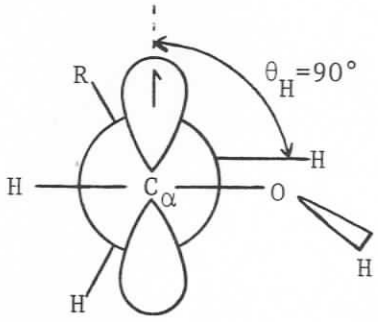

C_α-OH planar
higher $|a_{OH}|$
decreased $|a_\beta|$

SCHEME 1

(continued)

(iii)

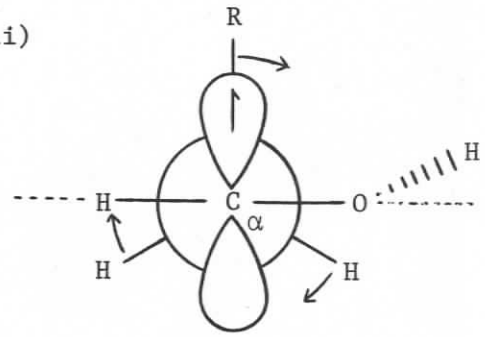

C_α-OH non-planar

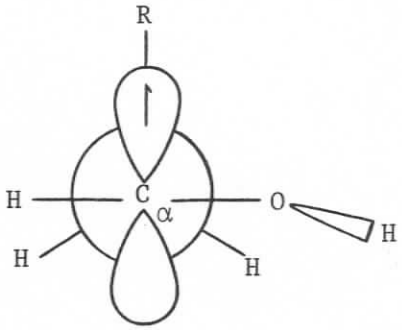

C_α-OH planar

(iv)

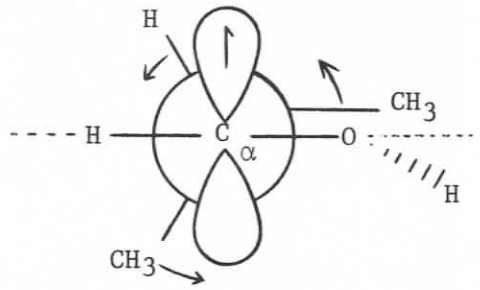

C_α-OH non-planar

low $|a_{OH}|$

low $|a_\beta|$

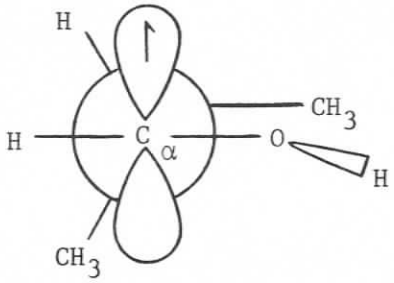

C_α-OH planar

higher $|a_{OH}|$

higher $|a_\beta|$

increases (i.e. $a_{\alpha H}$ continues to be modulated out-of-phase). A study of the radical (66) from diisobutyl ether could further define the source of the novel line broadening effects for the 1-hydroxy-2-methylprop-1-yl radical.

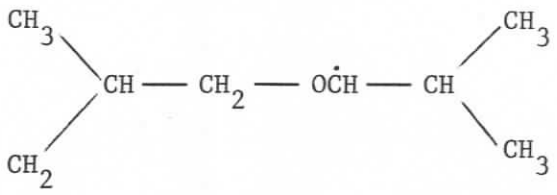

66

Barriers to internal rotation in the related isobutyl radical have recently been calculated by Pacansky and Schubert.[133] Their *ab initio* SCF study predicts a coupled C_α-C_β rotation—radical inversion for this species. There had been earlier a proposal that the isobutyl radical is subject to a deviation from tetrahedral geometry at C_β (67).[57,3]

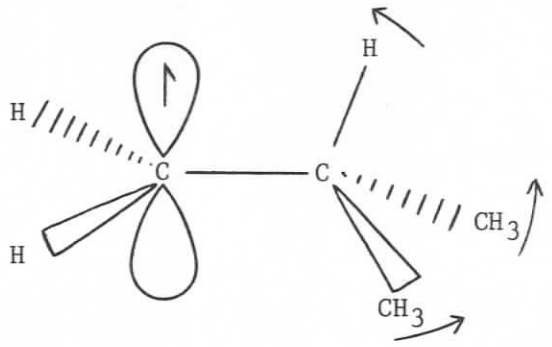

67

A related β-tilt effect in the alcohol radical (64) would also influence the rotational potential function. We do not consider that (68) represents the equilibrium conformation of radical (64) because of the unusual linewidth effect observed and because a_β would, in that case, be greater (cf. isobutyl radical, $a_\beta \simeq 32$ G @ -100°C).[3] Moreover, the

two similar radicals (49)(see section d,i) show even lower β-proton hfs than 1-hydroxy-2-methylprop-1-yl (64), indicative of equilibrium conformations (50) analogous to those found for related aldehydes (Table 5).

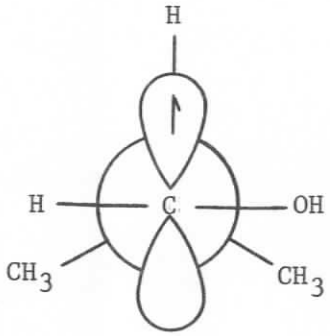

68

Finally, by -80°C some anisotropic broadening is evident in all lines in the spectrum (Figure 54c) of the radical (64)(*cf.* relatively high viscosity of isobutanol, Table 15).

(f) Further α Substitution—Radicals Derived from Complex Secondary Alcohols

(i) 2-Hydroxy-3,3-dimethylbut-2-yl Radical

The ESR spectrum of the 2-hydroxy-3,3-dimethylbut-2-yl radical (69) has not previously been reported. Splittings are given in Table 18. As the temperature was decreased the magnitude of a_{OH} decreased until at

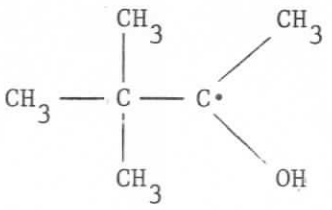

69

TABLE 18: Hyperfine splittings of 2-hydroxy-3,3-dimethylbut-2-yl radical (69)

Temp. °C	a_β	a_{OH}	$\lvert a_\gamma \rvert$
	±0.1	±0.1	
-10	19.15	0.86±0.04	
-20	19.15	0.90	
-30	19.05	0.66±0.01	0.07±0.01
-40	19.25	0.67±0.05	
-50	19.0	0.50	
-70	19.0	*ca.* 0	
-90	18.95	*	
-110	*ca.* 19.5	*	

* Unresolved.

ca. -70°C it was no longer resolved (Table 18, Figure 56). If the observed hydroxyl splitting is positive (at T = -50° to -10°C) then the conformation (70) in which $\theta_{OH} = \pm 90°$ is clearly much less favourable for this species than for the $R\dot{C}HOH$ radicals discussed earlier [i.e. positive contributions to a_{OH} from (hyperconjugative) spin delocalization will dominate]. The asymmetry of the spectrum at -70°C (Figure 56c) likely arises from anisotropy effects.

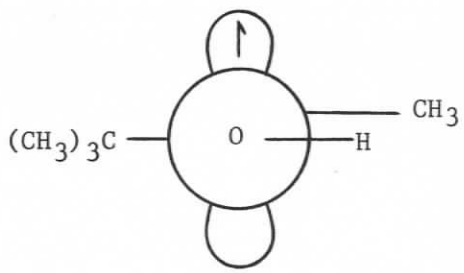

70a

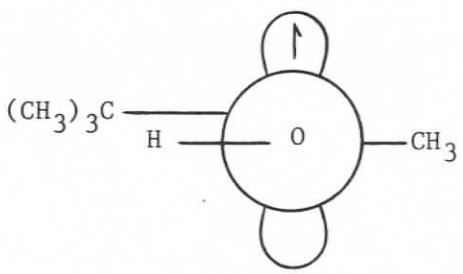

70b

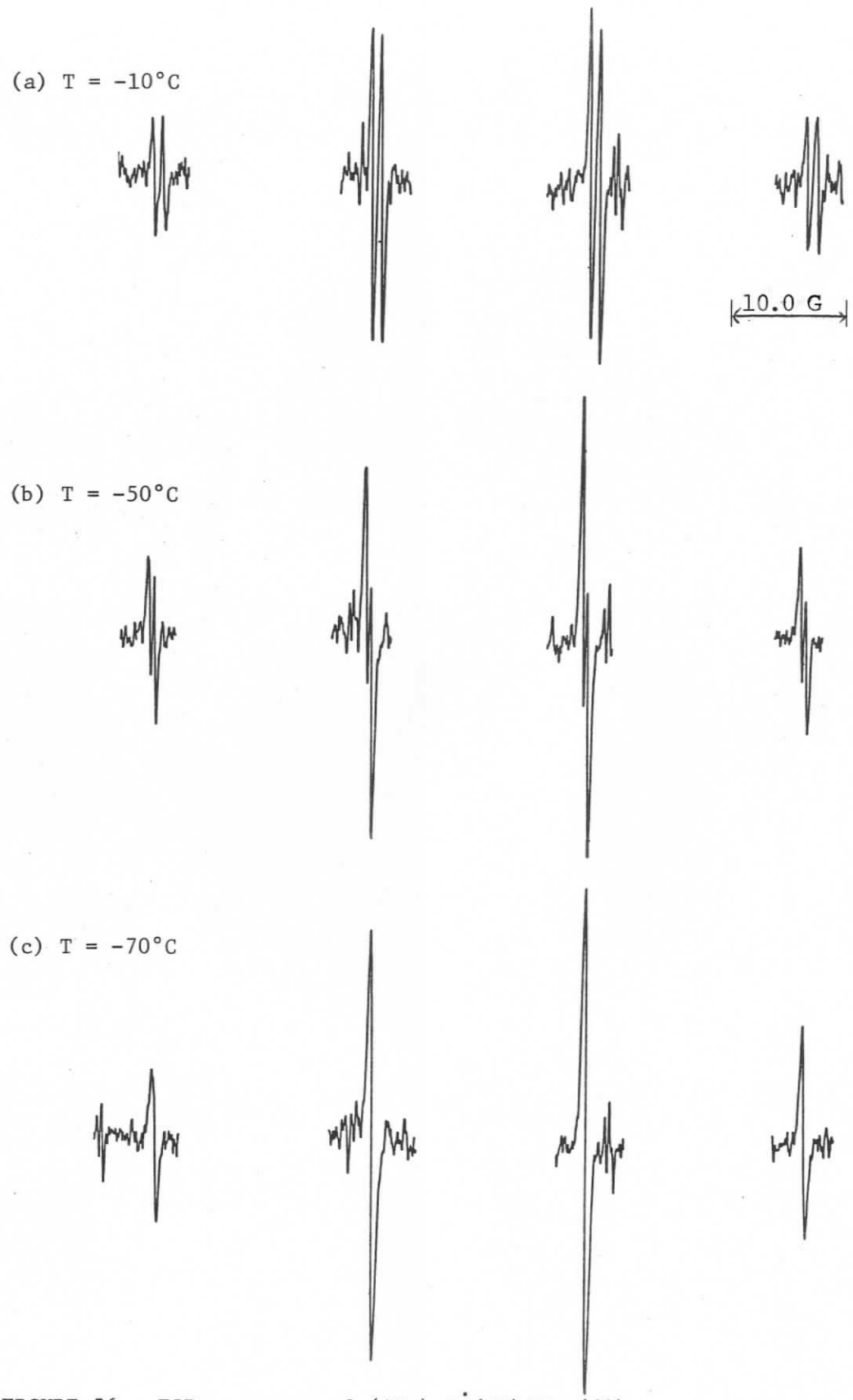

FIGURE 56: ESR spectrum of $(CH_3)_3C\dot{C}(OH)CH_3$ (69).

The γ-proton hfs is much smaller for this species (0.07 G) than in the case of $(CH_3)_3C\dot{C}HOH$ (26)(0.31 G). This is partially accounted for by removal of spin density from the radical center by its methyl substituent (*cf.* for $CH_3\dot{C}HOH$ a_β = 22.07 G @ -70°C, for $CH_3\dot{C}OHCH_3$ a_β = 19.4 G). Different equilibrium conformations involving the γ methyl groups can also be postulated. For example, while conformation (70c) seems appropriate for the relatively large $a_{\gamma H}$ observed for the radical (26) from

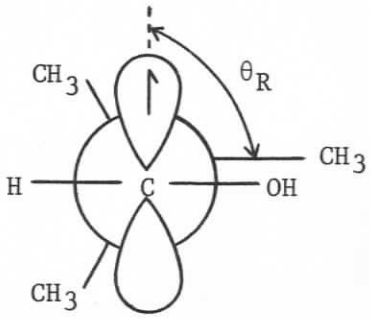

70c

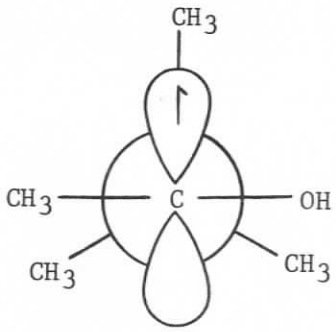

70d

neopentanol (Table 4), conformation (70d) can be postulated for the α-substituted radical (69) based on the suggestion for $(CH_3)_3C\dot{C}(CH_3)_2$.[3] Kochi[3] speculated that the θ_R = 0° group could have specific enhanced γ-H hfs but was unable to resolve any γ splittings. For radical (69) we see only the expected decet pattern.

The additional small sharp lines in the spectrum (Figure 56) are due to the radical (71) with resolved second order structure.

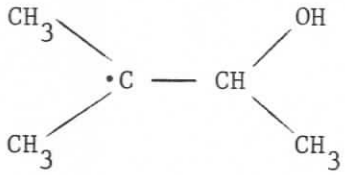

(ii) 3-Hydroxy-2,4-dimethylpent-3-yl Radical

The ESR spectrum of the 3-hydroxy-2,4-dimethylpent-3-yl radical (72) has not been reported. It consists of the expected triplet of

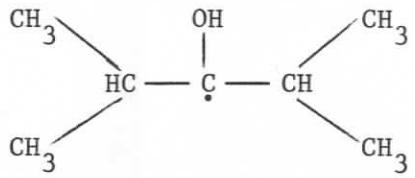

72

doublets (Figure 57, splittings in Table 19). The hfs of the twelve γ-protons could not be resolved.

TABLE 19: Hyperfine splittings for 3-hydroxy-2,4-dimethylpent-3-yl radical (72)

Temp. °C	a_β	$\lvert a_{OH} \rvert$
	±0.1	±0.1
+27	11.13	1.88
+20	10.83	2.07
+10	10.78	1.80
0	10.60	2.02
-20	10.45	1.75
-40	9.98	1.90
-50	9.85	1.87
-60	9.75	1.83
-70	9.74	1.69
-80	9.30±0.3	1.89
-90	9.75±0.2	1.95
-100	a possible assignment, see text	32.3±0.25
-110		32.6±0.25
-130		33.5±0.1

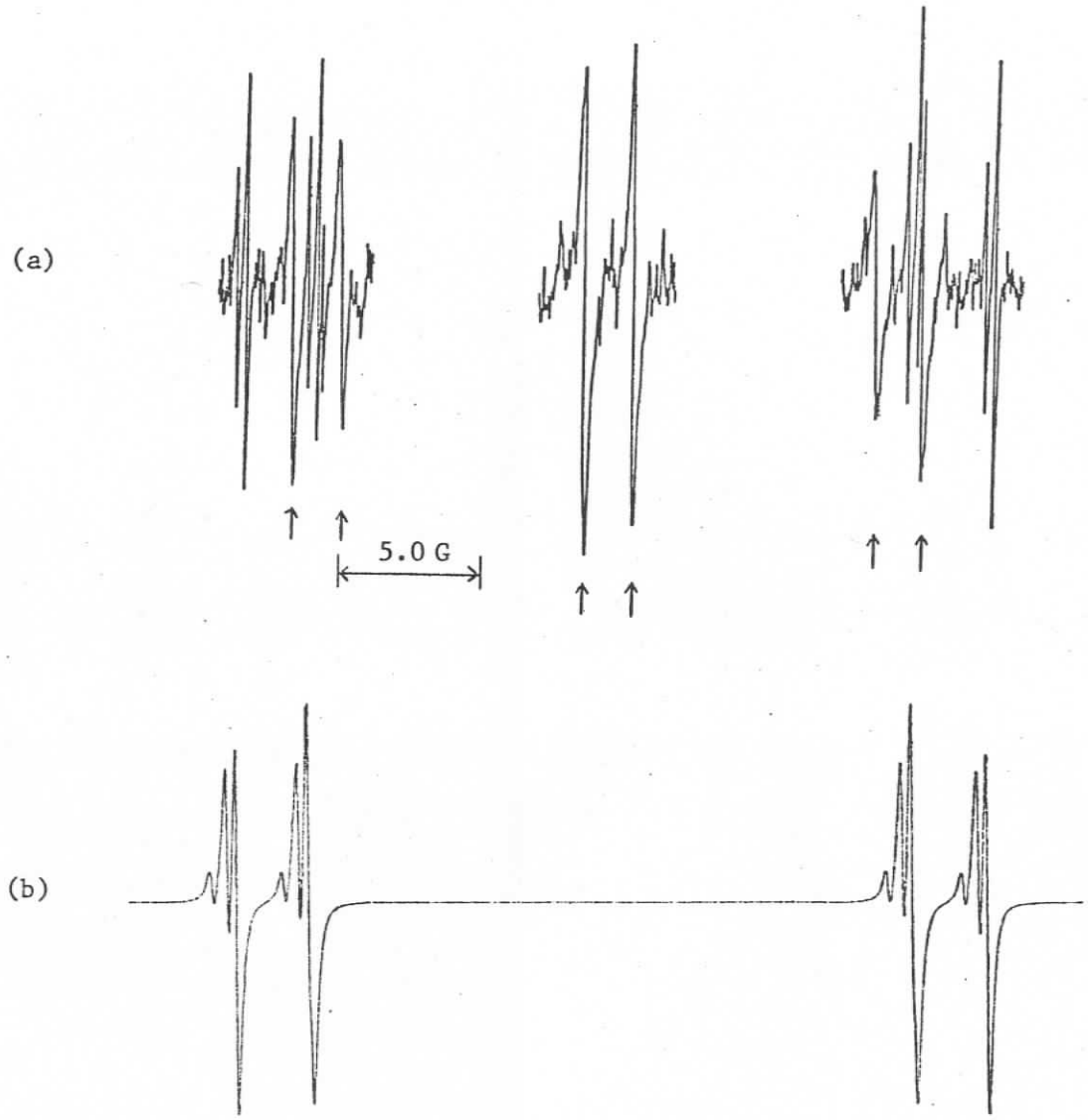

FIGURE 57: (a) ESR spectrum of radical (72) at -20°C (↑), (b) simulation of center peaks of ESR spectrum of radical (73). The smallest splittings are 2nd order structure.

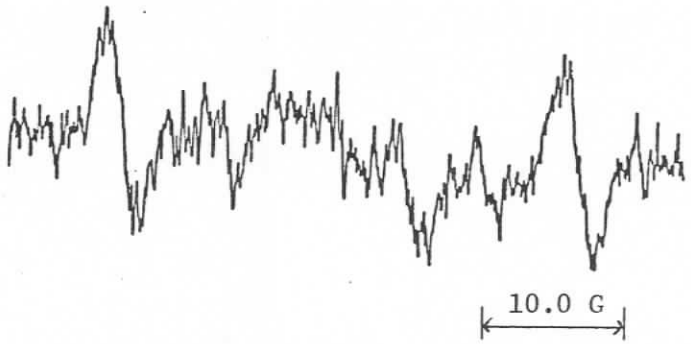

FIGURE 58: The ESR spectrum observed on initially irradiating $(CH_3)_2CHCH(OH)CH(CH_3)_2$ at -130°C and then increasing sample temperature to -110°C. (a = 32.6 ± 0.25 G)

Superimposed on the main spectrum is a second spectrum assigned to the species (73). The second spectrum is centered at a slightly higher field value (ΔH = +0.4 G, $\Delta g \simeq -0.0002$) than that of radical (72), and

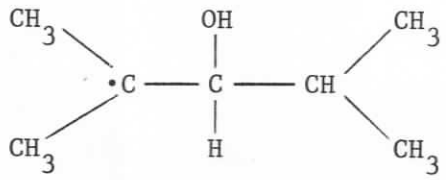

73

can be simulated (Figure 57) as a doublet (a = 21.45 ± 0.1 G) of septets (a = 24.10 ± 0.1 G) in which second order splitting is clearly resolved. We could not discern any linewidth effects in the spectrum of the α-hydroxy radical (72) which were not artifacts of overlap with the spectrum attributed to species (73).

Notable for the radical (72) are its very low β-proton hfs and its relatively high value of a_{OH} (Table 19). The former suggests favourable conformations in which the β-protons lie in or near the nodal plane of the semi-occupied p_z orbital. The value of a_{OH} is not only high but also remains relatively unchanged between +27°C and -90°C. We suggest, by comparison with the radicals $(CH_3)_2\dot{C}OH$ (32) and $(CH_3)_3\dot{C}COHCH_3$ (69) that a_{OH} is positive, which would indicate that conformations having $\theta = 90°$ for the hydroxyl group are effectively destabilized.

The radicals (74)[91] and (75)[139] have hydroxyl hyperfine splittings of 2.51 G and 3.72 G respectively. In the latter case the authors had hoped to observe a very high a_{OH} attributable to a significant potential minimum at $\theta = 0$ for the hydroxyl group rotation. They concluded,

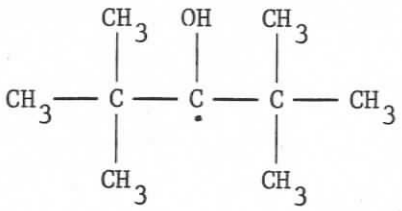

$a_{\gamma H}$ = 0.23 G

74

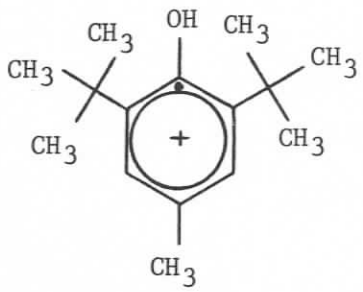

75

however, that the hydroxyl proton is constrained to lie in the plane of the aromatic ring and is sandwiched by two methyl groups of an adjacent *t*-butyl group. They imply, though, that the splitting is positive.

Davies and coworkers[140] have studied the ESR spectra of radicals of the type (76). When R is n-butyl or n-propyl the spectra showed[140]

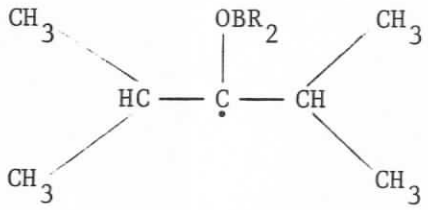

76

an alternating linewidth effect in which the $\tilde{M}_{\beta}$ = 0 components were broadened. They attributed this to the exchange 77a $\rightleftharpoons$ 77b. We observed no such linewidth effect in the spectrum of species (72). Note

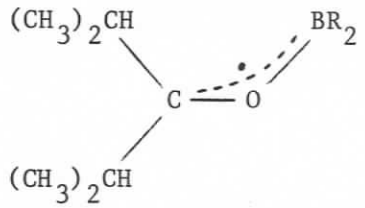

77a

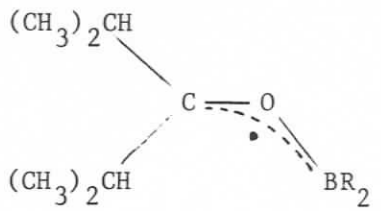

77b

that the $\tilde{M}_\beta = 0$ components for the radical (72) are not obscured by overlap with lines due to species (73).

We found that the spectrum of a sample of 2,4-dimethyl-3-pentanol initially irradiated at -130°C consists of a broad doublet (a = 33.5 ±0.1 G). This doublet is readily discernible as the temperature is increased to -100°C. Its appearance at -110°C is shown in Figure 58. As the temperature is further increased from -100° the "normal" spectrum of radical (72) appears at *ca*. -50°C.

This large splitting (33.5 G) is within the range calculated by Krusic et al.[57] for the hydroxyl proton of hydroxymethyl radical in a $\theta = 0°$ conformation (78). With the possible exception of this radical

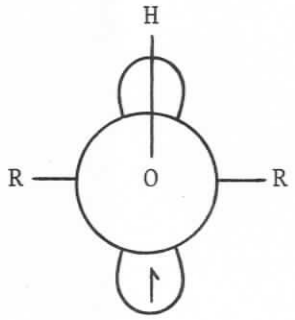

78

the observation of hfs due to a hydroxyl proton in a potential minimum at $\theta = 0°$ has not been reported.[37] However, further work with the deuterated analogue will be necessary to confirm such an assignment.

It should be pointed out that Krusic et al.[124] have assigned a significant splitting (16.5 G) to only *one* β-fluorine atom in their series of radicals (79, R = alkyl, phenyl). They suggest that the two perfluoroisopropyl groups are conformationally non-equivalent allowing only one β-fluorine to interact appreciably with the unpaired electron.

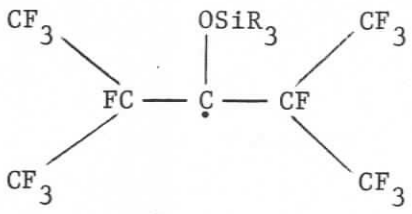

79

The simple doublet in Figure 58 could also arise from a similar single β-hydrogen splitting.

The low observed value of a_β for radical (72) (with $\frac{da_\beta}{dT}$ = +12 mG/C°) (Table 19) indicates a large dihedral angle with respect to the semi-occupied p_z orbital (Table 11). This in turn suggests a relatively small angle θ_R for the β-methyl groups (80).

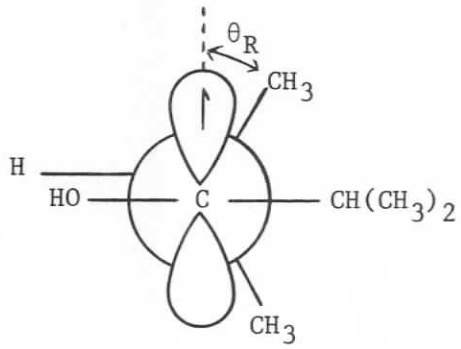

80

Thus we would expect to observe enhanced γ-proton splittings for this species. Experimentally the γ-splittings could not be resolved. Bending at C_α would decrease the γ-proton hyperfine interaction. However, since radical centers with extremely bulky substituents tend to prefer planarity,[117] the degree of bending for species (72) may actually be less than for the prototype $(CH_3)_2\dot{C}OH$. Since a θ_R = 30° conformation is

virtually mandatory, the contrast between the experimentally low a_γ and that anticipated on the basis of hydrocarbon models[32,132] demonstrates the caution that must be exercised when remote splittings are compared between species with widely different α-substituents.

(iii) 1-Hydroxycyclohexyl Radical

The ESR spectrum of the 1-hydroxycyclohexyl radical (81) has received much attention in the literature.[141-146,130] At 59°C the spectrum is a pentet due to four equivalent β-protons.[141] At -83°C the

81

spectrum is a triplet of triplets corresponding to two axially and equatorially non-equivalent pairs of β-protons.[141] Our low temperature spectra are in agreement with this exchange effect.(see Table 20)

TABLE 20: Hyperfine splittings of 1-hydroxycyclohexyl radical (81)

Temp. °C	$a_{\beta ax}$	$a_{\beta eq}$	$\lvert a_{\gamma_1} \rvert$	$\lvert a_{\gamma_2} \rvert$	Other (1H)
	±0.2	±0.1	±0.1	±0.1	±0.1
-70	35.86	10.44	0.60	0.60	0.60
-90	-	10.36	0.70	0.70	0.70
-100	36.12	10.40	0.72	0.72	0.72

Note: The calculated 2nd order hfs for 2H at 35.9 G is 0.38 G.

Corvaja et al.[130] have suggested that the twist-boat conformer is the most stable for this radical while Lloyd and coworkers[141,142] favour a chair conformation. The latter authors indicate that their theoretical[142] and experimental[141] results are best accounted for by chair-to-chair interconversion with concerted inversion of the radical center (82a $\rightleftharpoons$ 82b).

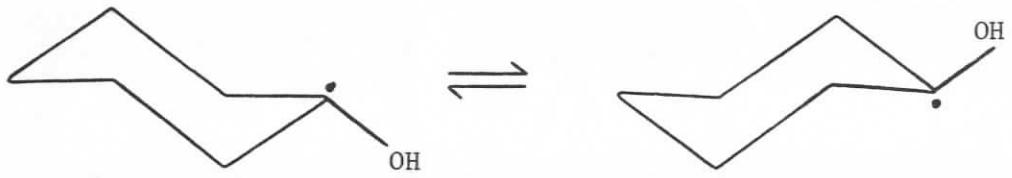

82a 82b

Unfortunately, in all these studies no further hyperfine splittings have been resolved. In this work it is demonstrated (Figure 59) that such additional splittings are present. The broadened appearance of the central triplet is due to incompletely resolved second order structure (Figure 59b). The optimum simulation of the observed multiplicity was achieved with coupling to five protons, in addition to H_β, all at 0.7 G. These are four γprotons and one other, either the hydroxyl proton or a single δ-proton. Lloyd et al.[141] indicated that in the analogous 4-methyl-1-hydroxycyclohexyl radical the hydroxyl proton did not contribute to observed splittings. In our work the multiplets were not strongly temperature dependent as might be expected for coupling to the hydroxyl proton. It should be noted that Lloyd's splittings[141] of a = 0.78 G (2H) and a = 0.39 G (3H) are based on a

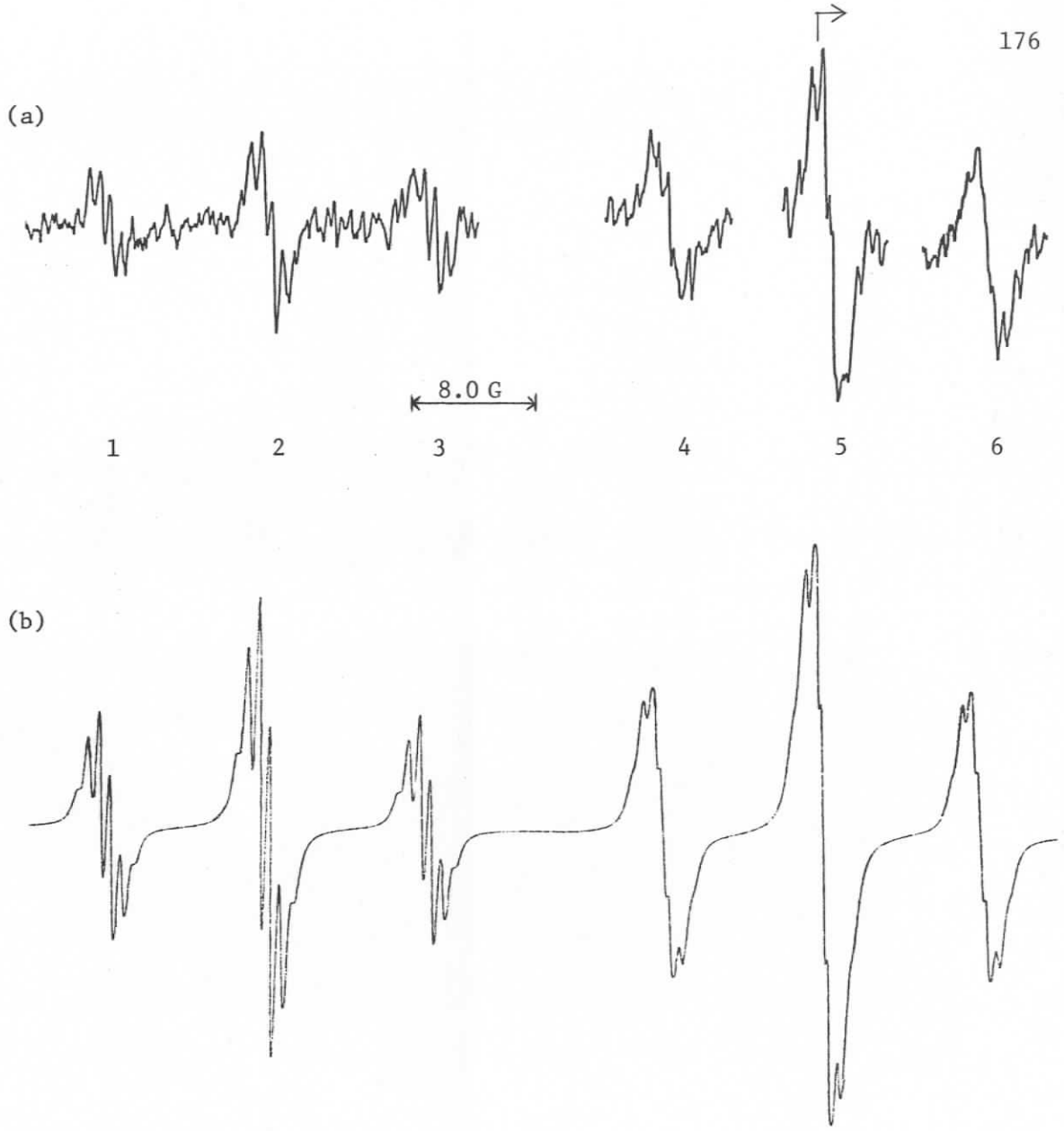

FIGURE 59: (a) Part of the ESR spectrum of 1-hydroxycyclohexyl radical (81) at -70°C. (b) Simulation of (a) which includes 2nd order splittings.

simulation of a severely broadened multiplet ΔH_{pp} = 0.40 G, so that the discrepancies in the γ-H splittings in the two determinations are not easily adjudicated.

The high resolution spectrum at -90°C (Figure 60) reveals a broadening of peaks 1, 4, 6 and 9. Exact simulations are hampered by the fact that the exchange program used[102] does not include second order effects. The best simulation we achieved involved modulation of $a_{\beta\text{-axial}}$ and $a_{\beta\text{-equitorial}}$ pairwise in phase (see Appendix A). Other splittings were not allowed to vary. Figure 61 illustrates the simulation at fast and intermediate rates.

Simulation models in which the two axial β-protons (and the two equitorial β-protons) are not completely equivalent, as would be expected if the modulating mechanism was restricted OH rotation, do not reproduce the observed linewidth effect. Peaks 4 and 6 are partially broadened by incompletely resolved second order splittings, and the onset of anisotropic broadening at -90°C cannot be ruled out completely. Further studies, for example using substituted cyclohexanols, other solvents and more dilute solutions are warranted. Notwithstanding the data show how higher resolution for 1-hydroxyalkyl radicals reveals additional information on the full range of line broadening effects that are actually operative.

The process that best fits the simulation model is inversion of the radical center (83a $\rightleftharpoons$ 83b). The following energy barriers result from *ab initio* calculations by Lloyd and coworkers:[142]

barrier	to	OH restricted rotation	2 Kcal/mol
barrier	to	inversion of radical center	3.5 Kcal/mol
barrier	to	ring inversion	$\geqslant$5 Kcal/mol

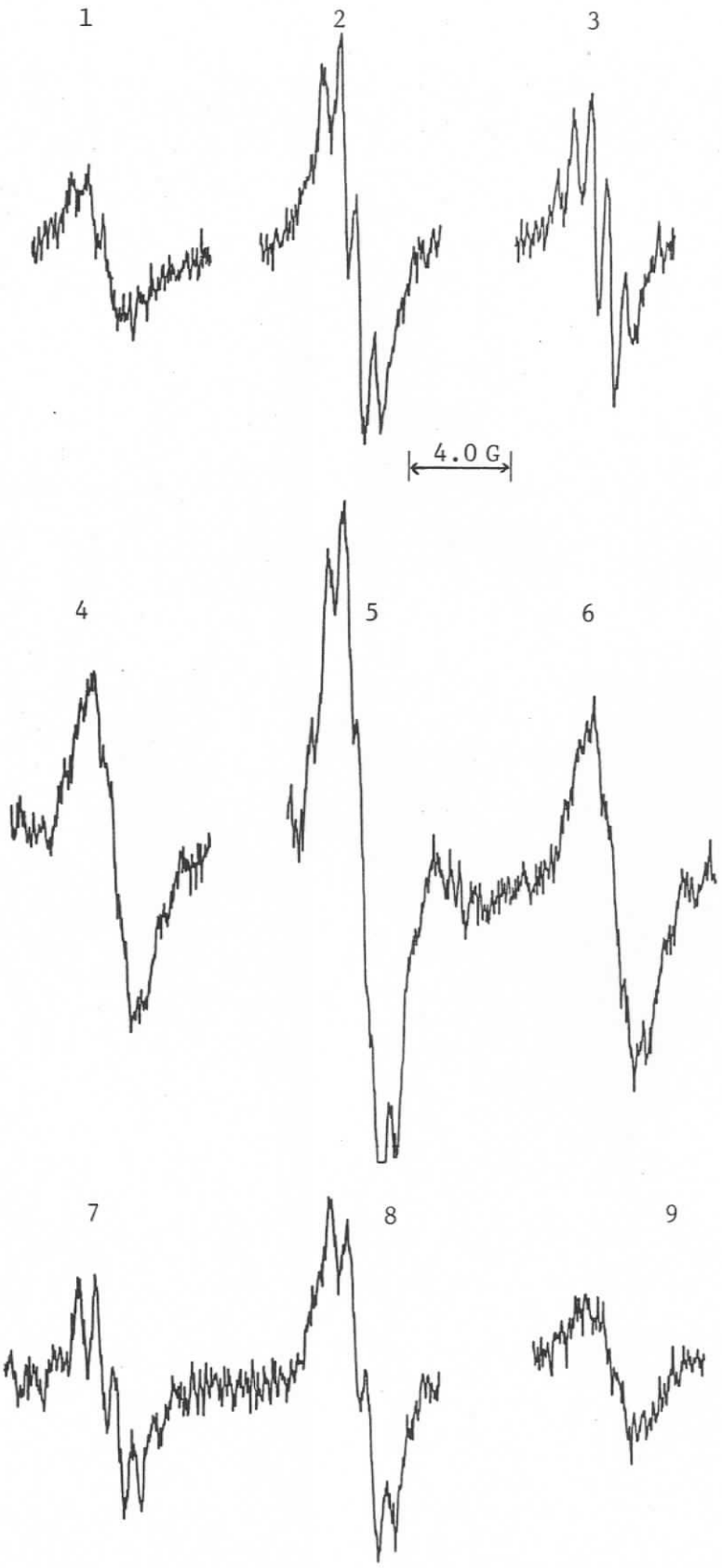

FIGURE 60: High resolution ESR spectrum of 1-hydroxycyclohexyl radical (81) at -90°C.

FIGURE 61: Simulated low temperature exchange spectrum of 1-hydroxycyclohexyl radical (81), (a) at fast exchange (*ca*. -70°C), (b) at slower exchange (*ca*. -90°C). (Second order splittings not included.)

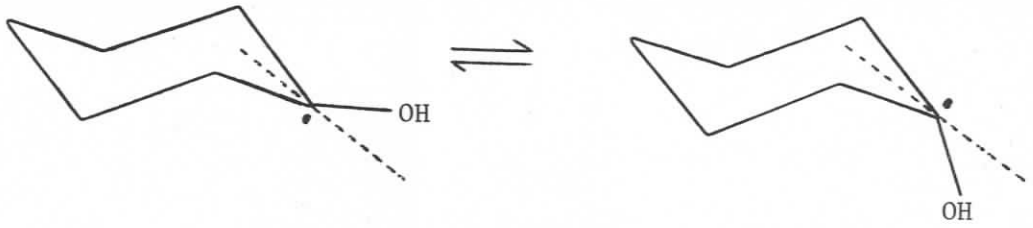

83a 83b

An out-of-plane angle of *ca*. ±36° was calculated to be the energy minimum.[142]

Hydroxyl group rotation may well be sufficiently fast (unrestricted) for this species that it does not give rise to observable modulation effects in the accessible temperature range. Radical center inversion would logically modulate the β-proton hfs in an axially and equatorially pairwise way. Our simulation model assumes also that the changes in $a_{\beta\text{-axial}}$ and $a_{\beta\text{-equatorial}}$ are in the same direction (see Appendix A).

Significant barriers to inversion for radicals have been observed previously. Malatesta and Ingold[70] found that inversion is completely inhibited in the radical (84) at temperatures as high as +20°C, implying a barrier $\geqslant$10 Kcal/mol. Accordingly, radical center inversion in

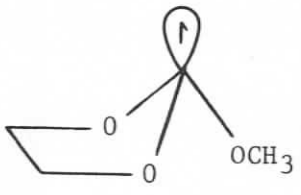

84

1-hydroxycyclohexyl radical (81), particularly with a (calculated) barrier of 3.5 Kcal/mol,[142] could cause observable linewidth effects.

(g) Summary, Conclusions and Suggestions for Further Work

The wide applicability of a general model to explain the linewidth effects observed in the low-temperature ESR spectra of α-hydroxyalkyl radicals (Figure 62) has been demonstrated. The model involves restricted rotation of the hydroxyl group and consequent modulation of the α, β and hydroxyl proton hyperfine splittings. Low energy conformations having the hydroxyl proton out of the nodal plane of the semi-occupied p_z orbital must be considered, and although in all cases a simple two-site exchange satisfactorily reproduces the experimental observations this number is not specifically required. Several rotational potential minima, some of which are degenerate, would in fact be expected. A possible test case for the importance of out-of-plane equilibrium conformations is the radical (85) from diisopropyl ether. The hfs of the γ'-proton could

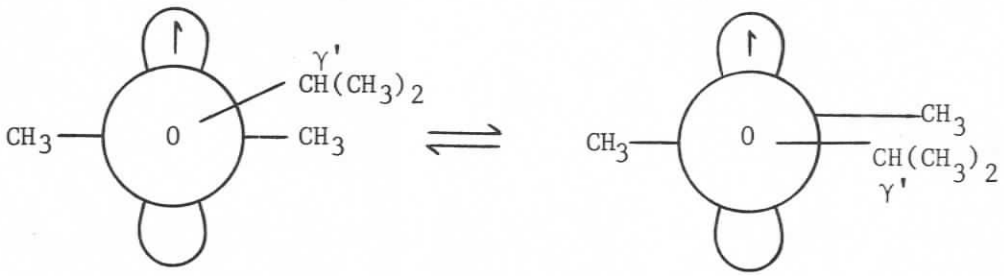

85a 85b

have two different observable values at low temperatures, corresponding to the conformations (85a) and (85b). The isopropyl group may be sufficiently bulky to induce these non-planar conformations.

FIGURE 62: Summary of model explaining ESR linewidth effects for α-hydroxyalkyl radicals.

A. Restricted Rotation About C_α-OH

1. (Refs. 57 and 125)

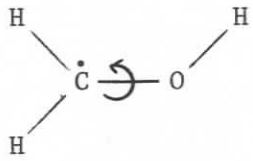

H_α hfs modulated out-of-phase, no change in a_{OH}

2.

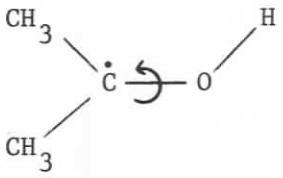

both β-CH_3 hfs modulated out-of-phase with a_{OH}

3.

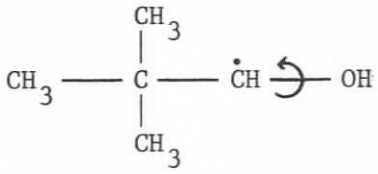

H_α hfs modulated out-of-phase with a_{OH}

4.

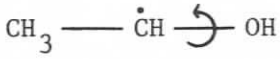

H_α and H_β hfs modulated out-of-phase with a_{OH}

—Figure 62 continues—

—Figure 62 continues—

B. Restricted Rotation About C_α-OH and C_β-C_γ

1. (See ref. 112)

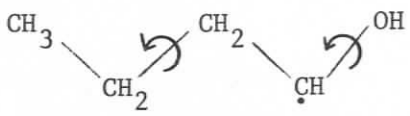

restricted C_β-C_γ rotation modulates the two H_β hfs mutually out-of-phase

2.

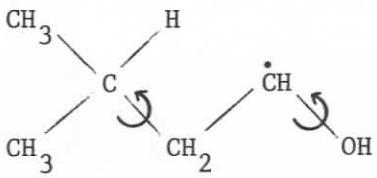

restricted C_β-C_γ rotation modulates the two H_β hfs mutually out-of-phase

3.

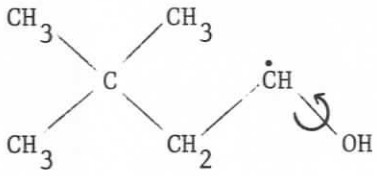

no apparent line broadening from restricted C_β-C_γ rotation

In the model used, mutual exchange was always assumed. In none of the examples in this chapter was the slow exchange spectrum obtained, nor is this likely to be possible due to the onset of severe anisotropic broadening for solutions of these alcohol substrates at low temperatures (*ca.* $\leqslant -100\,^{\circ}C$).

Superimposed on the hydroxyl group rotation effect is an out-of-phase modulation of the two β-proton splittings by restricted $C_{\beta}-C_{\gamma}$ rotation in some cases.

Based on recent results[132] for n-propyl radical it may now be possible to obtain limiting β-H and γ-H hyperfine splittings by studying n-butyl radical (obtained by reduction of the bromide) in liquid propane.

Moreover, diastereotopically induced non-equivalence of β-H hfs will be observed for such radicals as (86a) and (86b) even at temperatures where there is free rotation about $C_{\beta}-C_{\gamma}$.

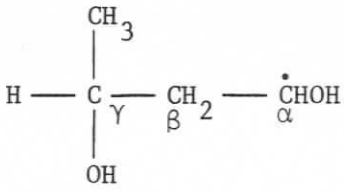

86a

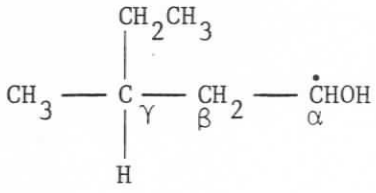

86b

Ether derived radicals such as (86c) will again prove useful in such studies.

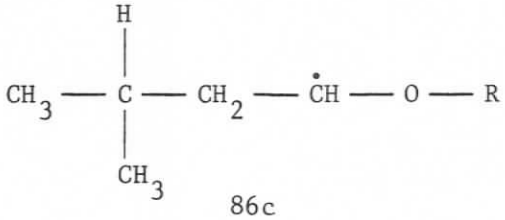

86c

Note that throughout the study we have commented on the usefulness of remote (γ) splittings in discussion of the preferred conformation (s) of radicals. As well, high resolution has been shown to be necessary to identify the inherent multiplicity of lines generated by second order effects in order to clearly isolate line broadening.

In cyclic radicals it has been shown that at low temperatures processes other than ring flip such as radical site inversion should be considered in generating an appropriate model for the high resolution spectrum of 1-hydroxycyclohexyl radical. Additional evidence, e.g. from 4-methyl-1-hydroxycyclohexyl radical and from hydroxycyclopentyl examples should be sought in support of this proposal.

In this work we have examined a series of β-alkyl alcohol-derived radicals where the conformations of the analogous aldehydes have been studied[134,135] (Table 5). The evidence, including β and γ-proton hfs, is consistent with the preferred conformation (87a) for the primary

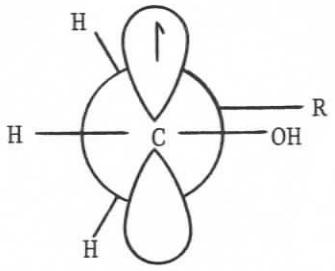

87a

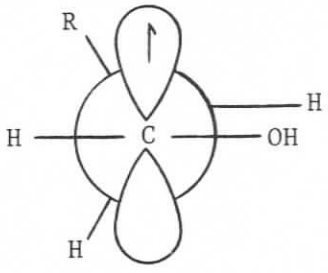

87b

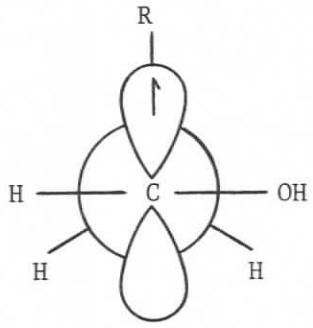

87c

alcohol radicals, except when R is bulky (e.g. isopropyl), in which case a preference for conformer (87b) is indicated. In the case of R = *t*-butyl, conformation (87c) is not specifically excluded by the observed parameters.

Hydrogen bonding must play an important role in these conformational equilibria for alcohol-derived radicals. Currently medium effects on such polar transients are poorly understood and are given scant attention in literature reports on the dynamic ESR of such radicals. Liquid alcohols are in association equilibria involving a variety of small polymers $(ROH)_n$, $n \leqslant 7$, which may be linear or cyclic in nature.[148,149,150] The enthalpy of dimerization of alcohols (in CCl_4 soln.) ranges from *ca.* -9.3 Kcal/mol for methanol to *ca.* -4.1 Kcal/mol for the more sterically hindered species di-*t*-butylcarbinol.[150] Alcohols are involved in two and only two hydrogen bonds per molecule.[148,150] If the properties of the alcohol-derived free radicals parallel these properties then the energy required to break two hydrogen bonds in a solution of hydroxyalkyl radicals is greater than the barrier determined for restricted rotation about C_α-OH (cf. hydroxymethyl radical, *ca.* 4 Kcal/mol)[57] and the barrier to C_β-C_γ rotation in 1-hydroxybut--1-yl radical (*ca.* 2 Kcal/mol).[112] Therefore an alternative model for C_α-OH rotation involves a relatively immobile hydrogen-bonded hydroxyl group attached to an alkyl chain which actually sweeps through the spatial arc in solution (87d).

A relevant experiment would be the observation of the radical $CH_3CH_2\dot{O}CHCH_3$ in the presence of *t*-butyl alcohol. The ESR spectrum,

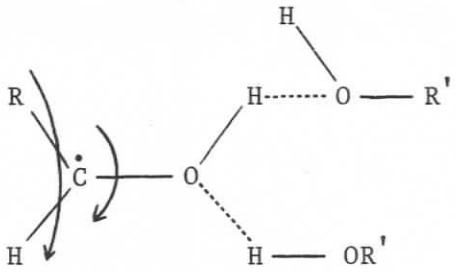

87d

normally isotropic to -145°C, might exhibit significant anisotropy if the radicals were hydrogen bonded. Clearly the effects of changing viscosity would be considered as well.

Further research involving simple hydroxyalkyl radicals should have as one of its objectives a clearer understanding of the role of hydrogen bonding in the conformational processes. Only through such studies can information be obtained that will indicate the preferred conformations of related polyol radical species in aqueous biological systems.

CHAPTER IV

CONFORMATIONS OF RADICALS FROM 1,3-DIOXANES AND 2,4,8,10-TETRAOXASPIRO[5,5]UNDECANES

1. BACKGROUND

In recent years the fixed geometry of cyclic ethers has been exploited to reveal dynamic processes (e.g. ring inversion) both in the parent compounds themselves[151,152] and in free radicals[40] derived from them. Some aspects of the conformational dependence of remote hyperfine splittings have been revealed by ESR studies of these latter species.[40]

Work on alcohols of increasing complexity prompted us to examine the effects of additional alkyl substitution in the 1,3-dioxane series in order to test the generality of conformational and configurational effects in radicals extensively substituted at C_β.

(a) ^{1}H NMR Studies of Parent Molecules

The conformational aspects of the 1,3-dioxane system have been thoroughly studied. The reviews presented by Eliel[151] and Wyn-Jones et al.[152] are most relevant to the present work.

Table 21 lists the ^{1}H NMR coalescence temperature, free energy of activation and activation energy (for chair-to-chair interconversion) for parent ethers of some of the radicals to be discussed. The table shows that dimethyl substitution at position 2 lowers the barrier to inversion (and the coalescence temperature) as revealed by comparison of (88) and (89), (90) and (91), and (92) and (93). This reflects the

TABLE 21: Some thermodynamic data for chair-to-chair interconversion of 1,3-dioxanes and related spiro ethers

Compound Number	Compound	Avg. T_c °C ^1H NMR	$\Delta G_c^{\ddagger}$ Kcal/mol	E_a Kcal/mol	Reference
88	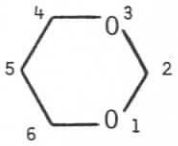	-82	9.7	11.5±1.0 in $CFCl_3$ Ref. 156	153,152
89	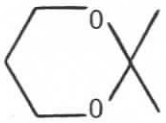	-126	7.8 for -73°C	6.7	154,152
				10.7±1.4	155
90	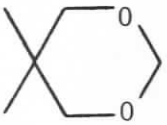	-57.5	10.5		153,152
			10.9±0.1	11.2±1.7	156
				13.5±0.8	155
91	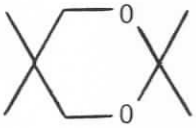	-102.7	8.2	9.5±0.9	154,152
				10.6±1.5	155
92	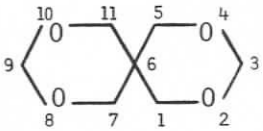	-72.9	9.7±0.1	9.6±0.6	156,152
93		-105	8.4±0.2	—	156,152
94	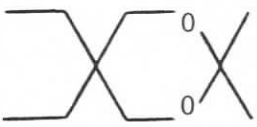	Only broadening of peaks at -110°	—	—	This work

fact that a 2-axial substituent is energetically unfavourable due to 1,3-diaxial interactions with the protons at positions 4 and 6. In all cases the energy minima correspond to chair conformers.[152] The simplicity of the ^{1}H NMR spectrum of 5,5-dimethyl-1,3-dioxane (90) and its relatively high coalescence temperature have made it a good example for the illustration of dynamic effects in ^{1}H NMR spectroscopy.[157]

The other dioxanes used as substrates in the present work are 2-methyl-1,3-dioxane (95), 2,5,5-trimethyl-1,3-dioxane (96), and 3,9-dimethyl-2,4,8,10-tetraoxaspiro[5,5]undecane (97). The conformer

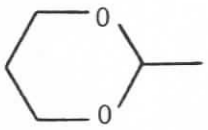

95

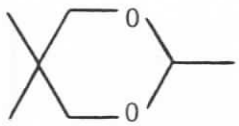

96

97

of compound (95) in which the 2-methyl group is equatorial is favoured by *ca.* 4 Kcal/mol,[152] and the marked preference of a 2-alkyl substituent for the equatorial conformation is quite general.[158] For example, it was found in this study that compound (97) exhibits the ^{1}H NMR spectrum of a single conformer even at +100°C (Figure 63).

(b) ESR Studies of Conformation for Derived Radicals

Radicals derived from 1,3-dioxanes have been the subject of much research. Attention has focussed on their configuration and conformation,[27,40,65,69,79,93] reactions in which they are involved,[69,159] and

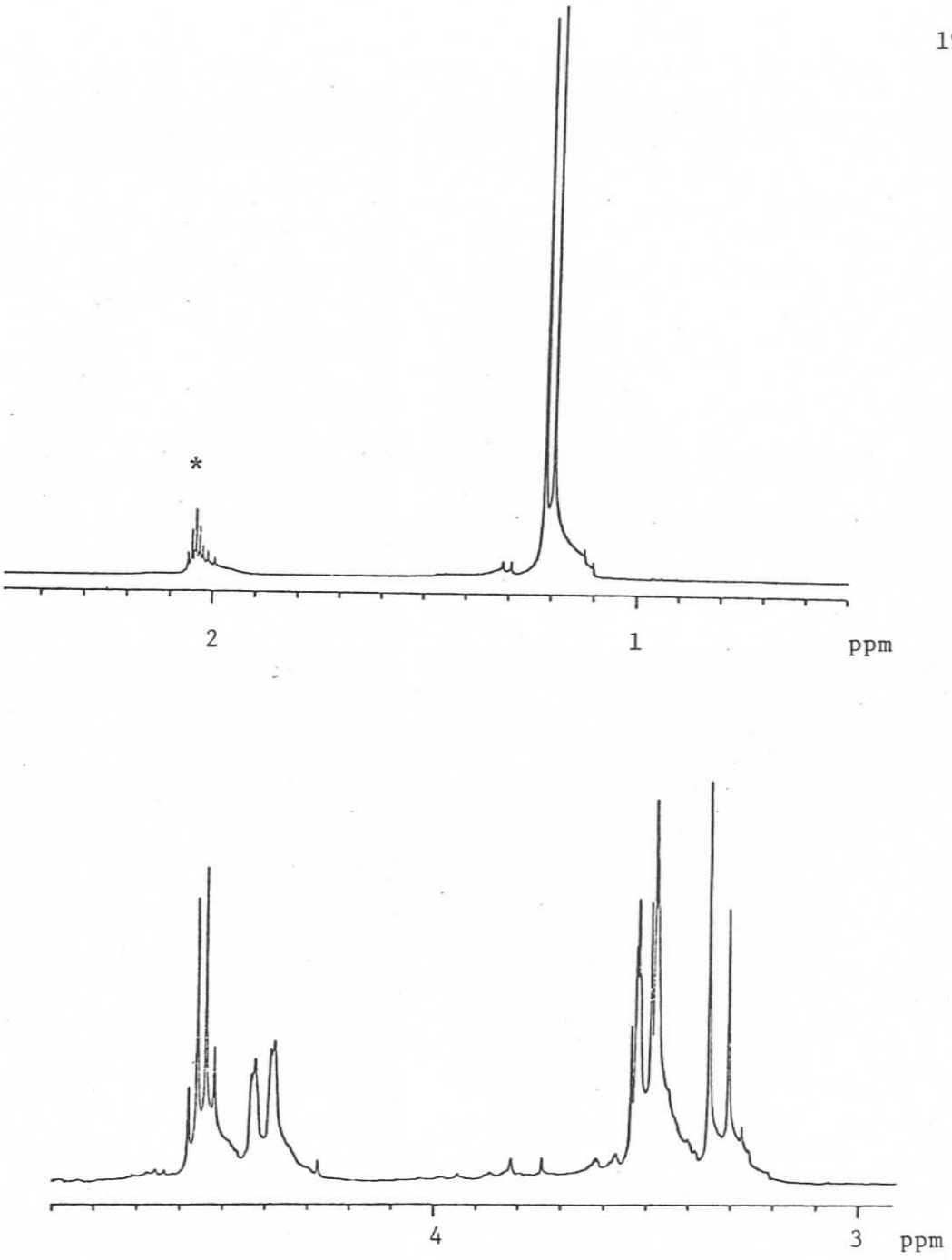

FIGURE 63: Ambient temperature ^{1}H NMR spectrum (250 MHz) of 3,9-dimethyl-2,4,8,10-tetraoxaspiro[5,5]undecane (97). *Solvent $(CD_3)_2CO$.

the stereoelectronic factors influencing their formation.[70,93,160] The configurational aspects of the radical center in such species were mentioned in Chapter II. To recapitulate briefly, radicals of the type (98) are significantly non-planar at C-2, causing a more positive α-

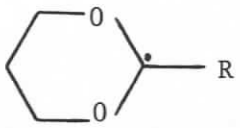

98

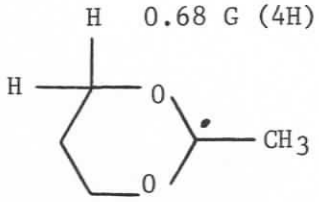

99

proton hfs (R = H, $|a_\alpha|$ = 0.19 G)[27] than in cyclohexyl radical (a_α = -21.3 G).[27] Additional proof of this bending was provided by Gilbert et al.[65] who reported that the spectrum of 2-methyl-1,3-dioxan-2-yl radical (99) at -120°C shows a decrease in relative intensity of the two central lines of the main quartet characteristic of restricted methyl group rotation. The spectrum of the radical (100) was also reported by

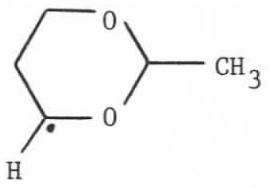

100a

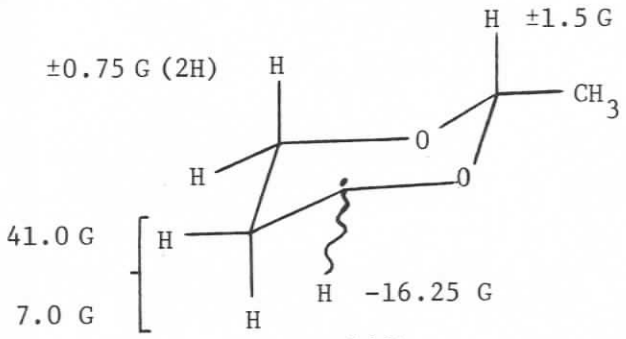

100b

these authors[65] with splittings assigned as shown. The related radical (101) had previously been reported[27] to have similar α and β splittings.

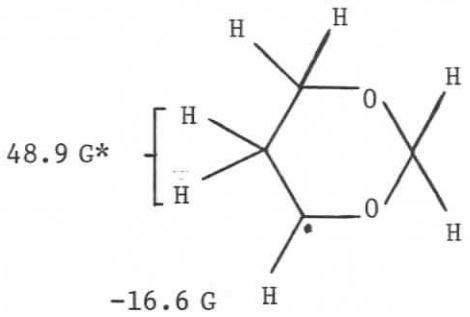

101

*Sum of values for axial and equatorial protons

Of special importance to this work is the thorough interpretation by Gaze and Gilbert[40] of the alternating linewidth effect in the spectrum of 1,3-dioxan-2-yl radical (98, R = H). The chair-to-chair interconversion (102a $\rightleftharpoons$ 102b) exchanges the axial and equitorial γ-protons

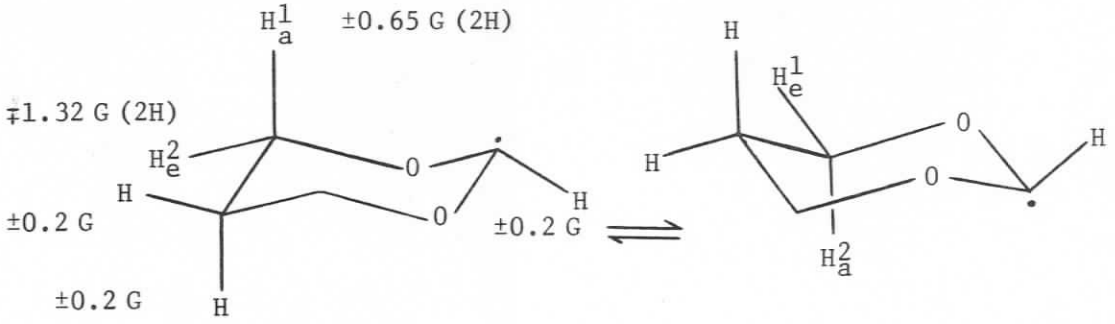

102a 102b

in pairs. Since their hyperfine splittings differ in sign (102a) the spectral width at intermediate exchange rates (e.g. -63°C) is much narrower than that observed when the slow exchange limit has been reached (-87°C).[40] Deterioration of signal-to-noise ratio at high temperatures precluded observation of the spectrum in the limit of fast exchange. Spectral simulation provided confirmation of the analysis,

which was also in good agreement with INDO calculations of the hyperfine splittings.[40] Similar linewidth effects were illustrated in the spectrum of 1,3,5-trioxan-2-yl radical (103).[40] The barrier to ring inversion

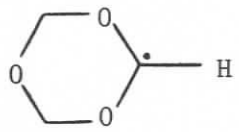

103

for this species was estimated to be 6.5 Kcal/mol.[40]

2. RESULTS OF THE PRESENT STUDY

(a) Radicals from 1,3-Dioxanes

(i) The 5,5-Dimethyl-1,3-dioxan-2-yl Radical

The ESR spectrum of the 5,5-dimethyl-1,3-dioxan-2-yl radical (104) exhibits the linewidth variation characteristic of this class of radicals. In this case the spectrum is simplified by the absence of δ-proton

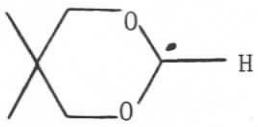

104

hfs, clarifying the broadening phenomenon. Moreover, in contrast to the previously reported work,[40] the spectrum has been observed much closer to the fast exchange limit, allowing calculation of the activation parameters for the process.

Figure 64 shows the spectrum of radical (104) at +25°C and -50°C corresponding to rapid and intermediate exchange rates for the process (105a $\rightleftharpoons$ 105b).

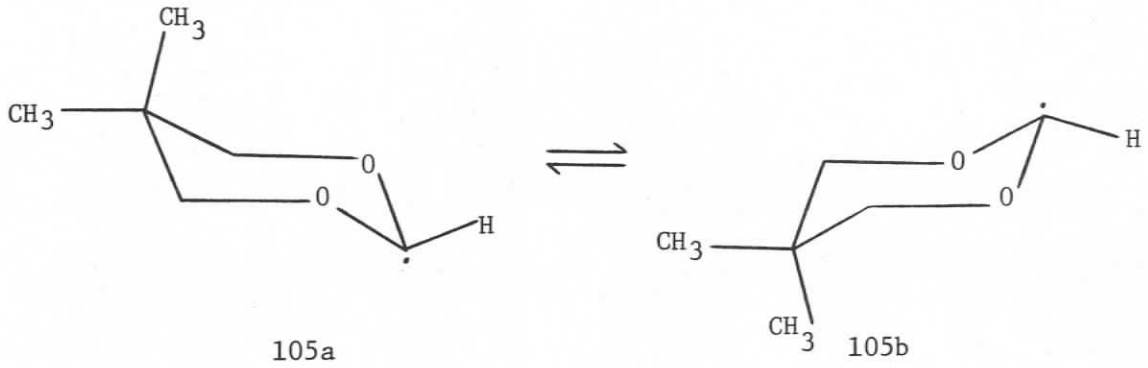

105a 105b

Simulations are based on the experimental splittings shown in Table 22 (see Appendix A).

TABLE 22: Hyperfine splittings for the 5,5-dimethyl-1,3-dioxan-2-yl radical (104)

Temp. °C	$\lvert a_{\alpha} \rvert$	$\lvert a_{\gamma e} \rvert$	$\lvert a_{\gamma a} \rvert$	$\lvert a_{\gamma\ avg} \rvert$
	±0.01	±0.01	±0.01	±0.01
+25	0.430	—	—	0.42
-50	0.385	—	—	$a_{\gamma e} - a_{\gamma a} = 0.80$
-110	0.430	1.50	0.70	—

Figure 65 shows the spectrum at the limit of slow exchange, its simulation, and a stick spectrum for interpretation of the observed lines. Figure 66 then provides the appropriate correlation diagram for such a system (cf. Gilbert et al.[40]).

The rate constants used to achieve satisfactory simulation of the spectra at various temperatures can be used to calculate the activation

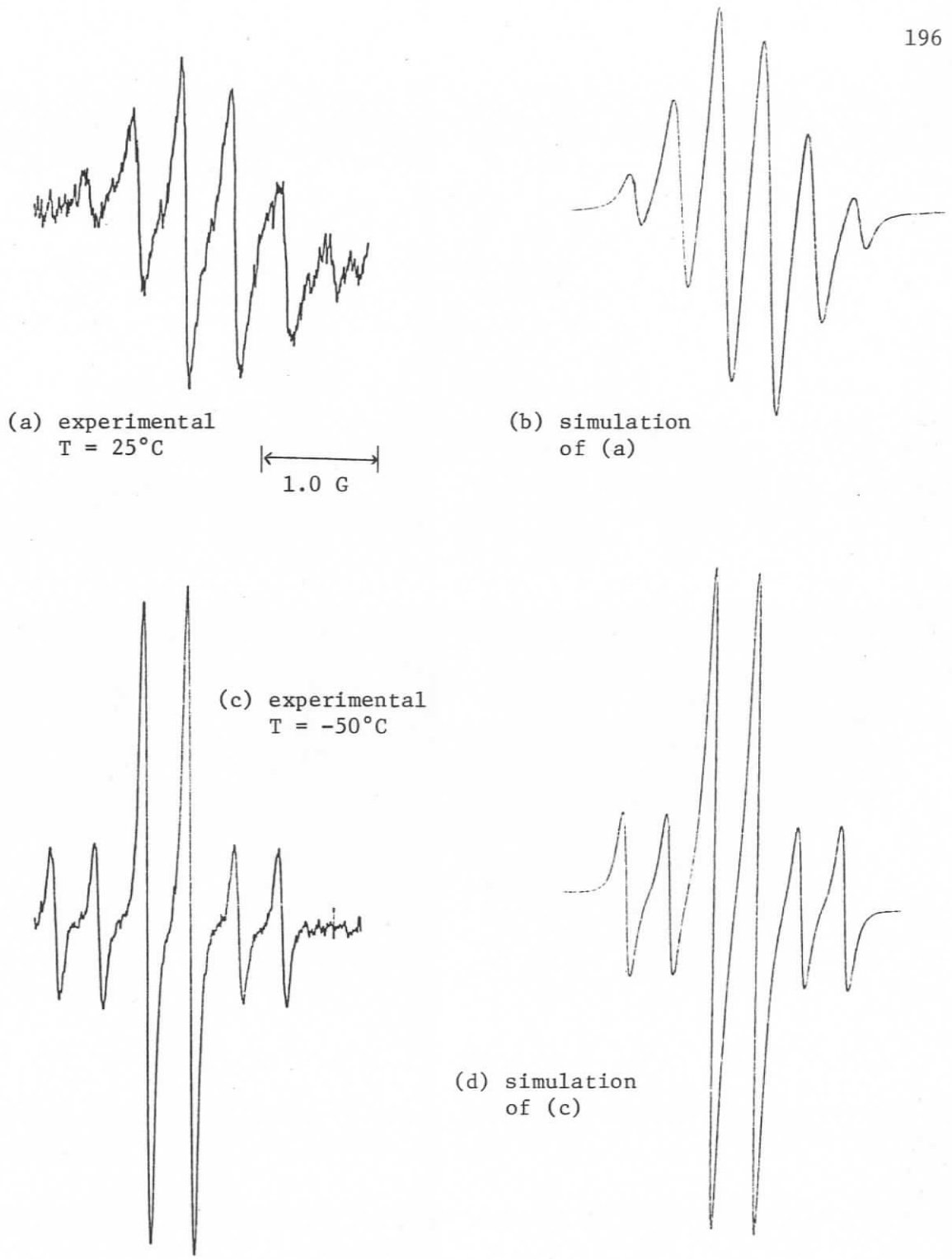

FIGURE 64: (a) ESR spectrum of 5,5-dimethyl-1,3-dioxan-2-yl radical (104) at 25°C, (b) simulation of (a), (c) the experimental spectrum at -50°C, (d) simulation of (c).

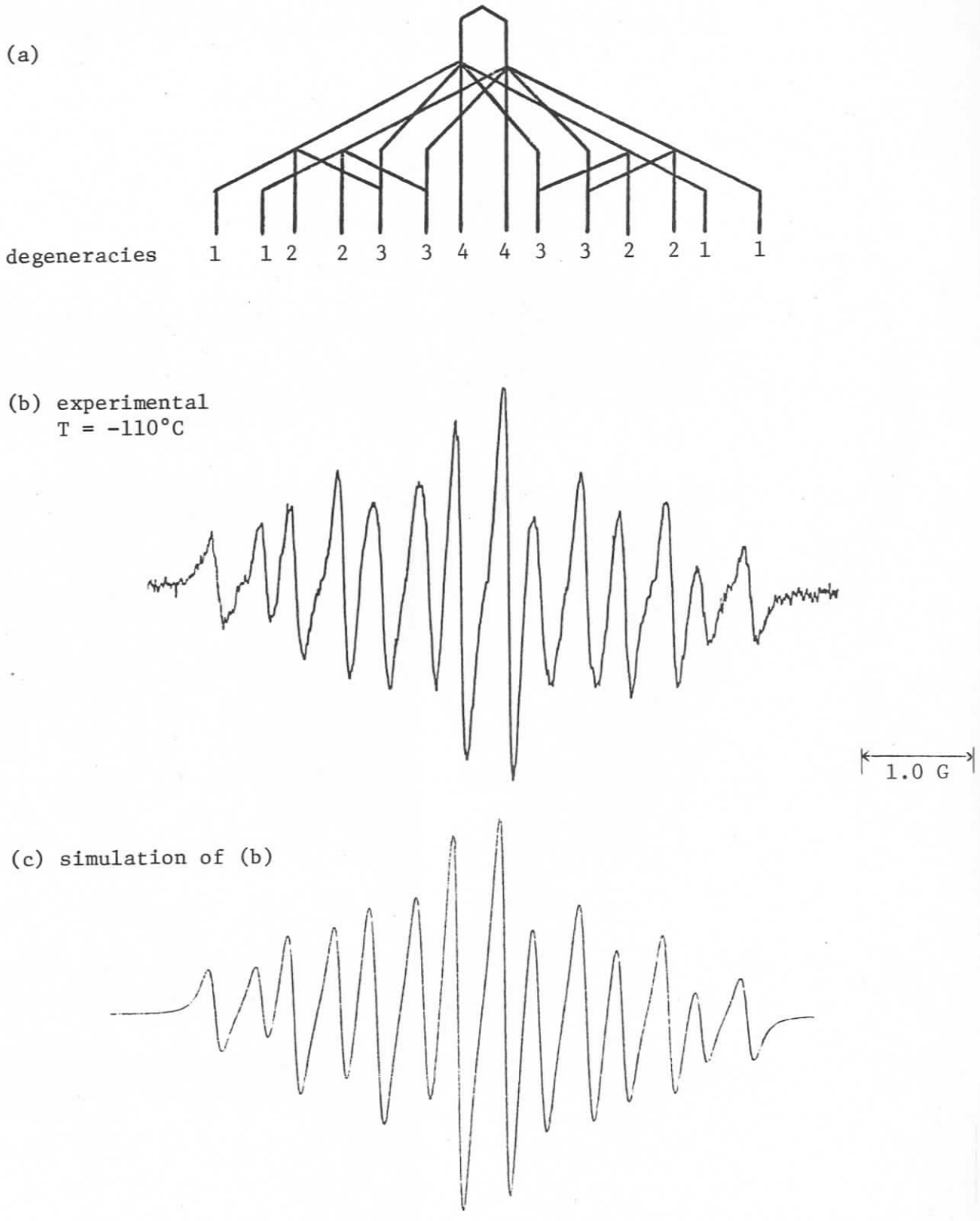

FIGURE 65: ESR spectrum of 5,5-dimethyl-1,3-dioxan-2-yl radical (104) in limit of slow exchange (a) stick spectrum, (b) experimental spectrum at -110°C, (c) simulation of (b).

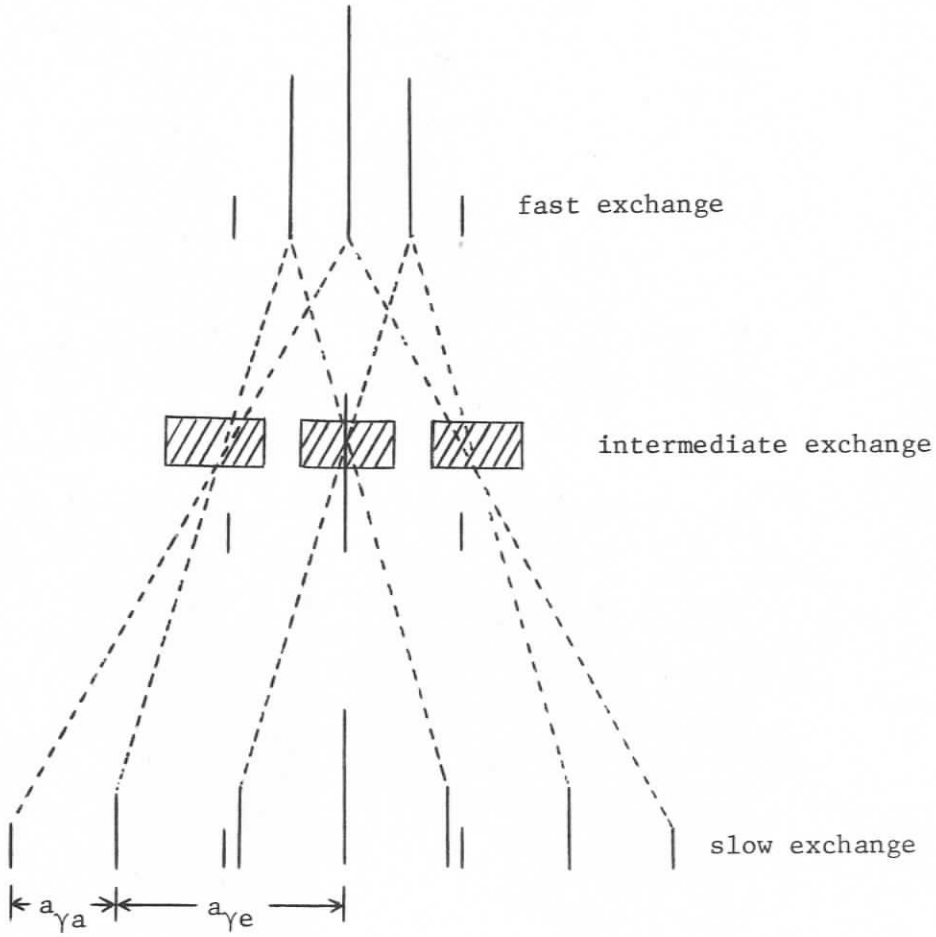

FIGURE 66: Stick spectrum representation of the effect of exchange in the spectrum of a radical showing interaction with two pairs of protons with splittings of opposite sign $|a_{\gamma e}| > |a_{\gamma a}|$ (a_{α} is omitted).

energy for the ring inversion process by means of the Arrhenius equation (15), where k is the rate constant at temperature T, E_a is the activation energy, R is the gas constant and A is a proportionality constant.

$$k = Ae^{-E_a/2.303\ RT} \qquad (15)$$

$E_a/2.303$ R.

TABLE 23: Temperatures and rate constants (from simulations) used to evaluate E_a for ring inversion in 5,5-dimethyl-1,3--dioxan-2-yl radical (104)

T (K)	$T^{-1} \times 10^3$	$(\frac{k}{2\pi})(s^{-1})$	$-\log_{10}(\frac{k}{2\pi})$
298	3.36	12.0	-1.079
223	4.48	0.16	+0.796
163	6.13	0.0040	+2.398

In practice some variation of the rate constants used in the simulation is possible without detectably altering the fit with the experimental spectra. The problem is particularly evident at the slow exchange limit, primarily because of the signal-to-noise ratio encountered for transient radicals in all studies using this technique. The calculated value of the activation energy, 5.9 Kcal/mol (Figure 67) should be regarded as an approximate minimum value. This is similar to the barrier to inversion for 1,3,5-trioxan-2-yl radical (103), 6.5 Kcal/mol.[40]

The free energy of activation for the process at the coalescence temperature (T_c) is calculated using Equation 16.[162]

$$\Delta G_c^{\ddagger} = 2.3\ RT_c\ (10.32 + \log T_c - \log k) \qquad (16)$$

Thus at coalescence (-50°C, 223 K), $\Delta G^{\ddagger} = 6.8$ Kcal/mol. This is similar to both the calculated value of E_a, and the barrier to ring flipping in the case of the 1,3,5-trioxan-2-yl radical (103).[40] The values of E_a and $\Delta G_c^{\ddagger}$ are somewhat lower than corresponding values for chair-to-chair

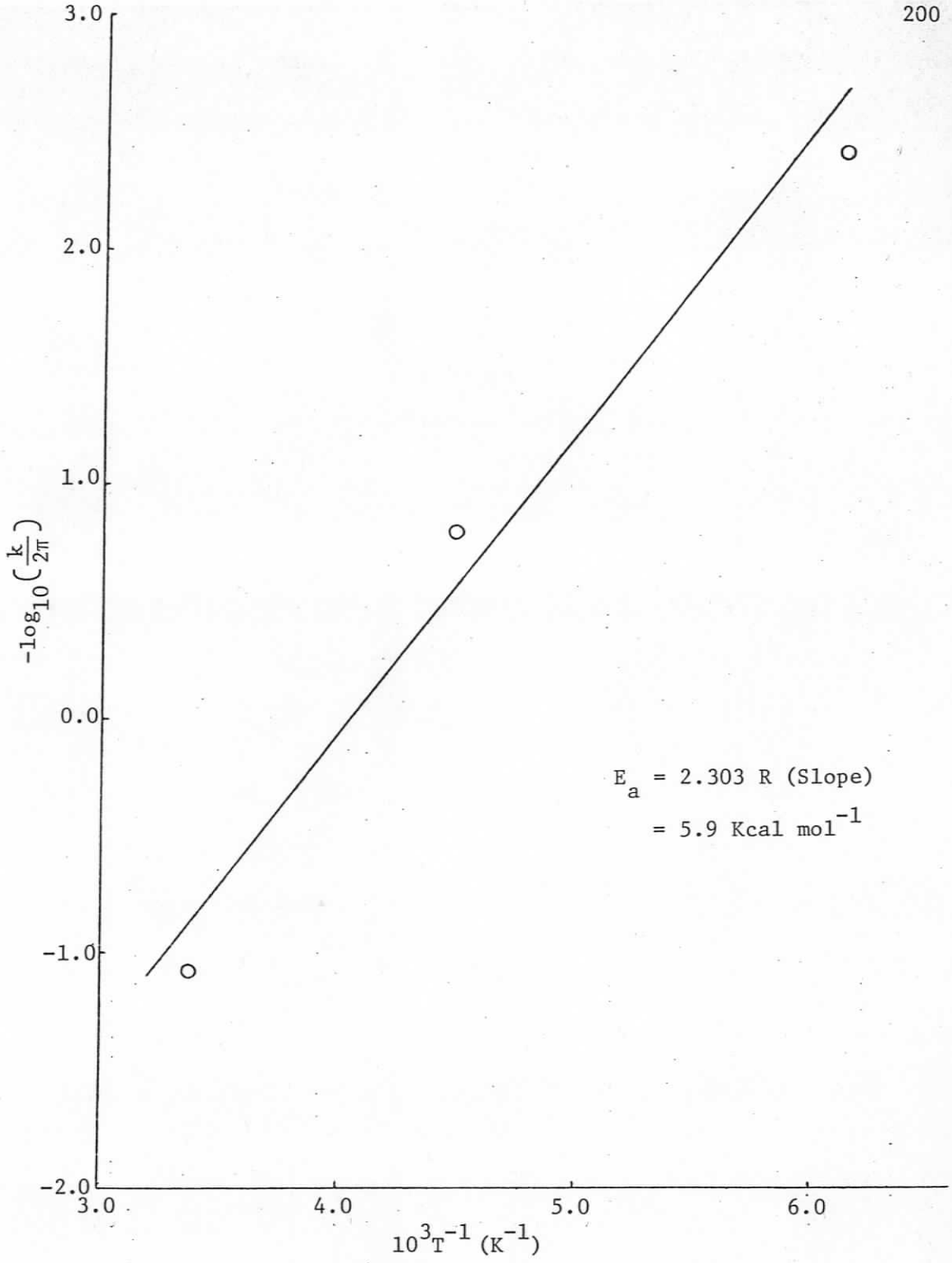

FIGURE 67: Plot of $-\log_{10}(\frac{k}{2\pi})$ (from simulations) vs. reciprocal of temperature of matching experimental spectrum for 5,5-dimethyl-1,3-dioxan-2-yl radical (104).

inversion of the parent molecule (Table 21) indicating more facile flipping in the radical. Note that the low value of a_α (Table 22) is indicative of significant bending (cf. Figure 12, Chapter I).

The relative simplicity of the spectra and the fact that both the fast and slow exchange spectra are accessible renders the 5,5-dimethyl--1,3-dioxan-2-yl radical (104) as useful a species for demonstrating the dynamic ESR phenomenon as the parent molecule is recognized to be in ^{1}H DNMR.[157]

Some spectra obtained at high modulation amplitude indicate the presence of additional signals [approximate doublet (15.5 G) of triplets (2.0 G)] which are due to the radical (106).

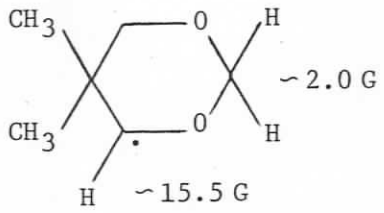

106

(ii) 2,5,5-Trimethyl-1,3-dioxan-2-yl Radical

The spectrum obtained upon irradiation of a solution of 2,5,5-trimethyl-1,3-dioxane was assigned to the 2-yl radical (107). It consists of the expected quartet further split by two non-equivalent

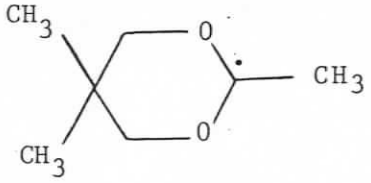

107

pairs of γ protons (Figure 68, hfs in Table 24).

TABLE 24: Hyperfine splittings of 2,5,5-trimethyl-1,3-dioxan-2-yl radical (107)

Temp °C	a_β	$\lvert a_{\gamma 1}\rvert$	$\lvert a_{\gamma 2}\rvert$
	±0.05	±0.06	±0.06
-54	13.60	0.955±0.01	0.68±0.01
-60	13.55±0.06	0.96	0.69
-90	13.60	0.90	0.75

Given the well-known preference of 2-alkyl substituents for the equatorial conformation in 1,3-dioxanes it is not surprising that no linewidth effects attributable to ring flipping are observed for this species (107). The spectrum is unchanged between -90°C and -50°C.

Peak group number 2 is shown under high resolution conditions in Figure 68b and can be simulated as a triplet of triplets (Figure 68c). While the signal-to-noise ratio is clearly less than optimal it should be noted that previous studies[65] on radical (108) did not achieve distinct γ-splittings but only relative changes in the intensity of the

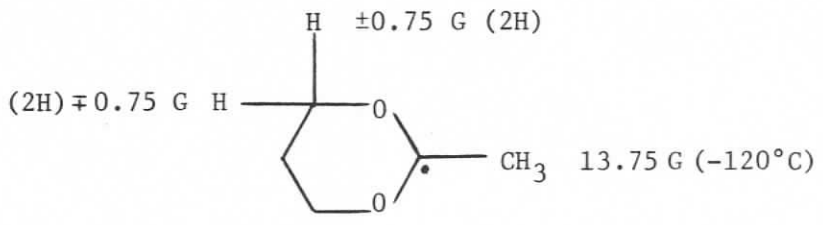

108

quintets. Here the single fixed conformation is clearly established by

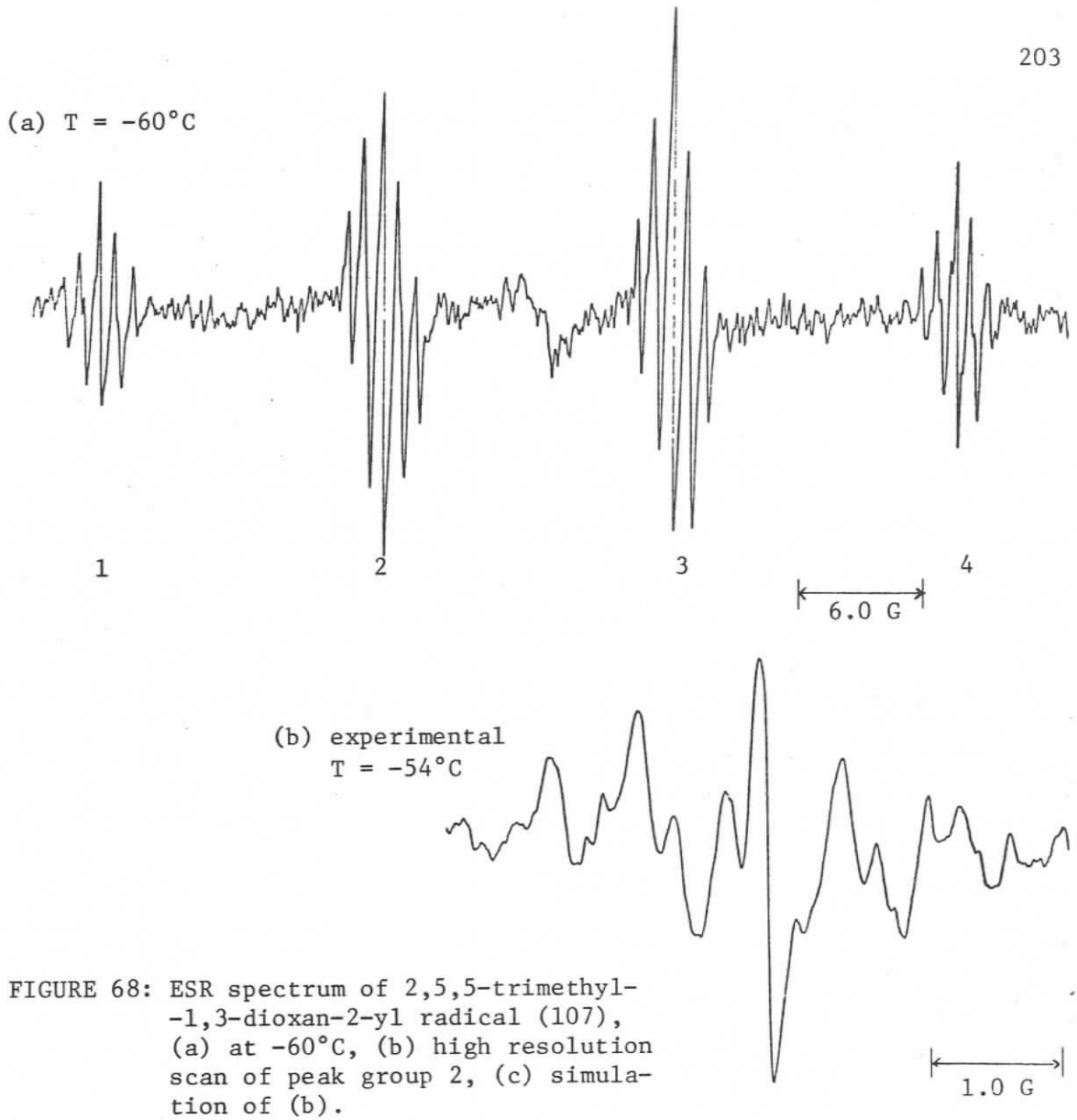

FIGURE 68: ESR spectrum of 2,5,5-trimethyl--1,3-dioxan-2-yl radical (107), (a) at -60°C, (b) high resolution scan of peak group 2, (c) simulation of (b).

the identification of two discrete γ-splittings.

The multiplet groups do not have the binomial 1:3:3:1 intensity relationship. The reduced intensity of the $\tilde{M}_\beta = \pm\frac{1}{2}$ lines may be due to restricted rotation about C_α-CH_3.[65] The β-proton hfs here is virtually the same as that observed in 2-methyl-1,3-dioxan-2-yl radical (108)[65] and supports the notion of a similar degree of bending at C_α in this species (107).

Under conditions of high sensitivity some spectra showed lines from one or more additional species. The radical (109) seemed a likely candidate but no splittings could be assigned under the signal-to-noise levels encountered.

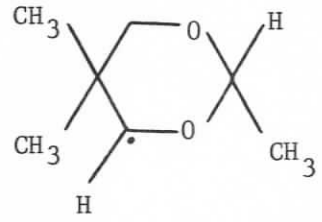

109

(iii) 2,2,5,5-Tetramethyl-1,3-dioxan-4-yl Radical

Hydrogen abstraction from the parent dioxane gave 2,2,5,5-tetramethyl-1,3-dioxan-4-yl radical (110), whose spectrum between +20°C and -110°C is a doublet of broad quartets (Figure 69a and b; hfs in Table 25).

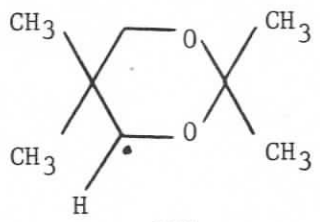

110

(a) T = -50°C

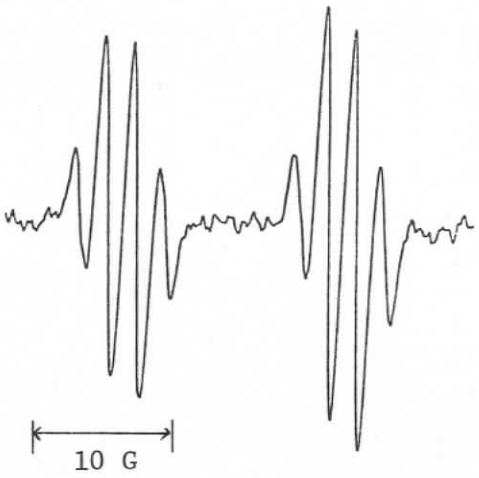

(b) T = -70°C

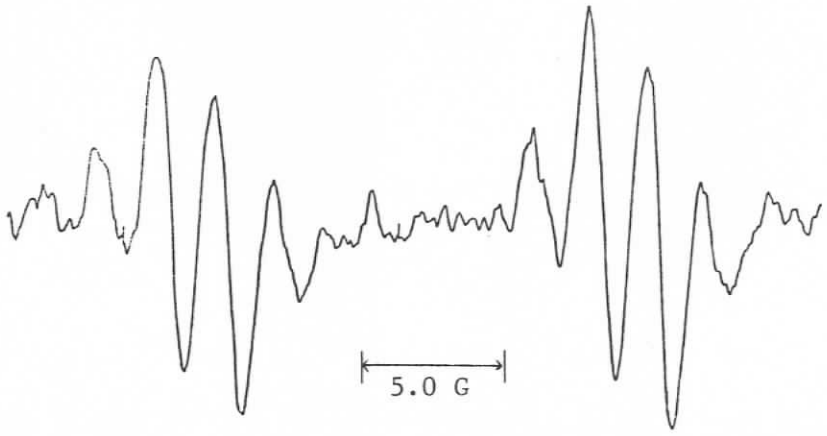

FIGURE 69: ESR spectrum of 2,2,5,5-tetramethyl-1,3-dioxan-4-yl radical (110) at (a) -50°C, (b) -70°C. (continued)

(c) T = -70°C

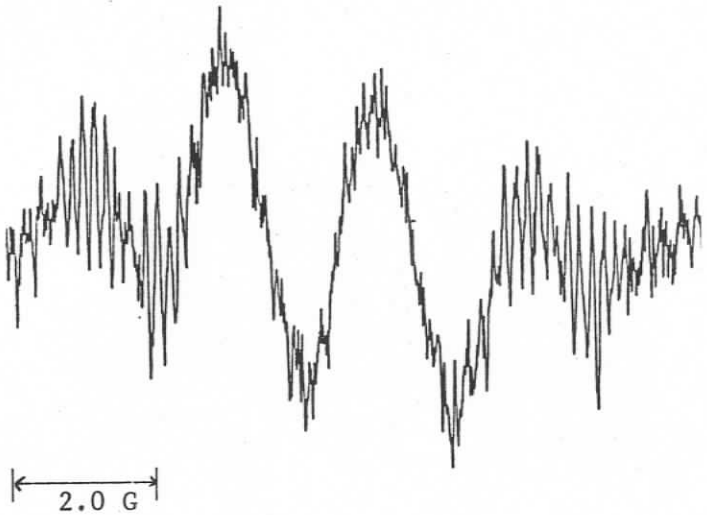

(d) simulation of (c)

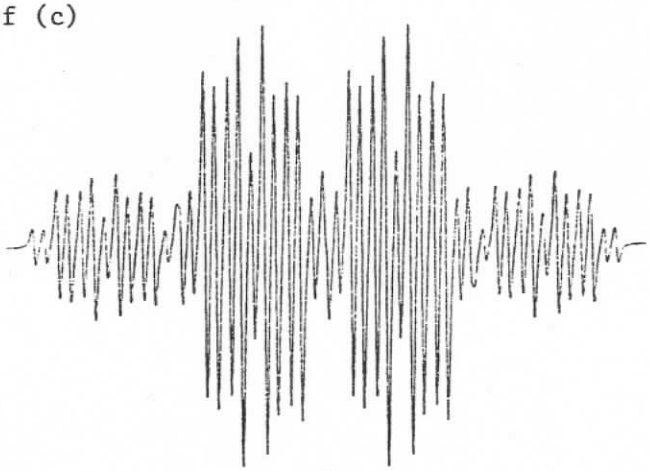

FIGURE 69 (continued): (c) high resolution scan of left-hand quartet.

TABLE 25: Hyperfine splittings of 2,2,5,5-tetramethyl-1,3-dioxan-4-yl radical (110)

Temp. °C	$-a_{\alpha H}$	$\lvert a_{\gamma CH_3} \rvert$	Other
	±0.05	±0.05	±0.05
+20	15.95±0.1	2.00±0.1	
-10	15.80±0.1	2.15±0.1	
-40	15.63	2.10±0.1	
-50	15.75±0.1	2.10±0.1	
-70	15.55	2.20	0.20
-80	15.78	2.18	
-100	15.55	2.03	
-110	15.60	2.20	

This indicates a selective hyperfine interaction with one methyl substituent. In fact the radical exists in one preferred conformation over the temperature range studied since there are no linewidth effects for exchange of methyl group hfs.

We propose structure (111) as the fixed conformation. The approximately axial 5-methyl group makes a small dihedral angle (θ_R) with the axis of the semi-occupied p_z orbital. This is a prerequisite for

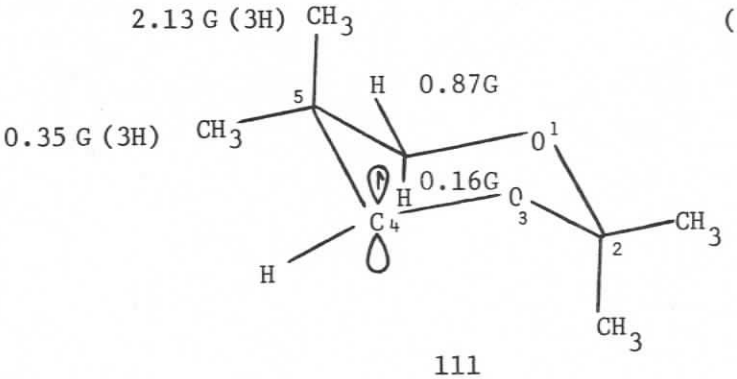

111

(splittings as used in simulation, Figure 69d)

γ-protons aligning according to the W-plan which results in large H_γ hfs (see Chapter I). (Ellinger et al.[32] have calculated that a large γ-proton hfs is likely for θ_R = 0° to 40°.) Therefore the preferred γ-coupling is assigned to the near-axial methyl group in conformer (111).

At -70°C under high resolution conditions additional hyperfine structure was observed, but only in the outer lines of each quartet (Figure 69c). The simulation (Figure 69d) reflects the approximate values assigned to the remaining γ-protons (see structure 111). As anticipated, it is sufficient to assign a large splitting ($a_{\gamma H}$ = 0.97 G) to only the equatorial proton of the methylene pair. At -50°C the quartets have the expected 1:3:3:1 intensity ratio but at -110°C the relative intensities of the $\tilde{M}_\gamma = \pm\frac{1}{2}$ components are significantly reduced (*ca.* 1:2:2:1). These observations can be created by restricted rotation of the near-axial β-methyl group (cf. 2-methyl-1,3-dioxan-2-yl radical, ref. 65).

(iv) <u>The 5,5-Diethyl-2,2-dimethyl-1,3-dioxan-4-yl Radical</u>

The ESR spectrum of the 5,5-diethyl-2,2-dimethyl-1,3-dioxan-4-yl radical (112) consists of a doublet of doublets throughout the temperature range +5°C to -120°C (Figure 70, Table 26). Based on the spectrum

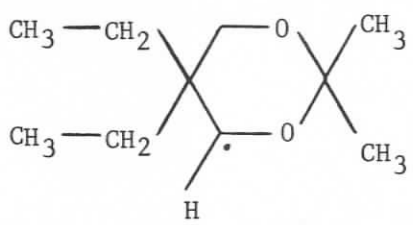

112

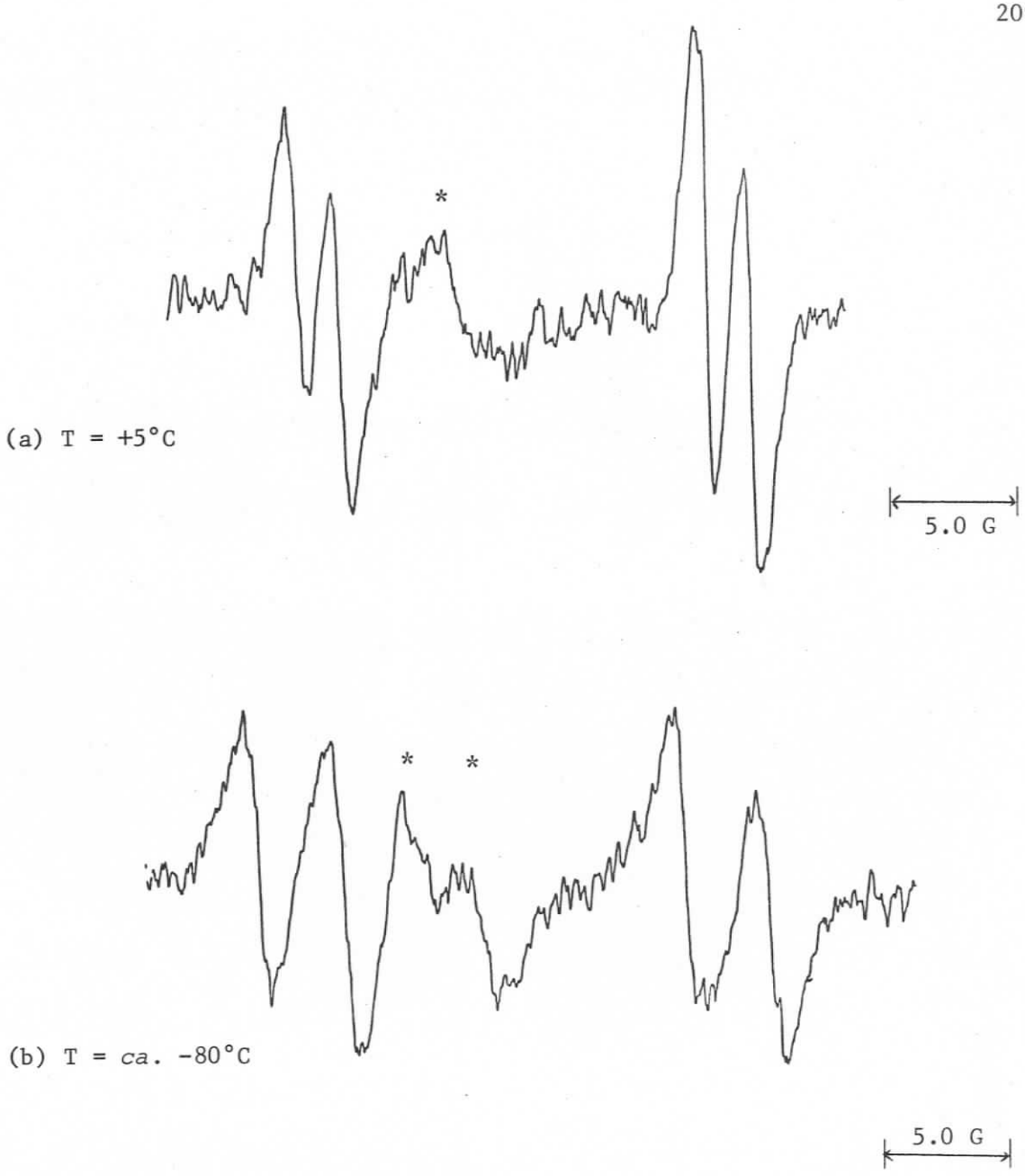

FIGURE 70: ESR spectrum of the 5,5-diethyl-2,2-dimethyl-1,3-dioxan-4-yl radical (112) (a) at +5°C, (b) at *ca.* -80°C. Additional broad absorptions (*) have not been identified but may be due to impurities.

TABLE 26: Hyperfine splittings of the 5,5-diethyl-2,2-dimethyl-1,3--dioxan-4-yl radical (112)

Temp. °C	$-a_\alpha$	$\lvert a_\gamma \rvert$
	±0.1	±0.1
+5	16.46	1.97
-10	16.50	2.05
-30	16.65	2.30
-60	17.13	3.12
-80	17.25	3.50
-100	17.12	4.12
-120	17.00	4.27

of the similar radical (110) the implication is coupling with only one of the substituent methylene protons. Indeed the CPK space-filling model of species (112) indicates not only that rotation of both ethyl groups (C_β-C_γ) is severely restricted but also that a favoured conformation must be one in which one methylene proton of the near-axial ethyl substituent is aligned exactly according to the W-plan (113).

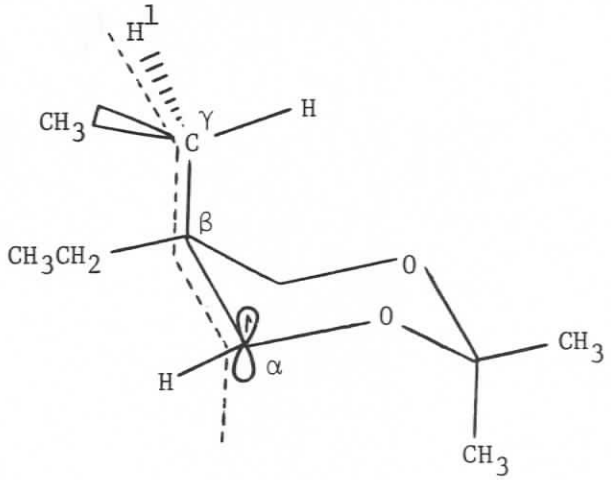

$\theta_R = 0°$

$\theta_{\gamma H^1} = 180°$

In this conformation the dihedral angle θ_R between the C_β-C_γ bond and the p_z axis is zero and the dihedral angle between the C_γ-H'_γ bond and the C_β-C_α bond (θ_γ) is 180° (113). The *ab initio* calculations of Ellinger et al.[32] for the n-propyl radical predict a hyperfine splitting of +4.37 G for the γ-proton in this conformation (θ_R = 0°, θ_γ = 180°).

The experimental H_γ splitting increases in magnitude as the temperature is decreased, from 1.97 G (5°C) to 4.27 G (-120°C) (Table 26). Thus our results provide quantitative and qualitative support for the non-empirical calculations.[32]

It was not possible to resolve any further hfs in the spectrum of the radical (112). The broad appearance of the multiplets suggests the presence of overlapping lines having small splittings arising from the other γ (and probably δ) protons.

Although in some spectra the outside lines appeared broadened we did not observe any linewidth effects which could be attributed to ring inversion or ethyl group rotation. The ring conformation is presumably frozen at all temperatures studied and the near-axial ethyl substituent oscillates about a conformational energy minimum in which it is more strictly constrained as the temperature decreases.

(b) Radicals from 2,4,8,10-Tetraoxaspiro[5,5]undecanes

(i) The 2,4,8,10-Tetraoxaspiro[5,5]undecan-3-yl Radical

The spectrum of the 2,4,8,10-tetraoxaspiro[5,5]undecan-3-yl radical (114) at +20°C is a sextet (Figure 71a) much like the spectrum of 5,5-dimethyl-1,3-dioxan-2-yl radical (104) and the splittings are similar (Table 27). The parent compound is known to have a barrier to ring

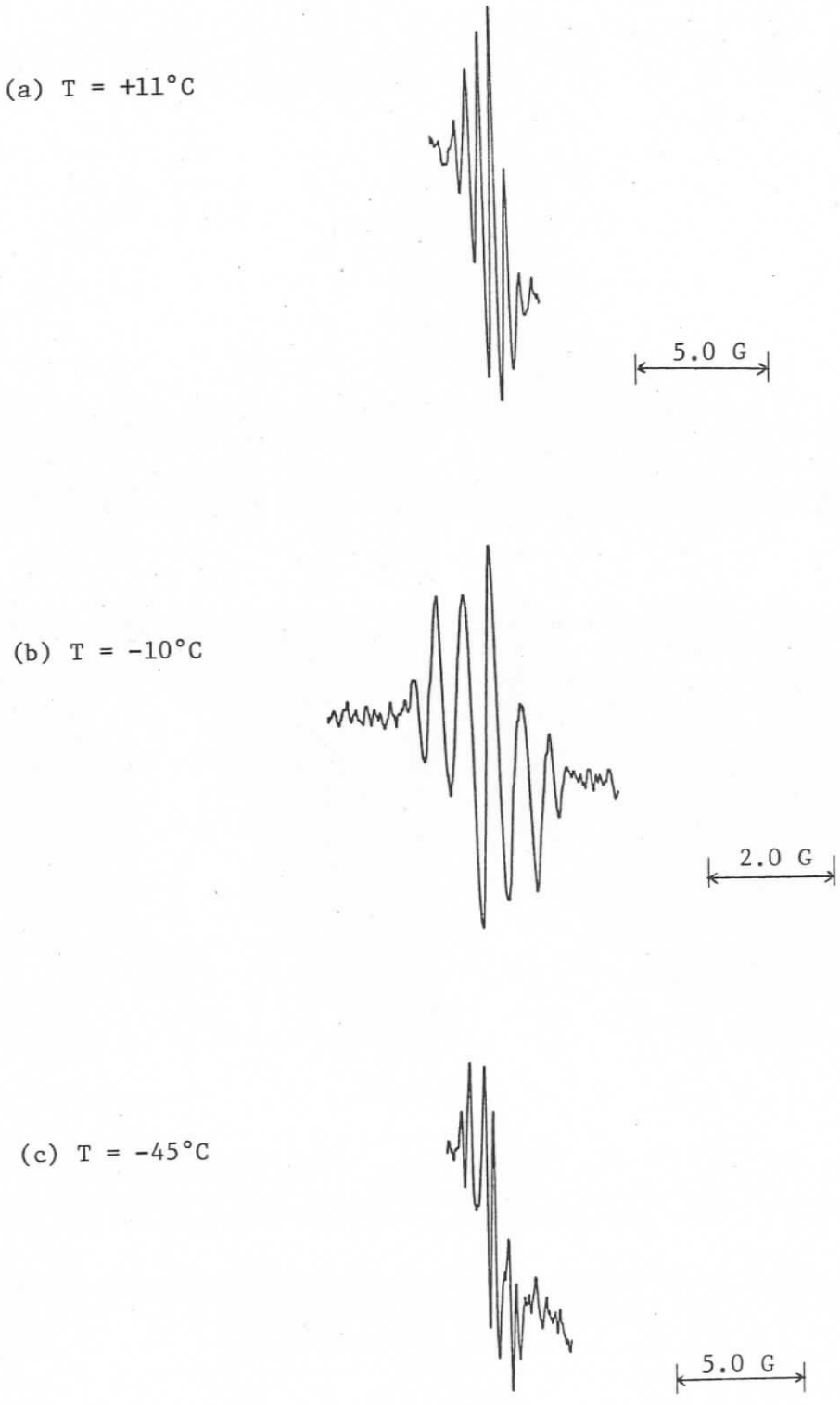

FIGURE 71: ESR spectrum of 2,4,8,10-tetraoxaspiro[5,5]undecan-3-yl radical (114) at various temperatures (all in neat di-*t*-butyl peroxide).

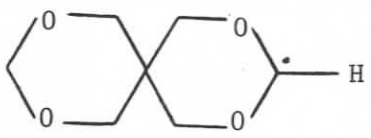

114

TABLE 27: Hyperfine splittings of the 2,4,8,10-tetraoxaspiro[5,5]-undecan-3-yl radical (114)

Temp. °C	$-a_\alpha$	$\lvert H_\gamma \text{hfs} \rvert$	
	±0.05	±0.05	
+20	0.48	0.50	average of axial and equatorial
+11	0.35	0.47	
-10	0.40±0.02	0.40±0.02	
-40	0.38	0.94	difference of γ-hfs at intermediate exchange
-45	0.33	0.93	

inversion not greatly different from 5,5-dimethyl-1,3-dioxane so that, by comparison with the radical (104) we expect ring flipping to be fast at room temperature for the spiro radical (114) as well. Once again, in contrast to other work, we observe the high temperature limit. At -45°C the spectrum (Figure 71c) is reminiscent of that obtained for radical (104) at -50°C, corresponding to an intermediate exchange rate for ring inversion. Unfortunately we were not able to obtain a resolved spectrum of the spiro radical (114) below -45°C. The relatively poor solubility of this solid substrate contributes to this problem. In contrast to the 1,3-dioxanes all the spiro substrates were solids at room temperature and precipitated easily from solution. (Note: A range

of solvents was employed in an attempt to improve the solubility; cyclopropane, cyclopentane, acetone, di-n-propyl ether.)

Additional lines that could not be clearly assigned were observed in some wider scans, possibly due to the radical (115).

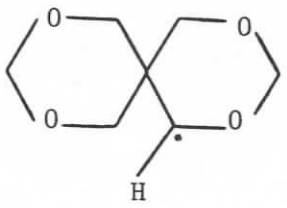

115

(ii) The 3,9-Dimethyl-2,4,8,10-tetraoxaspiro[5,5]undecan-3-yl Radical

The investigation of the 3,9-dimethyl-2,4,8,10-tetraoxaspiro[5,5]-undecan-3-yl radical (116) was again impeded by the low solubility of the parent compound in cyclopropane, n-pentane, cyclopentane, and di-*t*-butyl peroxide and by the rapid building of a yellowish solid on the inside wall of irradiated sample tubes on the lamp side. The low

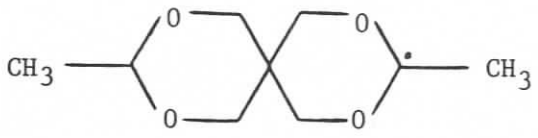

116

temperature spectrum of radical (116) (Figure 72) is a quartet further split by coupling to all four γ-protons, as observed for the monocyclic analog (107). The splittings are given in Table 28. The known

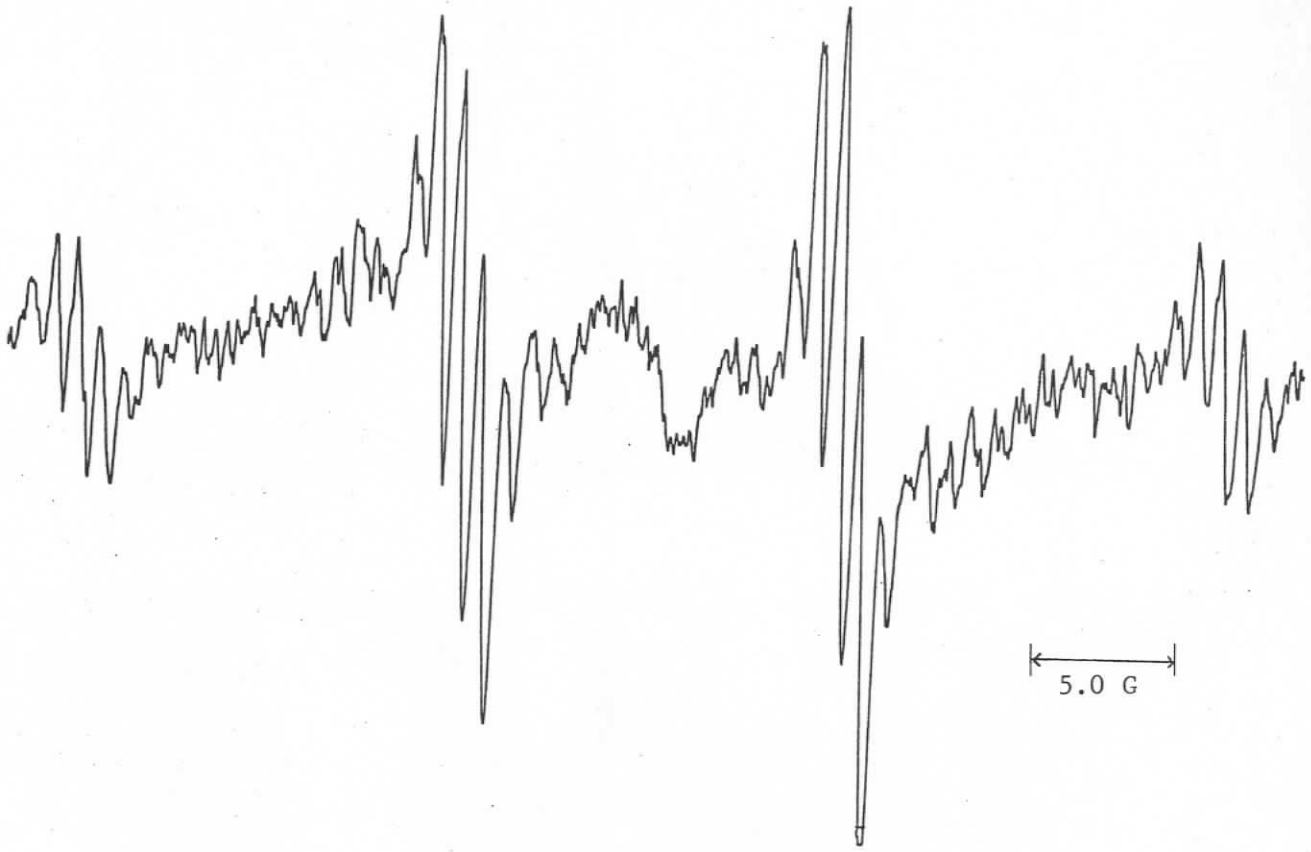

FIGURE 72: ESR spectrum of the 3,9-dimethyl-2,4,8,10-tetraoxaspiro-[5,5]undecan-3-yl radical (116) at -50°C.

TABLE 28: Hyperfine splittings of the 3,9-dimethyl-2,4,8,10-tetraoxaspiro[5,5]undecan-3-yl radical (116)

Temp. °C	a_β	$\lvert a_\gamma \rvert$
	±0.05	±0.05
-40	13.72±0.1	0.90±0.1
-50	13.88	0.85
-54	13.77	0.88
-60	13.85±0.1	0.90±0.1
-80	13.66	0.88

preference of 2-alkyl substituents for the equatorial conformation in related molecules leads us to expect no linewidth effects attributable to ring flipping. Experimentally this was the case, although at -10°C resolution of the multiplets was poor.

Some of the spectra showed additional lines but we were unable to assign them specifically to the other expected radical (117). Pursuit of resolution of the spectrum could afford additional confirmation of the remote γ-splittings through quaternary carbon.

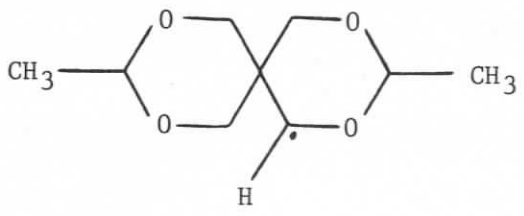

117

(iii) The 3,3,9,9-Tetramethyl-2,4,8,10-tetraoxaspiro[5,5]-undecan-1-yl Radical

Given the *a priori* possibility of a large specific γ-proton splitting in the spectrum of the 3,3,9,9-tetramethyl-2,4,8,10-tetraoxaspiro[55,]undecan-1-yl radical (118) we irradiated samples of the parent compound dissolved variously in trichlorofluoromethane, di-*t*-butyl peroxide, cyclopropane, and acetone. In most cases only a broadened

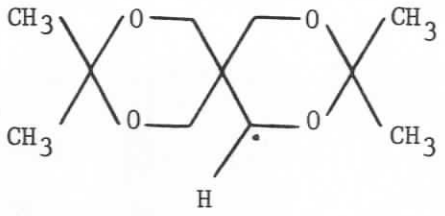

118

doublet (a_α = 16.4 G ±0.1 G) was observed, attributed to the radical (118). An additional hyperfine interaction (triplet, 0.6 G) appears partially resolved in the spectrum shown in Figure 73a (cf. simulation, Figure 73b). The H_α hfs did not vary significantly with solvent change or temperature change (+20° to -80°C). The substrate is rapidly hydrolysed in aqueous acid. Accordingly, an extended series of experiments employing both aqueous flow systems and irradiation in acetone solution did not improve the resolution shown in Figure 73a.

(c) Summary and Conclusions

The 5,5-dialkyl-1,3-dioxane systems (shown below) provided a conceptual link to the sterically hindered alcohol radicals $R\dot{C}HOH$ where R has a quaternary center at the point of attachment (see Chapter V).

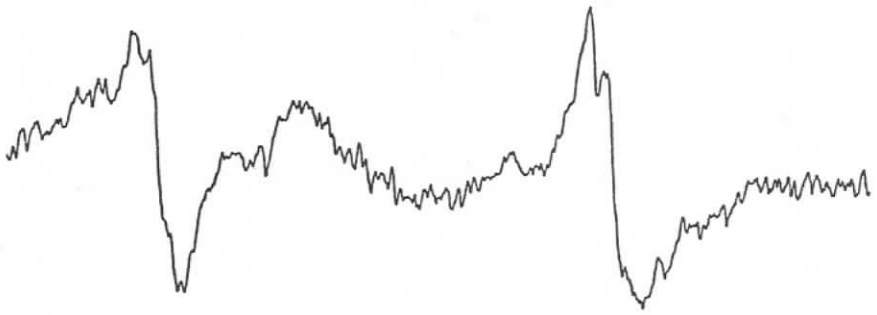

(a) experimental
T = -10°C

5.0 G

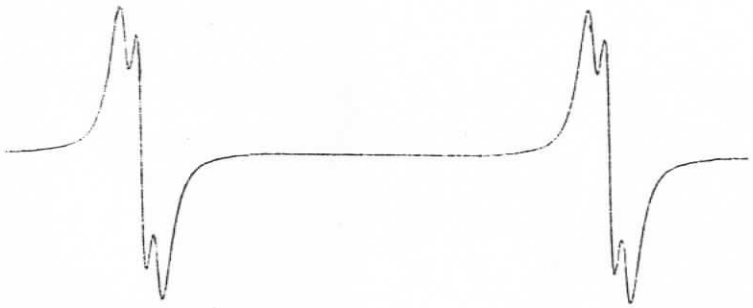

(b) Simulation
of (a)

FIGURE 73: (a) ESR spectrum of the 3,3,9,9-tetramethyl-2,4,8,10--tetraoxaspiro[5,5]undecan-1-yl radical (118) at -10°C in neat di-*t*-butyl peroxide. (b) Simulation of spectrum in (a), $|a_{\alpha}|$ = 16.4 G, a_{γ} = 0.60 G (2H).

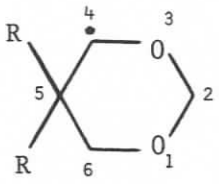

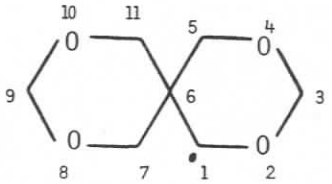

The results indicate the experimental difficulties of solubility and spectral overlap of several radical species for such relatively high molecular weight systems, particularly the spiro examples. However, 5,5-dialkyl substitution does reduce the complexity of individual spectra. For example, 5,5-dimethyl-1,3-dioxan-2-yl radical (104) illustrates the effect of ring inversion, at different rates, on the ESR spectrum. The energy of activation for the inversion was found to be *ca*. 5.9 Kcal/mol, comparable to the value of 6.5 Kcal/mol found by Gilbert et al.[40] for the 1,3,5-trioxan-2-yl radical (103).

In the cases where competition between attack at C-2 and C-4 is removed by fully alkylating C-2, we have obtained the first examples of these highly hindered C-4 radicals. Two interesting features of such species have been identified for the first time:

(1) The ring system, though highly mobile on the NMR time scale for the parent, appears completely fixed for the corresponding radical.

(2) The resulting fixed γ-R groups at $\theta_R \simeq 0$ provide markedly enhanced splittings fully consistent with theoretical predictions. Specifically, the 2,2,5,5-tetramethyl-1,3-dioxan-4-yl radical (110) exhibits a γ-CH_3 splitting of *ca*. 2 G and the 5,5-diethyl-2,2-dimethyl--1,3-dioxan-4-yl radical (112) has a single γ-H hyperfine splitting of 4.27 G (@ -120°C).

Agreement with the steric effects of alkyl groups in $R\dot{C}HOH$ radicals (see Chapter V) has been demonstrated both in the trends in $a_{\alpha H}$ and also in the packing of highly hindered ethyl groups to yield a specific single γ-H splitting in both series. Further information about specific γ-H splittings should be available from a study of the 2,2-dimethyl-1,3-dioxan-4-yl radical.

In the cases where C-3 radicals could be obtained from the previously unstudied spiro systems, the 1,3-dioxan-2-yl trends have been confirmed. Specifically the 3,9-dimethyl-2,4,8,10-tetraoxaspiro[5,5]-undecan-3-yl radical (116) is fixed in a single conformer, while the corresponding unsubstituted species (114) undergoes ring inversion, giving dynamic effects observable on the ESR time scale. In the latter case the high temperature (fast exchange) limit is available (in contrast to 1,3-dioxan-2-yl itself). Full analysis of the dynamics must await improved low-temperature limit spectra.

CHAPTER V

RADICAL CONFIGURATION: STERIC AND ELECTRONIC EFFECTS IN SOME ALCOHOL-DERIVED RADICALS

1. INTRODUCTION

The property of configuration, or degree of non-planarity at the radical center, was discussed in Chapter I. This "bending" was seen to arise from either geometrical constraints (e.g. small rings) or the presence of a substituent which could participate in conjugative (electron releasing) delocalization of the unpaired electron. The effect of electronegativity on bending at C_α has been difficult to evaluate since most electronegative substituents can also be involved in conjugative delocalization (i.e. have non-bonding electrons). Alkyl substituents will generate effects of smaller magnitude than substituents containing heteroatoms. Interpretation of these effects will also be difficult since steric, inductive, and delocalization (hyperconjugative) effects are possible.

While the small decreases in $|a_{\alpha H}|$ with increasing substitution of the methyl radical are well known[3] all these species are likely planar or nearly so.[3] The series of radicals obtained by substitution of methyl for β-hydrogen in ethyl radical displays $a_{\alpha H}$ values which show a modest but clear configurational trend related to increasing alkyl substitution at C_β (Table 29).[24]

TABLE 29: H_α hfs for the primary alkyl radicals obtained by increasing methyl substitution at C_β in ethyl radical[24]

Radical	$-a_{\alpha H}$	Temp. °C
$CH_3CH_2^\bullet$	22.38	-180
$CH_3CH_2CH_2^\bullet$	22.08	-180
$(CH_3)_2CHCH_2^\bullet$	22.0	-135
	21.3	-183[132]
$(CH_3)_3CCH_2^\bullet$	21.4	-177[132]

In the present work a more marked configurational trend is observed for the α-hydroxy analogs of these species. Moreover, increasingly bulky β substitution introduces an additional steric effect on the observed α-H hyperfine splittings.

2. RESULTS OF THE PRESENT STUDY

(a) Radical Configuration

The ESR spectra have been obtained for a series of α-hydroxyalkyl radicals (119-125 in Table 30) having different degrees of alkyl substitution at C_β. The change in $a_{\alpha H}$ along the series (Figure 74) provides information about the configuration at the radical center. The first four radicals (119-122) have been discussed (Chapter III). Within this group the α-proton hfs at a given temperature becomes steadily more positive (decreases in magnitude) with increasing β-substitution, implying an increasing degree of bending at C_α (see also Figure 75). Interestingly the series of radicals (119-122) corresponds to the increasing

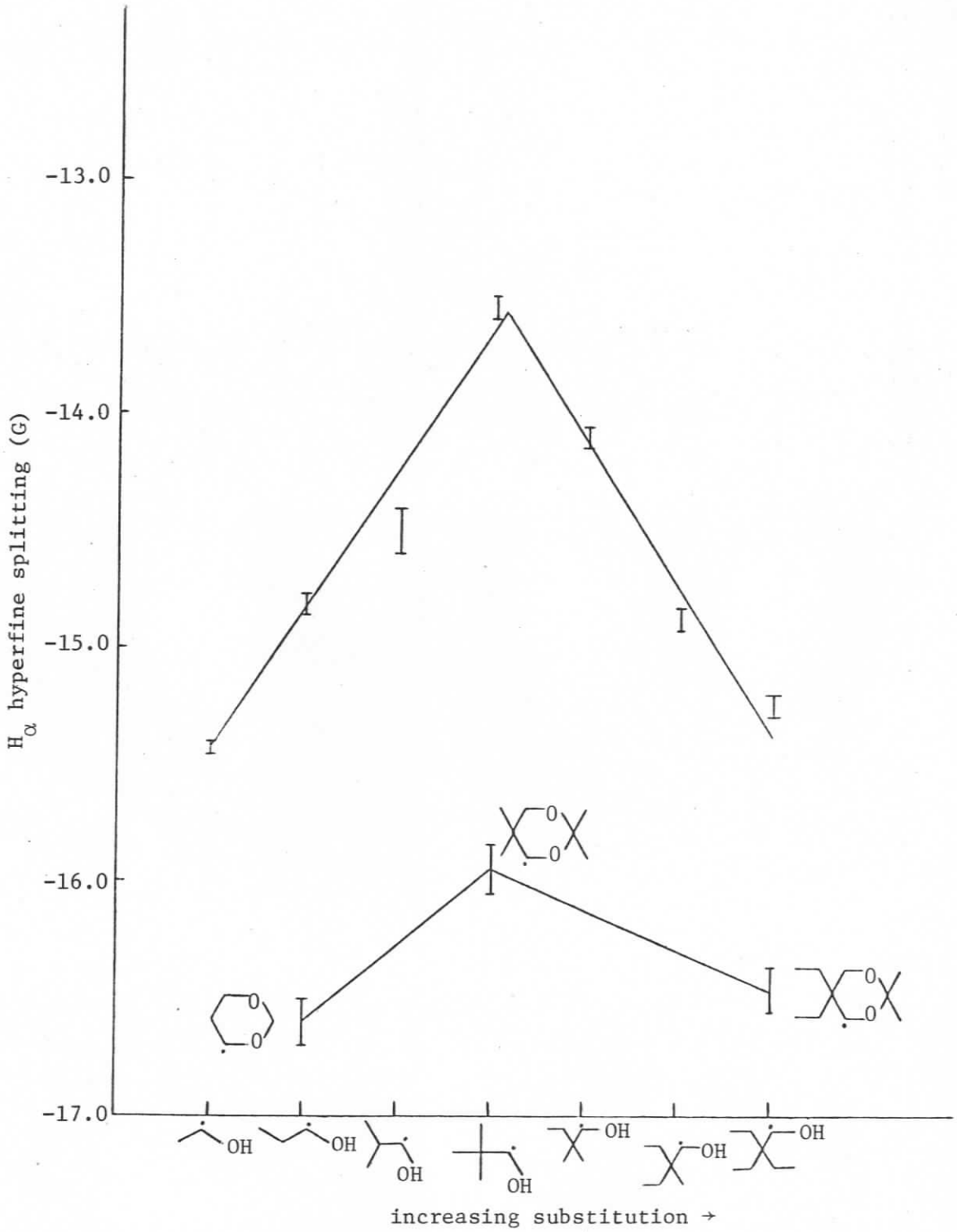

FIGURE 74: Plot of $a_{\alpha H}$ (G) at 0°C vs. substitution at C_β for 1-hydroxyalkyl radicals (119)-(125). Three related dioxane examples are also shown.

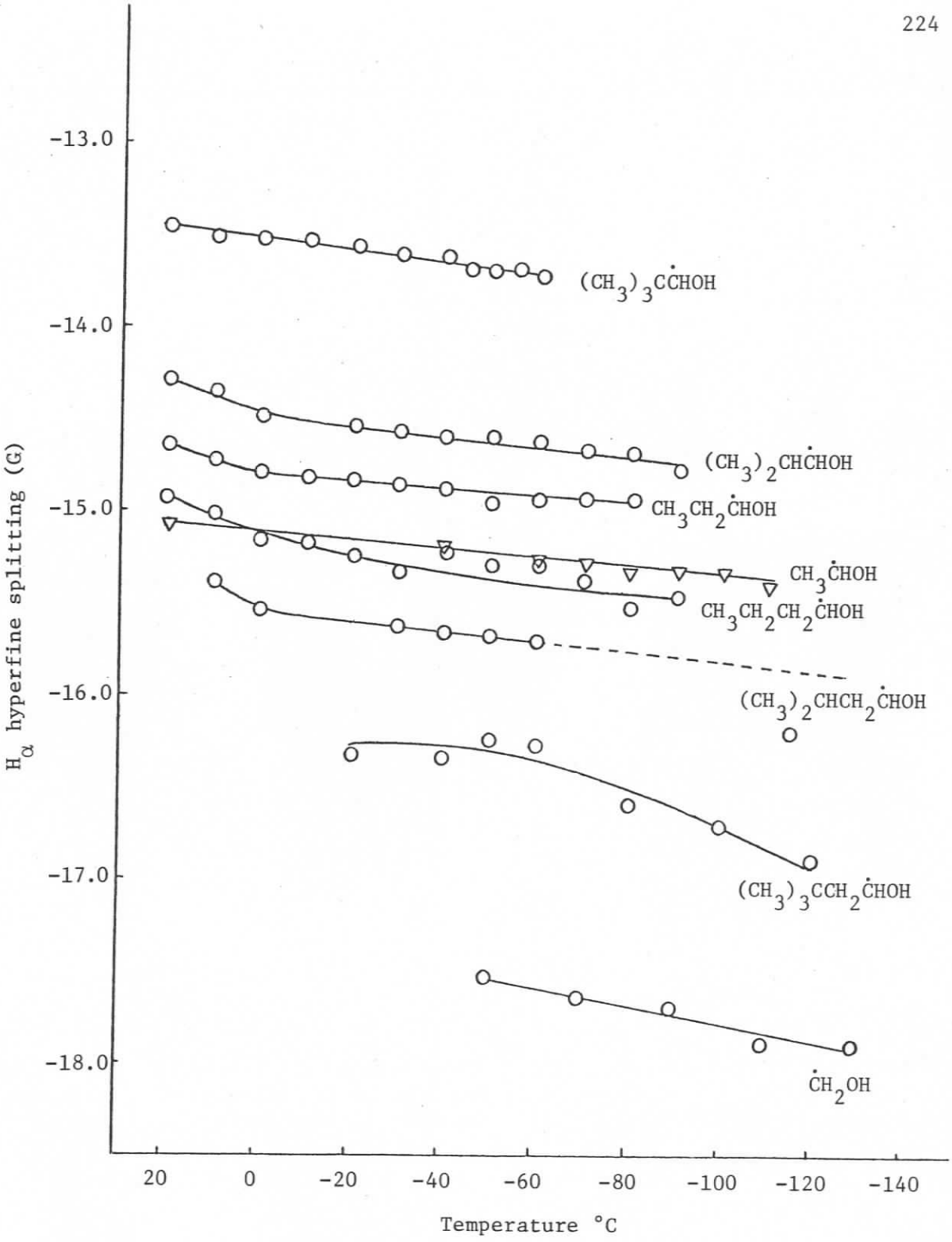

FIGURE 75: Plot of $a_{\alpha H}$ (G) vs. temperature (°C) for selected 1-hydroxyalkyl radicals.

TABLE 30: Values of $a_{\alpha H}$ for a series of 1-hydroxyalkyl radicals

Structure Number	Radical	$-a_{\alpha H}$ (G) @ 0°C	Steric Parameter, E'_s Ref. 161
119	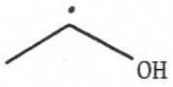	15.43^{25}±0.03 interpolated	
120		14.82±0.05	
121	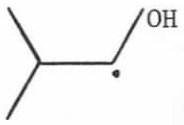	14.50±0.1	
122	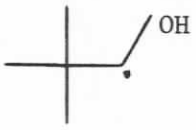	13.54±0.05	-1.43
123		14.10±0.05 interpolated	-2.28
124		14.88±0.05	-3.54*
125	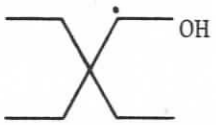	15.24±0.05	-5.29

* Value not specifically given in ref. 161; obtained by analogy.

order of electron releasing character,[163] or decreasing effective electronegativity, of the C_α alkyl substituent. [Note that theoretical predictions (Chapter I) require an *increase* in bending with substituent electronegativity.] Thus it appears that the *electron releasing* character of the substituent is the important property here in determining the degree of bending, as evidenced by H_α hfs values. However, in addition, increased population of the conformers shown below could influence the average value of $a_{\alpha H}$. Similar conformationally induced low values of $|a_{\alpha F}|$ have been proposed for the perfluoroneopentyl radical.[188]

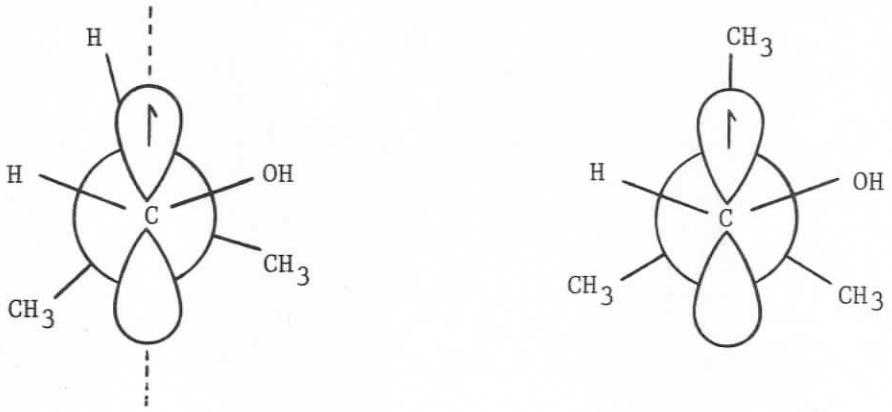

The radicals with increasingly complex alkyl substituents (122-125) do not demonstrate a simple levelling off of a_α as might have been expected. Rather, the trend is reversed and $|a_\alpha|$ increases linearly with increasing substituent size (Figure 74). Since the differences in inductive electronic properties of the C_α alkyl substituents in this series (122-125) are negligible they cannot account for the observed trend in $a_{\alpha H}$. Therefore the increasing steric bulk of the C_α substituent along this series (122-125) forces the radical to adopt a more nearly planar configuration. Consideration of models shows that the "packing"

of more bulky groups would drastically reduce any tendency toward bending induced by "staggered" conformations such as those shown above.

Note that the series of radicals (101),[27] (110), and (112) from cyclic ethers (Chapter IV) exhibit the same trend in their high temperature H_α hfs, indicative of steric "flattening" for the β,β-diethyl species (Figure 74).

Dubois et al.[161] have discussed the formal sequencing of alkyl groups based on their steric effects in the acid-catalysed esterification of carboxylic acids in methanol at 40°C. These authors provide a comprehensive list of steric parameters (E_S') for alkyl substituents. Figure 76 is a plot of $a_{\alpha H}$ for radicals (122-125) vs. the E_S' value corresponding to the respective C_α substituent. The clear trend in these points provides support for a controlling steric effect upon $a_{\alpha H}$ (and hence configuration) in this series of radicals.

The temperature dependence of the α-proton hyperfine splittings of the radicals (122-125) is shown in Figure 77, based on the data in Table 31. Uncertainty in the hfs in Figure 77 increases at low temperature due to the increasing anisotropy and the onset of modulation of the hydroxyl and α-proton hyperfine splittings.

The effects of two other C_α substituents, F_3C- and $(HOCH_2)_3C-$, support the analysis. Both are electronegative compared to alkyl substituents. The H_α splitting in $CF_3\dot{C}HOH$ (126) is significantly more negative than $a_{\alpha H}$ in $CH_3\dot{C}HOH$ (119) indicating less bending[27] (see Table 32). Increased flattening can be attributed to conjugative electron withdrawal by CF_3 as illustrated in (126a-c).

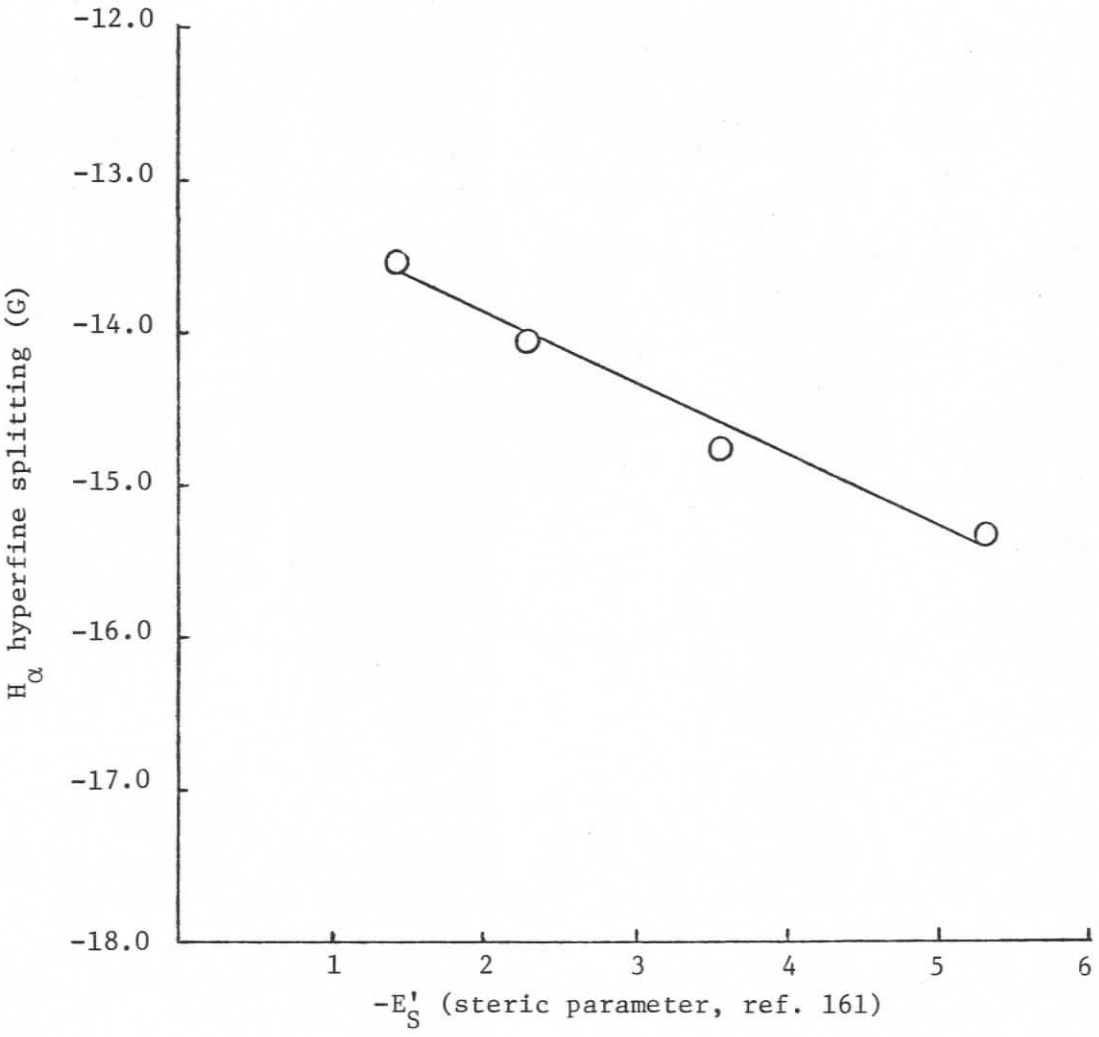

FIGURE 76: Plot of $a_{\alpha H}$ (G) at 0°C vs. steric parameter ($-E_S'$, ref. 161) for radicals (122-(125). (Line is least-squares fit, splittings were taken from the curves in Figure 77.)

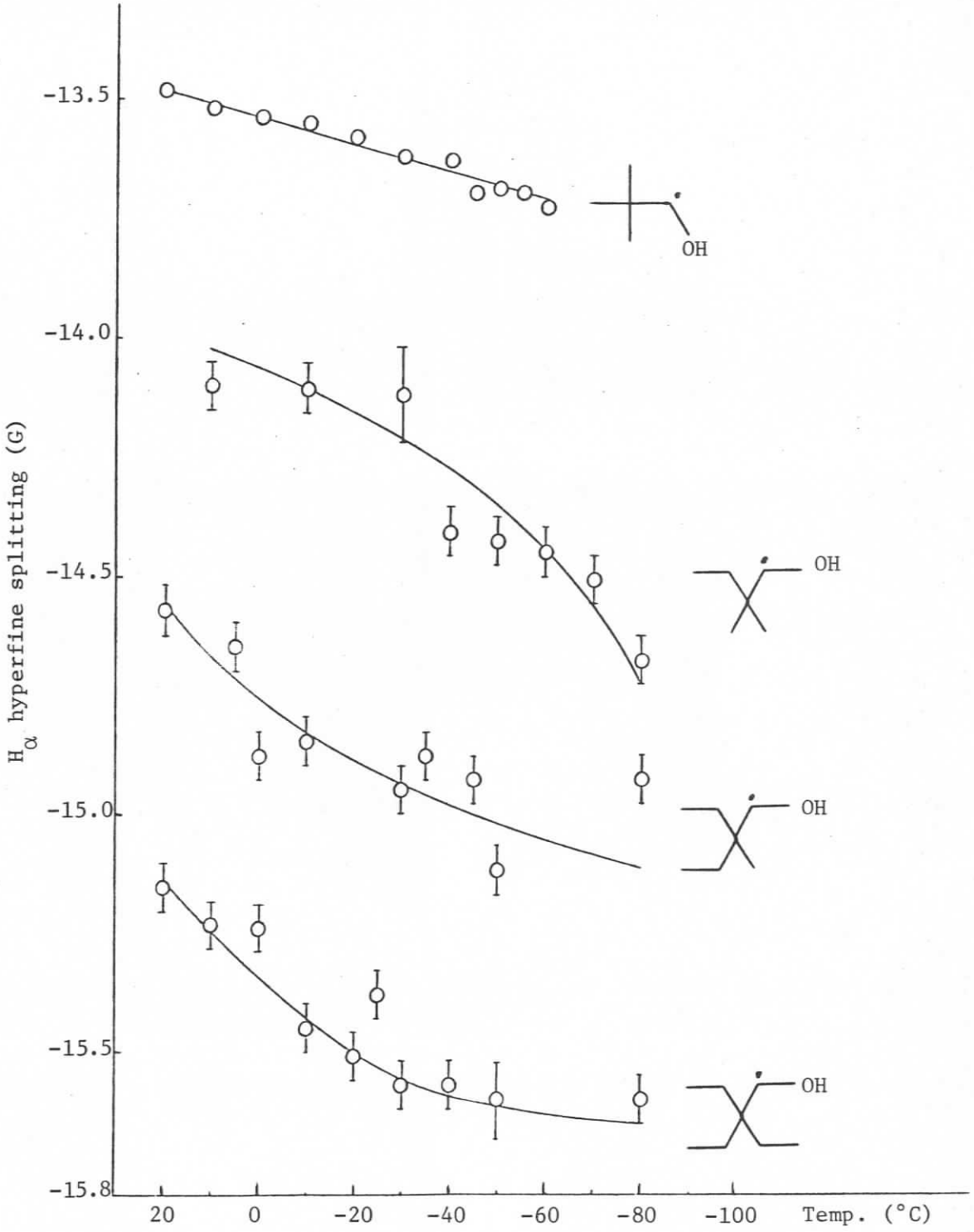

FIGURE 77: Plot of $a_{\alpha H}$ (G) vs. temperature (°C) for β-substituted 1-hydroxyalkyl radicals.

TABLE 31: Hyperfine splittings of the radicals (122-125)

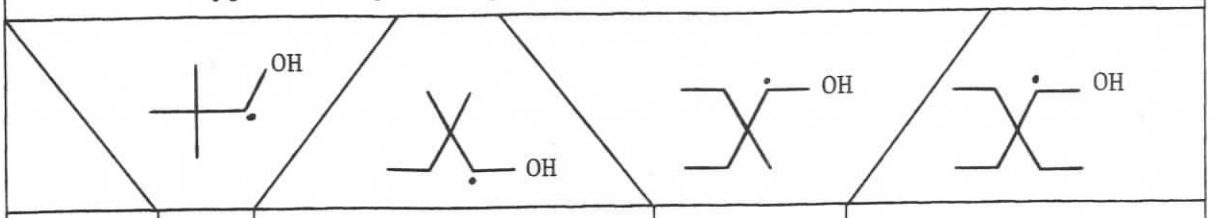

Radical	122	123			124		125	
Temp. °C	$-a_{\alpha H}$	$-a_{\alpha}$	$-a_{OH}$	$\lvert a_{\gamma} \rvert$	$-a_{\alpha}$	$-a_{OH}$	$-a_{\alpha}$	$-a_{OH}$
	±0.05	±0.05	±0.05	±0.05	±0.05	±0.05	±0.05	±0.05
+20	13.48				14.57	nr*	15.15	nr
+10	13.52	14.10	nr	nr			15.23	0.45
+5	-				14.65	nr		
0	13.54				14.88	nr	15.24	0.59
-10	13.55	14.11	nr	nr	14.85	0.72	15.45	0.58
-20	13.58						15.51	0.66
-25	-						15.38	0.75
-30	13.62	14.12±0.1	0.89±0.1	nr	14.95	0.75	15.57	0.71
-35	-				14.88	0.75		
-40	13.63	14.41	0.84	nr			15.57	0.83
-45	13.70				14.93	0.92		
-50	13.69	14.43	0.90	nr	15.12	0.80	15.60±0.08	0.74±0.08
-60	13.73	14.45	1.06	0.39				
-70	-	14.51	1.13	0.38				
-80	-	14.68	1.08	0.41	14.93	1.38	15.6±0.1	-

* Not resolved

TABLE 32: H_α hfs in the case of F_3C- and $(HOCH_2)_3C$- substituents

Structure Number	Radical	$-a_{\alpha H}$	Temp. °C
119	$CH_3\dot{C}HOH$	15.37[25]	26
126	$CF_3\dot{C}HOH$	18.1[164]	27
127	$(HOCH_2)_3C\dot{C}HOH$	16.32[136]	21-23

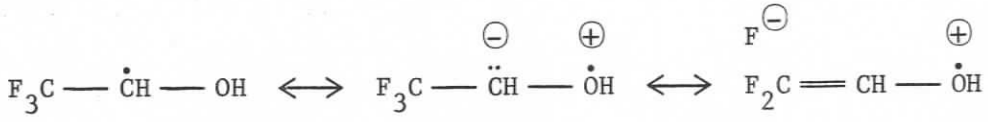

126a 126b 126c

The higher $|H_\alpha|$ hfs of the radical (127) from pentaerythritol (Table 32) indicates that this species is also less bent than 1-hydroxyethyl (119). The effect is less pronounced than in (126) although both conjugative electron withdrawal and steric bulk (cf. radical 125) are expected to lead to decreased bending. Thus the relative importance of the two effects in this species (127) is unclear. Intramolecular hydrogen bonding is a complicating factor.

Figure 75 shows that $|a_{\alpha H}|$ increases (relative to $CH_3\dot{C}HOH$) for the species $(CH_3)_2CHCH_2\dot{C}HOH$ and $(CH_3)_3CCH_2\dot{C}HOH$, possibly indicative of "steric flattening" for these species as well.

Clearly it would be desirable to obtain $^{13}C_\alpha$ hyperfine splittings to supplement our knowledge about the trends in bending in all the species discussed above. It was not possible to observe any signals

attributable to hyperfine coupling with ^{13}C in natural abundance in several attempts using the well-behaved substrate neopentyl alcohol. It would be possible to synthesize this alcohol enriched in ^{13}C at the α-position. Reaction of *t*-butyl magnesium chloride with $^{13}CO_2$ would give pivalic acid,[165,166] which has been reduced to the alcohol by $LiAlH_4$ in good yield.[167,168] The more direct reaction of *t*-butyl magnesium chloride with $H_2^{13}CO$ or $H^{13}COOCH_3$ is an alternative route. Isotopically enriched samples of the other hindered alcohols could also be prepared for study by similar methods.

(b) The ESR Spectra of Complex β-Branched 1-Hydroxyalkyl Radicals

(i) The 1-Hydroxy-2,2-dimethylbut-1-yl Radical

The ESR spectrum of the 1-hydroxy-2,2-dimethylbut-1-yl radical (123) at +10°C is a simple broad doublet, $\Delta H_{pp} \simeq 0.9$ G (Figure 78a).

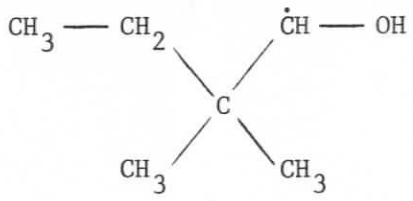

123

Upon cooling the sample $|a_{OH}|$ increases so that at -50°C the splitting is well resolved (Figure 78b). At -60°C two additional features become apparent (Figure 78c). First, the inside lines of the OH doublets are broadened by modulation of a_α and a_{OH} out-of-phase as observed for the radical from 2,2-dimethyl-1-propanol (neopentanol)(see Chapter III, section 3a). Second, an additional splitting is clearly resolved in the

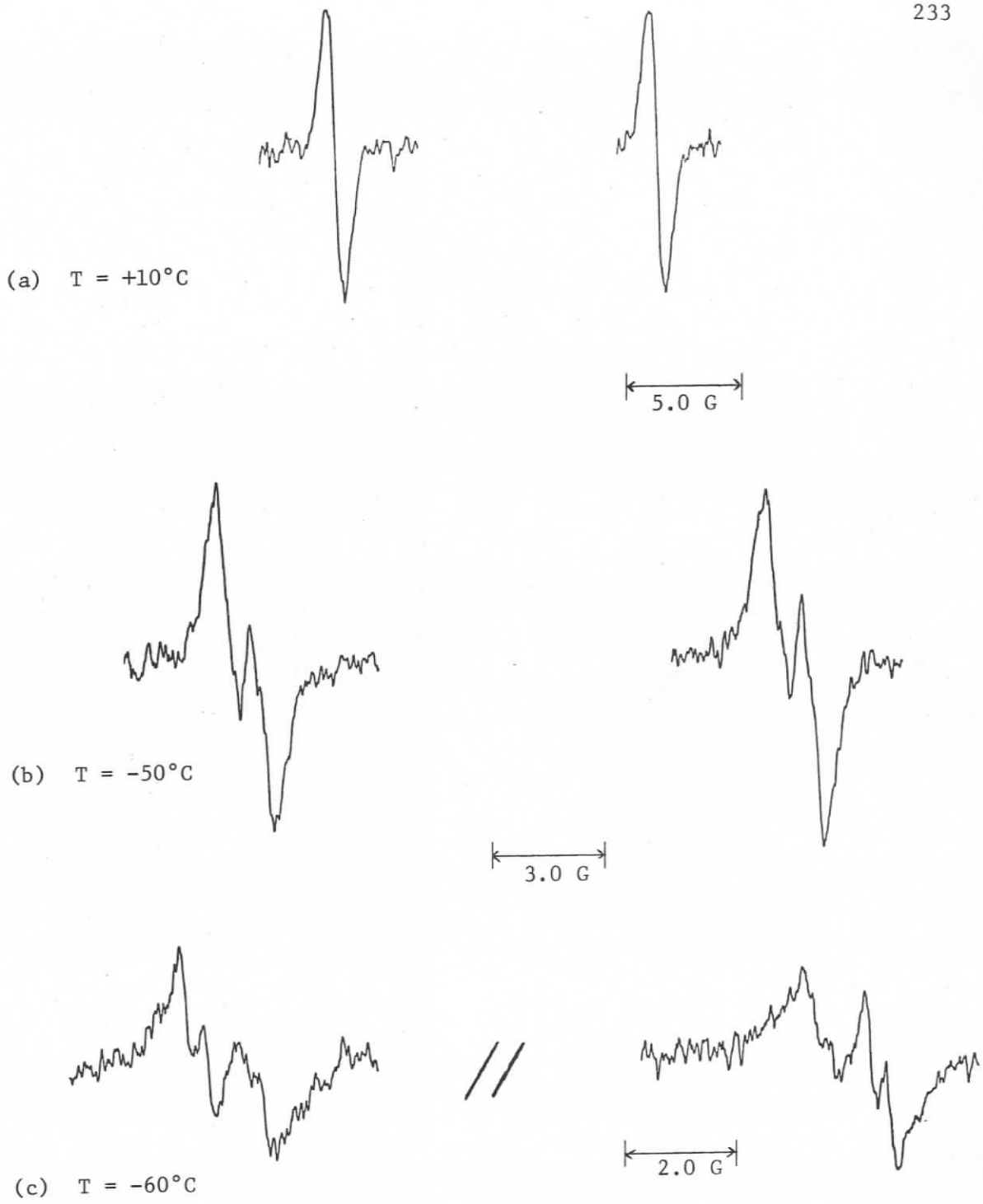

FIGURE 78: The ESR spectrum of the 1-hydroxy-2,2-diemthylbut-1-yl radical (123) at (a) +10°C, (b) -50°C, (c) -60°C. (Figure continues)

(d) T = -80°C

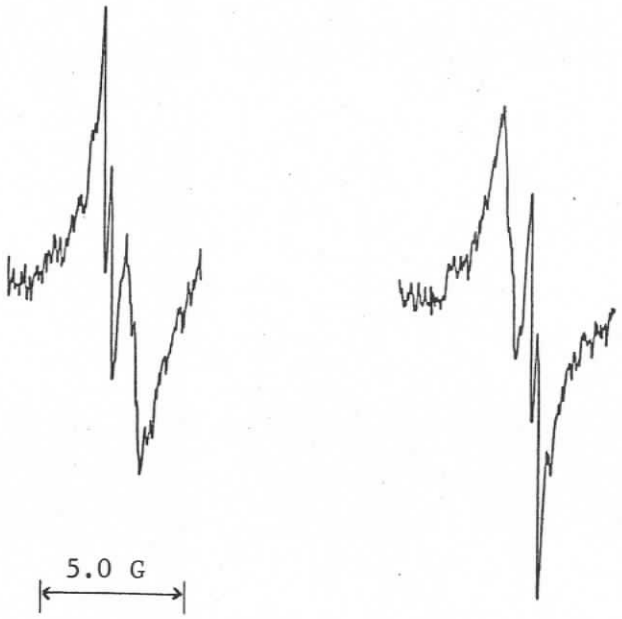

(e) T = -70°C

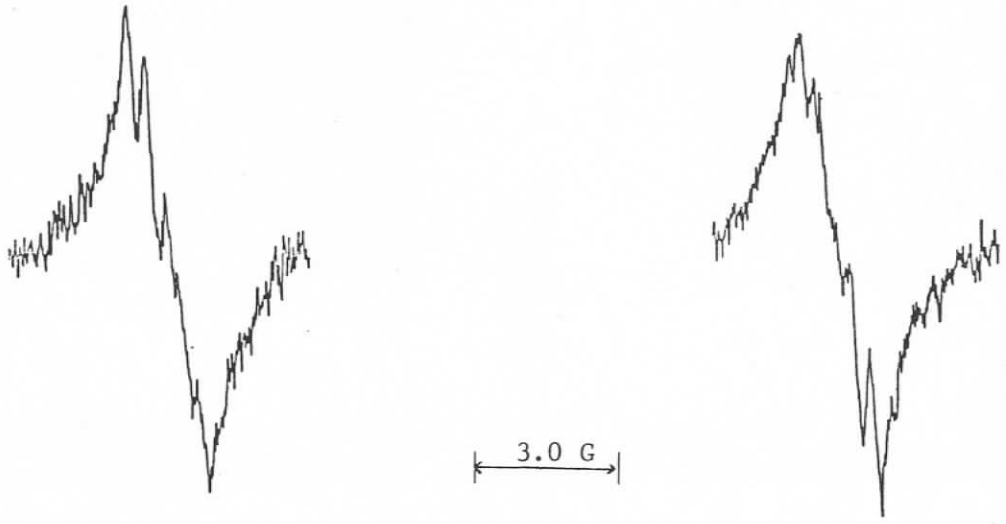

FIGURE 78 (continued): (d) spectrum of radical (123) at -80°C, (e) spectrum of a sample of radical (123) in which most of the OH had been exchanged to OD; at -70°C.

outer part of each OH doublet. This must represent a specific γ-proton interaction. The generally broad appearance of the lines is likely due to other unresolved H_γ splittings (hyperfine splittings are listed in Table 31). Deuteration of the hydroxyl group changed the appearance of the low temperature spectrum (cf. Figures 78d and e) in that a_{OH} was not clearly resolved but the smaller (γ) splitting (*ca*. 0.4 G) remained unchanged. (Note that Krusic et al.[57] found that for $\cdot CD_2OD$ the value of a_{OD} was *ca*. 15% greater than predicted on the basis of proton-deuteron moment ratio.) Attempts at simulation of the experimental spectrum (Figure 78c) were unsuccessful, probably because of significant overlap of signals arising from the undeuterated radical.

An equilibrium conformation which could give rise to a large specific γ-proton interaction is (128, $\theta_2 > \theta_1$). Here the single proton

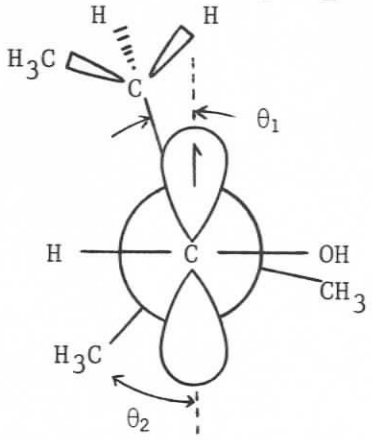

128

at $\theta_\gamma = 180°$ of the ethyl group would be expected to give a significantly larger splitting than other γ-protons.

(ii) The 2-Ethyl-1-hydroxy-2-methylbut-1-yl Radical

The ESR spectrum of the 2-ethyl-1-hydroxy-2-methylbut-1-yl radical (124) is a simple doublet at +20°C. The hydroxyl proton splitting is resolved at -10°C (Figure 79a and b). The hyperfine splittings are

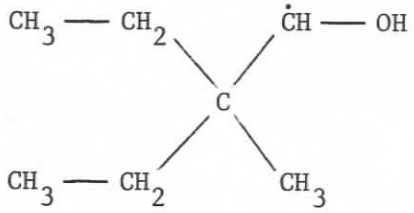

124

listed in Table 31. At -80°C, when the substrate is dissolved in cyclopropane, there is marked broadening of the inside lines of the hydroxyl doublets as observed in the spectrum of the radical from neopentanol (Chapter III) and ascribed to restricted rotation about C_α-OH. This broadening is not evident in the same solvent at -50°C. However, when the substrate was dissolved in di-*t*-butyl peroxide only, this broadening became evident at a much higher temperature, -35°C (Figure 79c). It appears that in solvents of higher viscosity than cyclopropane the modulation effects of restricted rotation set in at higher temperatures. Both solvent viscosity and hydrogen bonding between solvent and the radical could create this effect.

No further hyperfine structure was observed. Indeed extrapolation from theoretical calculations by Ellinger[32] for n-propyl radical suggests that average γ-proton splittings for a probable equilibrium conformation like (129) would be low. A uniquely favoured ethyl group (cf. structure 128) is now not anticipated.

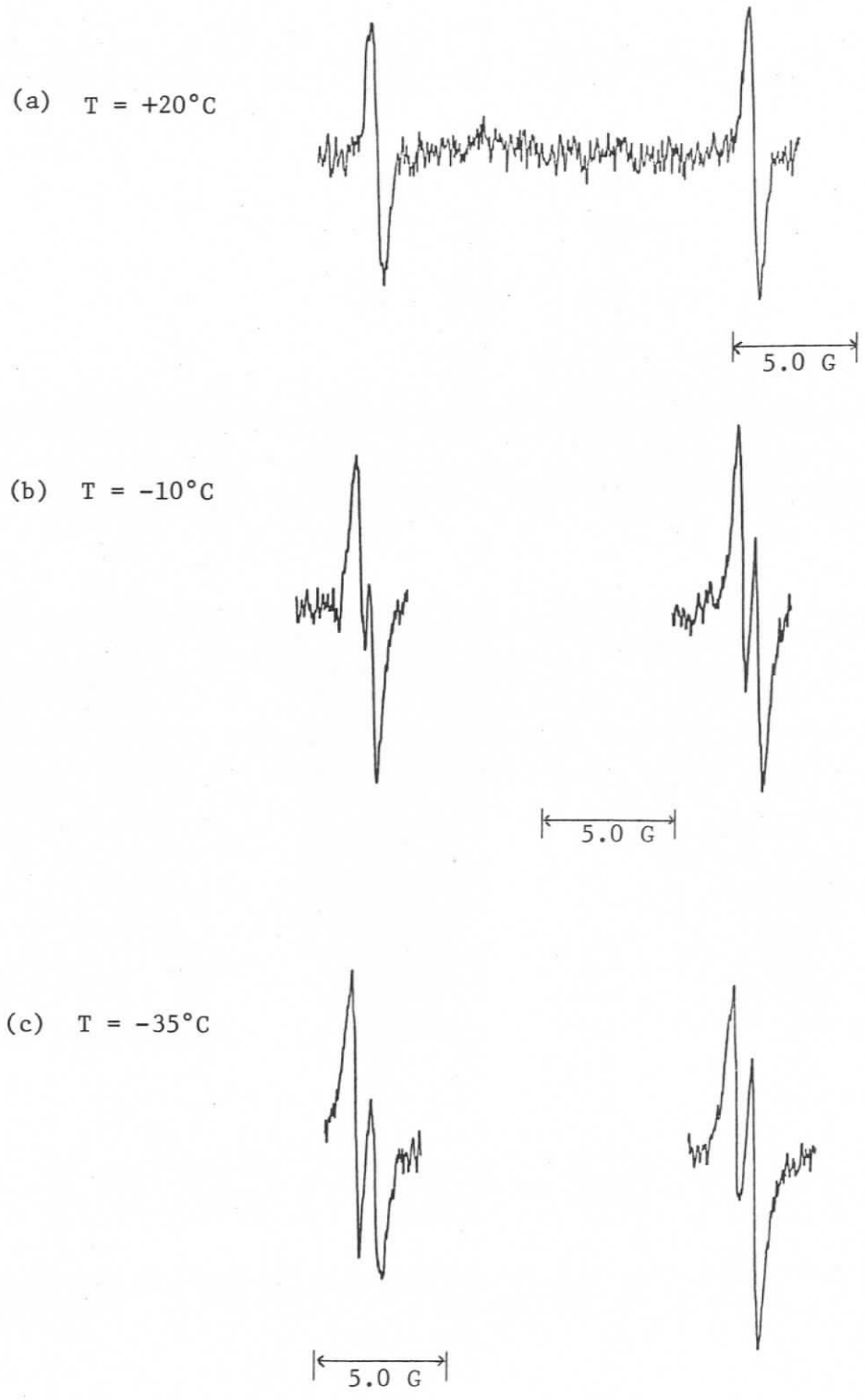

FIGURE 79: ESR spectrum of the 2-ethyl-1-hydroxy-2-methylbut-1-yl radical (124) (a) at +20°C, in dtbp solvent, (b) at -10°C in cyclopropane solvent, (c) at -35°C in di-*t*-butyl peroxide solvent, showing broadening of inside lines.

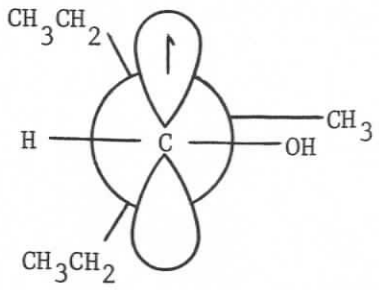

129

(iii) The 2,2-Diethyl-1-hydroxybut-1-yl Radical

The ESR spectrum of the 2,2-diethyl-1-hydroxybut-1-yl radical (125) is much like that of radical (124). At +20°C it consists of a simple doublet and at -10°C the hydroxyl splitting is resolved (Figure 80, splittings in Table 31). Spectral resolution deteriorated at low

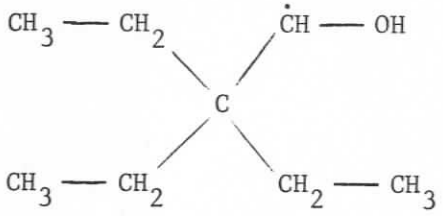

125

temperatures and the expected broadening of the inside lines was only weakly observed. Some of the additional signals (a = 17.3 G, marked * in Figure 80c) in the high temperature spectrum were attributed to the triethylmethyl radical, which has been previously reported.[170] Other signals were not assigned. Comparison with triethylmethyl radical gives the g-value of radical (125) as 2.0036.

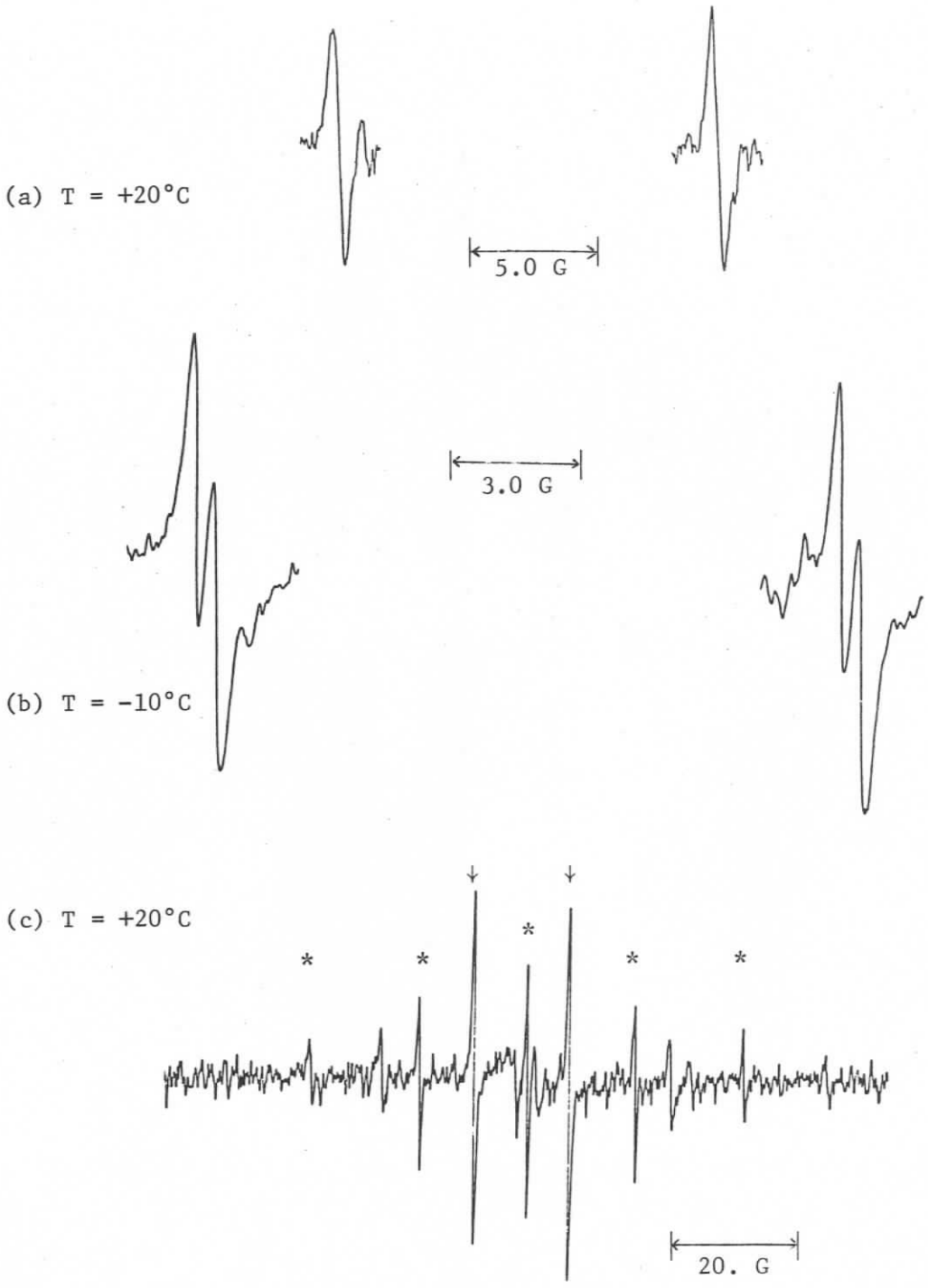

FIGURE 80: ESR spectrum of 2,2-diethyl-1-hydroxybut-1-yl radical (125), (a) at +20°C, (b) at -10°C, (c) at +20°C showing other signals present. The peaks (*) are assigned to triethylmethyl radical. The signals from the alcohol radical (125) are marked (↓), other signals are unassigned.

3. SUMMARY AND CONCLUSIONS

Based on the α-proton hyperfine splitting as a monitor of radical configuration it has been shown that C_α-alkyl substituents of increasing +I inductive effect cause increased bending in the α-hydroxy series ethyl, n-propyl, isobutyl, neopentyl (119-122). Increasing the bulk of the α-substituents causes an apparent decrease in bending which correlates well with the steric parameters of these groups as defined by Dubois et al.[161] (radicals 122-125). The α-proton splittings of certain other alcohol-derived radicals with bulky substituents (for example, $(CH_3)_2CHCH_2\dot{C}HOH$ and $(CH_3)_3CCH_2\dot{C}HOH$, see Figure 75) are likely also influenced by this steric flattening effect.

The spectra of the bulky radicals (123-125) show inside line broadening characteristic of restricted C_α-OH rotation as clearly demonstrated for the 1-hydroxy-2,2-dimethylprop-1-yl radical (1-hydroxyneopent-1-yl) in Chapter III. In the case of the 1-hydroxy-2,2-diemthylbut-1-yl radical (123) an additional splitting is assigned to interaction with a specific γ-proton.

CHAPTER VI

EXPERIMENTAL

1. GENERAL

(a) Instrumentation

^{1}HNMR spectra were recorded on Perkin Elmer R12 (60 MHz) and R32 (90 MHz) instruments. The latter was used for variable temperature studies. ^{13}CNMR and some ^{1}HNMR were obtained with a Nicolet TT14 spectrometer (^{13}C @ 15.1 MHz, 60 MHz Varian magnet). When high field spectra were deemed necessary the Brüker WM 250 multinuclear spectrometer was used (^{13}C @ 62.875 MHz, ^{1}H @ 250.132 MHz). Solvents and temperatures for NMR data are specified in each case. ^{1}H chemical shifts (δ) are given in ppm downfield from tetramethylsilane as internal reference. For ^{13}CNMR the deuterated solvent was used as the internal reference. The multiplicity symbols have their usual meanings (s = singlet, d = doublet, t = triplet, q = quartet, m = multiplet, b = broad).

Mass spectra were obtained with a Finnigan 3300 gc/ms (quadrapole) system employing methane chemical ionization.

Carbon and hydrogen analyses were performed by Canadian Microanalytical Service Ltd., Vancouver, B.C.

Melting points were obtained with a Reichert hot-stage aparatus equipped with an Omega Engineering digital thermometer.

(b) Solvents

Cyclopropane, cyclopentane, Freon-11, and Freon-113 were commercial products used without further purification. Cyclopropane (99%) was supplied by Union Carbide. Supply by this firm ceased early in 1982.

Acetone was spectroscopic grade (99%+). Acetone was dried by distillation from K_2CO_3 unless otherwise indicated.

Methanol was anhydrous reagent grade or distilled commercial grade.

Methylene chloride, hexanes, petroleum ether (30°-60°), and diethyl ether were distilled commercial solvents.

Benzene was dried by refluxing over sodium followed by distillation. It was stored over sodium wire.

Tetrahydrofuran was dried by refluxing with potassium until the persistent blue colour of benzophenone radical anion was established, followed by distillation. This procedure was followed before each use.

Di-*t*-butyl peroxide was purified by the method of Roberts et al.[66] Accordingly, the peroxide was washed with aqueous KI, dried over $MgSO_4$, distilled (b.p. lit.[66] 111°C @ 760 mm, 70°C @ 197 mm), and passed through a short column of basic alumina (activity $\leqslant$ 1). Note that the KI solution was not acidified in the present work.

(c) Substrates

The commercially obtained substrates from which some of the radicals studied were generated were either used as received or purified if required. A summary of the source of each material follows.

SUBSTRATE	*PURIFICATION/SOURCE*
methanol	anhydrous reagent
ethanol	100%, distilled commercial solvent
1-propanol	distilled reagent b.p. 95.5-96.5°C @ 760 mm, Fischer, Mallinckrodt
2-propanol	reagent grade as supplied by Amachem
1-butanol	distilled reagent b.p. 114-116°C @ 760 mm, Amachem
isobutanol(2-methyl-1-propanol)	reagent grade as supplied by MC&B
isopentanol(3-methyl-1-butanol)	distilled reagent b.p. 128-129°C @ 760 mm, Caledon
neopentanol(2,2-dimethylpropanol)	narrow b.p. fraction dist. from technical grade (78%), manuf. sugg. b.p. 113-114°C @ 760 mm, crystallized neat in some cases; Aldrich
3,3-dimethyl-1-butanol	98%, Aldrich, only trace impurities by ^{1}HNMR
3,3-dimethyl-2-butanol	99%, Aldrich
2,4-dimethyl-3-pentanol	94%, Aldrich, distilled b.p. 138.5-140°C @ 760 mm
cyclohexanol	distilled reagent 159-161°C, Fisher
diethyl ether	distilled reagent
di-n-propyl ether	99%+, Aldrich gold label
di-n-butyl ether	99%, Aldrich
2,4,8,10-tetraoxyspiro[5,5]undecane (pentaerythritol diformal)	as received from Eastman, pure by ^{13}C & ^{1}HNMR
2,2-dimethyl-1-butanol	as received from Chemicals Procurement Laboratories, trace impurity by ^{1}HNMR

2. PREPARATION OF SUBSTRATES

(a) 5,5-Dimethyl-1,3-dioxane (90)

A solution of 2,2-dimethyl-1,3-propanediol (107.4 g as 97%, 1.0 mol) in hexanes (600 mL) with *p*-toluenesulphonic acid (1 g, 0.5 mol %) was refluxed in a flask fitted with a Dean Stark trap and condenser, an inlet tube (i.d. 10 mm) for formaldehyde, and a magnetic stirrer.

Formaldehyde was generated by heating (oil bath, 180-200°C) powdered paraformaldehyde (*ca*. 150 mL, in a 500 mL flask) which had been dried over P_2O_5 in a dessicator for several days. A small positive pressure of nitrogen helped flush the gaseous formaldehyde into the reaction flask. The inlet tube projected *ca*. 3 cm below the surface of the alcohol solution. (Caution: polymerized formaldehyde may block some of the tubing.)

After 1 h all the diol had dissolved. At the end of 3 h all the paraformaldehyde had evaporated and 16 mL water had been collected. The clear colourless solution was treated with a saturated aqueous solution of $NaHCO_3$ (3 x 80 mL) and dried over $MgSO_4$. It was then evaporated to low volume and distilled at atmospheric pressure. The initial distillate (69-96°C) was discarded. Three fractions were then collected; 96-130°C (5.9 g), 130-142°C (11.2 g), and 142-214°C (9.1 g). A small portion of the second fraction was chromatographed on Sephadex using 35% CH_3OH in $CHCl_3$ as eluant. No product was recovered. The remainder of this fraction was redistilled from sodium through a short column of glass rings. The main portion was collected at 126°C.

The first and third fractions from the initial distillation were combined and fractionally redistilled in the same way. The main portion was collected at 125°C. The distillate in each case was 5,5-dimethyl-1,3-dioxane (90)(total yield *ca*. 13%), b.p. 125-126°C (lit. 126.5,[171] 126.6[172] @ 747 mm Hg).

Analysis found: C, 62.19; H, 10.82%

$C_6H_{12}O_2$ requires: C, 62.04; H, 10.42%

ms peaks used for identification at m/e 117(M+1), 115(M-1).

^{1}HNMR (neat, 60 MHz): δ 0.91 (s,6H,Me-5),3.36(s,4H,H-4,6),4.64(s,2H,H-2). (cf. ref. 182).

^{13}CNMR ($CDCl_3$): δ 22.56(q,CH_3,J_H = 125.1 Hz),30.91(s,C-5),77.29 (tt,C-4,6,J_H = 142.7,4.6 Hz),94.05(tt,C-2,J_H = 162.5,4.6 Hz). (cf. ref. 181).

(b) 2,5,5-trimethyl-1,3-dioxane (96)

A mixture of 2,2-dimethyl-1,3-propanediol (107.3 g as 97%, 1.0 mol) and acetaldehyde (44.05 g, 56 mL, 1.0 mol) with *p*-TsOH (1.0 g, 0.5 mol%) in hexanes (600 mL) was refluxed for 1.5 h under a Dean Stark trap. Eighteen mL of water were collected. After cooling, the reaction mixture was treated with saturated aqueous $NaHCO_3$ (3 x 200 mL), washed with water (3 x 200 mL), dried over $MgSO_4$ and evaporated to a low volume. The liquid was distilled at atmospheric pressure. The fraction (50 mL) collected at 130-131.5°C was redistilled from sodium yielding 2,5,5-trimethyl-1,3-dioxane (96), 18.69 g (14.4%) b.p. 128-129°C, (lit. 130-131°C,[171-172] 128-130°C[173]).

Analysis found: C, 64.72; H, 11.33%

$C_7H_{14}O_2$ requires: C, 64.58; H, 10.84%

ms peaks used for identification at m/e (relative intensity) 131(M+1,14), 129(M-1,16).

^{1}HNMR (CCl_4, 90 MHz): δ 0.69(s,3H,Me-5_e), 1.19(s,3H,Me-5_a), 1.21(d,3H,Me-2_e,$J_{2\text{-}H}$ = 4.5 Hz), 3.25(d,2H,H-4_a,6_a,J_{gem} = 10.8 Hz), 3.47(d,2H,H-4_e,6_e,J_{gem} = 10.8 Hz), 4.42(q,1H,H-2_a,$J_{2\text{-}Me}$ = 4.5 Hz). (cf. ref. 182).

^{13}CNMR ($CDCl_3$): δ 20.84(q,Me-2_e,J_H = 127.2 Hz), 21.76(q,Me-5_e,J_H = 125.6 Hz), 22.93(q,Me-5_a,J_H ≃ 126 Hz), 29.84(s,C-5), 77.15(t,C-4,6,J_H = 141.9 Hz), 99.12(d,C-2,J_H = 157.9 Hz). (cf. ref. 181).

(c) 2,2,5,5-tetramethyl-1,3-dioxane (91)

A mixture of 2,2-dimethyl-1,3-propanediol (26.84 g as 97%, 0.25 mol), dry acetone (31.9 g, 40.4 mL, 0.55 mol), *p*-TsOH (1. g), and dry benzene (50 mL) was refluxed under a Dean Stark trap. After 27 h a further portion of dry benzene (50 mL) was added. After a further 7 h, 4.4 mL water had been collected. Triethylamine (0.54 g) was then added and the mixture was distilled at atmospheric pressure yielding 2,2,5,5--tetramethyl-1,3-dioxane (91), 18.23 g (48%) at 143-152°C. This product was redistilled from sodium through a short column of glass beads to yield a major fraction at 143-145°C (lit. 143°C,[174] 143-144°C,[155] 144-145°C[171,172]).

Analysis found: C, 67.07; H, 11.63%

$C_8H_{16}O_2$ requires: C, 66.62; H, 11.19%

ms peaks used for identification at m/e 145(M+1), 143(M-1).

^{1}HNMR (neat, 60 MHz): δ 0.90(s,6H,Me-5), 1.30(s,6H,Me-2), 3.34(s,4H, H-4,6). (cf. ref. 182).

^{13}CNMR ($CDCl_3$): δ 22.56(q'd',Me-5,J_{qH} = 125.1 Hz,$J_{d'H}$ = 4.6 Hz), 23.75(q'd',Me-2,J_{qH} = 126.6 Hz,$J_{d'H}$ ≃ 3.1 Hz), 29.96(s,C-5), 70.61(t't',C-4,6,J_{tH} = 141.9 Hz,$J_{t'H}$ ≃ 4.6 Hz), 97.60(septet, C-2, J_H = 4.6 Hz). (cf. ref. 181).

(d) 5,5-diethyl-2,2-dimethyl-1,3-dioxane (94)

A mixture of 2,2-diethyl-1,3-propanediol (33.05 g, 0.25 mol, vac. dist. 117-120°C), dry acetone (17.4 g, 22.0 mL, 0.30 mol), *p*-TsOH (1. g, 0.5 mmol), and dry benzene (100 mL) was refluxed under a Dean Stark trap. After 3 h, 6 mL water had collected. The reaction was allowed to cool and triethylamine (0.54 g) was added. The solution was evaporated to low volume and distilled from sodium through a short column of glass rings. The product, 5,5-diethyl-2,2-dimethyl-1,3-dioxane (94) distilled at 183-193°C giving 25.72 g (59.7%).

Analysis found: C, 69.49; H, 12.31%

$C_{10}H_{20}O_2$ requires: C, 69.72; H, 11.70%

ms peaks used for identification at m/e (relative intensity) 173(M+1,11), 171(M-1,13), 97(M-75,100).

^{1}HNMR (CCl_4, 60 MHz): δ 0.79(t,6H,H-2',$J_{H-1'}$ = 7.2 Hz), 1.28(s,6H,Me-2), 1.35(q,4H,H-1',$J_{H-2'}$ obscured by overlap), 3.39(s,4H,H-4,6). (cf. ref. 182).

^{13}CNMR ($CDCl_3$): δ 7.04(qt,Me-2',$J_{H-2'}$ = 125.1 Hz,$J_{H-1'}$ = 4.6 Hz), 23.82(t'd',C-1',$J_{H-1'}$ = 125.1 Hz,$J_{H-2'}$ = 3.1 Hz), 23.82(q'd', Me-2,J_{H-Me} = 126.1 Hz,$J_{H-4(6)}$ = 3.1 Hz), 34.89(s,C-5),

67.64(t't',C-4,6,$J_{H-4(6)}$ = 141.9 Hz,J_{other} = 3.1 Hz), 97.89(bm, C-2,J_H = 4.6 Hz). (cf. ref. 181).

(e) 3,9-dimethyl-2,4,8,10-tetraoxaspiro[5,5]undecane (97)

Acetaldehyde (17.62 g, 22.4 mL, 0.40 mol) was added to an ice-cooled 250 mL flask containing pentaerythritol (38.41 g of 98% reagent, 0.20 mol, finely powdered with a mortar and pestle). Upon addition, through the condenser, of hydrochloric acid (conc., 2 mL) the acetaldehyde refluxed. After the initial reaction subsided the mixture was heated to *ca*. 100°C for 1.5 h, after which time the reaction was homogeneous. The oily liquid was allowed to cool and was extracted with boiling hexanes (4 x 100 mL) by decantation. An additional portion of hexanes (200 mL) was added to the cooled extracts and this solution was treated with dilute Na_2CO_3 (100 mL), washed with water (2 x 100 mL), dried over $MgSO_4$ and evaporated to a low volume. The residual clear colourless oil was transferred, using ether, to a 50 mL pear flask and vacuum distilled. The second fraction gave 3,9-dimethyl-2,4,8,10--tetraoxaspiro[5,5]undecane (97), (16.15 g, 42.9%) at 85-90°C (lit.[175,176] 93-95°C @ 8 mm Hg).

Analysis found: C, 57.39; H, 8.69%

$C_9H_{16}O_4$ requires: C, 57.43; H,8.57%

ms peaks used for identification at m/e 189(M+1), 217(M+29), 229(M+41)

^{1}HNMR ($CCl_3F/(CD_3)_2CO$, 250 MHz): δ 1.21(d,6H,Me-3,9,$J_{H-3,9}$ = 5.15 Hz), 3.30-3.54(m,6H,6 of H-1,5,7,11), 4.37-4.44(m,2H,2 of H-1,5,7,11), 4.55(q,2H,H-3,9,J_{Me} = 5.15 Hz), (see Figure 63).

^{13}CNMR ($CDCl_3$): δ 20.81(q,Me-3,9,J_H = 127.0 Hz), 31.81(s,C-6), 70.04 (t,two of C-1,5,7,11,J_H = 141.4 Hz), 70.51(t,two of C-1,5,7,11, J_H = 141.4 Hz), 99.79(d,C-3,9,J_H = 161.1 Hz). (cf. ref. 181).

(f) 3,3,9,9-Tetramethyl-2,4,8,10-tetraoxaspiro[5,5]undecane (93)

Dry acetone for this preparation was refluxed over K_2CO_3 and a few crystals of $KMnO_4$, and then distilled. Again the pentaerythritol was finely powdered with a mortar and pestle before use.

Dry acetone (580.8 g, 734 mL, 10 mol), pentaerythritol (138.9 g as 98%, 1.0 mol), and anhydrous $CuSO_4$ (79.8 g, 0.5 mol) were mixed in a 2 L, 3-neck RB flask equipped with a mechanical stirrer.[178] The reaction was stirred for 24 h at room temperature and then filtered. The filtrate was evaporated to dryness and extracted with boiling hexanes (4 x 400 mL). The hot extracts were filtered by suction through a sintered glass disc as they were obtained. A second similar filtration was performed on the extracts after cooling, leaving a solid (a) behind. This filtrate was evaporated to dryness leaving a solid (b). The solid (a) was redissolved in hot hexanes and filtered, while hot, into the flask containing the solid (b), and the mixture was made up to 400 mL with hexanes. After boiling and cooling a first crop of white prisms was obtained (19.02 g). The filtrate, evaporated to lower volume, yielded a second crop (13.19 g). The product was 3,3,9,9-tetramethyl-2,4,8,10-tetraoxaspiro[5,5]-undecane (93) (total 32.21 g, 14.9%), mp 114-118°C (lit.[175] mp = 115-115.5°C).

Analysis found: C, 60.98; H, 9.65%

$C_{11}H_{20}O_4$ requires: C, 61.09; H, 9.32%

ms peaks used for identification at m/e (relative intensity) 217(M+1,8), 215(M-1,4).

^{1}HNMR ($CDCl_3$, 90 MHz): δ 1.35(s,12H,Me-3,9), 3.67(s,8H,H-1,5,7,11).

^{13}CNMR ($CDCl_3$): δ 23.60(q'd',Me-3,9,J_{H-Me} = 126.5 Hz,J_{other} = 3.2 Hz), 32.57(s,C-6), 63.98(bt,C-1,5,7,11,J_H = 143.7 Hz), 98.48(bs,C-3,9).

(g) (i) 2-Ethyl-2-methylbutanal (130)

2-Ethyl-2-methylbutanal (130) was prepared following the method of van der Gen et al.[180] for alkylation of aldehydes.

A 50 g portion of KH suspension in oil (*ca*. 23%, or ⩾ 220 mmol KH) was washed three times with petroleum ether by decantation. (Suggestions for handling KH-oil dispersions have been given by Brown.[179]) With enough of the last wash remaining to cover the KH, dry tetrahydrofuran (500 mL) was added. The 1 L flask was fitted with a pressure-compensating dropping funnel containing 2-ethylbutanal (20.0 g, 200 mmol) in dry THF (100 mL). (2-Ethylbutanal for this reaction and that in subsection h(i) was dried over $CaCl_2$ and fractionally distilled, b.p. 113-115°C.) The flask was purged with argon and a positive argon pressure was maintained in the flask by means of a balloon attached to the top of the dropping funnel. The aldehyde solution was added to the KH suspension with magnetic stirring, at room temperature, over 20 min. As H_2 was evolved it was occasionally necessary to vent excess pressure. After a further 1 h the mixture was cooled in an ice-water bath. Using the same apparatus a solution of methyl iodide (31.23 g, 13.8 mL, 220 mmol, used without purification) in dry THF (100 mL) was added to the flask over *ca*. 12 min with stirring. After a further 20 min distilled water

(200 mL) was added. The layers were separated and the aqueous layer was extracted with petroleum ether (1 x 300 mL) and ether (1 x 300 mL). The combined extracts and the organic mother liquor were dried over $MgSO_4$ and evaporated to low volume. The dark amber liquid was distilled at atmospheric pressure through a short column of glass beads. 2-Ethyl-2--methylbutanal (130)(6.25 g, 27.4%) was collected at 130-133°C.

Analysis found: C, 73.39; H, 12.68%

$C_7H_{14}O$ requires: C, 73.63; H, 12.36%

ms peaks used for identification at m/e (relative intensity) 115(M+1,100), 143(M+29,6), 155(M+41,4).

^{1}HNMR (neat, 60 MHz): δ 0.97(s,3H,Me-2), 0.79(t,6H,H-4,$J_{3,4} \simeq 8$ Hz), 1.51(q,4H,H-3,$J_{3,4} = 8.0$ Hz), 9.39(s,1H,H-1).

^{13}CNMR ($CDCl_3$): δ 8.26(bq,C-4,$J_H = 125.8$ Hz), 17.23(bq,Me-2,J_H = 127.0 Hz), 27.64(bt,C-3,$J_H = 126.7$ Hz), 49.46(s,C-2), 207.04 (d,C-1,$J_H = 167.4$ Hz).

(ii) <u>2-Ethyl-2-methyl-1-butanol</u> (131)

A mixture of the aldehyde (130)(4.50 g, 40 mmol) and $NaBH_4$ (1.13 g, 30 mmol, finely powdered with a mortar and pestle) with THF (125 mL, reagent grade) was heated to reflux. After 18 h NaOH solution (5-10%, 40 mL) was added to the cooled reaction mixture, followed by water (100 mL). Ether (100 mL) was added to the mixture and the aqueous and organic layers were separated. The aqueous layer was extracted with ether (3 x 100 mL) and the combined extracts and mother liquor were washed with water (2 x 200 mL), dried over $MgSO_4$, and evaporated to a low volume. The product was vacuum distilled yielding 2-ethyl-2-

-methyl-1-butanol (131) (3.90 g, 83.8%) at 74-80°C, (lit.[177] b.p. 150-151°C @ 760 mm Hg).

Analysis found: C, 72,60; H, 13.54%

$C_7H_{16}O$ requires: C, 72.35; H, 13.88%

ms peaks used for identification at m/e (relative intensity) 99(M-OH, 100), 115(M-1,12).

^{1}HNMR (neat, 60 MHz): δ 0.80(s,3H,Me-2), 0.80(t,6H,H-4,$J_{3,4} \simeq 7$ Hz), 1.30(distorted q,4H,H-3,$J_{3,4} \simeq 7$ Hz), 3.28(bd,2H,H-1,$J_{1,OH} \simeq 4$ Hz), 4.51(bt,1H,H-OH,$J_{1,OH} \simeq 4$ Hz).

^{13}CNMR ($CDCl_3$): δ 7.71(q,C-4), 20.77(q,Me-2), 28.09(t,C-3), 37.26(s,C-2), 68.99(t,C-1).

(h) (i) 2,2-Diethylbutanal (132)

This preparation was carried out in the same manner as g(i) above, except for the use of ethyl iodide (34.4 g, 220 mmol). (Ethyl iodide for this reaction was washed with aqueous sodium thiosulphate, then water, dried over $CaCl_2$ and distilled from sodium and stored over mercury.) Also the ice bath was not used and the reaction was left 21 h before workup.

The distillation gave 2,2-diethylbutanal (132) (6.33 g, 24.7%) at 152-159°C.

Analysis found: C, 72.48; H, 13.28%

$C_8H_{16}O$ requires: C, 74.94; H, 12.58%

ms peaks used for identification at m/e (relative intensity) 129(M+1,100), 157(M+29,10), 169(M+41,4).

^{1}HNMR (neat, 60 MHz): δ 0.74(t,9H,H-4,$J_{3,4}$ = 7 Hz), 1.48(q,6H,H-3, $J_{3,4}$ = 7 Hz), 9.17(s,H-1).

^{13}CNMR ($CDCl_3$): δ 7.82(q,C-4), 23.64(t,C-3), 52.64(s,C-2), 207.52(d,C-1).

(ii) 2,2-Diethyl-1-butanol (133)

A mixture of the aldehyde (132) (4.02 g, 31.4 mmol), finely powdered $NaBH_4$ (0.76 g, 20 mmol), and THF (100 mL, reagent grade), was refluxed for 18.5 h. Workup was the same as for the alcohol (131) (*vide supra*). The resulting liquid was vacuum distilled yielding 2,2-diethyl--1-butanol (133) (3.11 g, 76%) at 120-140°C. This slightly coloured product was redistilled under vacuum yielding 2.93 g (72%) of colourless product (133) at 145°C (lit.[177] b.p. 76-77°C @ 11 mm Hg).

Analysis found: C, 73.43,73.25; H, 14.95,14.52%

$C_8H_{18}O$ requires: C, 73.78; H, 13.93%

ms peaks used for identification at m/e (relative intensity) 129(M-1,4), 113(M-OH,9).

^{1}HNMR (CCl_3F, 90 MHz, +10°C): δ 0.76(t,9H,H-4,$J_{3,4}$ = 6.8 Hz), 1.22(q,6H,H-3,$J_{3,4}$ = 6.8 Hz), 2.29(bs,1H,H-OH), 3.22(bs,2H,H-1).

^{13}CNMR ($CDCl_3$): δ 7.37(bq,C-4,J_H = 124.6 Hz), 25.11(bt,C-3,J_H = 124.4 hz), 39.54(s,C-2), 65.95(bt,C-1,J_H = 140.4 Hz).

REFERENCES

1. Geske, D.H. Prog. Phys. Org. Chem. 4, 125 (1967).

2. Fischer, H. *Free Radicals,* J.K. Kochi, ed. John Wiley and Sons, New York, 1973, Vol. 2, p. 435.

3. Kochi, J.K. Adv. Free Radical Chem. 5, 189 (1975).

4. Ladd, J.A.; Wardale, H.W. *Internal Rotation in Molecules,* W.J. Orville-Thomas, ed. John Wiley and Sons, London, 1974, Chap. 5.

5. Norman, R.O.C. Chem. Soc. Rev. 8, 1 (1979).

6. *Time Domain Electron Spin Resonance,* L. Kevan and R.N. Schwartz, ed. John Wiley and Sons, New York, 1979.

7. McGarvey, B.R. *Critical Evaluation of Chemical and Physical Structural Information,* D.R. Lide Jr. and M.A. Paul, ed. Nat. Acad. Sci., Washington, D.C., 1974, p. 415.

8. Swartz, H.M.; Bolton, J.R.; Borg, D.C. *Biological Applications of Electron Spin Resonance,* Wiley-Interscience, New York, 1972.

9. *Free Radicals in Biology,* W.A. Pryor, ed. Academic Press, New York, 1976, Vol. 1.

10. Knowles, P.F.; Marsh, D.; Rattle, H.W.E. *Magnetic Resonance of Biomolecules.* John Wiley and Sons, London, 1976.

11. Wasson, J.R.; Corvan, P.J. Analyt. Chem. 50, 92R (1978).

12. Stevenson, G.R. Magn. Reson. Rev. 6, 209 (1980).

13. Griller, D.; Ingold, K.U. Acc. Chem. Res. 13, 193 (1980).

14. *Specialist Periodical Reports—Electron Spin Resonance.* The Chemical Society, London:
    (a) Vol. 1 (1973), R.O.C. Norman, Sr. Reporter
    (b) Vol. 2 (1974), R.O.C. Norman, Sr. Reporter
    (c) Vol. 3 (1976), R.O.C. Norman, Sr. Reporter
    (d) Vol. 4 (1977), P.B. Ayscough, Sr. Reporter
    (e) Vol. 5 (1979), P.B. Ayscough, Sr. Reporter
    (f) Vol. 6 (1981), P.B. Ayscough, Sr. Reporter

15. Ayscough, P.B. *Electron Spin Resonance in Chemistry.* Methuen and Co. Ltd., London, 1967.

16. Carrington, A.; McLachlan, A.D. *Introduction to Magnetic Resonance*. Harper and Row, New York, 1967.

17. Wertz, J.E.; Bolton, J.R. *Electron Spin Resonance, Elementary Theory and Practical Applications*. McGraw-Hill, New York, 1972.

18. Atherton, N.M. *Electron Spin Resonance, Theory and Applications*. John Wiley and Sons, London, 1973.

19. Assenheim, H.M. *Introduction to Electron Spin Resonance*. Hilger and Watts, London, 1966.

20. Carrington, A. Chem. in Brit. 4, 301 (1968).

21. Norman, R.O.C. Chem. in Brit. 6, 66 (1970).

22. Wilmshurst, T.H. *Electron Spin Resonance Spectrometers*. Adam Hilger Ltd., London, 1967.

23. Poole, C.P. Jr. *Electron Spin Resonance, A Comprehensive Treatise on Experimental Techniques*. Interscience Publishers, New York, 1967.

24. Fessenden, R.W.; Schuler, R.H. J. Chem. Phys. 39, 2147 (1963).

25. Livingstone, R.; Zeldes, H. J. Chem. Phys. 44, 1245 (1966).

26. Zeldes, H.; Livingstone, R. J. Chem. Phys. 45, 1946 (1966).

27. Dobbs, A.J.; Gilbert, B.C.; Norman, R.O.C. J. Chem. Soc. (A) 124 (1971).

28. Press, R.E. *The Chemical Electron*, Longmans, London, 1969.

29. King, F.W. Chem. Rev. 76, 157 (1976). (N.B. also ref. 268 therein.)

30. Sales, K.D. Adv. Free-Radical Chem. 3, 139 (1969).

31. Adam, F.C.; King, F.W. J. Chem. Phys. 58, 2446 (1973).

32. Ellinger, Y.; Subra, R.; Levy, B.; Millie, P.; Berthier, G. J. Chem. Phys. 62, 10 (1975). (cf. ref. 9 therein.)

33. Luz, Z. J. Chem. Phys. 48, 4186 (1968).

34. Ingold, K.U. *International Symposium on Electron Spin Resonance in Chemistry—Summary of Plenary Lectures*, Thessaloniki, Greece, 1979.

35. Eisenstein, O.; Anh, N.T.; Jean, Y.; Deraquet, A.; Cantacuzène, J.; Salem, L. Tetrahedron 30, 1717 (1974).

36. Sweigart, D.A. J. Chem. Ed. 50, 322 (1973).

37. Sullivan, P.D.; Menger, E.M. Adv. Magn. Reson. 9, 1 (1977).

38. Smith, P.; Kaba, R.A.; Wood, P.B. J. Phys. Chem. 78, 117 (1974).

39. Kawamura, T.; Matsunaga, M.; Yonezawa, T. J. Am. Chem. Soc. 100, 92 (1978).

40. Gaze, C.; Gilbert, B.C. J. Chem. Soc. Perkin 2, 754 (1977).

41. (a) Russell, G.A.; Chang, K.-Y. J. Am. Chem. Soc. 87, 4381 (1965).

(b) Russell, G.A.; Chang, K.-Y.; Jefford, C.W. J. Am. Chem. Soc. 87, 4383 (1965).

42. Ellinger, Y.; Rassat, A.; Subra, R.; Berthier, G. J. Am. Chem. Soc. 95, 2372 (1973).

43. Fessenden, R.W. J. Chem. Phys. 37, 747 (1962).

44. de Boer, E.; Mackor, E.L Mol. Phys. 5, 493 (1962).

45. Pacansky, J.; Horne, D.E.; Gardini, G.P.; Bargon, J. J. Phys. Chem. 81, 2153 (1977).

46. Brunton, G.; Ingold, K.U.; Roberts, B.P.; Beckwith, A.L.J.; Krusic, P.J. J. Am. Chem. Soc. 99, 3177 (1977).

47. Pauling, L. J. Chem. Phys. 51, 2767 (1969).

48. Cooper, J.; Hudson, A.; Jackson, R.A. Mol. Phys. 23, 209 (1972).

49. Bernardi, F.; Cherry, W.; Shaik, S.; Epiotis, N.D. J. Am. Chem. Soc. 100, 1352 (1978).

50. Bingham, R.C.; Dewar, M.J.S. J. Am. Chem. Soc. 95, 7182 (1973).

51. Gregory, A.R.: Malatesta, V. J. Org. Chem. 45, 122 (1980).

52. Symons, M.C.R. Ann. Rep. Prog. Chem. (Physical and Inorganic) 75, 117 (1978).

53. Griller, D.; Ingold, K.U.; Fischer, H.; Krusic, P.J. J. Am. Chem. Soc. 100, 6750 (1978).

54. Symons, M.C.R.; Griller, D. J. Magn. Reson. 39, 355 (1980).

55. Kochi, J.K.; Bazkuzis, P.; Krusic, P.J. J. Am. Chem. Soc. 95, 1516 (1973).

56. Kawamura, T.; Sugiyama, M.; Matsunaga, M.; Yonezawa, T. J. Am. Chem. Soc. 97, 1627 (1975).

57. Krusic, P.J.; Meakin, P.; Jesson, J.P. J. Phys. Chem. 75, 3438 (1971).

58. Fessenden, R.W.; Schuler, R.H. J. Chem. Phys. 43, 2704 (1965).

59. Bent, H.A. Chem. Rev. 61, 275 (1961).

60. Bent, H.A. J. Chem. Phys. 32, 1582 (1960).

61. Dobbs, A.J.; Gilbert, B.C.; Norman, R.O.C. J. Chem. Soc. Perkin 2, 786 (1972).

62. Hudson, A.; Root, K.D.J. Tetrahedron 25, 5311 (1969).

63. Krusic, P.J.; Kochi, J.K. J. Am. Chem. Soc. 91, 6161 (1969).

64. Biddles, I,; Hudson, A.; Wiffen, J.T. Tetrahedron 28, 867 (1972).

65. Gaze, C.; Gilbert, B.C.; Symons, M.C.R. J. Chem. Soc. Perkin 2, 235 (1978).

66. Perkins, M.J.; Roberts, B.P. J. Chem. Soc. Perkin 2, 77 (1975).

67. (a) Buley, A.L.; Norman, R.O.C.; Pritchett, R.J. J. Chem. Soc. (B), 849 (1966).

(b) Buley, A.L.; Norman, R.O.C. Proc. Chem Soc. 225 (1964).

68. Hefter, V.H.; Fischer, H. Chem. Ber. 74, 493 (1970).

69. Beckwith, A.L.J.; Tindal, P.K. Aust. J. Chem. 24, 2099 (1971).

70. Malatesta, V.; Ingold, K.U. J. Am. Chem. Soc. 103, 609 (1981).

71. Gaze, C.; Gilbert, B.C. J. Chem. Soc. Perkin 2, 1161 (1977).

72. Krusic, P.J.: Bingham, R.C. J. Am. Chem. Soc. 98, 230 (1976).

73. Chen, K.S.; Kochi, J.K. Can. J. Chem. 52, 3529 (1974).

74. Giese, B.; Beckhaus, H.-D. Angew. Chem. Int. Ed. Engl. 17, 594 (1978).

75. Fischer, H. Mol. Phys. 9, 149 (1965).

76. Shiga, T. J. Phys. Chem. 69, 3805 (1965).

77. Stone, E.W.; Maki, A.H. J. Chem. Phys. 36, 1944 (1962).

78. Loth, K.; Graf, F. Helv. Chim. Acta 64, 1910 (1981).

79. Lucken, E.A.C.; Poncioni, B. J. Chem. Soc. Perkin 2, 777 (1976).

80. Griller, D. J. Am. Chem. Soc. 100, 5240 (1978).

81. Griller, D. Magn. Reson. Rev. 5, 1 (1979).

82. Eiben, K.; Fessenden, R.W. J. Phys. Chem. 75, 1186 (1971).

83. Fessenden, R.W.; Schuler, R.H. Adv. Radiat. Chem. 2, 1 (1970).

84. Symons, M.C.R. J. Am. Chem. Soc. 91, 5924 (1969).

85. Vanderkooi, N. Jr.; Fox, W.B. J. Chem. Phys. 47, 3634 (1967).

86. Krusic, P.J.; Kochi, J.K. J. Am. Chem. Soc. 90, 7155 (1968).

87. Krusic, P.J.; Kochi, J.K. J. Am. Chem. Soc. 93, 846 (1971).

88. Hudson, A; Hussain, H.A. J. Chem. Soc. (B), 793 (1969).

89. Calvert, J.G.; Pitts, J.N. *Photochemistry*. John Wiley and Sons, New York, 1966, p. 449.

90. Elson, I.H.; Kochi, J.K. J. Org. Chem. 39, 2091 (1974).

91. Griller, D.; Ingold, K.U. J. Am. Chem. Soc. 96, 630 (1974).

92. Gaze, C.; Gilbert, B.C.; Symons, M.C.R. J. Chem. Soc. Perkin 2, 235 (1978).

93. Beckwith, A.L.J.; Easton, C.J. J. Am. Chem. Soc. 103, 615 (1981).

94. Yamazaki, I.; Mason, H.S.; Piette, L.H. Biochem. Biophys. Res. Commun. 1, 336 (1959).

95. Saito, E.; Bielski, B.H.J. J. Am. Chem. Soc. 83, 4467 (1961).

96. Dixon, W.T.; Norman, R.O.C. J. Chem. Soc., 3119 (1963).

97. Dixon, W.T.; Norman, R.O.C. Nature 196, 891 (1962).

98. Norman, R.O.C.; Gilbert, B.C. Adv. Phys. Org. Chem. 5, 53 (1967).

99. Norman, R.O.C. *Essays on Free-Radical Chemistry*. Special Publication 24, The Chemical Society, London, 1970, p. 117.

100. Wong, S.K. J. Magn. Reson. 43, 331 (1981).

101. Dalal, N.S.; Miller, J.M. J. Magn. Reson. 42, 491 (1981).

102. Heinzer, J. Mol. Phys. 22, 167 (1971).

103. Vancamp, H.L.; Heiss, A.H. Magn. Reson. Rev. 7, 1 (1981).

104. Wladimiroff, W.W. Photochem. and Photobiol. 5, 243 (1966).

105. Kasha, M. J. Opt. Soc. Amer. 38, 929 (1948).

106. Griller, D.; Ingold, K.U.; Scaiano, J.C. J. Magn. Reson. 38, 169 (1980).

107. Sullivan, P.D.; Bolton, J.R. Adv. Free-Radical Chem. 4, 39 (1970).

108. Hudson, A.; Luckhurst, G.R. Chem. Rev. 69, 191 (1969).

109. Chen, K.S.; Hirota, N. *Techniques of Chemistry 6,* Part 2, *Investigation of Rates and Mechanisms of Reactions,* G.G. Hammes, ed. 1974, p. 565.

110. Fraenkel, G.K. J. Phys. Chem. 71, 139 (1967).

111. Edge, D.J.; Kochi, J.K. J. Am. Chem. Soc. 94, 6485 (1972).

112. Lloyd, R.V. J. Phys. Chem. 85, 1440 (1981).

113. Sullivan, P.D. J. Phys. Chem. 74, 2563 (1970).

114. Gaze, C.; Gilbert, B.C. J. Chem. Soc. Perkin 2, 116 (1977).

115. Sullivan, P.D. J. Phys. Chem. 75, 2195 (1971).

116. Derbyshire, W. Mol. Phys. 5, 225 (1962).

117. Ayscough, P.B.; McClung, R.E.D. Mol. Phys. 20, 35 (1971).

118. Ayscough, P.B.; Brice, M.C.; McClung, R.E.D. Mol. Phys. 20, 41 (1971).

119. Barnabas, A.B.; Forbes, W.F.; Sullivan, P.D. Can. J. Chem. 45, 267 (1967).

120. Sullivan, P.D.; Bolton, J.R. J. Am. Chem. Soc. 90, 5366 (1968).

121. Gough, T.E. Can. J. Chem. 47, 331 (1969).

122. Gough, T.E.; Taylor, G.A. Can. J. Chem. 47, 3717 (1969).

123. (a) Loth, K.; Graf, F.; Günthard, Hs.H. Chem. Phys. Lett. 45, 191 (1977).

(b) Rudin, M.; Loth, K.; Graf, F.; Günthard, Hs.H. Chem. Phys. Lett. 46, 29 (1977).

124. Krusic, P.J.; Chen, K.S.; Meakin, P.; Kochi, J.K. J. Phys. Chem. 78, 2036 (1974).

125. Hudson, A. J. Chem. Soc. (A), 2513 (1969).

126. Ha, T.-K. Chem. Phys. Lett. 30, 379 (1975).

127. Grossöhme, V.T.; Wünsche, P.; Roth, H.-K. Z. Phys. Chemie, Leipzig, 258, 129 (1977).

128. Sargent, F.P.; Grady, E.M. Chem. Phys. Lett. 38, 130 (1976).

129. Adams, J.Q. J. Am. Chem. Soc. 90, 5363 (1968).

130. Corvaja, C.; Giacometti, G.; Sartori, G. J. Chem. Soc. Faraday Trans. 2 70, 709 (1974).

131. Steven, J.R.; Ward, J.C. Aust. J. Chem. 20, 2005 (1967).

132. Ingold, K.U.; Walton, J.C. J. Am. Chem. Soc. 104, 616 (1982).

133. Pacansky, J.; Schubert, W. J. Chem. Phys. 76, 1459 (1982).

134. Karabatsos, G.J.; Hsi, N. J. Am. Chem. Sco. 87, 2864 (1965).

135. Karabatsos, G.J.; Fenoglio, D.J. Topics in Stereochemistry 5, 167 (1970).

136. West, P.R.; Sitwell, L.; Foster, T. unpublished results.

137. *Physico-Chemical Constants of Pure Organic Compounds*, J. Timmermans, ed. Elsevier Publishing Co., New York, 1950, Vol. 1.

138. *Techniques of Organic Chemistry*, Vol. 7, *Organic Solvents*, A. Weissberger, ed. Interscience, New York, 1955.

139. Nemoto, F.; Mukai, K.; Tsuzuki, N.; Ishizu, K. Chem. Lett. 307 (1981).

140. Davies, A.G.; Roberts, B.P.; Scaiano, J.C. J. Chem. Soc. (B), 2171 (1971).

141. Lloyd, R.V.; Causey, J.G. J. Chem. Soc. Perkin 2, 1143 (1981).

142. Lloyd, R.V.; Causey, J.G.; Momany, F.A. J. Am. Chem. Soc. 102, 2260 (1980).

143. Gilbert, B.C.; Trenwith, M. J. Chem. Soc. Perkin 2, 1083 (1975).

144. Dixon, W.T.; Norman, R.O.C. J. Chem. Soc., 4850 (1964).

145. Ohmai, T.; Sukurai, G. J. Chem. Phys. 46, 1865 (1967).

146. Shiga, T.; Boukhors, A.; Donzou, P. J. Phys. Chem. 71, 4264 (1967).

147. Griller, D.; Ingold, K.U. J. Am. Chem. Soc. 96, 6715 (1974).

148. Franks, F.; Ives, D.J.G. Quart. Rev. 20, 1 (1966).

149. Gordon, J.E. *The Organic Chemistry of Electrolyte Solutions*. John Wiley and Sons, New York, 1975, p. 161 ff., p. 234 ff.

150. Vinogradov, S.N.; Linnell, R.H. *Hydrogen Bonding*. Van Nostrand Reinhold, New York, 1971.

151. Eliel, E.L J. Chem. Educ. 52, 762 (1975), and references therein.

152. Gittins, V.M.; Wyn-Jones, E.; White, R.F.M. *Internal Rotation in Molecules*, W.J. Orville-Thomas, ed. John Wiley and Sons, London, 1974, Chap. 12.

153. Coene, E.; Anteunis, M. Bull. Soc. Chim. Belges 79, 37 (1970).

154. Anderson, J.E.; Brand, J.C.D. Trans. Farad. Soc. Lond. 62, 39 (1966).

155. Friebolin, H.; Schmid, H.G.; Kabuss, S.; Faisst, W. Org. Magn. Reson. 1, 67 (1969).

156. Greenburg, A.; Laszlo, P. Tet. Lett., 2641 (1970).

157. Greenburg, A. J. Chem. Educ., 575 (1972).

158. Eliel, E.L.; Knoeber, M.C. J. Am. Chem. Soc. 90, 3444 (1968).

159. Perkins, M.J.; Roberts, B.P. J. Chem. Soc. Perkin 2, 77 (1975).

160. Zorin, V.V.; Zlot-skii, S.S.; Shuvalov, V.F.; Moravskii, A.P.; Rakhmankulov, D.L.; Paushkin, Y.M. Doklady Akad. Nauk. S.S.S.R. 236, 106 (1977).

161. Panaye, A.; MacPhee, J.A.; Dubois, J.-E. Tet. Lett., 3297 (1978).

162. Atkins, P.W. *Physical Chemistry*. Oxford University Press, Oxford, 1978, p. 913.

163. March, J. *Advanced Organic Chemistry,* 2nd Edition. McGraw-Hill, New York, 1977, p. 21, Table 3.

164. Smith, P.; Pearson, J.T.; Tsina, R.V. Can. J. Chem. 44, 753 (1966).

165. Greenwood, F.L.; Whitmore, F.C.; Crooks, H.M. J. Am. Chem. Soc. 60, 2028 (1938).

166. *Organic Syntheses,* Roger Adams, ed. Vol. VIII, 104 (1928).

167. Nystrom, R.F.; Brown, W.G. J. Am. Chem. Soc. 69, 2549 (1947).

168. Sarel, S.; Newman, M.S. J. Am. Chem. Soc. 78, 5416 (1956).

169. Sommer, L.H.; Blankman, H.D.; Miller, P.C. J. Am. Chem. Soc. 76, 803 (1954).

170. Watts, G.B.; Ingold, K.U. J. Am. Chem. Soc. 94, 491 (1972).

171. Rondestvedt, C.S. Jr. J. Org. Chem. 26, 2247 (1961). (see also ref. 158).

172. Pihlaja, K.; Heikkilä, J. Acta Chem. Scand. 21, 2390 (1967).

173. Eliel, E.L.; Powers, J.R. Jr.; Nader, F.W. Tetrahedron 30, 515 (1974).

174. Conrad, W.E.; Gesner, B.D.; Levasseur, L.A.; Murphy, R.F.; Conrad, H.M. J. Org. Chem. 26, 3571 (1961).

175. Berlow, E.; Barth, R.H.; Snow, J.E. *The Pentaerythritols.* Reinhold, New York, 1958, Am. Chem. Soc. Monograph No. 136.

176. Skrabal, A.; Zlatewa, M. Z. Phys. Chem. 119, 305 (1926).

177. Rice, R.V.; Jenkens, G.L.; Harden, W.C. J. Amer. Pharm. Assn. 27, 303 (1938).

178. (a) Orthner, L. Chem. Ber. 61B, 116 (1928). [See CA1327 (1928)]

(b) Orthner, L.; Freyss, G. Annelen 484, 131 (1930).

179. Brown, C.A. J. Org. Chem. 39, 3913 (1974).

180. Groenewegen, P.; Kallenberg, H.; van der Gen, A. Tett. Lett., 491 (1978).

181. Pihlaja, K.; Nurmi, T. Israel J. Chem. 20, 160 (1980).

182. Pihlaja, K.; Äyräs, P. Acta Chem. Scand. 24, 531 (1970).

183. Scheffler, K.; Hieke, K.; Schuler, P.; Stegmann, H.B. Z. Naturforsch 31a, 1620 (1976).

184. Scheffler, K.; Digel, F.; Krieg, R.; Stegmann, H.B. Z. Naturforsch 35a, 1231 (1980).

185. Fischer, V. Ph.D. Dissertation, 1981, Eberhard-Karls-Universität zu Tübingen.

186. Felix, C.C.; Sealy, R.C. J. Am. Chem. Soc. 103, 2831 (1981).

187. Gilbert, B.C.; Trenwith, M. J. Chem. Soc. Perkin 2, 1834 (1973).

188. Yim, M.B.; Wood, D.E. J. Am. Chem. Soc. 98, 3457 (1976).

APPENDIX A

SIMULATION OF THE ESR SPECTRA

The hardware and software used for simulation of the ESR spectra in this dissertation have been outlined in Chapter II. In addition to adaptation of the programs to local plotting routines several other changes were necessary in the ESREXN program. These modifications are given on the following three pages, along with the comments of the installer.

```
C
C       COMPUTATION OF EXCHANGE-BROADENED ESR SPECTRA
C
C       BY J. HEINZER
C       LABORATORIUM FUER ORG. CHEMIE
C       EIDG. TECH. HOCHSCHULE ZUERICH
C       UNIVERSITAETSSTRASSE 6 - 8
C       CH-8006 ZUERICH
C       SWITZERLAND
C
C       ZUERICH, MAY 1971
C
C
C******** PROGRAM INSTALLED  JANUARY, 1982 BY C.WRENSHALL ***************
C******** ACADEMIC SYSTEMS  UNIVERSITY OF VICTORIA         ***************
C
C       GENERAL CHANGES INVOLVED:
C
C       1) CHANGING FORMAT OF CARD-IMAGE I/O FROM 8A10 (CDC 6500/6400)
C          TO 20A4 (IBM SYSTEM/370)
C       2) REPLACING PLOTTING ROUTINES WITH LOCAL ROUTINES
C       3) DELETING CALL TO FUNCTION SUBROUTINE 'SECOND', WHICH IS NOT
C          IMPLEMENTED AT UVIC.
C
C       IN THE COURSE OF MAKING THESE CHANGES, SOME FUNDAMENTAL FAULTS
C       IN THE PROGRAM DESIGN WERE ENCOUNTERED.  IN PARTICULAR,
C       A) IN THE MAIN PROGRAM, THERE ARE TWO POINTS AT WHICH A BRANCH
C          INTO THE RANGE OF A DO-LOOP (DO 51...) ARE INDICATED, AND
C       B) IN SUBROUTINE ESRLET, VARIABLE 'RS' IS UNDEFINED IN ALL
C          BUT THE FIRST CALL TO THAT SUBROUTINE.
C       IN ADDITION, IN EXECUTING THE DATA IN TEST EXAMPLE A, A
C       NUMBER OF DIVIDE CHECKS OCCUR, ALTHOUGH THE RESULTS SEEM
C       UNAFFECTED.
C
C       ANY ATTEMPT TO STRINGENTLY DEBUG THIS PROGRAM WOULD BE HAMPERED
C       BY THE COMPLEXITY OF THE PROBLEM TO BE SOLVED, THE COMPLEXITY
C       OF THE PROGRAM ITSELF, THE NEARLY TOTAL LACK OF PROGRAM
C       DOCUMENTATION, AND BUDGET CONSTRAINTS.
C
C       CONSEQUENTLY, THIS PROGRAM HAS BEEN TESTED ONLY TO THE EXTENT
C       THAT THE SUPPLIED TEST DATA REPRODUCES THE SUPPLIED RESULTS.
C
C***** THE USER SHOULD BE AWARE THAT DUE TO DETECTED PROGRAM ERRORS,*****
C***** RESULTS OF THIS PROGRAM SHOULD BE REGARDED AS LIABLE TO       *****
C***** ERROR, AND SHOULD BE VERIFIED BY OTHER MEANS IF AT ALL        *****
C***** POSSIBLE.                                                     *****
C
C*************************************************************************
```

```
0050                    CALL NUMBER(X,2.7,H,S(J),90.,1)
0051                    CALL SYMBOL(X,3.5,H,1H=,90.,1)
                  C
```

```
FORTRAN IV G1  RELEASE 2.0              ESRLET          DATE = 82279          13/21/09

                  C******** CHANGED JANUARY 1982 BY C. WRENSHALL  ACADEMIC SYSTEMS ********
                  C
                  C       LOCAL VERSION OF PLOTTING SUBROUTINE NUMBER LEFT JUSTIFIES
                  C       RATHER THAN RIGHT JUSTIFIES VALUES PLOTTED, RESULTING IN A
                  C       DIFFICULT TO READ TABLE.  TO OVERCOME THIS, THE VALUE TO BE
                  C       PLOTTED IS TESTED TO DETERMINE THE NUMBER OF DIGITS TO BE
                  C       PLOTTED.  THE STARTING POSITION OF THE PLOTTED VALUE IS
                  C       ALTERED ACCORDINGLY.
                  C
                  C       ALSO, BY REQUEST OF USER, A-VALUES ARE CONVERTED FROM MM TO
                  C       GAUSS AND K-VALUES ARE CONVERTED FROM MM TO MHZ FOR PLOTTING
                  C       PURPOSES.  (A-VALUES ARE MULTIPLIED BY UM.  K-VALUES ARE
                  C       MULTIPLIED BY UM AND BY 2.80442.)
                  C
                  C*************************************************************************
                  C
0052                    XA = UM * A(J,I)
0053                    IF (XA.LE.9.99)CALL NUMBER(X,4.6,H,XA,90.,2)
```

```
FORTRAN IV G1  RELEASE 2.0                XSTEP                  DATE = 82279

0001                    SUBROUTINE XSTEP(NC,NA,NTEST,NSTEP,STEP,FMIN)
                C
                C       DETERMINES THE NUMBER OF STEPS
                C
0002                    LOGICAL NTEST
0003                    COMMON/ESR1/ AMP(1000),SP(1000,7)
0004                    COMMON/ESR2/ NU(7),S(7),A(7,15)
0005                    COMMON/ESR3/ B(15,15),W(15),P(15)
0006                    COMMON/FILE/ IN,IO
0007                5   FORMAT(//32H TEST OUTPUT OF SUBROUTINE XSTEP//
                       110X28HFMIN, EMAX, WMAX, WMIN, STEP,5F10.3/)
                C
0008                    NDIM=1000
0009                    EMAX=0.
0010                    WMAX=0.
0011                    WMIN=1000.
0012                    DO 1  J=1,NC
0013                    H=0.
0014                    DO 2  I=1,NA
                C
                C          FEBRUARY MODIFICATION.
                C          23 FEBRUARY 1982
                C          MOIRA GLEN
                C
                C          THE ABSOLUTE VALUE OF ARRAY 'A' HAS BEEN USED IN THE
                C          CALCULATION OF THE MAX AND MIN VALUES.
                C
0015                2   H=H+ABS(A(I,J))*SP(1,1)
0016                    IF(H.GT.EMAX) EMAX=H
0017                    IF(W(J).GT.WMAX)  WMAX=W(J)
0018                    IF(W(J).LT.WMIN) WMIN=W(J)
0019                1   CONTINUE
0020                    FMIN=-EMAX-8.*WMAX
0021                    STEP=WMIN/8.
0022                3   NSTEP=2*INT(-FMIN/STEP)+1
0023                    IF(NSTEP.LE.NDIM) GO TO 4
0024                    STEP=STEP*FLOAT(NSTEP)/FLOAT(NDIM-10)
0025                    GO TO 3
0026                4   IF(NTEST) WRITE(IO,5) FMIN,EMAX,WMAX,WMIN,STEP
0027                    RETURN
0028                    END
```

The following sections list, by figure and page, the parameters used in the simulations that appear in the dissertation. Note that in all cases involving exchange, satisfactory results were obtained assuming mutual exchange (i.e. equal populations of all conformers). The rate constants (k) given are those appearing on the plotted output in each case. Without an accurate knowledge of the splittings in the limit of slow exchange these rate constants are of use only in a relative sense, and have no *absolute* significance.

Figure 27b, page 86

B-NC 12 data system

a_{OH} = 0.48 G, $a_{\gamma H}$ = 0.313 G

linewidth = 0.07 G, modulation amplitude 0.06 G

Figure 28b,e, page 88

ESREXN

	configuration 1	configuration 2
$a_{\alpha H}$	13.50 G	13.90
a_{OH}	-1.64 G*	-0.10
$a_{\gamma H}$	0.30 G	0.30

linewidth = 0.11 G

k = 4.690 MHz, 2.339 MHz

---

*The lower value of a_{OH} (-1.64 G) is that used in the calculations of Krusic et al.[57] for θ = 90° in the planar hydroxymethyl radical. This value is applied in all the exchange simulations involving restricted C_{α}-OH rotation. The other values of a_{OH} must then be chosen such that the average is the experimentally observed value.

Figure 30a, page 97
Figure 31b,d, pages 98, 99
Figure 32b,e,g, pages 101, 102

Second order simulation program using the appropriate experimental splittings, Table 6.

Figure 32d,i, pages 101, 102
Figure 33a,b, page 103

ESREXN

(i) Two-site exchange model:

	configuration 1	configuration 2
$a_{\beta 1}$	19.55 G	19.10
$a_{\beta 2}$	19.45 G	18.90
a_{OH}	+0.44 G	-1.64

linewidth = 0.15 G

k = 24.329 MHz, 5.835 MHz

(ii) Compare the six-site exchange model referred to on page 104; structures 35a-f, page 105. The spectra from the six-site simulation model appear below.

Configuration	1	2	3	4	5	6
$a_{\beta 1}$	19.55	19.45	19.55	19.45	19.10	18.90
$a_{\beta 2}$	19.45	19.55	19.45	19.55	18.90	19.10
a_{OH}	-0.08	-0.08	-0.08	-0.08	-1.64	-1.64

linewidth = 0.15 G Norris subroutine option used.

k = 4.253 MHz, 1.013 MHz respectively, see figure

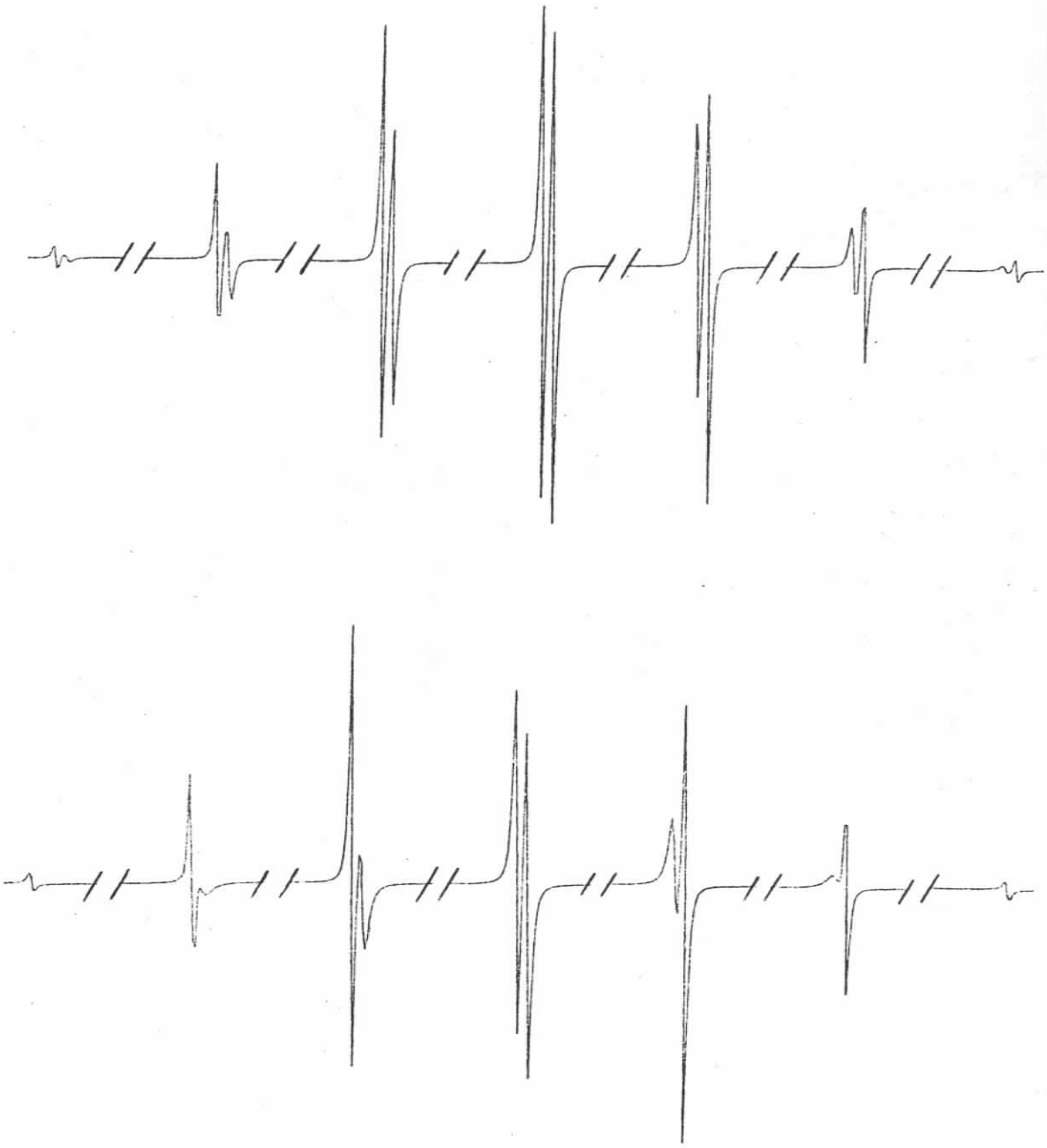

Spectra from simulation of six-site exchange model for 2-hydroxyprop--2-yl radical. See previous page.

Figure 36a,b,c, page 110

ESREXN

	configuration 1	configuration 2
a_{α}	15.10 G	15.70
a_{β}	22.00 G	22.20
a_{OH}	-1.64 G	-1.16

linewidth = 0.54 G

k = 3.75 MHz, 1.68 MHz, 0.56 MHz respectively

Figure 38c, page 114

Second order simulation program using the appropriate experimental splittings, Table 9.

Figure 41, page 118

ESREXN

	configuration 1	configuration 2
$a_{\alpha H}$	14.74 G	15.14
$a_{\beta H}$	21.87 G	22.27
a_{OH}	-1.60 G	-0.80
$a_{\gamma H}$	0.44 G	0.44

linewidth = 0.10 G

k = 3.889 MHz, 2.24 MHz, 0.97 MHz respectively

Figure 45c, page 129

B-NC 12 data system

peak group #5 a_{OH} = 0.97 G, $a_{\gamma H}$ = 0.74 G,

$a_{\delta H}$ = 0.13 G

linewidth = 0.06 G

modulation amplitude = 0.09 G

peak group #4 a_{OH} = 0.97 G, $a_{\gamma H}$ = 0.74 G

$a_{\delta H}$ = 0.13 G, $a_{2nd\ order}$ = 0.13 G

linewidth = 0.06 G

modulation amplitude = 0.09 G

Figure 47, page 131

ESREXN

Configuration	1	2	3	4
$a_{\alpha H}$	15.30 G	15.70	15.70	15.30
$a_{\beta 1}$	15.20 G	15.60	25.20	24.80
$a_{\beta 2}$	24.80 G	25.20	15.60	15.20
a_{OH}	-1.64 G	-0.90	-0.90	-1.64
$a_{\gamma H}$	0.80 G	0.80	0.80	0.80

linewidth = 0.49 G

(a) $k_{1,2} = k_{2,1} = k_{3,4} = k_{4,3}$ = 211.8 MHz

$k_{1,3} = k_{3,1} = k_{2,4} = k_{4,2}$ = 0.0 MHz

$k_{1,4} = k_{2,3} = k_{3,2} = k_{4,1}$ = 2742. MHz

(b) $k_{1,2} = k_{2,1} = k_{3,4} = k_{4,3}$ = 2.119 MHz

$k_{1,3} = k_{3,1} = k_{2,4} = k_{4,2}$ = 0.0 MHz

$k_{1,4} = k_{2,3} = k_{3,2} = k_{4,1}$ = 27.421 MHz

Figure 48e-h, p. 137

ESREXN

	configuration 1	configuration 2
$a_{\alpha H}$	-14.20 G	-14.20
$a_{\beta 1}$	26.32 G	11.32
$a_{\beta 2}$	11.32 G	26.32
$a_{\gamma 1}$	1.90 G	-0.30
$a_{\gamma 2}$	-0.30 G	1.90
$a_{\gamma'}$	1.84 G	1.84

linewidth = 0.44 G

k = 747.8, 224.3, 22.43, 6.281 MHz respectively

Figure 50, page 145

ESREXN

	configuration 1	configuration 2
$a_{\alpha H}$	15.70 G	15.70
$a_{\beta 1}$	12.66 G	24.26
$a_{\beta 2}$	24.26 G	12.66
a_{OH}	-1.10 G	-1.10
$a_{\gamma H}$	1.20 G	1.20

linewidth = 0.32 G

k = 807.7, 161.5, 32.3 MHz respectively

Figure 52d, page 152

ESREXN

	configuration 1	configuration 2
$a_{\alpha H}$	16.52 G	16.92
$a_{\beta H}$	15.60 G	16.00
a_{OH}	-1.60 G	-1.20

linewidth = 0.41 G

k = 0.872 MHz

Figure 53b, page 155

ESREXN (no exchange)
simulation of high resolution "doublet"

a_{OH} = 0.76 G

$a_{\delta H}$ = 0.10 G

linewidth = 0.07 G

Figure 53c, page 155

ESREXN

	configuration 1	configuration 2
$a_{\alpha H}$	16.04 G	16.44
$a_{\beta H}$	16.04 G	16.44
a_{OH}	-1.60 G	-1.20

linewidth = 0.41 G

k = 0.872 MHz

Figure 55a, page 158

ESREXN

	configuration 1	configuration 2
$a_{\alpha H}$	14.90 G	14.50
$a_{\beta H}$	23.30 G	22.90
a_{OH}	-0.83 G	-1.63
$a_{\gamma H}$	0.17 G	0.17
linewidth	0.07 G	

k = 3.74 MHz

Figure 55b,c, page 158

ESREXN

	configuration 1	configuration 2
$a_{\alpha H}$	14.50 G	14.90
$a_{\beta H}$	23.30 G	22.90
a_{OH}	-1.63 G	-0.83
$a_{\gamma H}$	0.17 G	0.17
linewidth	0.07 G	

k = 18.7, 3.74 MHz respectively

Figure 57b, page 169

Second order simulation program

$a_{\beta 1H}$ = 21.40 G

$a_{\beta 6H}$ = 24.00 G

linewidth = 0.19 G

Figure 59b, page 176

Second order simulation program

$a_{\beta 2H}$ (axial) = 35.92 G

$a_{\beta 2H}$ (equatorial) = 10.32 G

a_{OH} = 0.70 G

$a_{\gamma 4H}$ = 0.70 G

linewidth = 0.49 G

Figure 61a,b, page 179

ESREXN

	configuration 1	configuration 2
$a_{\beta 2H}$ (axial)	36.12 G	35.72
$a_{\beta 2H}$ (equatorial)	10.62 G	10.02
$a_{\gamma 4H}$	0.70 G	0.70
a_{OH}	-0.70 G	-0.70

linewidth = 0.43 G

k = 59.8, 1.2 MHz respectively

Figure 64b, page 196

ESREXN

	configuration 1	configuration 2
$a_{\alpha H}$	-0.43 G	-0.43
$a_{\gamma 2H}$ (equatorial)	-1.50 G	0.72
$a_{\gamma 2H}$ (axial)	0.72 G	-1.50

linewidth = 0.12 G

k = 75.5 MHz

Figure 64d, page 196

ESREXN
parameters as for Figure 64b
except $a_{\alpha H}$ = 0.39 G, linewidth = 0.09 G, k = 1.00 MHz

Figure 65c, page 197

ESREXN
parameters as for Figure 64b
except k = 0.025 MHz

Figure 68c, page 203

B-NC 12 data system

$a_{\gamma 1}$ (2H) = 0.955 G

$a_{\gamma 2}$ (2H) = 0.68 G

linewidth = 0.15 G
modulation amplitude 0.04 G

Figure 69d, page 206

ESREXN (no exchange)
See structure (111), page 207

$a_{\gamma 1}$ (3H) = 2.13 G

$a_{\gamma 2}$ (3H) = 0.35 G

$a_{\gamma 3}$ (1H) = 0.87 G

$a_{\gamma 4}$ (1H) = 0.16 G

linewidth = 0.05 G

Figure 73b, page 218

ESREXN (no exchange)

$a_{\alpha H}$ = 16.4 G

$a_{\gamma H}$ (2H) = 0.60 G

linewidth = 0.53 G